MULTI-CHAMBER TYRE DESIGN AND ANALYSIS FOR LOW ROLLING RESISTANCE

BY

HAMAD SARHAN DHEYAB HAMAD ALDHUFAIRI

A thesis submitted to the College of Engineering and Physical Sciences of the University of Birmingham for the degree of DOCTOR OF PHILOSOPHY

Department of Mechanical Engineering

School of Engineering

College of Engineering and Physical Sciences

University of Birmingham

July 2019

UNIVERSITY OF
BIRMINGHAM

University of Birmingham Research Archive

e-theses repository

This unpublished thesis/dissertation is copyright of the author and/or third parties. The intellectual property rights of the author or third parties in respect of this work are as defined by The Copyright Designs and Patents Act 1988 or as modified by any successor legislation.

Any use made of information contained in this thesis/dissertation must be in accordance with that legislation and must be properly acknowledged. Further distribution or reproduction in any format is prohibited without the permission of the copyright holder.

ABSTRACT

Rolling-resistance drives the focus of the majority of tyre developments because of its considerable impact over fuel economy and CO2 emissions considering the enormous amount of vehicles in use worldwide. Many efforts were carried out to lower the rolling-resistance but had no to little gains due to the tyre's complexity and the resultant trade-offs in the overall performance. This research offers a promising novel and simple tyre solution of four inner chambers to decrease the rolling-resistance while maintaining the other key driving performances satisfactorily. In this research, a full 3D finite element model of the tyre was developed using Abaqus 6.13-1 and validated against several experimental prototypes of single, dual and five multi-chambers respectively for targeted rolling performances. Using the validated finite element model as a base model, the "total design" approach of Stuart Pugh was followed to generate and select the best sub-optimum design of multi-chamber tyre solution. With parametric investigation using the full-factorial design of experiments, an optimum structural design with the best cavity volume and inflation settings were reached. The optimum design provided a 28% decrease in the rolling-resistance, a matching grip, a satisfactory cushioning and an enhanced cornering to that of the standard (baseline) tyre.

ACKNOWLEDGEMENTS

Foremost, I would like to express my sincere thanks and greatest gratitude to Allah Almighty who blessed me with everything I have and achieved. Thereafter, I would like to express my thanks and gratitude to my grandmother (Najeya Faris Al-Dkheel) who raised and took care of me for her support, encouragement and prayers. I pray to Allah Almighty to reward her and bestow his mercy upon her. Also, I would like to express my thanks and gratitude to my parents (Sarhan and Maryam) for their support, encouragement and prayers. Furthermore, I would like to show my gratitude and thanks to my dear wife (Meriem Benbarghout), her family especially her mother (Fettouma), my siblings (Abdulghani, Najiya, Theyab, Isa and Khalifa) and the rest of my family for their support, encouragement and prayers.

I would like to express my appreciation, gratitude and thanks to my supervisors Dr Khamis Essa and Dr Oluremi Olatunbosun for their support, guidance and help throughout my study as they were as a second family to me. Moreover, I would like to thank the Ministry of Education in the Kingdom of Bahrain for sponsoring me to study abroad and the University of Birmingham for welcoming me to study as one of its students.

In addition, I would like to extend my appreciation and thanks to Dr Karl Dearn, Dr Raya Al-Dadah, Dr Leung Soo, Mr Carl Hingley, Mr Peter Thornton and Mr Lee Gauntlett for their support and help in doing my research work. Finally, I would like to thank my colleagues Dr Adebola Ougunoiki, Dr Shahriar Parisouz, Dr Ammar Kubba, Dr Nasim Mahmoudi, Dr Alessandro Abena, Dr Ahmed Daboo, Dr Omar Efkirin, Dr Abdalqader Ahmad, Abror Tolipov, Olalere Kayode, Mohamed Hafez, Harith Ayoob, Ramy Abdallah, Abdullah Alqhatani and many more people whom I can not mention all here for their support and encouragement during my study.

TABLE OF CONTENTS

CHAPTER (1): GENERAL INTRODUCTION 1

1.1 BACKGROUND AND MOTIVATION 1

1.2 AIMS AND OBJECTIVES 4

1.2.1 Overall Aim 4

1.2.2 Objectives 4

1.3 SCOPE AND LIMITATIONS 5

1.4 THESIS LAYOUT AND CONTENTS 7

CHAPTER (2): LITERATURE SURVEY 11

2.1 INTRODUCTION 11

2.2 WORKING PRINCIPLE OF PNEUMATIC TYRES 12

2.2.1 Basic Representation 12

2.2.2 Forces and Torques/Moments 14

2.2.3 Deformational Behaviour 18

2.3 ROLLING-RESISTANCE 20

2.3.1 Description and Concept 21

2.3.1.1 Rolling-Resistance as a “Force” 21

2.3.1.2 Rolling-Resistance as an “Energy Consumed” 24

2.3.2 Rolling-Resistance Calculation 27

2.3.2.1 Analytical Approach 27

2.3.2.2 Experimental Approach 29

2.3.2.3 Finite Element Approach 30

2.4 ROLE OF OPERATIONAL CONDITIONS 35

2.4.1 Normal Load 35

2.4.2 Rolling Velocity 39

2.4.3 Inflation Pressure 44

2.5 TYRE ADVANCES FOR LOW ROLLING-RESISTANCE 49
2.5.1 Body Configuration and Construction *49*
2.5.2 Geometrical Dimensions *64*
2.5.3 Material Compounds *74*
2.6 SUMMARY 84
CHAPTER (3): MATERIAL PROPERTIES ACQUISITION 88
3.1 INTRODUCTION 88
3.2 DATA ACCURACY AND PRECISION 94
3.3 RUBBER COMPONENTS 98
3.3.1 Hyperelasticity *98*
3.3.2 Viscoelasticity *106*
3.3.2.1 Linear Viscoelasticity 106
3.3.2.2 Non-Linear Viscoelasticity 110
3.3.3 Density *122*
3.4 REINFORCEMENT COMPONENTS 122
3.4.1 Elasticity *123*
3.4.2 Lay-up Structure *129*
3.4.3 Density *134*
3.5 SUMMARY 134
CHAPTER (4): DEVELOPMENT AND VALIDATION OF FINITE ELEMENT MODEL FOR STANDARD TYRE 136
4.1 INTRODUCTION 136
4.2 GEOMETRICAL FEATURES CAPTURE 139
4.3 FE MODEL SET-UP 141
4.3.1 2D Axisymmetric Modelling *141*
4.3.1.1 Rubber and Wheel-Rim Components 142

4.3.1.2 Reinforcement Components 145
4.3.2 3D Modelling of 2D Profile, Air Cavity and Road 146
4.3.3 Simulation (Analysis) Steps 150
4.4 MESH REFINEMENT 155
4.4.1 Shape Quality 155
4.4.2 Sensitivity Analysis 156
4.4.3 Energy Outputs Analysis 158
4.5 FE MODEL VALIDATION 161
4.5.1 Validation (Experimental) Tool 162
4.5.2 Validation Scope 166
4.5.2.1 Assessment of Static Tyre Properties 168
4.5.2.2 Assessment of Dynamic Tyre Properties 173
4.5.3 Static Validation and Analysis 180
4.5.3.1 Geometrical Inflation Analysis 180
4.5.3.2 Vertical Stiffness Analysis 182
4.5.3.3 Footprint Analysis 184
4.5.4 Dynamic Validation and Analysis 187
4.5.4.1 Non-Uniformity Analysis 187
4.5.4.2 Rolling-Resistance Analysis 189
4.5.4.3 Cornering Analysis 192
4.6 SUMMARY 193

CHAPTER (5): DEVELOPMENT AND VALIDATION OF FINITE ELEMENT MODEL FOR DUAL-CHAMBER TYRE 195

5.1 INTRODUCTION 195
5.2 FE MODEL SET-UP AND REFINEMENT 197
5.3 FE MODEL VALIDATION 200
5.3.1 Validation Scope 200

5.3.2 Static Validation and Analysis *203*
5.3.2.1 Geometrical Inflation Analysis 203
5.3.2.2 Vertical Stiffness Analysis 205
5.3.2.3 Footprint Analysis 207
5.3.3 Dynamic Validation and Analysis *210*
5.3.3.1 Non-Uniformity Analysis 210
5.3.3.2 Rolling-Resistance Analysis 212
5.3.3.3 Cornering Analysis 214
5.4 FE MODELLING AND VALIDATION OF FIVE CHAMBERS TYRE 215
5.5 SUMMARY 216
CHAPTER (6): PROTOTYPE DESIGNING, EVALUATION AND CHARACTERISATION 218
6.1 INTRODUCTION 218
6.2 TARGETED DESIGN SPECIFICATIONS (PDS) 219
6.3 DESIGN CONCEPTS GENERATION 224
6.3.1 Global Behaviour of Tyre Cavity Air *224*
6.3.2 Concepts of Multi-Chamber Solution *225*
6.3.3 FE Development of Inner Chambers *229*
6.4 CONCEPTS EVALUATION 231
6.5 BEST SUB-OPTIMUM DESIGN 241
6.6 SUMMARY 242
CHAPTER (7): OPTIMUM MULTI-CHAMBER DESIGN FOR LOW ROLLING-RESISTANCE 245
7.1 INTRODUCTION 245
7.2 EFFECT OF INNER CHAMBER DESIGN 246
7.2.1 Designing Constraints *246*
7.2.2 Finite Element Model Development *247*
7.2.3 II-1 Designs Evaluation *248*
7.3 EFFECT OF CAVITY VOLUME 254

7.4 EFFECT OF INFLATION PRESSURE 265
7.5 OPTIMUM DESIGN VERSUS STANDARD DESIGN 271
7.6 SUMMARY 275

CHAPTER (8): SUMMARY, CONCLUSION AND FUTURE RECOMMENDATIONS 277

8.1 SUMMARY AND CONCLUSION 277
8.2 FUTURE RECOMMENDATIONS 280
8.2.1 Improvements to Finite Element Tyre Model 281
8.2.2 Improvements to Experimental Work 282
8.2.3 Practicality Evaluation of Multi-Chamber Design 282

APPENDICES 287

APPENDIX (A): BASIC BACKGROUND ABOUT PNEUMATIC TYRES 287
A.1 Main Function(s) 287
A.2 General Construction 288
A.2.1 Outer Geometrical Profile 288
A.2.2 Body Structure 290
A.2.3 Material(s) 292
APPENDIX (B): FE VALIDATION FOR PROTOTYPE 0.5 TYRE 295
B.1 Prototype 0.5 Tyre (Experimental Prototype) 295
B.2 Material Properties 296
B.3 FE Model 298
B.4 FE Validation 300
APPENDIX (C): WRITTEN PERMISSION FOR PROTOTYPE 0.5 TYRE 305
APPENDIX (D): FULL-FACTORIAL DOE RUNS FOR DIFFERENT VOLUME SETTINGS OF II-1-1B DESIGN 307
APPENDIX (E): FULL-FACTORIAL DOE RUNS FOR DIFFERENT INFLATION SETTINGS OF II-1-1B-20 DESIGN 308

LIST OF REFERENCES 309

LIST OF ILLUSTRATIONS

Figure 1.1 Thesis Chapters in the Context of Research Project.....8

Figure 2.1 Basic Mass-Spring-Damper Model of a Rubber Tyre [13, 32, 34].....13

Figure 2.2 Forces and Moments Acting on Tyre using SAE J670e Coordinates [25].....15

Figure 2.3 Deformation of Tyre's Contact Patch during Cornering [36].....16

Figure 2.4 Forces and Angles of Tyre from its Top View (on left) and Front View (on right) [37].....17

Figure 2.5 Typical Phase Lag between the Stress and Strain Responses as a Function of Time [10].....19

Figure 2.6 Typical Stress-Strain Response for a Strain Cycle [43].....20

Figure 2.7 Tyre's Rolling-Resistance as "Force" and "Moment" for Steady-State Conditions [11].....22

Figure 2.8 Loaded and Unloaded Tyre Radiuses [11].....24

Figure 2.9 Main Mechanisms Responsible for Tyre Rolling-Resistance [20].....26

Figure 2.10 Rolling-Resistance at Different Normal Loads for Passenger-Car Tyre [20]36

Figure 2.11 Impact of Tyre Size and Speed on Aerodynamic Drag [20].....40

Figure 2.12 Rolling-Resistance under Different Speeds for Passenger-Car Tyres [20]..41

Figure 2.13 Rolling-Resistance under Different Pressures for Passenger-Car Tyres [20] 45

Figure 2.14 Tyre Advances for Rolling-Resistance Reduction [20] 50

Figure 2.15 Impact of using Wider Belts on Overall Tyre Performance [28].....56

Figure 2.16 “Stiffness Enhanced Tread” Tyre [114].....58

Figure 2.17 Non-Pneumatic (Air-Free) Tyre Construction [118] 59

Figure 2.18 Bridgestone’s 2nd Generation Non-Pneumatic Tyre [119] 60

Figure 2.19 Common Trade-Offs between Rolling-Resistance and Other Features [20]82

Figure 3.1 Acquisition Approach for Material Properties 89

Figure 3.2 “Standard” and “Dual Chamber” Tyres [30].....90

Figure 3.3 Material Sample(s) Extraction from Investigated Tyre(s).....92

Figure 3.4 Reading Error (%) for a Tensile Test using 500 N Load Cell.....95

Figure 3.5 Reading Error (%) for a Tensile Test using 50 N Load Cell.....95

Figure 3.6 Relative Uncertainty Analysis.....97

Figure 3.7 Instron Testing Machine with Z-Load Cell 99

Figure 3.8 Fitting of Various Strain Energy Functions against Experimental Data for (a) Tread, (b) Sidewall, (c) Apex/Chafer, and (d) Inner Chamber Tube 103

Figure 3.9 PRF Model [206] 110

Figure 3.10 Normalised Stress Relaxation Test Data for (a) Tread, (b) Sidewall, (c) Apex/Chafer, and (d) Inner Chamber Tube 113

Figure 3.11 Isight Optimisation Model [29] 114

Figure 3.12 Single-Unit Element Cubes 3D FE Model 116

Figure 3.13 Tread Stress-Time Results of Linearised PRF Model and Test Data 118

Figure 3.14 Tread Stress-Time Results of Optimised PRF Model and Test Data [29] .120

Figure 3.15 Experimental Stress-Strain Data for (a) Cap Ply, (b) Carcass (Body) Ply, (c) Inner Chamber Housing Top, and (d) Inner Chamber Housing Side 126

Figure 3.16 Experimental Stress-Strain Data for (a) Steel Belt and (b) Bead 127

Figure 3.17 Instron Machine with 2 KN Load Cell 128

Figure 3.18 Cord Diameter Measurement using Precision Micrometer 130

Figure 3.19 Image Processing Technique for Reinforcement Lay-Up Capture 131

Figure 3.20 Cords Spacing and Orientation 133

Figure 4.1 Standard (Baseline) Tyre 137

Figure 4.2 Tyre FE Model Development.....138

Figure 4.3 Image Capturing and Processing for Cross-Sectional Tyre Profile 140

Figure 4.4 2D Axisymmetric Model of Standard Tyre 142

Figure 4.5 Groove-Less Tyre Rubber Profile with Fine Mesh and Wheel-Rim Assembly 144

Figure 4.6 2D to 3D Tyre Model Development 147

Figure 4.7 FE Simulation Steps for Complete Tyre Analysis 153

Figure 4.8 Tyre/Drum Model Orientation for (a) Cornering and (b) Straight-Line Rolling 154

Figure 4.9 Mesh Convergence Analysis for 3D Standard Tyre Model.....157

Figure 4.10 Total Energy (ETOTAL) for 3D Standard Tyre Model.....159

Figure 4.11 ALLAE/ALLIE Ratio for 3D Standard Tyre Model 161

Figure 4.12 “Straight-Line Rolling” Set-Up of Tri-Axial Electro-Hydraulic Tyre/Drum Rig 163

Figure 4.13 “Cornering” Set-Up of Tri-Axial Electro-Hydraulic Tyre/Drum Rig.....164

Figure 4.14 Experimental Set-Up of Faro Edge ScanArm.....166

Figure 4.15 Mass Balancing of Standard Tyre/Wheel Assembly using Wheel Balancer 168

Figure 4.16 Experimental Capture Process of Tyre Footprint Area 173

Figure 4.17 Rolling-Resistance Computation in FE Simulation [187] 178

Figure 4.18 Tread Centre Displacement due to Inflation 181

Figure 4.19 Sidewall Outermost Displacement due to Inflation 181

Figure 4.20 Tyre Vertical Stiffness at (a) 180 KPa, (b) 200 KPa, (c) 220 KPa, (d) 240 KPa and (e) 260 KPa 184

Figure 4.21 Footprint Area under Different Vertical Loads [30] 185

Figure 4.22 Footprint Area under Different Inflation Pressures 185

Figure 4.23 Footprint Profile at 220 KPa Inflation and 4000 N Vertical Load [30].....186

Figure 4.24 History of Radial and Lateral Forces of Standard Tyre at (a) 2000 N and (b) 4000 N Vertical Loads 188

Figure 4.25 Rolling-Resistance under Different Vertical Loads for Standard Tyre [187] 190

Figure 4.26 Rolling-Resistance under Different Inflations for Standard Tyre [187].....190

Figure 4.27 Contribution to Energy Dissipation (ALLCD (%)) by Region for Standard Tyre 192

Figure 4.28 Cornering Performance for Standard Tyre 193

Figure 5.1 Experimental Prototype of Dual-Chamber Tyre.....196

Figure 5.2 Outer Profile Capture of Inner Chamber Housing of Dual-Chamber Tyre ...198

Figure 5.3 2D Axisymmetric Model of Dual-Chamber Tyre 199

Figure 5.4 3D Model of Dual-Chamber Tyre.....200

Figure 5.5 Mass Balancing of Dual-Chamber Tyre/Wheel Assembly.....201

Figure 5.6 Experimental Set-Up for Inflation Validation of Dual-Chamber Tyre 202

Figure 5.7 Experimental Set-Up of Dual-Chamber Tyre for (a) Vertical Stiffness, Footprint and Rolling-Resistance and (b) for Cornering and Non-Uniformity Validations 203

Figure 5.8 Vertical Stiffness of Dual-Chamber Tyre at (a) 280-180 KPa, (b) 280-200 KPa, (c) 260-220 KPa, (d) 280-220 KPa, (e) 300-220 KPa and (f) 280-240 KPa.....207

Figure 5.9 Footprint Area under Different Vertical Loading [30] 208

Figure 5.10 Footprint Area under Different Inflation Pressures of (a) Outer Chamber and (b) Inner Chamber.....209

Figure 5.11 Footprint Profile for Dual-Chamber Tyre and Standard Tyre [30] 210

Figure 5.12 Rolling-Resistance at Different Vertical Loads for Dual-Chamber Tyre [30] 212

Figure 5.13 Rolling-Resistance under Different Inflations of (a) Outer Chamber and (b) Inner Chamber for Dual-Chamber Tyre 213

Figure 5.14 Cornering Performance for Dual-Chamber and Standard Tyres [30] 215

Figure 6.1 Potential Designs I, II and III of Multi-Chamber Tyre Solution [30] 226

Figure 6.2 Lay-up Orientation of Inner Wall Reinforcements for Design II 231

Figure 6.3 Performance of Designs I, II and III at Normal Inflation for (a) Rolling-Resistance Coefficient, (b) Static Vertical Stiffness (N/mm), (c) Footprint Area at Straight Rolling (mm^2), (d) Radial Non-Uniformity (N), (e) Lateral Non-Uniformity (N) 233

Figure 6.4 Performance of Designs I, II and III at Economy Inflation (a) Rolling-Resistance Coefficient, (b) Static Vertical Stiffness (N/mm), (c) Footprint Area at Straight Rolling (mm^2), (d) Radial Non-Uniformity (N), (e) Lateral Non-Uniformity (N) 234

Figure 6.5 Vertical Deflection and Footprint Width of Designs I, II and III 235

Figure 6.6 Tyre Deformation under Vertical Loading [30] 238

Figure 6.7 Cornering Performance of Designs I, II and III at Normal Inflation for (a) Cornering Stiffness (N/deg) and (b) Footprint Area (mm^2) at 3° Slip 241

Figure 7.1 II-1 Designs of Multi-Chamber Tyre Solution [292].....248

Figure 7.2 Straight-Line Free-Rolling Performance of II-1 Designs at Normal Inflation for (a) Footprint Area (mm^2), (b) Static Vertical Stiffness (N/mm) and (c) Rolling-Resistance Coefficient [292] 249

Figure 7.3 Cornering Performance of II-1 Designs at Normal Inflation for (a) Cornering Stiffness (N/deg) and (b) Footprint Area (mm^2) at 3° Slip [292].....252

Figure 7.4 (a) 2D Axisymmetric and (b) 3D Cross-Sectional Models of II-1-1B Multi-Chamber Design [292] 253

Figure 7.5 Effect of (a) Width and (b) Height of LW on Footprint Area at Straight Free-Rolling [292] 256

Figure 7.6 Influence of LW's Height on (a) Vertical Stiffness (N/mm), (b) Rolling-Resistance Coefficient and (c) Radial Non-Uniformity (N) and LW's Width on (d) Rolling-Resistance Coefficient during Straight Free-Rolling [292] 259

Figure 7.7 Performance of II-1-1B Designs at Normal Inflation for (a) Footprint Area (mm^2) at Straight Rolling, (b) Cornering Stiffness (N/deg), (c) Footprint Area (mm^2) at 3° Slip, (d) Rolling-Resistance Coefficient and (e) Static Vertical Stiffness (N/mm) [292].262

Figure 7.8 Effect of Zone 2's Inflation on (a) Vertical Stiffness (N/mm), (b) Contact-Patch Area (mm^2) and (c) Rolling-Resistance Coefficient at Straight Free-Rolling [292].....267

Figure 7.9 Performance of II-1-1B-20 Design at Different Inflations for (a) Footprint Area (mm^2) at Straight Rolling, (b) Cornering Stiffness (N/deg), (c) Footprint Area (mm^2) at 3° Slip, (d) Rolling-Resistance Coefficient and (e) Static Vertical Stiffness (N/mm) [292].268

Figure 7.10 Straight Free-Rolling Performance of II-1-1B-20 and Standard Designs at Normal and Economy Inflations for (a) Footprint Area (mm^2), (b) Rolling-Resistance Coefficient, (c) Vertical Stiffness (N/mm) and (d) Contact Pressure Pattern (MPa) [292] 270

Figure 7.11 Straight Free-Rolling Performance of II-1-1B-20 Design under Different Vertical Loadings for (a) Rolling-Resistance (N) as Energy Lost per Unit Distance, (b) Footprint Area (mm^2) and (c) Vertical Stiffness (N/mm) 272

Figure 7.12 Cornering Performance of II-1-1B-20 Design at Different Slip Angles for (a) Lateral Force (N) and (b) Footprint Area (mm^2).....274

Figure 8.1 Proposed On-Drum Building Approach of II-1-1B-20 Design [292] 284

Figure 8.2 Suggested Curing Method of II-1-1B-20 Design [292].....285

Figure A.0.1 Outer Layout of Today's Vehicle Tyre and its Key Features [298] 288

Figure A.0.2 Basic Geometrical Dimensions of Common Vehicle's Tyre [303] 290

Figure A.0.3 Detailed Radial Tyre Construction [304] 291

Figure A.0.4 General Ingredients of Final Tyre's Material(s) 293

Figure A.0.5 Experimental Prototype 0.5 Tyre.....295

Figure A.0.6 Uniaxial Tensile Test using Instron Machine.....296

Figure A.0.7 2D Axisymmetric Model of Prototype 0.5 299

Figure A.0.8 3D Model of Prototype 0.5 299

Figure A.0.9 Experimental Set-Up for Inflation Validation of Prototype 0.5 300

Figure A.0.10 Experimental Set-Up for Static and Dynamic Contact Validation of Prototype 0.5.....301

Figure A.0.11 Inflation Validation of Prototype 0.5 at (a) Tread Centre and (b) Sidewall Outermost Point 302

Figure A.0.12 Vertical Stiffness Validation of Prototype 0.5 303

Figure A.0.13 Footprint Validation of Prototype 0.5.....303

Figure A.0.14 Rolling-Resistance Validation of Prototype 0.5 304

Figure A.0.15 Cornering Validation of Prototype 0.5 304

LIST OF TABLES

Table 2.1 Influence of Vertical Load on Tyre's Rolling-Resistance [8].....37

Table 2.2 Role of Rolling Velocity on Tyre's Rolling-Resistance [8] 42

Table 2.3 Effect of Inflation Pressure on Tyre's Rolling-Resistance [8] 46

Table 2.4 Advances in Body Construction [8].....51

Table 2.5 Advances in Dimensional Settings [8] 65

Table 2.6 Advances in Tyre Materials [8] 76

Table 3.1 Yeoh Coefficients for Rubber Components 104

Table 3.2 Yeoh "D_1" Coefficients for Tyre Rubbers 105

Table 3.3 Prony Coefficients for Tyre Rubbers.....109

Table 3.4 Linearised PRF Model Parameters for Tread 117

Table 3.5 Optimised Yeoh and PRF Model Coefficients for all Rubbers 121

Table 3.6 Yeoh "D1" Coefficients for all Rubbers (Re-Calculated) 122

Table 3.7 Finalised Elastic Young's Moduli for all Reinforcements 128

Table 3.8 Lay-Up Settings for all Tyre Reinforcements 134

Table 3.9 Reinforcements' Density.....134

Table 4.1 Testing Settings for Inflation Validation of Standard Tyre.....169

Table 4.2 Testing Settings for Stiffness Validation of Standard Tyre.....170

Table 4.3 Testing Settings for Footprint Validation of Standard Tyre 172

Table 4.4 Rolling Conditions for Non-Uniformity and Rolling-Resistance Validations of Standard Tyre.....174

Table 4.5 Rolling Settings for Cornering Validation of Standard Tyre 180

Table 4.6 Radial and Lateral Non-Uniformities of Standard Tyre 187

Table 5.1 Testing Conditions for Inflation Validation of Dual-Chamber Tyre 204

Table 5.2 Displacement of Tread Centre and Sidewall Outermost due to Inflation [30]205

Table 5.3 Testing Conditions for Footprint Validation of Dual-Chamber Tyre 208

Table 5.4 Non-Uniformity in Dual-Chamber Tyre during Rolling.....211

Table 5.5 Cornering Settings for Dual-Chamber Tyre and Standard Tyre.....214

Table 6.1 Contact Pressure Pattern of Designs I, II and III [30].....237

Table 7.1 Full-Factorial DoE for Further Development of Design II 247

Table 7.2 Contact Pressure Distribution of II-1 Designs Contact-Patch [292] 250

Table 7.3 Full-Factorial DoE for Cavity Volume Settings of II-1-1B Design [292].....255

Table 7.4 Contact Pressure Distribution for Several II-1-1B Designs [292] 258

Table 7.5 Contact Pressure Distribution for II-1-1B-15, II-1-1B-20 and II-1-1B-25 Designs 264

Table 7.6 Full-Factorial DoE for Inflation Settings of II-1-1B-20 Design [292] 266

Table 7.7 Contact Pressure Distribution of II-1-1B-20 Design under Different Vertical Loadings 273

Table A.0.1 Material Model Coefficients for Hyperelasticity and Viscoelasticity of Rubber Components 297

Table A.0.2 Density for Rubber Components 297

Table A.0.3 Elastic Properties for Reinforcement Components 298

Table A.0.4 Lay-Up of Reinforcement Components in Tyre Structure 298

Table A.0.5 Economy Inflation Mode of Prototype 0.5 302

Table A.0.6 Evaluation Results of 25 Different Volume Versions of II-1-1B Design 307

Table A.0.7 Evaluation Results of Nine Different Inflation Versions of II-1-1B-20 Design 308

LIST OF ABBREVIATIONS

IEA	International Energy Agency
CO2	Carbon Dioxide
FE	Finite Element
FEM	Finite Element Modelling
PDS	Product Design Specification
F	Vertical Force applied on Tyre
m_u	Unsprung Mass
a	Acceleration
c_u	Damping Coefficient
v_u	Damping Velocity
k_u	Spring Stiffness
x_u	Spring Displacement
F_X	Longitudinal Force
Ω	Angular Velocity
T	Wheel Torque
M_X	Overturning Moment
F_y	Lateral Force

α	Cornering Angle (i.e. Slip Angle)
γ	Camber Angle (i.e. Inclination Angle)
M_y	Rolling-Resistance Moment
F_Z (or) Z	Normal Force (Load)
R_l (or) R_L	Loaded Tyre Radius
M_Z	Aligning Moment
δ	Phase Lag Angle
NVH	Noise, Vibration and Harshness
t_r	Longitudinal Shift
$-F_Z$	Reaction to the Normal Load
$F_R = F_{RR}$	Rolling-Resistance Force
R_e	Loaded Tyre Radius
R	Unloaded Tyre Radius
θ	Angle
RRE	Energy Lost per Unit Distance
P_{in}	Input Mechanical Power to Tyre
P_{out}	Output Mechanical Power of Tyre
$P_{in} - P_{out}$	Net Mechanical Power Input to Tyre

V	Tyre Linear Velocity
U	Internal Energy of Tyre
t	Time
$\dot{Q}$	Rate of Heat Transfer to Tyre
V_S	Instantaneous Velocity
FEA	Finite Element Analysis
PRF	Parallel Rheological Framework
RR	Rolling-Resistance
$C_R = C_{RR}$	Rolling-Resistance Coefficient
MTIS	Meritor Tire Inflation System
TPCS	Tire Pressure Control System
AMT	Air Maintenance Technology
SIT	Self Inflating Tire
Exp.	Experimental
UHP	Ultra-High Performance
R_w	Wheel Radius
H	Tyre Section Height
NR	Natural Rubber

IIR	Butyl Rubber
BR	Polybutadiene
SBR	Styrene-Butadiene
IR	Polyisoprene
ERF	Electro-Rheological Fluid
PVDF	Polyvinylidene Fluoride
PCL	Polycaprolactone
TPMS	Tyre Pressure Measurement System
EU	European Union
A_R	Rebar Area
r_R	Rebar Radius
σ	Nominal Stress
F_T	Measured Tensile Force
A_0	Original Cross-Sectional Area
ε	Nominal Stain
δ	Total Elongation (Displacement)
L_0	Original Gage Length
E_R	Relative Error

T_i^{th}	Stress Value based on Hyperelastic Strain Energy Function Model
T_i^{test}	Stress Value from Test Data
U_Y	Strain Energy Stored per Unit of Reference Volume
C_{i0} and D_i	Temperature-Dependent Material Coefficients
$\bar{I_1}$	First Deviatoric Strain Invariant
J^{el}	Elastic Volume Ratio
K_0	Initial Bulk Modulus
μ_0	Initial Shear Modulus
D_1	Material Coefficient related to Compressibility
v_p	Poisson Ratio
E	Young Modulus
$g(t) = g_i$	Normalised Shear Relaxation Modulus at Time (t = i)
$G(t)$	Shear Relaxation Modulus at Time (t)
$G(0)$	Instantaneous Shear Relaxation Modulus at Time (0)
$g(\infty)$	Normalised Long-term Shear Relaxation Modulus
E_m	Relaxation Model's Young Modulus
E_{Exp}	Experimental Young Modulus
E_∞	Long-term Young's Modulus at time (∞)

E_i	Young's Modulus at time (*i*)
τ_i	Relaxation Time at Loading Time (*i*)
N	Number of Prony Series Terms
$\mathrm{G}(\infty)$	Long-term Shear Relaxation Modulus
$\overline{g_i}$	Prony Series Coefficient
D^{cr}	Symmetric Part of Velocity Gradient
$\bar{\mathrm{q}} = \mathrm{G}^{\mathrm{cr}}$	Equivalent Deviatoric Cauchy Stress
$\overline{\sigma}$	Deviatoric Cauchy Stress
$\tilde{\mathrm{q}}$	Equivalent Deviatoric Kirchhoff Stress
$\bar{\mathrm{T}}$	Deviatoric Kirchhoff Stress
A (or) A_i, n and m	Material Constants
$\bar{\varepsilon}^{\mathrm{cr}}$	Equivalent Creep Strain
$\dot{\bar{\varepsilon}}^{cr}$	Equivalent Creep Strain Rate
SR (or) SR_i	Stiffness Ratio of (i)th Viscoelastic Network
R.P. (or) RP	Reference Point
PVC	Polyvinyl-Chloride
PPI	Pixels Per Inch
CPU	Central Processing Unit

2D	Two Dimensional
3D	Three Dimensional
CAD	Computer Aided Design
ETOTAL	Model’s Total Energy
ALLAE	Artificial Strain Energy
ALLKE	Kinetic Energy
ALLIE	Total Strain Energy
ALLVD	Viscous Energy Dissipation
ALLFD	Frictional Energy Dissipation
ALLWK	External Work
ALLPW	Work Done by Contact Penalties
LVDT	Linear Variable Displacement Transducer
LVD	Linear Variable Displacement
PC	Personal Computer
CAREA	Total Area in Contact
HR	Hysteresis Damping Ratio
ALLCD	Energy Dissipated by Viscoelasticity
Cp	Mean Contact Pressure

CPRESS	Contact Pressure
Ac	Footprint Area
D_E	Deflection Energy
F_C	Mean of Normal Contact Force
D_V	Vertical Deflection
E_{LC}	Energy Lost at Contact-Patch
L_C	Contact-Patch Length
R_D	Radius of Road Wheel Drum
DoE	Design of Experiment
LW	Lateral Inner Wall
LWH	Lateral Inner Wall Height
LWW	Lateral Inner Wall Width
CFD	Computational Fluid Dynamics

LIST OF PUBLICATIONS

1) Aldhufairi HS, Olatunbosun OA. Developments in tyre design for lower rolling resistance: a state of the art review. Proceedings of the Institution of Mechanical Engineers, Part D: Journal of Automobile Engineering. 2018;232(14):1865–82. doi: https://doi.org/10.1177/0954407017727195

2) Aldhufairi HS, Essa K. Tire Rolling-Resistance Computation based on Material Viscoelasticity Representation. Advances in Automotive Engineering. 2019;1(2):167-83. Available from: http://www.techno-press.org/?page=container&journal=aae&volume=1&num=2# . doi: https://doi.org/10.12989/aae.2019.1.2.167

3) Aldhufairi HS, Olatunbosun OA, Essa K. Determination of a Tyre's Rolling Resistance using Parallel Rheological Framework. SAE Technical Paper. 2019. doi: https://doi.org/10.4271/2019-01-5069

4) Aldhufairi HS, Essa K, Olatunbosun OA. Multi-chamber Tire Concept for Low Rolling-Resistance. SAE International Journal of Passenger Cars - Mechanical Systems. 2019;12(2):111-26. doi: https://doi.org/10.4271/06-12-02-0009

5) Aldhufairi HS, Olatunbosun OA, Essa K. Multi-Chamber Tyre Designing for Fuel Economy. Proceedings of the Institution of Mechanical Engineers, Part D: Journal of Automobile Engineering. 2019. doi: https://doi.org/10.1177/0954407019857026

CHAPTER (1): GENERAL INTRODUCTION

1.1 BACKGROUND AND MOTIVATION

Although they have been around for a long time, for over a century, the pneumatic rubber tyres in vehicles are still being used worldwide in the transportation of over 60% of the population and goods [1]. There is a growing demand for pneumatic rubber tyres that have reached over one billion annually in the global market and that figure is expected to keep rising in the upcoming years [2, 3]. Such growing demand is accompanied with increasing needs for further developments and improvements of pneumatic tyres to meet the diverse functional driving requirements more conveniently and the changing economic, environmental and health necessities and concerns [4, 5].

Furthermore, those demands and needs for pneumatic tyres are to be understood and expected due to the benefit and the crucial role the tyres play in vehicles as they are the only dominant alternative that can efficiently and effectively handle the vehicle ride under a wide diverse range of driving conditions [6]. In fact, there are no other practical alternatives to pneumatic rubber tyres; it is unrivalled and unmatched in its applications and strength and resilience properties in the automotive sector [6]. Moreover, tyres are the only medium and connection between the vehicle and the road; between which the tyres transmit vertical, longitudinal and lateral forces that would govern and control the vehicle's dynamical handling and driving performance [7].

One of those needs for further improvement is the crucial need to minimise the tyre's rolling-resistance which is continually drawing a great deal of focus and consideration [8]. This is since the rolling-resistance can have a serious negative impact on the vehicle driving performance, the energy source(s) sustainability, and the environmental wellbeing [9]. In order for the vehicle to move, the vehicle's engine needs to exert certain mechanical energy on the drive wheels to overcome all the opposing forces to the vehicle's movement such as inertial forces, gravity forces, wind resistance and tyre's rolling-resistance [10]. The rolling-resistance of the tyre is the main contributor among those opposing forces that try to oppose the vehicle's movement and causes energy loss which in turn leads to more fuel consumption and hence more vehicle's CO2 emissions [8].

Although vehicle engines, nowadays, are more efficient with the help of advanced technology, it is not of good use if the rolling-resistance is not lowered. This is because higher rolling-resistance means further lowering vehicle performance in terms of limiting its speed, causing more power loss and reducing its fuel economy (i.e. higher fuel consumption), which in return leads to more undesired vehicle emissions and hence air pollution and global warming (Greenhouse phenomenon) [10, 11].

The tyre's rolling-resistance can be held accountable for around 20% to 30% of the total fuel consumption of vehicle depending on the drive cycle and the vehicle's category used [8]. Many experimental measurements have been performed that show that fuel consumption corresponds almost linearly with the variations in rolling-resistance in

general [10]. A ~10% reduction in rolling-resistance would result in ~1% improvement in fuel economy depending on the vehicle's type [12-14]. Even though it might seem a small improvement, it holds a remarkable effect on lowering CO2 emissions and improving the environment considering the massive amount of vehicles in use around the globe [15]. In 2008, the International Energy Agency (IEA) described the use of lower rolling-resistance tyres as the best approach to decrease CO2 emissions in the transportation field [13, 16].

Such effect of the rolling-resistance has made vehicle manufacturers, governments and research institutions place huge interest and put forward tremendous efforts toward reducing rolling-resistance in tyres and improving fuel economy in vehicles [17-19]. According to Europe technical centre of Nexen tire, the rolling-resistance of the tyre is beginning to drive and hold the focus of tyres' developments worldwide in which it is anticipated that, in the future, the research on tyre's rolling-resistance will continue to grow to be intense and very demanding [18]. The legislation across the globe is placing very strict and challenging requirements for enhancing the vehicle's fuel efficiency. Europe's 2021 emissions regulations demand a limit of 95g/km of CO2 emissions from vehicle manufacturers which, in terms of fuel consumption, is 4.1 L/100Km for petrol and 3.6 L/100Km for diesel. To meet those limits, car makers are targeting the rolling-resistance coefficient of 7.0 kg/tonne dropping to 6.5 by 2020 [18].

1.2 AIMS AND OBJECTIVES

1.2.1 Overall Aim

The core aim of this research project is to develop an advanced tyre structural design, which is capable of controlling the tyre's profile and its stiffness, for lowering tyre's rolling-resistance without compromising other essential features, like the tyre's grip and cornering performance, in accordance with the driving/road conditions.

1.2.2 Objectives

In order to accomplish the aim of this research project, the following key objectives are specified and targeted:

A. Experimentally evaluate the standard design of the chosen tyre for rolling-resistance and other driving requirements.
B. Introduce basic practical changes to the standard tyre design to have a different structural design prototype to evaluate for the same performance outputs experimentally.
C. Develop and validate working finite element (FE) models of the standard and the structurally altered tyres to compute the rolling-resistance correctly.
D. Generate novel design concepts of the tyre structure which have the potential to reduce the rolling-resistance.
E. Develop and evaluate the proposed novel structural designs using the validated FE models to select the best sub-optimum design for low rolling-resistance and meeting the other driving requirements.

F. Perform parametric analyses using the validated FE models to investigate the influence of various main structural aspects on the rolling-resistance and the other requirements and identify the best structural settings for all the driving requirements.

1.3 SCOPE AND LIMITATIONS

Based on the aim and objectives of this research project, the scope of the research will involve investigating mainly the effect of introducing different novel structural designs to a standard tyre on the rolling-resistance and the other driving requirements like the tyre's grip, cushioning and cornering performance. To independently examine the structural effects of the tyre, the principal rolling-resistance as a result of only the internal losses (i.e. hysteresis damping) in the tyre structure is assessed, which can represent up to 95% of the tyre's total rolling-resistance at steady-state rolling on a straight flat path [8]. In that regard, the selected tyres are evaluated at straight and steady-state free-rolling settings on a smooth road-surface drum to eliminate the effects of acceleration, deceleration, and road roughness on the tyre's rolling-resistance. In addition, the tyres are to roll at constant low velocity (i.e. 30 Km/h) to remove the impact of aerodynamic drag on the tyre's rolling-resistance [20, 21].

There are several limitations which have restricted the research scope of this project. First of all, this research project is self-funded with limited resources at hand and a tight time frame to accomplish. Given the tyre is a highly complex product, the task of manufacturing new and actual structural prototypes of the targeted tyres to test

empirically is found to be very expensive, highly time-consuming, and extremely difficult to achieve especially if it is to involve a “trial-and-error” approach which usually yields no or little gains in return in practice [8]. With that in mind, the evaluation of the “design manufacturability” is another research aspect that was not possible to include within the scope of this research project due to the lack of the required resources. Likewise, the inflation mechanism of the different tyre chambers is excluded. Once this research project is published, the author looks forward to attracting potential sponsor(s) to evaluate the “design manufacturability” as future work.

Nevertheless, some measures were taken to minimise those limitations and address them to a degree. Finite element modelling (FEM) is used as a credible, cost-effective, and time-saving alternative to the expensive experimental solution of developing and testing new structural designs of the tyre [22]. Furthermore, for selecting the best novel design, apart from considering all the driving requirements, careful consideration is given for the “design manufacturability” by ensuring the simplicity and conciseness of the selected structural design of the tyre. Also, some considerations on the “design manufacturability” and the “inflation mechanism” are given as novel concepts for future work in chapter (8) of this thesis.

Another limitation to this project’s scope is the incapability of the laboratory tyre/drum test rig to provide a testing rolling speed above 50 Km/h or acceleration/deceleration rolling conditions. Due to that, the effect of the travelling speed over the rolling-resistance was not possible to verify and investigate since such an effect is only

perceptible at around 80-100 Km/h and above whereas below 80 Km/h there is no apparent effect except for aerodynamic drag influence [20, 23]. Similarly, the effect of the tyre's net weight on the rolling-resistance was not included because the tyre's rotational inertia has almost no influence over the rolling-resistance during straight free-rolling whereas its impact is more observable during "acceleration-and-braking" conditions, which are not supported by the tyre/drum test rig. This goes in line with Walter [24].

Regardless, again, care is taken to ensure having a proposed structural design of the tyre that is simple and concise in a way that would avoid gaining unnecessary extra weight and have a marginal increase in the net weight. In addition, if any further weight is gained, it would be easily compensated by equivalent weight reduction either in the wheel, the vehicle or both.

1.4 THESIS LAYOUT AND CONTENTS

The work carried out in this research project in order to achieve the aim and the objectives in section 1.2 is covered and documented by this thesis over eight chapters in total as illustrated in Figure 1.1 and laid out as follows:

This chapter (i.e. chapter (1)) serves as a general introduction to the research work carried out and presented in this thesis. It highlights the context and the rationality behind the research work conducted, the research aim and objectives achieved, the scope of the research, and the different aspects of research covered in this thesis.

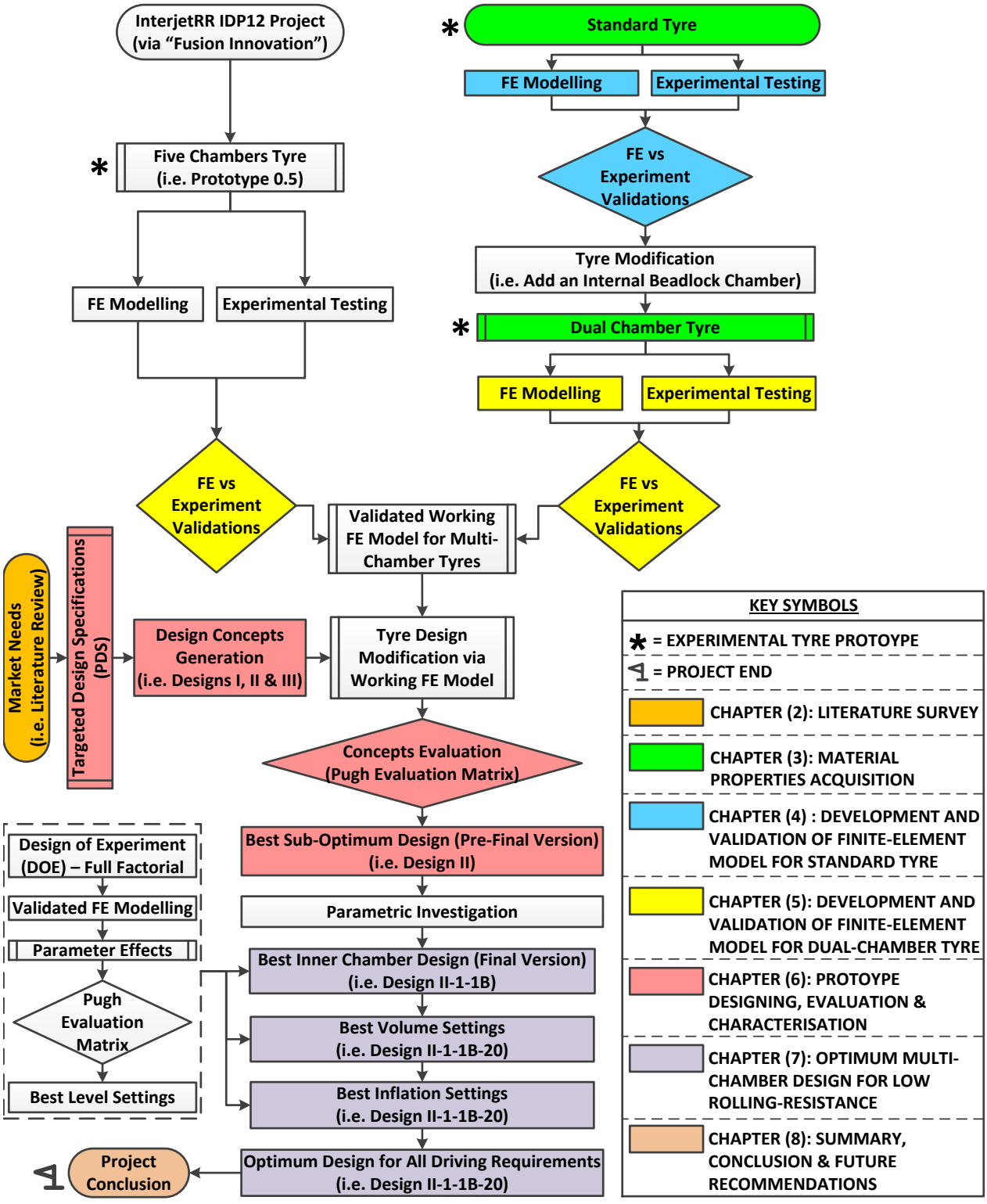


Figure 1.1 Thesis Chapters in the Context of Research Project

For chapter (2), a brief introduction about the concepts of pneumatic tyres and its rolling-resistance relevant to the research project is given. This is followed by critical analysis and criticism of the current literature work on the subject of both the rolling-resistance determination and the tyre developments for low rolling-resistance. Based on this, the best practices to follow, the ineffective practices to avoid, the norms and regulations to meet, the targeted specifications to achieve, and the potential research gaps to exploit for the new tyre design to be achieved in this research project are identified.

In chapter (3), the process used to capture the material physical properties of the different components of the real tyre(s) and incorporate it into the FE solution to simulate tyre rolling is explained and described. This involves both the “standard” and “dual chamber” tyres adopted especially for this research project excluding “prototype 0.5” tyre for confidentiality reasons since its design, manufacture and ownership belongs to an external third party under different development project.

With regard to chapter (4), it illustrates the development process of the full 3rd FE tyre model in Abaqus software for the “standard” tyre from capturing the actual geometrical profile of the tyre, converting the profile into a full FE model with proper mesh refinement and validating the model against relevant experiments for static and dynamic tyre properties. “Prototype 0.5” tyre is not included in this chapter too for the same confidentiality reasons.

Chapter (5) shows further validation of the proposed FE capability in chapter (4) to simulate the multi-chamber tyre solution. This involved validating two multi-chamber solutions, one with dual chambers and the other with five chambers (i.e. prototype 0.5), against the corresponding experiments for static and dynamic tyre properties.

As for chapter (6), the chapter covers the initial designing for several potential prototypes of the targeted multi-chamber tyre design (i.e. designs I, II and III) and their evaluation using the validated FE model(s) for low rolling-resistance and satisfactory levels of the other driving requirements like tyre's grip, cushioning and cornering performance.

In chapter (7), a parametric investigation of the most promising design (i.e. design II) from the initial designs covered in chapter (6) is shown and discussed in order to reach the optimum design settings that would address all the driving requirements satisfactorily. The investigation includes studying the effects of inner-chamber design (i.e. designs II-1 and II-2), cavity volume and inflation pressure for the best settings.

Chapter (8) is the closing chapter of this thesis where a summary of the main research findings is given highlighting the research novelty and contributions to the current research field. In addition, the potential areas in this research work that can be expanded and subjected to further research in the future are identified and suggested.

CHAPTER (2): LITERATURE SURVEY

2.1 INTRODUCTION

For over a century, the “pneumatic rubber tyre” has been existent since its first practical invention by John Boyd Dunlop in 1888 [4]. Across the past nearly 100 years, the “pneumatic tyre” went through many improvements such as incorporating carbon black by Pirelli into tyre’s compound in 1907, inventing the first radial tyre design(s) by Arthur Savage in 1915, further developing and commercializing the radial tyres by Michelin in 1946, and introducing Tubeless tyres by Goodrich in 1952 [25-28].

To this day, the cycle of tyre improvements is still on-going with growing increase in the development needs due to the vital role played by the tyre, as the sole choice with no equivalent contender yet, in enabling and maintaining the complicated vehicle operation [6]. This is since it is the only physical link between the vehicle and the road which transmits the necessary driving forces between them in attempt to meet the wide diverse ride and handling requirements over different road conditions [4].

In line with this research project’s aim and objectives, this chapter mainly aims to explore, investigate and analyse in-depth the existing research on “tyre structural design” and its developments with respect to lowering “tyre rolling-resistance”. This involves looking at the implications, merits and limitations of the current development studies along with indicating any relevant gaps or opportunities to exploit further for

future research. Prior to that, this chapter gives coverage to some relevant fundamental and principal information on tyres and its rolling-resistance to serve as background material for the subsequent chapters and to understand this research. Henceforth, the “rubber” term is used to indicate the vulcanised and filled polymer compounds of the tyre.

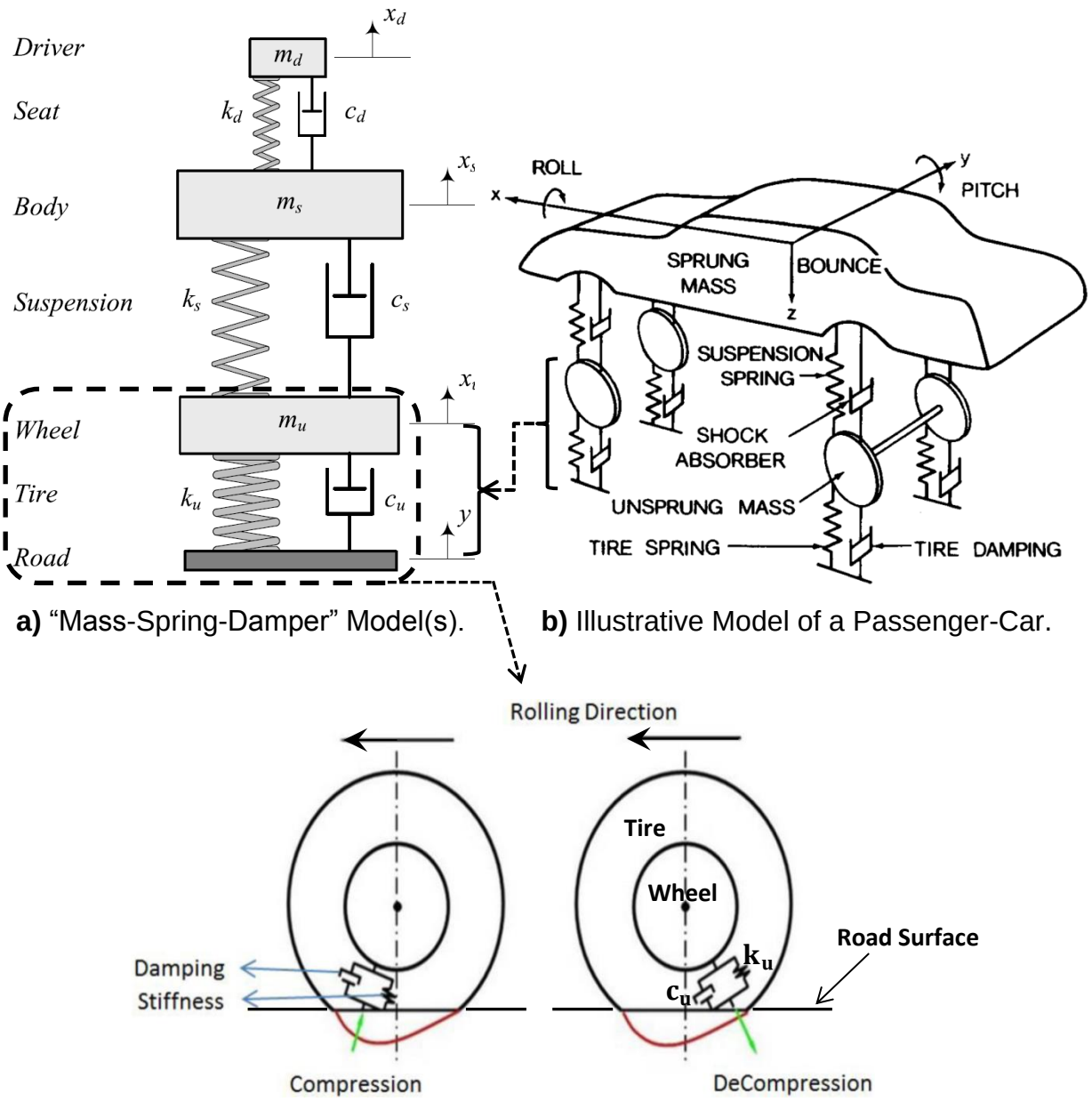
Several sections of the review work done by the author in this chapter, as the main owner and contributor, especially sections 2.3, 2.4 and 2.5, were published as a part of a publication plan for this research project work. Those publications can be referred to through [8, 29, 30].

2.2 WORKING PRINCIPLE OF PNEUMATIC TYRES

As an introduction to the topic of pneumatic tyres, basic background on pneumatic tyres in terms of their functions and general construction can be found in appendix (A). Furthermore, the common terminologies and definitions used for the pneumatic tyres in today’s tyre industry can be found by referring to ISO 4223-1:2017 standard [31]. In this section, a generic overview of how tyres work and behave under the most common driving conditions are highlighted as follows.

2.2.1 Basic Representation

A very basic and simple representation of the tyre alone (i.e. excluding the vehicle body and its suspension) is the following single degree-of-freedom system shown in Figure 2.1 below [32, 33]:



a) "Mass-Spring-Damper" Model(s). **b)** Illustrative Model of a Passenger-Car.

c) A Tire undergoing Compression and Decompression in its Contact Patch as it rolls on Road.

Figure 2.1 Basic Mass-Spring-Damper Model of a Rubber Tyre [13, 32, 34]

Although the tyre representation in Figure 2.1 does not reflect the actual nature and behaviour of the tyre in vehicles, it still does give a general understanding of how the tyre behaves. Here, the spring along with the damper is supposed to reflect the visco-elastic properties of the tyre and how it acts when it is subjected to load/deformation. In other words, the tyre acts as a cushion (i.e. damper) to absorb the deformations due to loads or road irregularities and then returns back (i.e. functioning like a spring) to its original shape once the source of deformation ceases. Basically, the equation of motion for such a model would be as follows:

$$F(t) = m_u \cdot a + c_u \cdot v_u + k_u \cdot x_u \qquad (2.1)$$

2.2.2 Forces and Torques/Moments

According to Erdogan [35], the tyre's forces are produced as a result of two elements and they are the friction at the contact patch and the elastic deformation of the tyre. Using SAE J670e coordinate system, the forces and its moments/torques to act on a tyre in general are represented as follows in Figure 2.2:

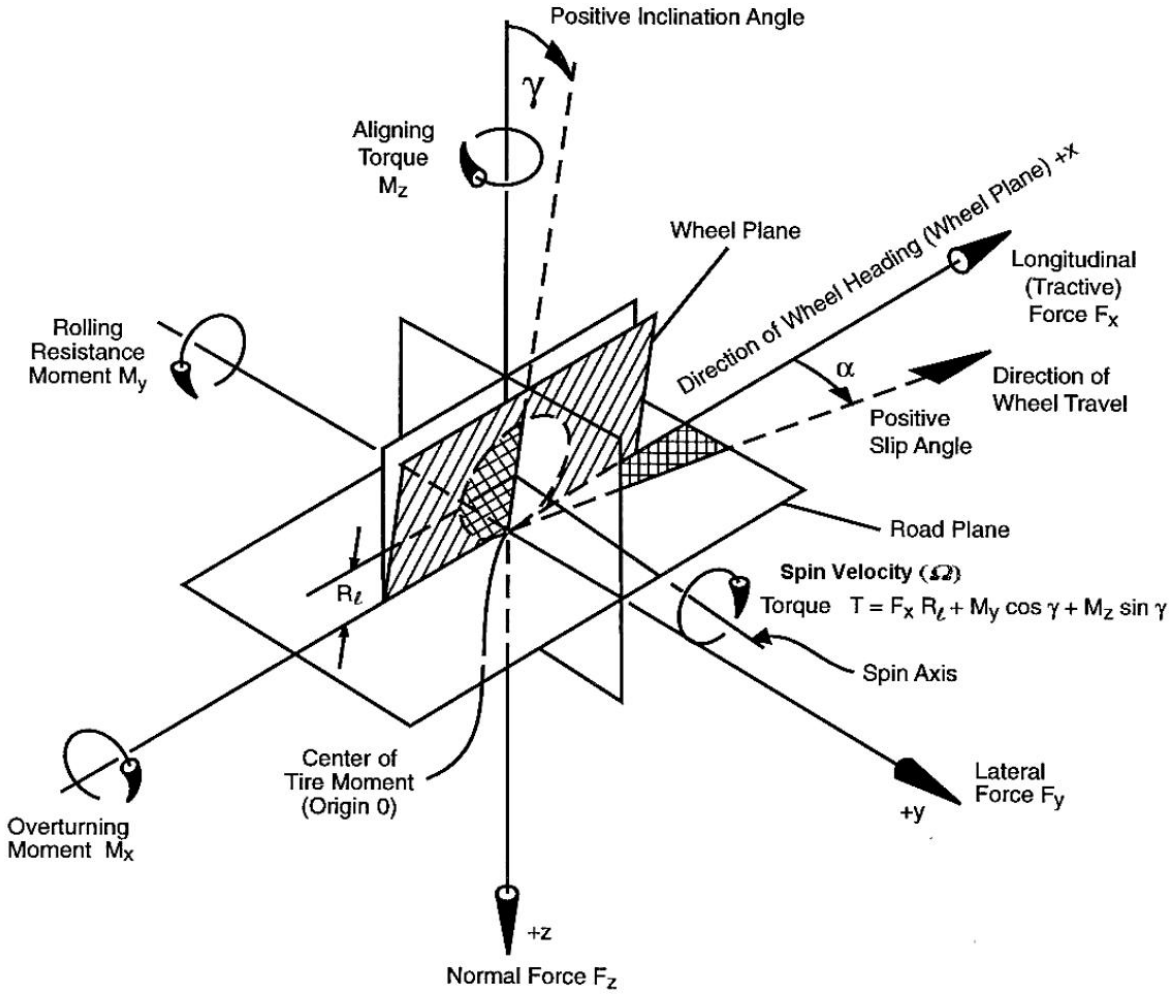


Figure 2.2 Forces and Moments Acting on Tyre using SAE J670e Coordinates [25]

In Figure 2.2, along the x-axis, ideally, a longitudinal force (F_X) acts from the road on the tyre during the tyre's acceleration or deceleration. The longitudinal force is generated based on the "angular velocity" (Ω) of the tyre about the spin axis of the wheel; which in turn is determined by the "wheel torque" (T) that is produced from the drive axle of the vehicle's engine and acts about the spin axis of the wheel on the tyre. This longitudinal force of the tyre is responsible for the vehicle's rolling performance, in terms of traction and braking, and overcoming the opposing force (F_R) to tyre's forward movement which

is to be discussed in section 2.3.1.1 [5]. About the x-axis, a moment/torque called the "overturning moment" (M_X) acts on the tyre as a result of the lateral transferal of the vertical load (i.e. normal force) between the tyre and the road, with reference to the contact centre, due to cornering or road irregularities.

Along the y-axis, ideally, a lateral force (F_y) acts from the road on the tyre during cornering and/or if the tyre was cambered to a side. However, in reality, the lateral force acts away or off from the ideal y-axis and the contact centre due to the deformation of tyre's contact patch during cornering. The distance between the "contact centre" and "where the lateral force is actually applied" is called "pneumatic trail"; which acts as a moment arm for the lateral force as seen in Figure 2.3 below.

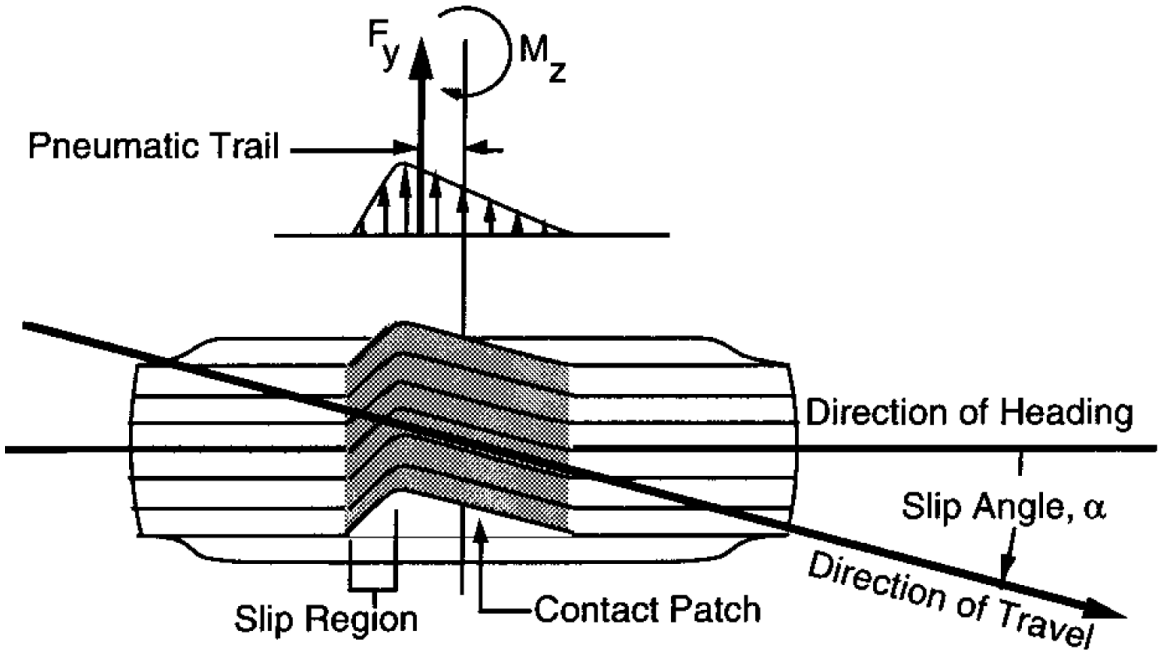


Figure 2.3 Deformation of Tyre's Contact Patch during Cornering [36]

Basically, the lateral force of the tyre is generated as a result of the forces formed due to two non-zero angles during cornering/turning; namely the “slip angle” ($\boldsymbol{\alpha}$) and the “camber angle (i.e. inclination angle)” (γ) as shown in both Figure 2.2 and Figure 2.4.

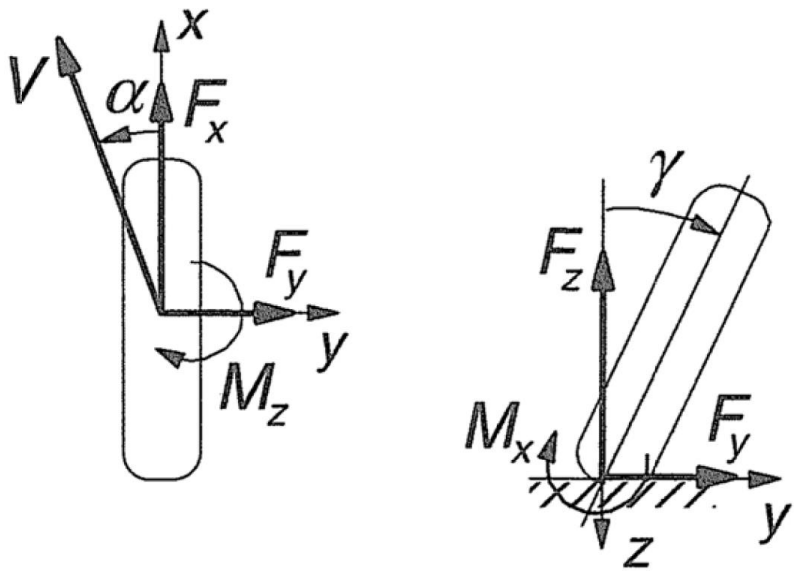


Figure 2.4 Forces and Angles of Tyre from its Top View (on left) and Front View (on right) [37]

The tyre’s lateral force, caused by those two angles, is accountable for the vehicle’s stability and the cornering performance [5]. About the y-axis, a moment/torque called the “rolling-resistance moment” (M_y) acts on the tyre as a result of the fore-aft shift of the normal pressure (i.e. normal force) between the tyre and the road at the contact-patch in the direction of tyre rolling (i.e. forward or backwards) with reference to the contact centre [32]. Principally, this is because of the hysteresis effect induced by the tyre

deformation at the contact-patch during rolling [38]. Such a phenomenon is to be discussed further in the next section.

Along the z-axis, ideally, a normal force (F_Z) acts from the road on the tyre once the tyre gets into contact with the road surface. Such force is largely responsible for the deformation of tyre's structure, the production of frictional forces, and the determination of "tyre loaded radius" (R_l) as shown in Figure 2.2 [39]. About the z-axis, a moment/torque called the "aligning moment" (M_Z) acts on the tyre as a result of a combination of two shear forces on the road surface, namely the longitudinal force (F_X) and the lateral force (F_y) [39]. In the case of a non-zero slip angle ($\boldsymbol{\alpha}$), such a moment can act as a restoring moment for the tyre from the travel direction to the heading direction [25].

2.2.3 Deformational Behaviour

Mainly, as indicated previously, the conventional pneumatic tyre is made up of a filled and cross-linked synthetic rubber (i.e. long-chain polymers) due to its special characteristics, which provide the tyre with the necessary strength (i.e. with the aid of reinforcement plies), resilience, adhesion and cushioning to perform the wide diverse and sophisticated requirements of vehicle driving on the road [40]. However, once it has undergone a deformation, the tyre rubber displays both an elastic-solid and a viscous-fluid like mechanical responses (i.e. viscoelastic behaviour) after it is restored back to its original shape [41, 42]. The "elastic" part is related to returning the tyre to its original

shape (i.e. restoring the tyre's remaining mechanical energy) while the "viscous" part represents the delay in the tyre restoration (i.e. mechanical energy dissipation as heat).

This delay, often called "hysteresis effect", can be seen in the phase lag between the applied stress and the resulting strain responses during repetitive cycles of loading/unloading as indicated in Figure 2.5. This occurs as a result of the rubbing of the intertwined long-chain molecules against each other in the internal rubber structure (i.e. internal damping) leading to heat generation and dissipation during the repetitive tyre deformation and restoration process [42].

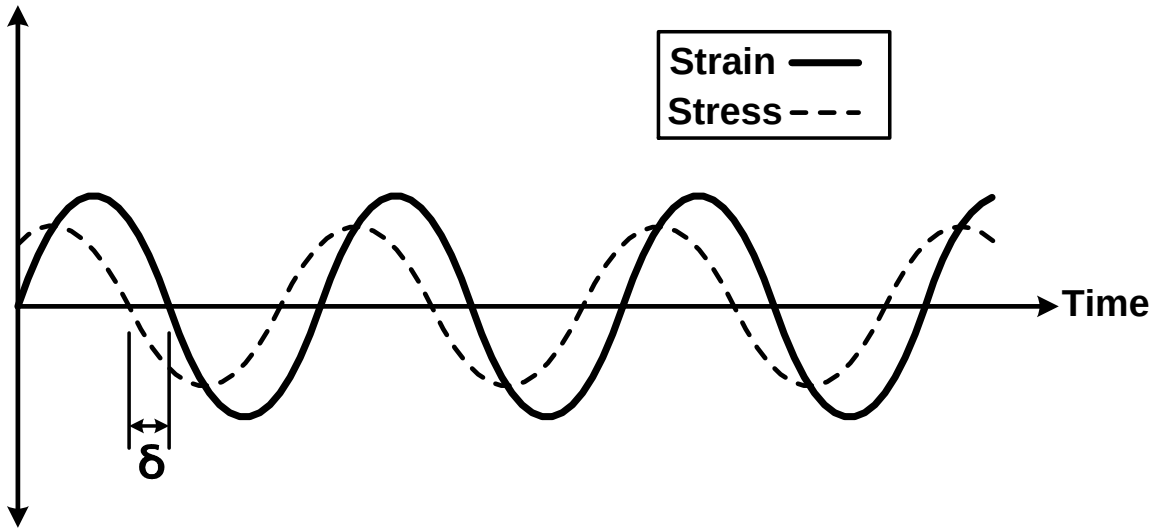


Figure 2.5 Typical Phase Lag between the Stress and Strain Responses as a Function of Time [10]

In Figure 2.6, a closer look at the stress-strain response for a full strain cycle (i.e. one complete loading/unloading cycle) reveals the occurrence of energy loss (in the form of

heat) per each strain cycle as the unloading path follows a different route to that of the loading one. Such a difference forms an “ellipse”, often called the “Hysteresis Loop”, in which its area represents the energy loss (i.e. the shaded area in the stress-strain curve).

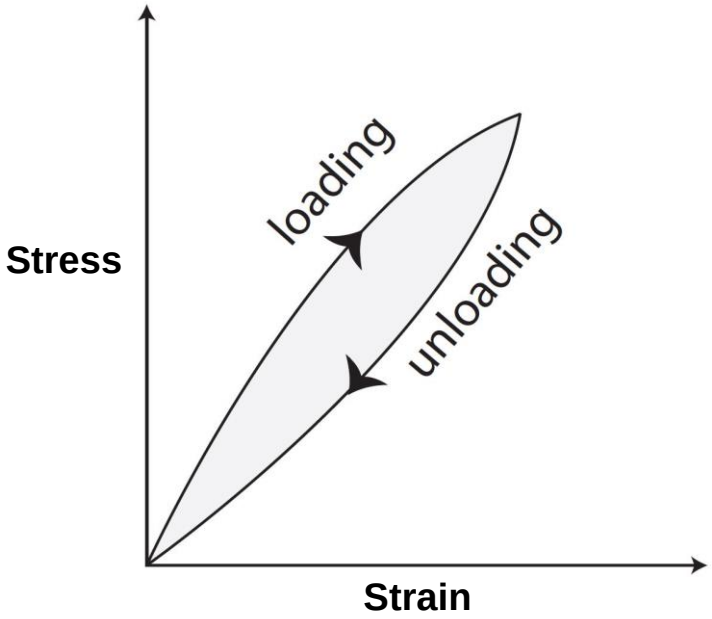


Figure 2.6 Typical Stress-Strain Response for a Strain Cycle [43]

In addition to viscoelasticity’s effect in terms of tyre’s hysteresis, the rubber’s viscoelasticity is also greatly responsible for the “surface adhesion” between the tyre and the road [44]. The “surface adhesion” can be considered primarily accountable for the “tyre’s friction”, namely “grip” [11, 36].

2.3 ROLLING-RESISTANCE

“Rolling-resistance” is a term that is frequently heard and used in vehicle ride with respect to the operational interaction between the tyre and the road surface; as a

performance indicator and an assessment criteria especially for fuel economy, braking distance, tread-wear and other operational aspects related to noise, vibration and harshness (NVH) [4, 45].

2.3.1 Description and Concept

Over most of the literature, it can be observed that rolling-resistance is being interpreted and viewed through one of two distinct perspectives [9-11, 46-48]. Traditionally, the rolling-resistance has been investigated and viewed as a “force” that opposes the tyre travel path and hence resists its rolling. This concept is limited only to the cases of free-rolling tyres on flat road surfaces under steady-state conditions, whereas for other scenarios of driving conditions, it tends to be inconsistent and inadequate. A later and more comprehensive concept of rolling-resistance is the one where rolling-resistance is investigated and treated as an “energy loss” caused due to tyre rolling. Those two concepts of rolling-resistance are further discussed below:

2.3.1.1 Rolling-Resistance as a “Force”

In this perspective, the rolling-resistance is tackled and interpreted in terms of “force” and “moment” balance at the contact patch. According to the “force” concept of rolling-resistance, when a pre-loaded tyre freely rolls on a flat and hard road surface under steady-state conditions; the resistance to the tyre’s rolling is generated as follows in Figure 2.7 below [11, 49]:

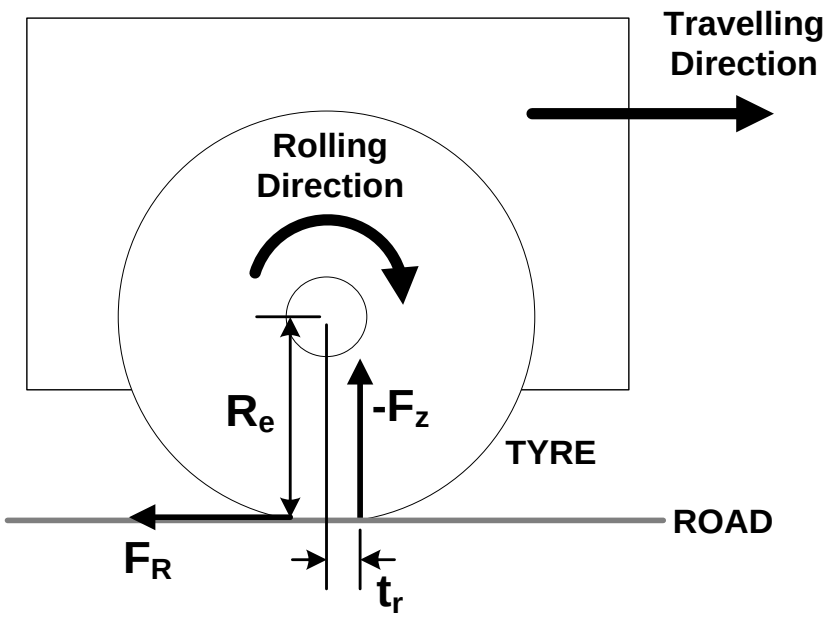


Figure 2.7 Tyre's Rolling-Resistance as "Force" and "Moment" for Steady-State Conditions [11]

During tyre rolling, the front half of tyre's contact patch experiences compression accompanied with some losses in the form of heat as a result of the tyre deformation, under a vertical load and against the road surface as it rolls, and the viscoelastic nature of its material (i.e. hysteretic damping effect). As the tyre continues to roll, at the rear half of the contact patch, the tyre starts to return back to its normal shape but only after a certain period of time has passed (i.e. "relaxation time") as not all of the stored elastic energy at tyre's interface region with the road is recovered back to the tyre. Again, this is due to the hysteresis damping.

Such behaviour leads to a longitudinal shift (t_r) in the application point of the "reaction to the normal load" ($-F_Z$) at the contact patch from being exactly underneath the wheel spin

axis toward being in the first half of the contact patch as illustrated in Figure 2.7. This shift produces a moment about the wheel spin axis that opposes and resists the tyre rolling (i.e. rolling-resistance moment (M_y)). Furthermore, there is the generation of a longitudinal shear force (i.e. rolling-resistance force (F_R)) at the contact patch that opposes and resists the forward movement of the tyre. The rolling-resistance force (F_R) creates a moment about the wheel spin axis that counteracts the rolling-resistance moment (M_y).

To maintain the steady-state rolling condition, a force is required to be implemented from vehicle's engine to the wheel centre that is equivalent to the rolling-resistance force (F_R) in magnitude but in-line with the tyre rolling direction. This way both the rolling-resistance moment (M_y) and the rolling-resistance force (F_R) will be balanced out and cancelled. For steady-state conditions, basically, the rolling-resistance (F_R) can be calculated from the longitudinal shift (t_r) as indicated below:

$$F_R = \frac{\text{Rolling Resistance Moment}}{\text{Loaded Tyre Radius}} = \frac{(\mathbf{F_Z}) \times (\mathbf{t_r})}{\mathrm{R_e}} = \frac{(\mathbf{F_Z}) \times (\mathbf{t_r})}{\mathrm{R}\,.\,\cos\theta} \qquad (2.2)$$

Where

θ = Angle between "R" and "R_e" as shown in Figure 2.8.

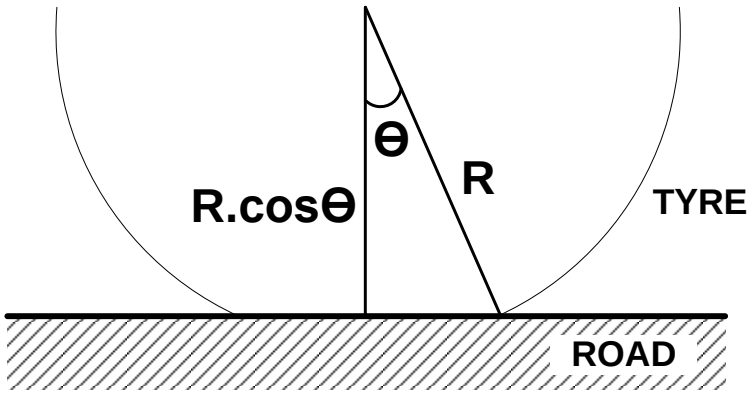


Figure 2.8 Loaded and Unloaded Tyre Radiuses [11]

2.3.1.2 Rolling-Resistance as an "Energy Consumed"

At this perspective, the rolling-resistance is viewed as the "loss incurred in mechanical energy" of a rolling tyre deflected under a vertical load. In this concept, it is emphasized that the rolling-resistance to be taken as a scalar quantity, which is the "energy per unit distance", and not to be regarded as a "force" (i.e. a vector quantity) despite both quantities having the same measuring units (i.e. Joule/Metre = Newton) [48].

With this alternative concept, the rolling-resistance is seen as a representation of all the mechanical energy losses of the tyre in the form of heat as a result of the tyre rolling for a unit distance [9, 10]. According to thermodynamics principles, the energy losses of the rolling tyre occur due to multiple work and heat transfer mechanisms. For straight-line and steady-state free-rolling on a flat road surface, those mechanisms are mainly as follows and seen in Figure 2.9 [10, 11, 50-53]:

a) Most of the energy transformation or loss happens internally within the tyre's structure in the form of heat dissipation as an outcome of the "viscoelastic behaviour of tyre material(s) (i.e. mechanical hysteresis)" when the tyre rolls and experiences deformation due to a vertical load and/or road irregularities (i.e. 80 to 95% of total rolling-resistance). Further details on tyre deformation and hysteresis effect were covered in section 2.2.3.

b) "Aerodynamic drag" as a result of tyre rolling against surrounding air causing the air to act as a barrier that is rubbing against the tyre and slowing down from its rolling movement leading to thermal energy generation or heat exchange. This mechanism starts to be perceptible after 30 km/h and becomes significant when the tyre is rolling at high velocities (i.e. 0 to 15% of total rolling-resistance) [20, 21].

c) "Friction/slip" between the tyre and road surface and between the tyre and wheel-rim during tyre rolling. Mainly, during rolling, a part of the contact patch of the tyre tends to stick momentarily to the road surface while the rest of the contact patch area starts to rub against the road surface causing slipping or friction to occur at the interface and hence heat generation. This mechanism is the least contributing to rolling-resistance (i.e. ~5% of total rolling-resistance).

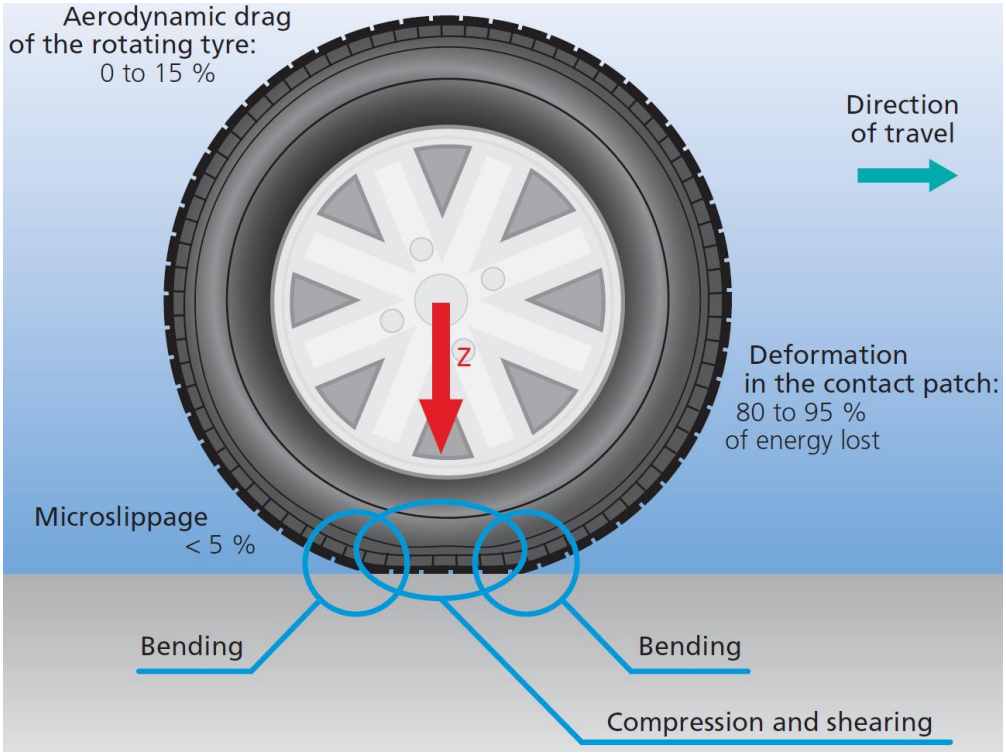


Figure 2.9 Main Mechanisms Responsible for Tyre Rolling-Resistance [20]

In general, the intensity and extent of rolling-resistance rely on the sort of tyre, the type of road surface, and the vehicle operating conditions (e.g. tyre's load, inflation pressure and speed) in use [10]. Unlike the "force" concept, here, rolling-resistance can be calculated for both "steady-state" and "transient" driving conditions as indicated below according to both Pillai [9] and LaClair [10]:

For any "Steady-State" conditions, according to "conservation of energy" principle, the rolling-resistance can be determined based on the "net mechanical power input" of the tyre (i.e. the rate at which energy is transformed into heat due to tyre rolling) as follows:

$$RRE = \frac{P_{in} - P_{out}}{V} \quad (2.3)$$

For “Transient” conditions, the rolling-resistance can be determined through the modification of the earlier Eq. (2.3) in which the rolling-resistance is calculated based on the “changes of the tyre’s thermal energy” as indicated below:

$$\mathrm{RRE} = \frac{\left(\frac{dU}{dt} - \dot{Q}\right)}{V_S} \quad (2.4)$$

2.3.2 Rolling-Resistance Calculation

In this section, a careful review is conducted over the mainstream approaches used to measure the tyre’s rolling-resistance in the current research field to select the best methods possible to evaluate the tyre’s rolling-resistance properly in this research project in accordance with the research aim and objectives in section 1.2. From the literature, three main approaches are found and they are as follows:

2.3.2.1 Analytical Approach

Generally, the analytical approach uses mathematical modelling to describe certain physical mechanisms in the tyre application. This involves representing the tyre structure through a basic physical set-up, like a ring, plate or string, which can be expressed mathematically based on empirical tyre parameters/constants to approximate the mechanical response of interest [5, 54, 55].

Commonly, in the analytical models, the tread is treated as a pre-stressed interface with a given bending stiffness whereas the sidewall is of either elastic or viscoelastic foundation upholding the tread region [5, 55]. As highlighted previously, the tyre is a highly non-linear and complex product whether it was for its geometry, material response or contact boundary conditions [56]. This has made it extremely difficult to develop analytical models capable of predicting tyre's rolling-resistance accurately over the tyre structure [22].

Nevertheless, several efforts were made to estimate the overall tyre rolling-resistance. Stutts and Soedel [57] introduced a model where the tread is represented as a fixed extension band supported by a sidewall of elastic foundation in which the rolling-resistance is determined based on the deflection at the contact-patch. Kim and Savkoor [58] predicted the hysteretic loss using an elastic ring model with viscoelastic foundation. Various analytical models, including a flexible ring model, for rolling-resistance calculation were performed by Miège and Popov [59]. Li *et al.* [60] proposed an elastic brush model to compute the energy lost based on the integral of the loading/unloading curve functions at the contact patch.

In general, the available analytical models are found to be simple, inexpensive and time-saving and sometimes give useful perceptions about the physical mechanisms and the total rolling-resistance. Nevertheless, those models have oversimplified geometrical and material definitions compared to the actual tyre. This has made those models incapable

of capturing the rolling-resistance accurately given the tyre's complexity and the diverse rolling conditions especially the dynamic, non-linear and more sophisticated contact problems. In addition, the analytical approach is found unable to predict the energy dissipation in detail across the tyre structure. Those findings go in line with that of Yang [5], Hoever [54] and Andersen *et al.* [22].

2.3.2.2 Experimental Approach

Many researchers have pointed out that, with drum testing, it is possible to precisely predict the direct rolling-resistance of tyre (i.e. due to tyre's internal losses) at the desired testing conditions and protocols without the interference of other factors like changes in temperature, road roughness and dryness unlike the other methods [12, 22, 61-63]. In that regard, Smith [61] commented that the drum method allows for consistent and repeatable measurements to be achieved enabling evaluating, rating and comparing tyres and their characteristics. Contrarily, this forms a big challenge and an obstacle that needs to be addressed for the other measuring methods, specifically, the "trailer" and the "on-vehicle" (i.e. coast-down and fuel consumption) according to Sandberg [50], Andersen *et al.* [22] and Ejsmont *et al.* [63].

However, both Smith [61] and Ejsmont *et al.* [63] highlight that the drum method is very limited when it comes to replicate the actual-world scenarios accurately and to measure everything related to the rolling-resistance contribution in the vehicle. Such limitation can be largely overcome by using, for example, the on-vehicle testing which is a broad way to measuring all things influencing the rolling-resistance in the vehicle. In line with this

research project goal(s), the “laboratory drum testing” is chosen as the best method to measure experimentally the rolling-resistance due to the tyre deformational behaviour (hysteresis damping) at the contact patch, at free-rolling condition, compared to other measuring methods like the “trailer” and “on-vehicle” tests.

2.3.2.3 Finite Element Approach

Many studies on the tyre rolling-resistance prediction were conducted utilising finite element approach as a cost-effective, time-saving and adequate substitute to the time-consuming and expensive experimental method [22, 54, 64-66]. In the existing literature, various methods were used to estimate the tyre’s rolling-resistance in terms of either “drag force” or “energy dissipation” [54, 67]. The second term is broadly used to describe the tyre rolling-resistance since it is more comprehensive and valid regardless of the given rolling condition [65, 67, 68].

Generally, to evaluate the tyre rolling-resistance as an energy loss, the finite element (FE) model would need to have both a deformational module and a dissipative module of the tyre [22, 66]. For the deformation component, the FE approach is found to be capable of providing detailed geometrical tyre models subjected to exact boundary/loading conditions with well-developed and precise hyperelastic/elastic material models (e.g. Yeoh, Neo-Hooke and Arruda-Boyce models) [54, 66, 68]. For the dissipation component, generally, one of two methods is implemented to calculate the tyre energy dissipation and it is either by a “viscoelastic theorem inside a post-FEA processing code” or “viscoelastic material functions within the FEA solution”.

In the “viscoelastic theorem” option, commonly, a commercial FE platform is utilised together with an external in-house developed code. The FE platform would have a 3D elastic FE tyre model subjected to either a static contact (non-rolling) analysis or a steady-state rolling analysis. Separately, the loss properties of the tyre materials are obtained experimentally. The external code is used as a post-FEA processing tool to analyse either the elastic strain energy outputs or the time records of the stress-strain cycles of the FE tyre model with the material loss properties captured experimentally to compute the tyre rolling-resistance as per the given viscoelastic theory.

Luchini *et al.* [69] proposed a strain-based viscoelastic theory (i.e. “Directional Incremental Hysteresis”) that is applied with a quasi-static FE tyre model to compute the rolling-resistance. A reasonable match was observed between the computed and the experimental results. Ebbott *et al.* [70] introduced a semi-coupled approach in a thermomechanical analysis. The tyre energy loss was calculated through a linear dissipation module based on the strain history obtained from an elastic static-contact FE model and the experimental loss parameters. However, some deviations were found between the computed and the experimental rolling-resistance results.

Ghosh [65] conducted a similar investigation to Ebbott *et al.* [70] but with a non-linear viscoelastic in-house code to determine the energy dissipation. Nearly 10% error was found between the estimated and the experimental results. Cho *et al.* [71] calculated the tyre rolling-resistance using an in-house Fortran code and a static-contact FE model.

Similarly, an error of ~13% was noticed between the computed and the experimental results. Other investigations including Shida *et al.* [72], Wei *et al.* [68], Ma *et al.* [73], Hoever [54], and Golbakhshi and Namjoo [74], have used similar approaches and very similar results were reported.

Evidently, the majority of the available "viscoelastic theorem" studies normally use in-house developed codes which are not accessible to the public. A further drawback is the involvement of linear viscoelasticity based assumptions within the theory solution to describe the highly non-linear viscoelasticity of the tyre rubbers. Nandi *et al.* [40] highlighted the same conclusion. Moreover, the viscoelastic theory comprises of a detailed and long dynamic analysis of the tyre that would usually include simplifications and assumptions to arrive at an approximated solution of restricted precision. The theorem method is best suited to use with static-contact FE models rather than dynamic rolling especially when the complexity of the contact problem increases.

For the method of the "viscoelastic functions of the FEA solution", it would involve the usage of a "viscoelastic material model" within a commercial FEA solution to estimate the tyre rolling-resistance. The viscoelastic model is defined by inserting its material coefficients into the FEA solution matrix. These coefficients are computed based on time-domain or frequency-domain experimental data, in some cases, under various strain or frequency cycles.

Ghosh *et al.* [75] attempted to compute the tyre rolling-resistance by using an equation of Pillai and Fielding-Russell [76] and extracting its parameters from a steady-state rolling FE simulation with a linear viscoelastic model (i.e. Prony series). A single rolling condition was validated only with ~12% error between the computed and the experimental results. Kim *et al.* [77] proposed a method for fitting the prony series model of a dynamic rolling-tyre FE simulation against the experimental material loss-tangents for different loading frequencies. The tyre rolling-resistance was calculated based on the dissipation energy output. A good agreement was achieved between the computed and the experimental outcomes.

Hernandez *et al.* [64] used an equation of Schuring [78] to calculate the tyre rolling-resistance based on the longitudinal reaction force obtained from a free-rolling FE simulation with a prony series model fitted under different temperatures and frequencies. No experimental validations were provided to support the FE results. Rafei *et al.* [79] have used a non-linear viscoelastic model called “Bergstrom-Boyce” model based on the “parallel rheological framework” (PRF) to predict the tyre’s rolling-resistance at a steady-state rolling using Abaqus/Standard. A poor validation was provided with differences between the FE and the experimental results which may refer due to the insufficient fitting of the adopted material model and the inadequacy of the Abaqus/standard procedure to the non-linear PRF-based model, especially for a dynamic rolling case. Both Nandi *et al.* [40] and Nyaaba *et al.* [80] made the same remarks.

Observably, most of the available “viscoelastic models in the FE solution” treat the tyre viscoelasticity as linear instead of being non-linear as in reality. The validity of the FE solution relies greatly on the accuracy and scope of the experimental fitting procedure used to compute the viscoelastic model’s parameters and its suitability to the rolling condition(s) investigated. A further matter is the trade-off involved between the output accuracy, the set-up complexity, and the computational resources needed for the FE tyre model.

Overall, the tyre rolling-resistance can be estimated with a reasonable degree of accuracy using the current FE approaches. Nevertheless, the tyre FE solution for the rolling-resistance is yet an incomplete task and more improvements are still required. The reason behind that is the complexity of the mechanism bonding the hysteresis phenomenon with the rolling-resistance which becomes more sophisticated with the involvement of the various tyre design and operational parameters [8]. The main challenge lies in obtaining a realistic material model for the rolling-resistance FE solution that is capable of capturing the non-linear viscoelasticity of the tyre rubbers.

For this research project, the “power-law strain hardening model” (i.e. a non-linear viscoelastic model) of the “parallel rheological framework” is used to calculate the tyre’s rolling-resistance through a proposed new method as shown in chapters (3) and (4) of this thesis.

2.4 ROLE OF OPERATIONAL CONDITIONS

The operational parameters of the tyre play an important role in influencing the tyre's physical properties especially the rolling-resistance in which their consideration is necessary to take into account whenever a new tyre design is sought along with their maintenance during operation. In this section, only three core operational parameters are considered with respect to their relationship to rolling-resistance because they are controllable parameters with a significant effect on the rolling-resistance and they are as follows:

2.4.1 Normal Load

In general, the normal load (vertical force) is exerted on the tyre as a result of the vehicle's weight coming into contact with the road surface through the tyre as a medium. Across the literature, it is evident that increasing normal load has a remarkable impact on increasing rolling-resistance too in a nearly linear manner. This is because an increase in normal load would mean further bending and shearing of tyre construction at the contact-patch and hence higher deformation and hysteresis damping [10, 15, 20]. Being a major player in influencing rolling-resistance, the coefficient of rolling-resistance (C_R) is basically expressed with respect to normal load (F_Z) as follows:

$$C_R = \frac{F_R}{F_Z} \tag{2.5}$$

Michelin [20] conducted an experimental measurement of rolling-resistance under different loads, for passenger-car tyre according to ISO 8767 standard, in which it has been found that the rolling-resistance force ($F_R = F_{RR}$) increased proportionally with the increase of load (F_Z) while the rolling-resistance coefficient ($C_R = C_{RR}$) has actually moderately decreased with the load as indicated in Figure 2.10. LaClair [10] refers the reason behind the decrease of the rolling-resistance coefficient to the increase of tyre's temperature because of load increasing which leads to reducing the coefficient of rubber hysteresis losses and in return decreasing the rolling-resistance coefficient.

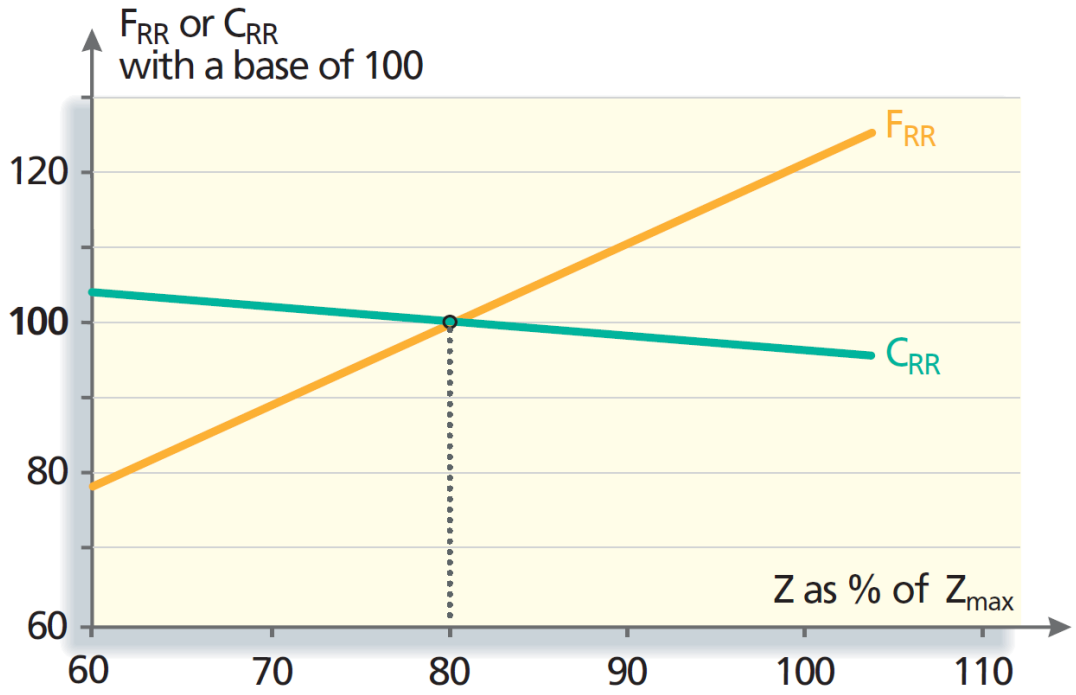


Figure 2.10 Rolling-Resistance at Different Normal Loads for Passenger-Car Tyre [20]

Many other investigative studies reflect the same pattern of the almost linear proportional relationship between the rolling-resistance and the vertical load. Examples of such studies are indicated in Table 2.1 below:

Table 2.1 Influence of Vertical Load on Tyre's Rolling-Resistance [8]

Study No.	Source	Investigation					Tyre's Dimensions								Remarks
		Method	Operating Conditions				Aspect Ratio	Section Width	Section Height	Outer Diameter	Inner Diameter	Tread Depth	Wheel Diameter	Effect on Rolling Resistance	
			Speed	Vertical Load	Inflation Pressure	Others									
1	[81]	Mathematical & Experimental	?	↑	–	Radial Passenger-Car Tyre	–	–	–	–	–	–	–	↑	
2	[70]	Numerical (Coupled Thermo-mechanical FE model)	?	↑	–	Passenger & Radial Medium Truck Tyres	–	–	–	–	–	–	–	↑	Numerical & Experimental
3	[72]		?	↑	–	Passenger Radial Tyre	–	–	–	–	–	–	–	↑	Numerical & Experimental
4	[68]		–	↑	–	Radial Tyres	–	–	–	–	–	–	–	↑	
5	[20]	Experimental	–	↑	–	Passenger Car Tyres	?	?	?	?	?	?	?	↑	According to ISO 8767 standard
6	[9]	Analytical & Experimental	–	↑	–	Passenger Radial Tyre & Radial Truck	–	–	–	–	–	–	–	↑	According to SAE J1269

						Tyres									
7	[82]	Experimental	–	↑	–	Radial (FR78-14) Tyre	–	–	–	–	–	–	–	↑	
8	[83]	Experimental & Thermal Modelling	–	↑	–	Radial Tyre	–	–	–	–	–	–	–	↑	
9	[84]	Numerical (FE Modelling) with Experimental Validation	–	↑	–	Radial Passenger-Car Tyre	–	–	–	–	–	–	–	↑	

Key Indicators:

– : Fixed, Constant or No Change	↑ : Increase	↘ : Slight Decrease
→ : Marginal Change (i.e. Negligible)	↓ : Decrease	**?** : Not Stated / Unknown
↕ : Variable or Fluctuating (No Particular Pattern)	↗ : Slight Increase	**N/A** : Not Applicable

Improvements that can be made to lower the effect of normal load on rolling-resistance are limited and constrained by the vehicle's size and the nature of usage. Yet, many developments were made to minimise vehicle's weight especially in passenger-cars such as replacing vehicle engine's parts, wheel (rim) and vehicle body panels with lightweight materials like aluminium alloys, plastics and fibres.

2.4.2 Rolling Velocity

Across the literature, increasing rolling speed exerts nearly no change on rolling-resistance until the speed reaches ~100km/h where rolling-resistance starts to slightly increase then dramatically increase as the speed arrives at and exceeds ~120km/h. Such influence of higher speeds is due to several phenomena that take place. As speed increases so do the centrifugal (inertial) forces in the tyre which with higher speeds lead to the creation of standing waves (i.e. vibrational energy) in the tyre's circumference and hence increasing rolling-resistance through hysteresis effect [10, 15]. Increasing the speed would also raise the frequency at which tyre deformation occurs increasing in return the loss-tangent (dissipation factor) of tyre material(s) [10]. Moreover, at higher speeds, there is the growth of aerodynamic drag as seen in Figure 2.11 that acts against tyre movement and hence causes rolling-resistance to rise significantly [20].

However, sometimes, rolling-resistance might decrease with speed increase due to the rise in tyre's temperature to the point where the loss-tangent (dissipation factor) gets affected and decreased and hence the rolling-resistance too as indicated previously with the case of the normal load in section 2.4.1 [10, 15].

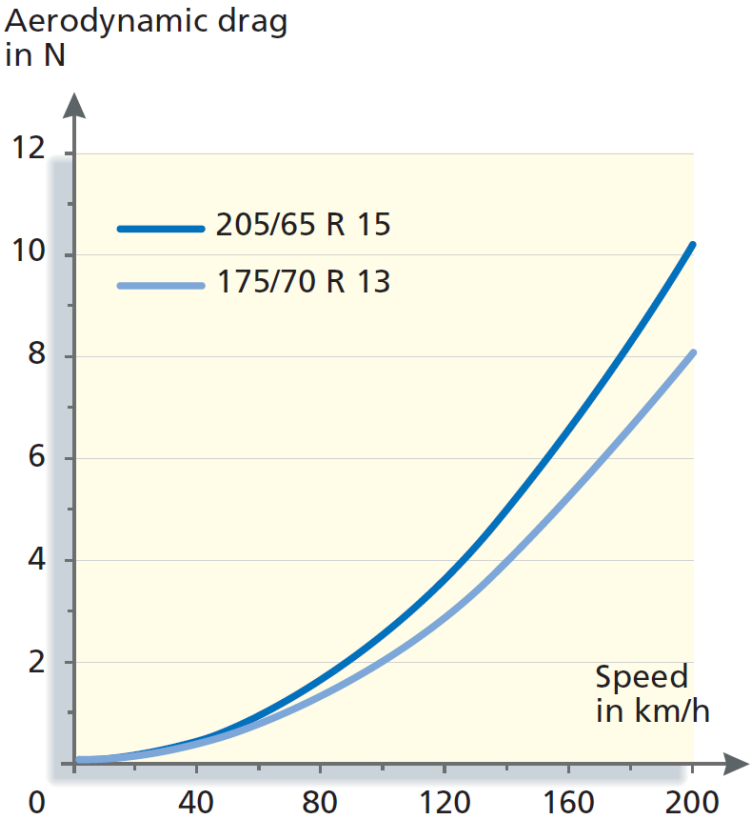


Figure 2.11 Impact of Tyre Size and Speed on Aerodynamic Drag [20]

Michelin [20] performed an experimental measurement of rolling-resistance under different speeds, for passenger-car tyres according to ISO 8767 standard, in which it has been found that the rolling-resistance (F_{RR}) increased significantly as the speed reached and exceeded ~120km/h as shown in Figure 2.12.

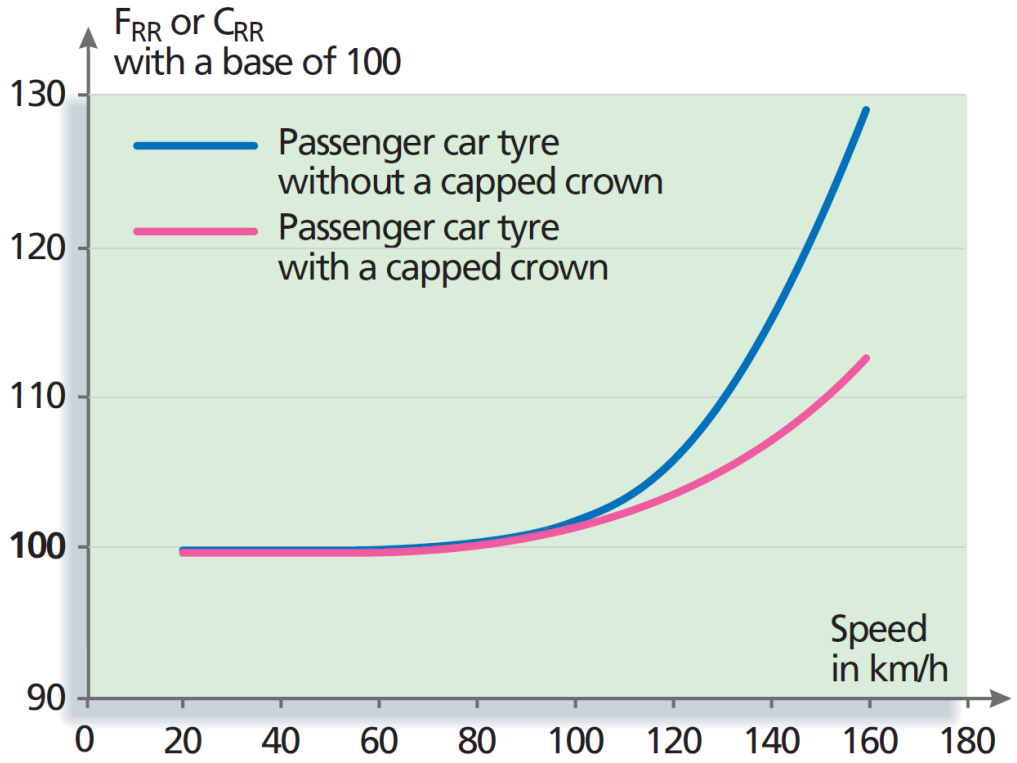


Figure 2.12 Rolling-Resistance under Different Speeds for Passenger-Car Tyres [20]

Many other studies exhibit a good agreement with Michelin's experimental results in Figure 2.12 in terms of the relationship of rolling-resistance with speed. Examples of those studies are given in Table 2.2 below:

Table 2.2 Role of Rolling Velocity on Tyre's Rolling-Resistance [8]

Study No.	Source	Investigation					Tyre's Dimensions						Wheel Diameter	Effect on Rolling Resistance	Remarks
		Method / Approach	Operating Conditions												
			Speed	Vertical Load	Inflation Pressure	Others	Aspect Ratio	Section Width	Section Height	Outer Diameter	Inner Diameter	Tread Depth			
1	[81]	Mathematical & Experimental	↑	?	?	Passenger-Car Tyres / On Dry & Wet Road Surfaces	?	?	?	?	?	?	?	↑	
2	[20]	Experimental	↑	–	–	Passenger-Car Tyre	?	?	?	?	?	?	?	↑	According to ISO 8767 standard / RR increases sharply after 120 km/h
3	[85]	Experimental	↑	–	–	(7.50-14) Tubeless Tyre	–	–	–	–	–	–	–	↑	RR increases sharply after 120 km/h
4	[23]	Experimental	↑	–	–	Radial and Bias Car Tyres on Smooth Flat Surface	?	?	?	?	?	?	?	↑	RR increases sharply after 120 km/h

5	[83]	Experimental & Thermal Modelling	↑	–	–	Radial Tyre	–	–	–	–	–	–	–	↑	
6	[84]	Numerical (FE Modelling) with Experimental Validation	↑	–	–	Radial Passenger-Car Tyre	–	–	–	–	–	–	–	↑	RR increases sharply after 120 km/h

Key Indicators:

– : Fixed, Constant or No Change	↑ : Increase	↘ : Slight Decrease
→ : Marginal Change (i.e. Negligible)	↓ : Decrease	**?** : Not Stated / Unknown
↕ : Variable or Fluctuating (No Particular Pattern)	↗ : Slight Increase	**N/A** : Not Applicable

Attempts were made to keep the vehicle's speed within the range where the rolling-resistance is stable and not experiencing an increase like including the "cruise control" unit to enable the driver to maintain constant speed of vehicle or the "warning indicator" in vehicle's dashboard to warn the driver when reaching high speed (i.e. 120km/h). Alternatively, developments were made to the tyre construction, especially the design and materials of the reinforcement cords, to minimise the intensity of standing waves or make sure the standing waves occur at very high speed [86-89].

2.4.3 Inflation Pressure

With respect to the existing literature, compared to the impact of load and speed, the inflation pressure has the most notable influence over rolling-resistance where rolling-resistance tends to be inversely proportional to pressure for hard road-surfaces. With temperature increase, besides the material effect indicated previously, the rolling-resistance would decrease more because of the further increase in pressure due to the thermal expansion of air inside the tyre [15].

Such effect on rolling-resistance is because the increase in pressure would make the tyre harder and holds its shape more firmly compared to a lower pressure tyre. This would lead to a lower area of contact-patch with the road along with lesser bending and shearing stresses created in the tyre; which means less tyre deformation and hence less tyre hysteretic damping [10, 11, 15, 20, 32].

Michelin [20] conducted an experimental measurement of rolling-resistance under different pressures, for a passenger-car tyre according to ISO 8767 standard, in which it has been found that the rolling-resistance decreased significantly with the pressure increase as seen in Figure 2.13.

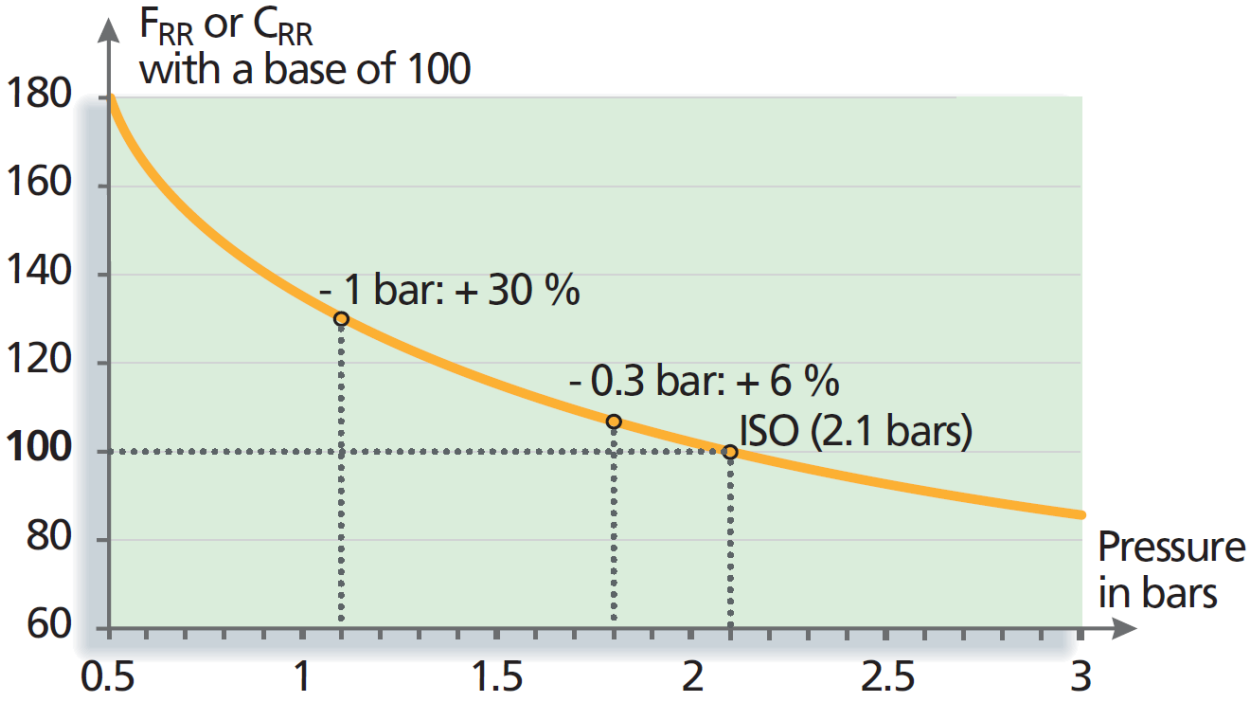


Figure 2.13 Rolling-Resistance under Different Pressures for Passenger-Car Tyres [20]

Many other studies generally match Michelin's experimental results in Figure 2.13 in terms of the relationship of rolling-resistance with pressure for normal hard road-surfaces. Examples of those studies are indicated in Table 2.3 below:

Table 2.3 Effect of Inflation Pressure on Tyre's Rolling-Resistance [8]

Study No.	Source	Investigation					Tyre's Dimensions						Wheel Diameter	Effect on Rolling Resistance	Remarks
		Method	Operating Conditions				Aspect Ratio	Section Width	Section Height	Outer Diameter	Inner Diameter	Tread Depth			
			Speed	Vertical Load	Inflation Pressure	Others									
1	[81]	Mathematical & Experimental	**?**	**–**	↑	Radial Passenger-Car Tyre	**–**	**–**	**–**	**–**	**–**	**–**	**–**	↓	
2	[70]	Numerical (Coupled Thermomechanical FE model)	?	**–**	↑	Passenger and Radial Medium Truck Tyres	**–**	**–**	**–**	**–**	**–**	**–**	**–**	↓	Numerical & Experimental
3	[72]		?	**–**	↑	Passenger Radial Tyre	**–**	**–**	**–**	**–**	**–**	**–**	**–**	↓	Numerical & Experimental
4	[68]		?	?	↑	Radial Tyres	**–**	**–**	**–**	**–**	**–**	**–**	**–**	↓	
5	[20]	Experimental	**–**	**–**	↑	Passenger-Car Tyre	**?**	**?**	**?**	**?**	**?**	**?**	**?**	↓	According to ISO 8767 standard
6	[9]	Analytical & Experimental	?	**–**	↑	Passenger Radial Tyre & Radial Truck Tyres	**–**	**–**	**–**	**–**	**–**	**–**	**–**	↓	

7	[90]	Experimental	↕	?	↑	Under different Types of Road Surfaces (Medium Hard Soil & Concrete)	?	?	?	?	?	?	?	↘	For Soft (Sand) Surface, the increase in Pressure causes the RR to increase too.
8	[82]	Experimental	–	–	↑	Radial (FR78-14) Tyre	–	–	–	–	–	–	–	↓	
9	[83]	Experimental & Thermal Modelling	–	–	↑	Radial Tyre	–	–	–	–	–	–	–	↓	

Key Indicators:

– : Fixed, Constant or No Change	↑ : Increase	↘ : Slight Decrease
→ : Marginal Change (i.e. Negligible)	↓ : Decrease	**?** : Not Stated / Unknown
↕ : Variable or Fluctuating (No Particular Pattern)	↗ : Slight Increase	**N/A** : Not Applicable

It is economically and environmentally wise to maintain the tyres at the proper inflation pressure to help to keep rolling-resistance down. This is as a decrease in inflation pressure by 15% below the targeted pressure can lead to a rise of 2.7% in fuel consumption [91]. To minimise from such drawback, pressure monitoring and self-inflation mechanisms are increasingly introduced and utilised. However, they are mostly applied in military and commercial transportation sectors such as the Tiremaax-Pro, MTIS, and TPCS systems. In contrast, for passenger-car vehicles, only the pressure monitoring solution is commonly applied [92-99].

Most of those developments were done on the commercial vehicles rather than the passenger-cars due to the profound gains it has on fuel economy for commercial vehicles which far exceed that of the passenger-cars. This is especially as the commercial vehicles can house the inflation systems properly unlike the passenger-cars where it could be of an issue [15, 100, 101].

Regardless, there are two potential prototypes of self-inflation systems that can be included as a part of the tyre assembly. While those prototypes are set initially for commercial vehicle usage, there are current plans in motion for the passenger-car usage too [94, 100-102]. The first prototype is the Goodyear AMT or Coda SIT where the inflation is induced from the peristaltic pumping (loading/unloading) effect of the tyre and the second one is the Aperia's Halo in which the inflation is supplied by a pendulum pump fitted to the wheel hub and operated from tyre rolling motion [99, 102, 103].

2.5 TYRE ADVANCES FOR LOW ROLLING-RESISTANCE

Principally, the way the tyre is designed and constructed determines its performance and response under different drive/road conditions. In this section, a state of the art review is conducted on the existing development research related to the tyre structural design and its effect on rolling-resistance with focus on the deformational hysteresis effect since it is the key contributor to the dominant majority of the tyre's rolling-resistance. In addition, this is to independently investigate the tyre structural role in reducing the rolling-resistance in line with this research project's aim and objectives. Accordingly, the current literature is found to fall under three categories of the tyre structural design and those categories are as follows:

2.5.1 Body Configuration and Construction

This section concerns the studies done on the building-up parts of tyre's structural body and its overall effect on rolling-resistance. One of the major advances done in this field is the production of "Radial-Ply" tyres, by Michelin in 1946, and its replacement of the energy-consuming "Bias-Ply" tyres [27]. The adoption of radial tyres, as an alternative tyre construction, has brought a remarkable reduction in tyre's rolling-resistance as seen in Figure 2.14, which can count up to an average of ~25% or more, compared to that of older Bias tyres constructions [78, 104, 105]. There is even the claim of this reduction reaching ~40% for the conventional radial tyres [106].

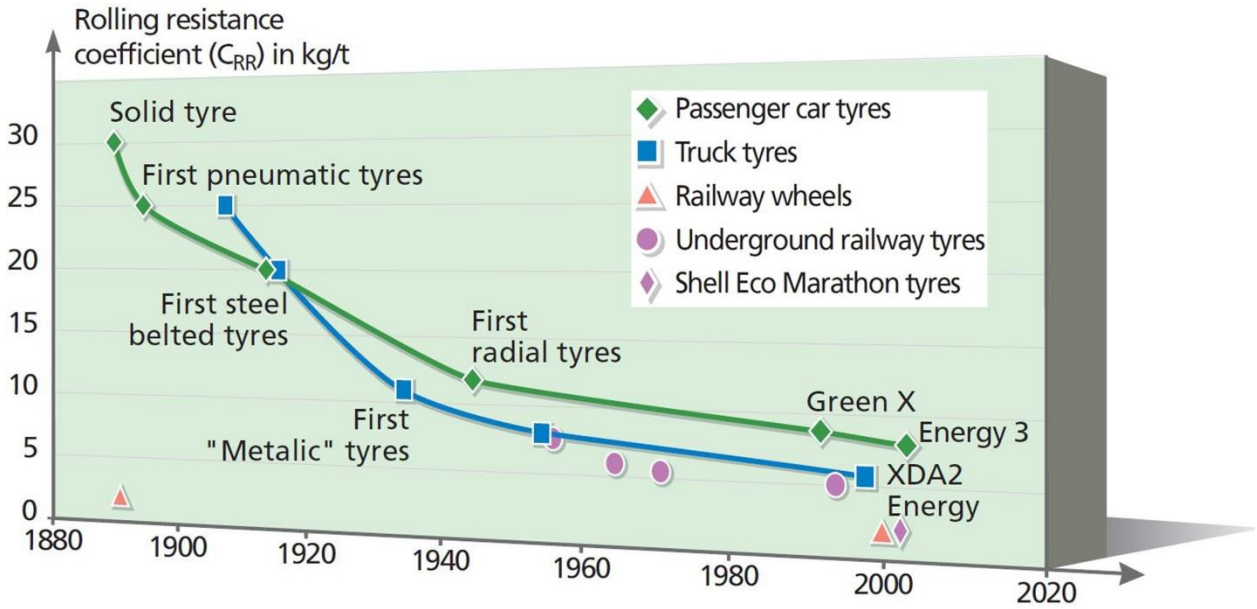


Figure 2.14 Tyre Advances for Rolling-Resistance Reduction [20]

Across the literature, many studies confirm the fact that radial tyres provide much lower rolling-resistance compared to that of bias tyres as summarised in Table 2.4.

Table 2.4 Advances in Body Construction [8]

Study No.	Source	Body Construction (Change Introduced)	Influence on Rolling Resistance (RR)	Method / Approach	Operating Condition			Others	Remarks
					Speed	Vertical Load	Inflation Pressure		
1	[107]	Radial-Ply VS Bias-Ply Constructions	Radial tyres has lower RR than that of Bias tyres	Exp.	↑	?	?	48 radial samples and 16 bias samples	
2	[23]	Radial-Ply VS Bias-Ply Constructions	Radial tyre has lower RR than that of Bias tyre	Exp.	↑	–	–	On smooth flat surface	
3	[105]	Radial-Ply VS Bias-Ply Constructions	Radial tyres has lower RR than that of Bias tyres	Exp.	↑	–	–	For both passenger-cars and trucks	Same tyre sizes.
4	[107]	Radial-ply Tyres from different Tyre Manufacturers	Clear difference in RR between the tyres of the same construction type	Exp.	↑	?	?	Radial-ply tyres	
5	[20]	Tyre with Cap-Ply	Below ~120kph, Cap-ply causes RR to slightly increase. Above ~120kph, Cap-ply leads to significant reduction in RR.	Exp.	↑	–	–	Passenger-car tyre	According to ISO 8767 standard

6	[108]	“Belt-width/tread-arc width (belt/arc ratio)”, “rubber thickness above belt-edge (shoulder gauge)”, “rubber thickness underneath belt-edge (insert gauge)”, &“crown angle”	- RR reduction with the decreasing of belt/arc ratio, shoulder gauge & insert gauge. - Crown angle had negligible impact on RR.	Exp.	?	?	?	Four tyre versions each containing twenty-five passenger-car tyres of the same outer size	Investigation on tyre's belt geometry
7	[109]	“Belt/arc ratio”, “crown angle”, “tread radius”, & “tread-arc width/section width (arc/section ratio)”	- RR reduction with decreasing of belt/arc ratio. - Arc/section & Crown angle had negligible impact. - Tread radius had a weak impact compared to belt/arc.	Exp.	?	?	?	Four tyre versions each containing 27 various tyres of different aspect ratios.	Investigation on tyre's belt geometry
8	[110]	Tyres With and Without Tread Patterns	- Pattern-less had 8% lower RR than patterns. - Various Tread Patterns had no impact on RR.	Exp.	?	?	?	The tested tyres were identical.	
9	[111]	Tyres With Different Tread Patterns	No significant changes in RR between different patterns except for snow tread had 27% higher RR.	Exp.	?	?	?	Passenger-car tyres	
10	[112]	Tread-Patterns of different block sizes and arrangements	A change of 5% in RR at 40km/h minimised to less than 2% at 150km/h.	Exp.	↑	?	?	N/A	Identical tyres.

11	[113]	Block Tread Pattern VS Rib Tread Pattern	A block-pattern led to an increase in RR by 15% more than a rib-pattern.	Exp.	?	?	?	Truck tyres	Block-pattern had a deeper tread.
12	[114]	Stiffness enhanced tread (i.e. by embedding plugs into the tread-cap)	Less deformational energy which led to lower RR	Exp.	?	?	?	Plugs, tread-cap and tread-base come in different materials.	
13	[115]	“Non-pneumatic (Air-free) Tyres” (i.e. Discrete (thin) Spokes Distribution)	- Low RR, inflation maintenance-free, and no flat-run. - Limited to usage with small vehicles of low to moderate speeds. - Handling and ride comfort problems.	Exp.	↓	↓	N/A	Flexible spokes that link the wheel hub to an outer composite shear ring where a rubber tread is mounted	
14	[116]	Different Non-pneumatic tyre's spokes (i.e. Spoke Pairs, Honeycomb, & Curved Spokes)	- The Spoke Pairs model had the lowest RR followed by the Honeycomb model and then the Curved spokes models as the last.	Numerical	–	–	N/A	Quasi-static 2D FE model(s) using Abaqus	Spoke pairs have highest vertical stiffness.
15	[117]	Four inner-chambers tyre	Lower RR than single chamber tyre	Exp.	–	–	–	Basic (initial) Prototype	

Key Indicators:

– : Fixed, Constant or No Change	↑ : Increase	↘ : Slight Decrease
→ : Marginal Change (i.e. Negligible)	↓ : Decrease	**?** : Not Stated / Unknown
↕ : Variable or Fluctuating (No Particular Pattern)	↗ : Slight Increase	**N/A** : Not Applicable

The advantage of the radial tyre over bias tyre with respect to rolling-resistance reduction can be referred obviously to the difference in the ply-construction between the two in terms of the number and orientation (angle) of body-plies and the existence of belts. Generally, the radial tyre contains a single radial-ply with several belts while the bias tyre consists of several diagonally oriented plies with no belt(s). Such construction makes the radial tyre have quite low friction internally along with a lot easier cord(s) deflection when under loading; which results in less heat generation and therefore less deformational energy and lower rolling-resistance [15, 28, 104, 106].

Although the existing studies indicate positive effects of radial tyres over fuel economy, most of those studies were conducted under inconsistent experimental conditions compared to each other which need standardisation to have more proper comparative investigations. Moreover, the radial tyres' advantage in fuel economy can be easily lost if other interrelated factors were not properly maintained like insufficient levels of inflation pressure or improper driving style [105].

LaClair [10] has reported that the addition of "nylon cap-ply" to the radial tyre construction can lead to an increase in rolling-resistance by a few percent if the tyre speed is below ~120kph especially when the tyre is not originally designed to accommodate the cap-ply. This is because including a cap-ply in the tyre would mean more mass to include producing further energy dissipation under cyclic deformation that could count up to ~2% of rolling-resistance. Above ~120kph, the cap-ply has a different impact on rolling-resistance in which it actually aids in lowering the tyre's rolling-

resistance. The reason behind this is that the cap-ply acts as crown reinforcement that decreases the impact of the centrifugal forces generated, limiting the crown's curvature change when in the contact-patch, and hence lowers the increase of rolling-resistance with higher speeds as was illustrated earlier in Michelin's investigation in Figure 2.12 of section 2.4.2.

For the "belt" geometry of the tyre, Lindemuth [28] indicated that having "wider belts" layer would have diverse effects on the overall tyre performance as shown in Figure 2.15 where the red-dots outside the circle represent an improvement in performance and vice versa. For tyres with wider belts, the speed-capacity, handling and traction performances were improved but at the expense of negatively impacting the ride, rolling-resistance and weight aspects. The increase in rolling-resistance, here, is because the wider the belt layer would mean the greater the tread area that would be supported directly by the belt under vertical loading for more contact flatness with the road resulting in greater deformation of the tread region at the contact-patch. This is in addition to causing a reduction in tread's flexibility and more added mass that would consume more deformational energy [15].

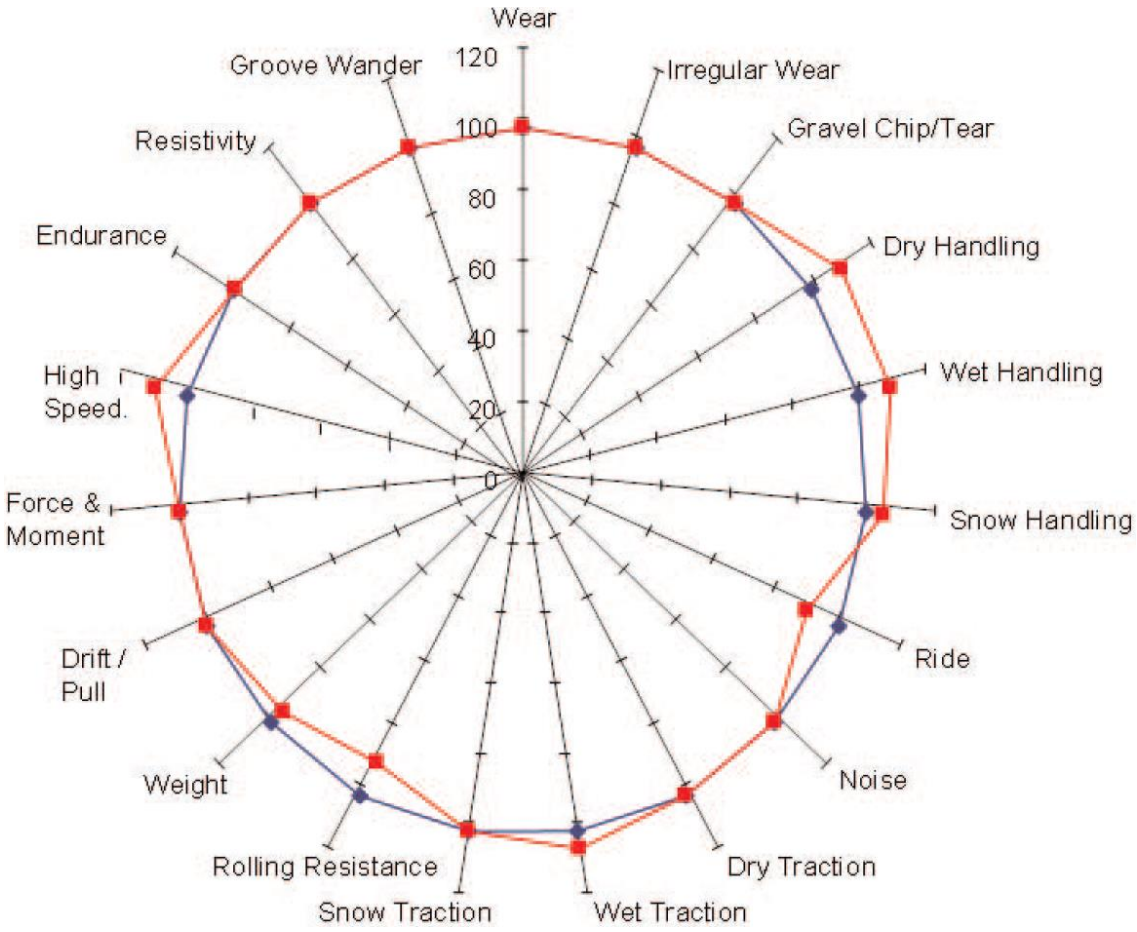


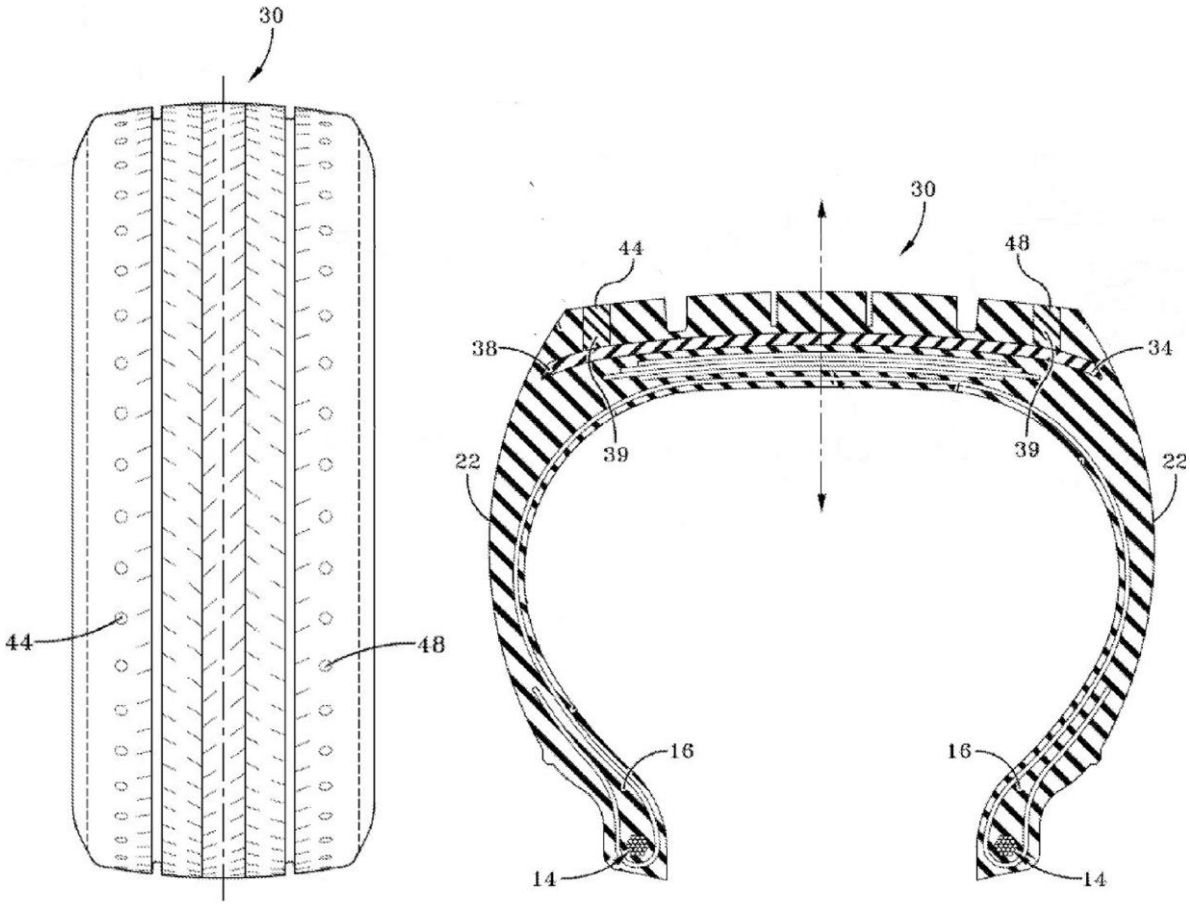
Figure 2.15 Impact of using Wider Belts on Overall Tyre Performance [28]

Both Yurjevich [108] and Walter [109] have carried out extensive work on designing, building and testing numerous tyres for the influence of belt geometry on rolling-resistance as indicated in Table 2.4. In general, the reduction of rolling-resistance in both Yurjevich [108] and Walter [109] works was achieved whenever there was a reduction in the size of the belt geometry which meant having less mass and hence less deformational energy consumed. This investigative work of both Yurjevich [108] and Walter [109] took tremendous time and costs to complete in which more than a year was spent on designing, building-up, and testing the tyres.

As for the “tread” geometry of tyre, there were several investigations done on the effect of “tread patterns” on rolling-resistance. For example, Keefe and Koralek [110] examined tyres both with and without tread patterns. They found out that pattern-less tyres exhibited 8% lower rolling-resistance than that with patterns. For tyres with patterns, they concluded that the same tyres but with different tread-patterns had no clear change in rolling-resistance among them. Williams [111] had similar results as illustrated in Table 2.4. On the other hand, Gerresheim [112] showed that there is a change of 2-5% in rolling-resistance for similar tyres but with tread-patterns of different block sizes and arrangements. Those findings can be supported through Knight's [113] work where he experimented on truck tyres with different tread-patterns and concluded that a block-pattern led to a rise in rolling-resistance by 15% more than a rib-pattern. Nonetheless, Knight [113] indicated that such a difference between those patterns might be due to block-pattern having a deeper tread of 3-5mm (i.e. see the next section 2.5.2 for the impact of tread-depth on rolling-resistance).

A recent invention by Sandstrom *et al.* [114] was made which introduces a stiffness enhanced tread to the tyre by embedding plugs into the tread-cap as seen in Figure 2.16. The embedded plugs, tread-cap and tread-base come in different materials to each other. Those embedded plugs are supposed to provide the tread with a higher stiffness vertically meaning less compressive strains to the tread under loading and hence less deformational energy which in turn lead to lower rolling-resistance without

largely affecting other tyre's characteristics. Such a conclusion was claimed to be reached based on experimental work, but no results of this work were presented.



A) Tyre Outside Layout (Side View)

B) Tyre Cross Section

Key Indicator:			
14	Beads	30	Tread-Cap
16	Apex	34 & 38	Tread-Base
22	Sidewall	39, 44 & 48	Embedded Plugs

Figure 2.16 "Stiffness Enhanced Tread" Tyre [114]

A growing trend in tyre construction is the movement toward developing "Non-pneumatic (Air-free) tyres" due to its potential gains over pneumatic tyres with respect to lower

rolling-resistance, inflation maintenance-free, and no flat-run [115]. According to Rhyne and Cron [115], those non-pneumatic tyres are usually made-up from flexible spokes that link the wheel hub to an outer composite shear ring on which a rubber tread is mounted as shown in Figure 2.17.

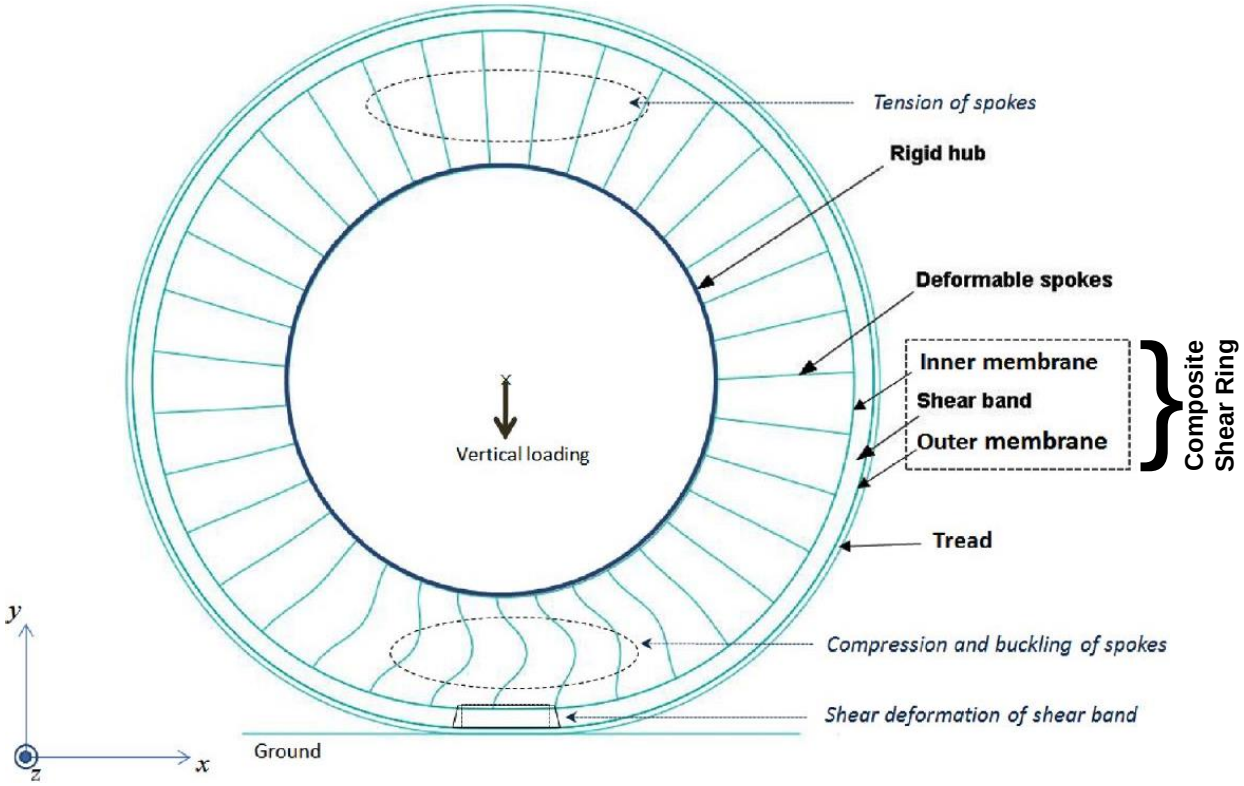


Figure 2.17 Non-Pneumatic (Air-Free) Tyre Construction [118]

Commonly, the spokes and shear band of the outer ring come with a hyperelastic material, like polyurethane, that promotes flexibility along with lower damping and hence less viscoelastic energy loss leading in turn to lower rolling-resistance [118]. A practical example of non-pneumatic tyres is that of Bridgestone's 2nd generation air-free tyre for small vehicles with a maximum speed of 60km/h presented in Figure 2.18.



A) Tyre Layout **B) Tyre(s) fitted on Vehicle**

Figure 2.18 Bridgestone's 2nd Generation Non-Pneumatic Tyre [119]

Despite the potentials the Non-pneumatic tyres hold, there are yet limitations and challenges facing the non-pneumatic tyres that need to be tackled and overcome. One of those limitations is that the non-pneumatic tyres may sometimes give greater rolling-resistance than that of the pneumatic tyres due to the usage of a large number of dissipative lattice spokes to sustain a targeted loading and maintain certain ride comfortability as the case of "Michelin Tweel" tyre. Such spokes would cause additional mass, further heat generation, and more inter-spokes friction [116, 118, 120, 121]. Also, generally, the non-pneumatic tyres are limited to usage with small vehicles of low to moderate speeds under normal conditions where the usage for conventional vehicles operation is yet to be realised. However, there are multiple researches and attempts that were conducted to further improve the non-pneumatic tyres like Kaufman *et al.* [122], Ju *et al.* [123] and Ma *et al.* [124] on the usage for lunar rovers and passenger-cars and

Rutherford *et al.* [125] and Narasimhan *et al.* [126] on minimising vibration of non-pneumatic tyres for high speeds usage.

An emerging and prospective design concept of tyre construction is the development of multiple internal chambers inside the tyre's cavity (i.e. Multi-chamber tyre) to control the tyre profile and its stiffness according to the drive/road conditions. Such a concept has the potential to serve as an alternative improvement to lowering rolling-resistance without adversely affecting other tyre central characteristics due to the current tyre structure complexity. Different concepts of multi-chamber tyres are introduced as untested patent designs in the public domain [30]. Majority of those designs are made to reinforce tyre beads mounting to the wheel, ensure air-sealed cavity, and address run-flat conditions [127-131]. Generally, those designs come either as internal tubing partitioned by radial separators or circular dual to triple chambers placed adjacently or concentric to each other. Nevertheless, the validity and reliability of those patents are to be questioned since they claim satisfaction of specific needs only and no investigations were done to support their solution's practicality and achievement of various driving needs.

To enhance off-road grip, further patents were proposed involving the use of either circular concentric multi-chambers or attachable circular shoe-housing to the tread-outside containing internal multi-chambers [132-134]. Each of Lambe [135] and Francesco *et al.* [136] suggested through their patented designs that better ride comfort and fuel-saving are possible through having concentric and circular dual-chambers at

which the internal chamber is inflated at a lower pressure than that of the external chamber. Such a proposition can be confronted with the chance that the proposed design settings may negatively affect in turn the tyre's grip, beads mounting, and structure balance during rolling. This is especially since the designers did not supply any validations to back-up their proposition.

Coyote [137] developed an attachable inner chamber that can be used to turn the conventional tyre into concentric and circular dual-chambers. The internal chamber is set at higher pressure to back-up both beads mounting and run-flat conditions whereas the external chamber is set at lower pressure to provide better off-road grip. Each of Bridgestone [138] and Goodyear [139] has provided separately a prospective design model of a circular multi-chamber tyre for enhanced handling, comfortability and fuel-saving by altering chambers' inflations independently and variously according to driving/road conditions. Both tyre makers are exerting extensive efforts to further improve their notional models into actual, makeable and working prototypes.

In an uncompleted project by Fusion Innovation [140], Kubba [117] evaluated a basic tyre prototype of four inner-chambers empirically and concluded that multi-chamber solution could influence reducing the rolling-resistance. His evaluation involved building-up a tyre FE model through Abaqus/Standard which was restricted to estimating the quasi-static responses besides the cornering performance to a specific range. However, the FE model was incapable of computing the tyre's rolling-resistance and the inner cavity response since neither the medium of cavity air nor its interaction with the tyre

structure was accounted for. The tyre inflation was compensated by just applying the relevant distributed loading pressure along the tyre inner-liner in accordance with each chamber domain.

In the context of multi-chamber tyres, there is weak coverage and shallow literature on the topic especially with respect to reducing the rolling-resistance since the multi-chamber tyre is relatively new and immature research area in which it is still in the designing phase or laboratory prototyping with no actual usage yet. The existing research projects on this field are on-going and confidential ones belonging to automobile and tyre institutions. Therefore, it is a research field that is yet to be explored and investigated in-depth with rich research opportunities and infinite designing possibilities.

Overall, the existing literature on tyre construction shows that the radial tyre construction, once its generic design became standardised, has contributed to lowering the rolling-resistance greatly at one go. Subsequent constructional improvements for lowering the tyre's rolling-resistance were done on an incremental basis over a prolonged period of time. This could be since the experimental development work is a very difficult task to accomplish because of the high costs, the large time-taken, and the little or no gains involved in the process due to the complexity of the tyre structure. An instance on that would be the works of both Yurjevich [108] and Walter [109] mentioned earlier.

In addition, usually, the small improvements made in the tyre construction to lower the rolling-resistance are restricted to the specific tyre that was investigated due to the complexity of the tyre design and the involvement of many interrelated design factors at particular settings in the process. A good example is Thompson and Myriam [107] investigation conducted on different manufacturers tyres as seen in Table 2.4.

2.5.2 Geometrical Dimensions

One of the main dimensional characteristics of the tyre is the “Aspect ratio”. It is the ratio of tyre’s section height to section width which defines the tyre profile as seen in Figure A.0.2 in section A.2.1 of appendix (A). On investigating the overall aspect ratio, various studies indicated different influences of the aspect ratio on the rolling-resistance indicating the involvement of other design/operating factors in the process. An example of such studies can be seen from the studies numbered 1 to 8 in Table 2.5.

Table 2.5 Advances in Dimensional Settings [8]

Study No.	Source	Tyre's Dimensions						Investigation					Influence on RR	Remarks
									Operating Conditions					
		Aspect Ratio	Section Width	Section Height	Outer Diameter	Inner Diameter	Tread Depth	Method / Approach	Speed	Vertical Load	Inflation Pressure	Others		
1	[141]	↑	↕	–	–	–	?	Analytical & Experimental	?	–	–	Radial passenger-car tyres	→	
2	[112]	↓	?	?	?	?	?	Experimental	?	–	–	Passenger-car tyres	→	
3	[142]	↓	↕	?	–	↕	?	Experimental	↓	?	?	Radial truck tyres	↘	Fixed material compound & construction
4	[143]	↓	↑	–	–	–	?	Experimental	?	?	?	Passenger-car tyres	↓	Fixed material compound & construction
5	[113]	↓	?	?	?	?	?	Experimental	?	?	?	Radial truck tyres	↓	
6	[144]	↑	?	?	–	?	?	Analytical Modelling	?	?	?	Radial passenger-car tyres	↕	Minimum RR at 70% aspect ratio
7	[145]	?	–	?	↕	–	?	Experimental	?	?	?	Fixed material compound & construction	?	Minimum RR at 85% aspect ratio
8	[146]	?	?	?	–	?	?	Experimental	?	–	–	Passenger-car tyres	?	Minimum RR at 65% aspect ratio

9	[147]	↑	↓	–	–	–	–	Analytical + Experimental	?	–	↑	Truck tyres / fixed carcass thickness & tread thickness	↓	Inflation pressure has greater impact on RR than section width
10	[147]	↓	↑	–	–	–	–	Analytical + Experimental	?	↑	↑	Truck tyres / fixed carcass thickness & tread thickness	↓	Inflation pressure has greater impact on RR than section width & load
11	[148]	?	↑	?	?	–	?	Experimental	↓	–	↑	N/A	↓	Inflation pressure & speed have greater impact on RR than section width
12	[147]	–	↓	?	↑	?	–	Analytical + Experimental	?	–	↑	Truck tyres / fixed carcass thickness & tread thickness	↓	Inflation pressure & outer diameter have greater impact on RR than section width
13	[24]	↑	↓	↑	–	↓	?	Experimental	↑	?	?	UHP radial tyres of the same brand & type	↓	Faster rolling (from 0 60mph)
14	[141]	↑	–	↑	↑	–	?	Analytical & Experimental	?	–	–	Radial passenger-car tyres	↓	
15	[141]	↑	–	↑	↑	↑	?	Analytical & Experimental	?	–	–	Radial passenger-car tyres	↓	
16	[141]	↑	–	↑	↑	↓	?	Analytical & Experimental	?	–	–	Radial passenger-car tyres	↓	Increase in section height is more than decrease in wheel diameter
17	[141]	↑	–	↑	–	↓	?	Analytical & Experimental	?	–	–	Radial passenger-car tyres	–	Increase in section height is equal to the decrease in wheel diameter
18	[20]	–	–	–	↑	–	?	Experimental	↓	?	**?**	Radial passenger-	↓	According to ISO 8767

												car tyre		standard of testing
19	[90]	?	?	?	↑	?	?	Experimental	?	?	?	Under different road surfaces	↓	Outer diameter has greater impact on RR in soft surfaces compared to harder surfaces
20	[107]	?	?	?	↑	?	?	Experimental	↓	?	?	Radial tyres	↓	
21	[142]	?	?	?	?	?	↓	Experimental	?	?	?	Truck tyres	↓	Linear relationship between RR & tread depth
22	[113]	?	?	?	?	?	↓	Experimental	?	?	?	Various truck tyres	↓	Linear relationship between RR & tread depth
23	[149]	?	–	?	?	–	↓	Experimental	?	↕	↑	Radial passenger-car tyres	↓	
24	[150]	?	–	?	?	–	↓	Experimental	?	?	?	Radial truck tyres	↓	Non-Linear relationship between RR & tread depth
25	[151]	?	–	?	?	–	↓	Experimental	?	↕	↕	Low profile radial truck tyres	↓	Non-Linear relationship between RR & tread depth

Key Indicators:

– : Fixed, Constant or No Change	↑ : Increase	↘ : Slight Decrease
→ : Marginal Change (i.e. Negligible)	↓ : Decrease	**?** : Not Stated / Unknown
↕ : Variable or Fluctuating (No Particular Pattern)	↗ : Slight Increase	N/A : Not Applicable

In this context, more detailed investigations were conducted that involved studying independently the impact of the components of the aspect ratio (i.e. section height and width), taking into account the role of operating factors too, on the rolling-resistance. In studies 9 to 11 in Table 2.5, Clark [147] and Curtiss [148] illustrated that the tyre's section width had small to marginal impact on the rolling-resistance in which it was inconsistent. On the other hand, the inflation pressure had an obvious and consistent influence on the rolling-resistance of inverse proportionality as indicated previously in section 2.4.3. Furthermore, in Table 2.5, both Treichel [142] and Curtiss [148] showed that the decrease in rolling speed would help in reducing the rolling-resistance, in line with the previous findings in section 2.4.2, regardless of the type of change introduced in section width.

As illustrated earlier in Table 2.5, in some cases, it may appear that an increase in section width would help in lowering rolling-resistance although it is the influence of the operating parameters (i.e. inflation pressure and speed). There is the claim that wider tyres will promote a larger area of tyre's contact patch and hence less applied force to each part of the contact patch. In return, this will cause less compression or deformation to each patch's part than that of narrower tyres and therefore leading to lower material hysteresis effect and energy losses at the end [152]. However, this claim might be held true and valid more toward "solid" tyres rather than "pneumatic" tyres as indicated in Evans' [153] work.

Given the anisotropic and viscoelastic nature of the tyre's rubbers, a wider tyre may lead to a higher rolling-resistance considering the deformation of the tyre crown curvature at the contact-patch under vertical loading. This is especially as the crown region at the contact-patch can account for ~70% of the overall energy losses of the tyre compared to the tyre's other regions [10, 154]. Wong [32] comments on this matter by indicating that the wider the tyre the more aerodynamic drag (wind resistance) it creates; especially at high speed where its effect on increasing rolling is more evident as seen in the previous example in Figure 2.11 in section 2.4.2.

For the role of other dimensional parameters together with the aspect ratio on influencing the rolling-resistance, further investigations were performed and they are listed as studies 12 to 17 in Table 2.5. As study number 12, Clark [147] highlighted that both the outer diameter and the inflation pressure had an apparent impact on the rolling-resistance of inverse proportionality. In study 13, Walter [24] revealed that the wider and shorter the tyre (i.e. lower aspect-ratio) became, the more the time taken for the car to reach from 0 to 60mph and the more the fuel consumption reaching 10% more as the aspect-ratio reduced from 65 to 35. This is because of the reduction in the overall tyre-and-wheel net-weight (i.e. effective-mass) that higher-profile tyres achieve over lower-profile ones. This is seen by the increase in the effective-mass from being 2.6% for 195/65R15 tyre to 4.2% for 235/35R19 tyre; equal to an increase by 59kg to vehicle-weight. Apparently, the more the section-height and the less the section-width of the tyre, the less the wheel mass will be, resulting in lower net-weight of both tyre and wheel

meaning lower rotational inertia-resistance since tyre rubber is much lighter than that of the metal wheel.

Pillai and Fielding-Russell [141] conducted a series of studies on the impact of aspect ratio, section height and wheel-diameter on the rolling-resistance as seen in Table 2.5. In the assessment of their overall work, Pillai and Fielding-Russell [141] concluded the following:

- If the “tyre radius (R)” is constant, the rolling-resistance would be independent of the aspect ratio. An example of that is study 1 in Table 2.5 where the change in section width did not influence the rolling-resistance.
- If the “tyre radius (R)” is changed as a result of changing the aspect ratio, the rolling-resistance would become affected by the aspect ratio. Higher aspect ratio would mean longer outer diameter and hence lower rolling-resistance. An example of that would be studies 14 and 15 in Table 2.5.
- If the “wheel radius (R_w)” and the “section height (H)” are changed oppositely to each other, rolling-resistance might increase, remain the same or decrease depending on the resultant change of “tyre radius (R)”. An example of that would be studies 16 and 17 in Table 2.5.

Other investigations confirming the obvious effect of the outer diameter on the rolling-resistance, which is of inverse proportionality, are studies 18 to 20 in Table 2.5. Such evident impact of tyre outside diameter on rolling-resistance can be attributed to the fact

that tyre radius is interconnected to the length of contact patch area and hence to the normal load on the tyre. Having larger (longer) tyre radius gives the tyre more stiffness and less vertical deformation for the same normal load which means lower bending of tyre radius when it enters and leaves the contact patch region and in return lesser hysteresis losses [15, 20]. The outer tyre diameter is closely related to the aspect ratio as it contains one of the aspect ratio's components and it is the section height as a part of its dimension. Therefore, this makes the aspect ratio have an influential impact on rolling-resistance through the tyre's outer diameter whenever the introduced change is involving the tyre's section height.

Another tyre dimension of an impact on the rolling-resistance is the "tread depth (thickness)". According to the studies 21 to 25 in Table 2.5, it is apparent that the reduction in tread depth would result in a decrease in rolling-resistance too and the rate of rolling-resistance reduction will vary based on certain factors like inflation pressure, tyre type and tread material. The main reason behind the consistent impact of tread depth on rolling-resistance is the fact that the principal cause for rolling-resistance is the energy losses due to rubber deformation (hysteresis effect); so the less the rubber material the less the deformation will be and hence the less the rolling-resistance will be in return. Walter [24] highlights that decreasing tread mass for passenger-car-radial tyres is more effective and important in lowering rolling-resistance (i.e. inertia-resistance) than changing the wheel material from steel to alloy (i.e. a lighter material). In general, having a thinner tread for the tyre would help lower rolling-resistance and hence the fuel

consumption along with manufacturing costs, but on the other hand, it will shorten the lifespan of the tyre (wear life) and lower from its traction capability.

An overall look at the trend of the existing literature on the dimensional design of pneumatic tyre for low rolling-resistance reveals that there are infinite possibilities of configuring and altering the dimensional parameters of the tyre. Every possibility holds and dictates certain changes to the tyre construction and its capabilities leading in turn to diverse impacts on rolling-resistance depending on the given tyre. As such, the investigative researches' results on the tyre's dimensional impact on rolling-resistance are found to be almost mixed. This is because of the high likelihood of interactions and interferences between the numerous design elements of the tyre with each other, like material(s), components orientation and dimensional constraints, in which compromises in some features over the others are inevitable. Furthermore, added to the equation is the influence of operational tyre parameters, like the inflation pressure, normal load and speed which the tyre needs to meet and withstand. The inconsistency of testing conditions can be taken as another reason for the diversity of literature results on the impact of dimensional tyre changes on rolling-resistance. Such findings are in agreement with that of LaClair [10] and Schuring and Futamura [81].

However, there have been on-going developments in the tyre field which provide promising opportunities to exploit for further improvement of tyre's rolling-resistance. Among which is the evident, notable and consistent impact of "tyre outside diameter" on rolling-resistance as proved across many relevant pieces of literature where increasing

the outside diameter would clearly help in decreasing the rolling-resistance [10, 15, 20, 32, 141]. There is an increasing movement toward this trend of developing “tall and narrower” tyres by tyre manufacturers like “Fiat Chrysler Automobiles” which is putting a fruitful effort toward developing tall and narrow tyres as a new promising approach for minimising rolling-resistance and trade-off between the tyre’s characteristics like rolling-resistance, handling, braking and NVH [155]. Nevertheless, there are vehicle manufacturers that use low profile (shorter and wider) tyres for better vehicle driving performance in terms of improved road-grip, steering response, cornering capability, traction and braking but at the expense of increasing rolling-resistance (i.e. higher fuel consumption) and lowering ride comfort (i.e. poor cushioning against road shocks and damages) [20, 156]. For higher profile tyres, it is the opposite scenario.

Choosing between having a low profile (shorter and wider) tyre and a higher profile (taller and narrower) one will always involve trade-offs in the tyre’s features and characteristics as highlighted earlier. A promising concept that could further lower the trade-offs between tyre’s characteristics especially between low profile and higher profile tyres is having “dynamically changing tyre profile” that is capable of accommodating both low and higher profile for the same tyre according to the driving and road situation at hand. Such a concept was already highlighted in the previous section as the “multi-chamber tyre” concept. This concept holds a potential solution that could be far better than most of the existing tyres designs if it is to be successfully made real. This is since the current literature only offers fixed/permanent changes to the tyre’s profile (i.e. aspect ratio) that were not so effective in addressing the diverse and conflicting needs of the

vehicle whether it was in terms of driving performance or fuel economy which require different characteristics of the tyre especially the dimensional ones.

2.5.3 Material Compounds

The tyre has a complex structure as it is made up from over 200 raw materials, to form its rubber compounds and cord reinforcement, in order to carry out the diverse driving functions under different operating conditions from normal to extreme ones [157, 158]. The literature addresses the tyre's material(s) improvement, for better rolling-resistance, through looking at one of two areas or both, i.e. less hysteresis in the material(s) through modifying "rubber compounds" and/or less tyre deformation through modifying "cord-reinforcement" [53, 106, 159]. This is with the focus on the "rubber compounds" as it has a dominant impact on rolling-resistance [53, 82]. The hysteresis losses of tyre's rubber-compounds, due to its viscoelastic behaviour under cyclic deformation, can be held responsible for 80-95% of total rolling-resistance of the tyre as indicated previously. Among the tyre's regions, the hysteresis losses occur mostly in the tread (crown) region which typically represents ~70% of energy dissipation compared to the tyre's other regions; the sidewalls and the bead, which hold ~15% each [82, 154]. In addition, to having large rubber mass and being the only part of the tyre in contact with the road, there are rigorous efforts toward improving tread material(s) for lower rolling-resistance and better traction (grip) [10, 15, 81].

One of the development areas of tread compounds is where Hunt *et al.* [82] investigated the influence of implementing different tread polymers on rolling-resistance respectively

as indicated in Table 2.6. It was concluded that changing tread polymer has an apparent impact on rolling-resistance where the natural rubber (NR) tread had the lowest rolling-resistance and the butyl (IIR) tread had the highest rolling-resistance.

Table 2.6 Advances in Tyre Materials [8]

Study No.	Source	Tyre's Material(s) (Change Introduced)	Influence on Rolling Resistance (RR)	Approach	Speed	Vertical Load	Inflation Pressure	Others	Remarks
1	[82]	Different tread polymers	Polymers of low to high RR respectively: Natural rubber, cls-(BR), solution (SBR), emulsion (SBR), (BR), (IR), and butly.	Exp.	–	–	–	Radial passenger-car tyres of the same size, tread design & tread hardness.	All had same composition percentage of carbon-black & aromatic-oil
2	[160]	Different tread polymers in shoulders & centre	Lower RR and Better Traction (grip).	Exp.	–	–	–	Radial passenger-car tyres of the same size	ISO 28580 / US Patent 20160016435
3	[161]	Different tread material (i.e. Polymer, carbon-black, oil and curatives)	A decrease in dry-traction by 5% and wet-traction by 7% at 30km/h to 15% at 100km/h for a 10% decrease in RR.	Exp.	↑	?	?	N/A	
4	[162]	A tread with different hysteresis properties at different temperature & frequency ranges	Tread material to offer low hysteresis at low temperatures & frequencies for low RR. The opposite for better traction.	Analytical	?	?	?	For RR, at (~50°C) and (~10-150Hz). For wet traction, at (~100-150°C) and (~50kHz - 1 MHz).	Occurrence of grip and RR at different temperatures & deformational frequencies

5	[143]	A tread with a close glass-transition temperature to that of traction domain	Tread to provide high loss-tangent at low temperature for higher traction & the opposite for lower RR both for same frequency.	Analytical	?	?	?	For frequency of 1 to 110 Hz, at 50 to 70 °C for RR & at -20 to 20 °C for Wet Traction	Time-temperature superposition principle
6	[163]								
7	[164]								
8	[164]	Modification to Polymer's Macrostructure: Decreasing chain-end concentration through reducing molecular weight distribution	Decrease material hysteresis and hence RR too.	Exp.	?	?	?	Manipulate molecular weight distribution by blending polymers with different molecular weights	
9	[165]							Different molecular weight distribution by blending various monodisperse polymers	
10	[166]							Random Branching to change molecular weight & its distribution	
11	[167]	A better dispersion of carbon-black	Significant minimization in RR.	Exp.	?	?	?	Increasing the interaction between polymer-chains and carbon-black via modifying chain-ends	
12	[168]								
13	[81]								
14	[20]	Reduce filler concentration in rubber (i.e. widen distance between filler aggregates)	Minimize energy dissipation and RR.	Exp.	?	?	?	A) Minimising filler volume without changing the filler aggregate size or vice versa (i.e. limited improvements). B) Improving the filler distribution in the rubber compound (i.e. more difficult & expensive).	
15	[169]	"Nano-molecular base" for cap-ply	Enhance grip and minimise heat dissipation.	Exp.	?	?	?	Nokian's WR-A3 tyre	
16	[169]	Nano-coating for tread	Lower heat dissipation and RR.	Exp.	?	?	?	Bridgestone's Ecopia tyre	

17	[169]	Tyre with carbon Nano-tubes	Enhance tensile strength (by ~600%) and hardness (by ~70%) leading to lower tyre's deformation compared to SBR tyres.	Exp.	?	?	?	N/A
18	[170]	Nano-meter Silica fillers for improved distribution with styrene butadiene	Better grip and RR.	Exp.	?	?	?	Giti radial Champiro UHP tyres
19	[53]	Different cords reinforcement materials (i.e. for carcass & belts)	- Aramid had a significant impact on lowering RR. - Rayon carcass caused higher RR. - Others did not exhibit major differences on RR.	Exp.	–	–	–	- HR78-15 Poly-steel radial tyres of the same design. - Cost down & constant speed wheel testing.
20	[53]	Different carcass & belt weight	Increase in weight lead to significant increase in RR.	Exp.	–	–	–	HR78-15 Poly-steel radial tyres of the same design
21	[171]	"Electro-rheological fluid (ERF)" as a smart filler for two tyre polymers	Adjustable tyre viscosity (internal dampening) and tuneable RR.	Exp.	N/A	N/A	N/A	- ERF reinforced electrospun polymer(s), ERF/PVDF (Polyvinylidene fluoride) and ERF/PCL (Polycaprolactone). - Silicon rubber.

Key Indicators:

– : Fixed, Constant or No Change	↑ : Increase	↘ : Slight Decrease
→ : Marginal Change (i.e. Negligible)	↓ : Decrease	**?** : Not Stated / Unknown
↕ : Variable or Fluctuating (No Particular Pattern)	↗ : Slight Increase	N/A : Not Applicable

Volk *et al.* [160] performed a more innovative way by using different polymers for the shoulders and the central portions respectively for the same tyre tread, in which the shoulders' polymer had lower rolling-resistance, in attempt to achieve lower rolling-resistance and other desired features like better traction with a minimum trade-off. Generally, those two features, lower rolling-resistance and better traction (grip), are both important and vital to achieve in the tyre in order to function efficiently but the problem is that one feature cannot be achieved without compromising the other feature and vice versa [10]. This is due to the tyre's material hysteresis which needs to be low to reduce rolling-resistance and vice versa to enhance the traction (grip) at the same time which is a conflicting requirement. An example of that can be seen in Martini [161] experimental work in Table 2.6.

An alternative approach to improve tread-compounds in a way that would minimise the trade-off between rolling-resistance and traction (grip) is taking advantage of the dependency of tyre's material hysteresis on "polymer's glass-transition temperature" and "frequency of tyre surface deformation" along with the occurrence of grip and rolling-resistance at different temperatures and deformational frequencies [10, 81]. In Table 2.6, Bond *et al.* [162] proposed to have a tread material that would offer low hysteresis properties at low temperatures and frequencies where normally rolling-resistance occurs and high hysteresis at high temperatures and frequencies where generally grip (traction) occurs. Other researchers suggested having a tread material with a close glass-transition temperature to that of traction domain, in an attempt to meet the opposing requirements for both low rolling-resistance and enhanced traction, by providing high

loss-tangent at low temperatures for higher traction and low loss-tangent at higher temperatures for lower rolling-resistance both for the same frequency range [143, 163, 164] .

Further development works on tread polymers to meet the rolling-resistance and traction requirements involved improvements through using different “polymerisation methods” (i.e. emulsion to solution), changes to both “polymer’s microstructure and macrostructure”, and “polymer chain-end alterations” [172]. On polymer’s macrostructure, several researchers concluded that decreasing chain-end concentration through reducing molecular weight distribution would decrease the material hysteresis and hence rolling-resistance [164-166]. Fujimaki *et al.* [167] and Oshima *et al.* [168] reported significant minimisation in rolling-resistance through achieving a better dispersion of carbon-black as a result of increasing the interaction between polymer-chains and carbon-black via modifying chain-ends. Futamura [81] showed similar findings to the earlier effects of macrostructure and chain-end modification on rolling-resistance.

With regard to polymer’s microstructure, many studies point out the need to control the composition and microstructure in a way that would give an adequate balance between the glass-transition temperature, hysteresis and tensile strength properties of the polymers to satisfactorily meet the rolling-resistance and traction requirements [173-175]. However, it is not easy to modify the polymer’s microstructure without influencing the macrostructure too. If the macrostructure is to be considered in tyre design, the

influence of composition and microstructure would be negligible on rolling-resistance [81].

“Filler chemicals”, like Carbon-black and Silica, used for strengthening and reinforcing the rubber compound is another way of further developments for low rolling-resistance. According to both LaClair [10] and Michelin [20], the fall in modulus (i.e. rigidity) and increase in energy losses of rubber compounds become greater when the filler concentration is bigger (i.e. smaller distance between the filler aggregates). Therefore, to minimise the energy dissipation and rolling-resistance in return, a number of solutions were introduced to widen the spaces between the reinforcing filler aggregates as indicated under study 14 in Table 2.6 which have some limitations that could lead to a trade-off between the tyre core features as seen from the example in Figure 2.19.

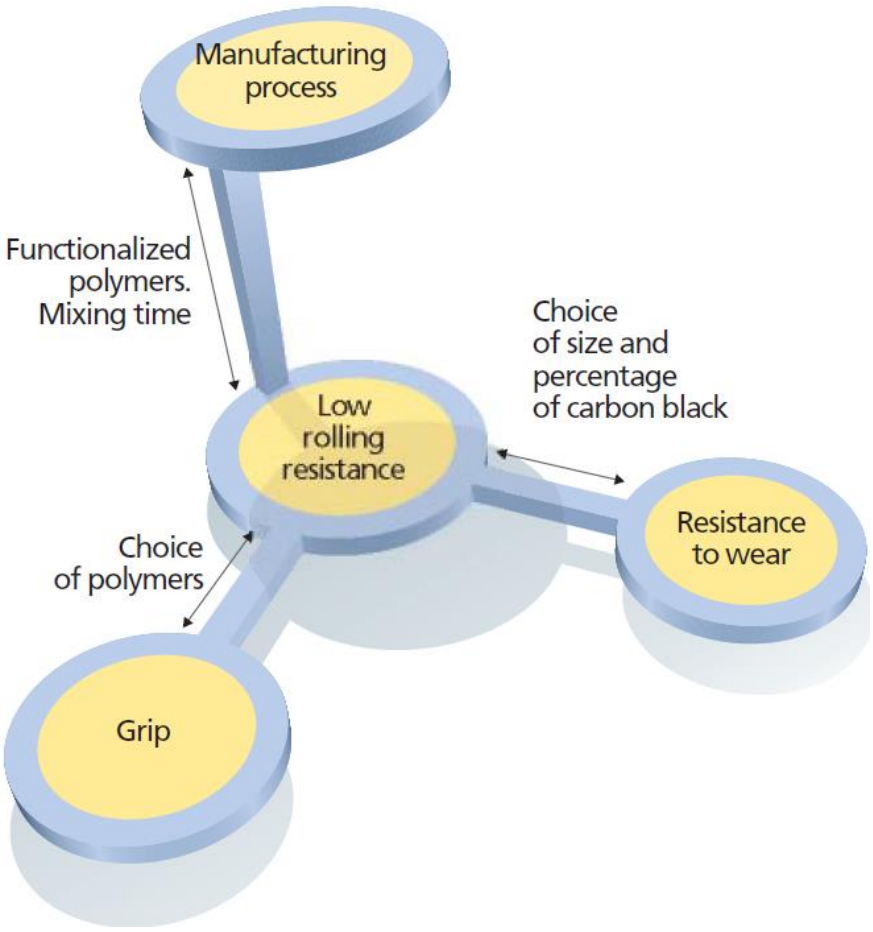


Figure 2.19 Common Trade-Offs between Rolling-Resistance and Other Features [20]

A growing trend in tyre developments for low rolling-resistance is the usage of “Nano-technology” in building-up the material(s) for the tyre different parts to improve their properties and features further in order to reduce rolling-resistance. On this subject, several investigations were conducted from which studies 15 to 18 in Table 2.6. Another emerging trend is the “intelligent or smart materials” which involves the usage of tyre materials with a built-in sensor, actuator, and control system altogether to react to particular stimuli in a predetermined way [5, 176, 177]. The intelligent materials started

as a part of the “tyre monitoring technology” then evolved into the “intelligent tyre technology”. However, generally, the only practical intelligent tyre technology in use currently in the market is the “tyre pressure monitoring system” (TPMS) where usually a “piezoelectric material” is used for the tyre pressure sensor [5, 177, 178].

The intelligent tyre technology is yet to be fully efficient and well established. Most of the developments done on intelligent tyre materials are still lab-based, and yet to be practical, and put for market use. An example would be Chen [171] research on the use of “electro-rheological fluid” as a smart filler for the tyre polymer material(s) to adjust the tyre’s viscosity and hence lower the rolling-resistance as indicated in Table 2.6. Such slow development progress can be attributed to the technical difficulties facing intelligent material(s) application in terms of manufacturing requirements, communication barriers, coping with extreme operating conditions, service life, and cost incurred [179].

Although its influence is marginal compared to tyre rubbers, Vorachek *et al.* [53] illustrated that introducing changes to the tyre reinforcement cords can still influence rolling-resistance as shown from studies 19 and 20 in Table 2.6.

Overall, the tyre’s material(s) developments for rolling-resistance are a predominant research field in vehicle tyres with a rich literature and on-going intensive efforts of research. This is because of the tyre’s rubber and cords material hysteresis which is responsible for the majority (~95%) of tyre’s rolling-resistance. However, having said that, the development changes made to tyre’s material(s) have the least level of design

freedom compared to other design aspects of the tyre (i.e. body construction and dimensions) where it is unlikely to have significant future developments [82, 154]. One of the main reasons is the trade-off between the rolling-resistance and the other performance features if the tyre's material(s) to involve modifications to meet certain driving requirements of the vehicle [32, 81]. Another reason would be the difficulty in the manufacturing process of tyre's rubber compounds for low rolling-resistance and other conflicting features which demand different material properties and manufacturing conditions [10, 20].

Looking at the literature on tyre's material(s), potential trends for future research can be seen that may further improve rolling-resistance. One of these trends is the attempts to reach an enhanced silica (filler) approach to natural rubber for truck tyres which would result in a remarkable improvement to rolling-resistance if it was to be successful [180]. This is as, currently, there is the problem of being unable to completely couple silica with the polymer chains of natural rubber for truck-tyres which leads to rising rolling-resistance and lowering wear-resistance [15]. Another largely growing trend of research is the field of intelligent material(s) such as nano-materials, magnetic rubber materials, and so on [180].

2.6 SUMMARY

A major challenge faced in the literature is lowering rolling-resistance without compromising other performance aspects of the tyre which is extremely difficult. Apparently, this is due to the many interactions and complex relationships between the

rolling-resistance and the design and operating parameters of the tyre which make it very difficult to express such relationship quantitatively or predict rolling-resistance analytically under such conditions without making simplifications. Therefore, improving the tyre design for specific features usually includes compromising other features in unpredictable ways in most cases. That is why rolling-resistance improvement depends almost completely on experimental results for the targeted tyre(s). Lately, this has been aided by the use of numerical modelling to help in saving time and cost.

Normally, the improvement in the rolling-resistance would be specific and limited to the investigated tyre alone due to the tyre complexity. As such, sometimes, results of investigations of the impact of certain tyre structural design parameters on rolling-resistance are found to be quite mixed in the literature. The inconsistency of testing conditions is another reason for this. Also, there are limitations on the availability of information, on the construction of tyres and their relation to rolling-resistance, from the manufacturers' side due to confidentiality reasons.

Regardless of such challenge(s), there are several operating and design parameters whose effect on rolling-resistance is quite apparent and consistent. With the complexity of the tyre structure, the operating conditions have a much bigger room for change and hence have a greater influence on rolling-resistance compared to the changes in the tyre's structure. Nonetheless, for the tyre structure itself, the tyre's material(s) have the least level of design freedom, and hence less effective, compared to tyre's body construction and dimensional aspects.

In the tyre's construction, the radial-ply construction brought a large immediate improvement to rolling-resistance in which it was ~20-30% lower in rolling-resistance compared to the old bias-ply construction depending on the operating conditions [82]. The subsequent developments to the tyre's construction were minor ones done on a gradual basis as it usually consumes a lot of time, costs and efforts due to tyre complexity. Among the common improvements to rolling-resistance are the reduction and re-distribution of mass in the tyre's construction and the usage of non-pneumatic tyres (Air-free). However, the current designs of non-pneumatic tyres are not as competitive as the pneumatic tyres in carrying out conventional vehicle(s)' operations.

For the tyre's dimensional aspects, there are infinite possibilities for configuring the dimensional parameters to affect rolling-resistance. One dimensional parameter that has an evident, notable and consistent impact on rolling-resistance is the tyre's outer diameter. A new promising concept that could lower the trade-off between low and high tyre profile characteristics is a "tyre with dynamically changing profile". Despite being in its very early stage of development with no practical application yet, this concept offers a potential opportunity for research that, if it is successful, would be much better in addressing the conflicting requirements of the tyre than the fixed/permanent changes to the tyre's profile. Based on the operating conditions, a rolling-resistance difference of ~10-20% can be found between the use of low and high tyre profiles (i.e. aspect ratio) [82].

The subject of tyre's materials is a prominent research field due to material hysteresis being the primary source (~95%) of rolling-resistance. However, it is unlikely to have significant developments in the near future as it has the least level of design freedom. Potential areas for future researches would be tread compounds, silica filler solution to natural-rubber and intelligent-materials for tyres.

To conclude, based on the extensive literature review done, the concept of "multi-chamber tyre" for low rolling-resistance is chosen as the research topic of this thesis. This is because this topic is a promising new research opportunity of little findings and no actual applications yet that can be a potential alternative solution to reducing rolling-resistance with marginal trade-offs especially for the current compromises between low and high profiles tyres. Furthermore, the necessary main resources to carry-out such research are available in terms of laboratory testing equipment and FE capabilities.

CHAPTER (3): MATERIAL PROPERTIES ACQUISITION

3.1 INTRODUCTION

To achieve this research project aim and objectives, the FE modelling of the targeted tyre(s) is necessary to save time and costs and to investigate the tyre with greater details. One of the fundamental and crucial inputs to the tyre FE model is the actual tyre material properties which are required in order to be able to simulate the real-like mechanical response of the tyre for given contact conditions.

This chapter shows the complete process followed to capture the required material properties from extracting the material samples from the actual tyre for experimental testing up to calculating the material coefficients and the reinforcement's lay-up needed as the material property input for the FE model. The overall process is summarised and indicated in Figure 3.1 below.

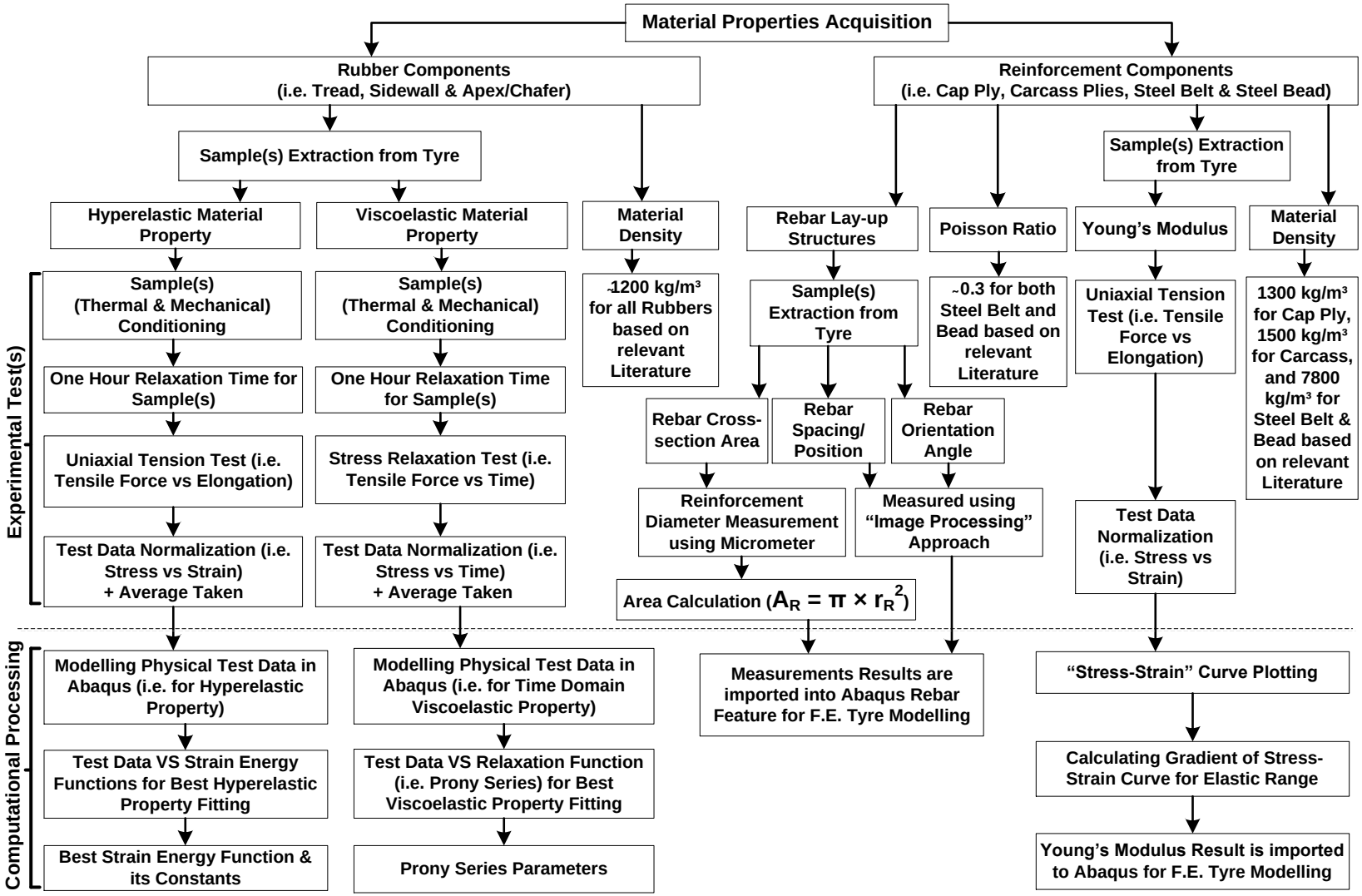


Figure 3.1 Acquisition Approach for Material Properties

A conventional passenger-car tyre of 225/55 R17 size is chosen as the baseline tyre to be investigated and structurally improved for this research project which is of adequate internal cavity space to accommodate the multi-chamber solution, flexible sidewalls, lightweight, and good fuel efficiency of “B” class according to EU (1222/2009) regulation. Hereafter, this tyre is to be called the “standard” tyre. At a later stage of this research project, the standard tyre is modified to accommodate an internal cavity chamber becoming a “dual chamber” tyre, as seen in Figure 3.2, which is used to validate the tyre FE modelling further. An inner-chamber housing with an internal tube is used. The housing is used to hold-in the internal tube and give the inner-chamber its profile shape whereas the inner tube is used to seal and keep the inflation air inside the inner-chamber.

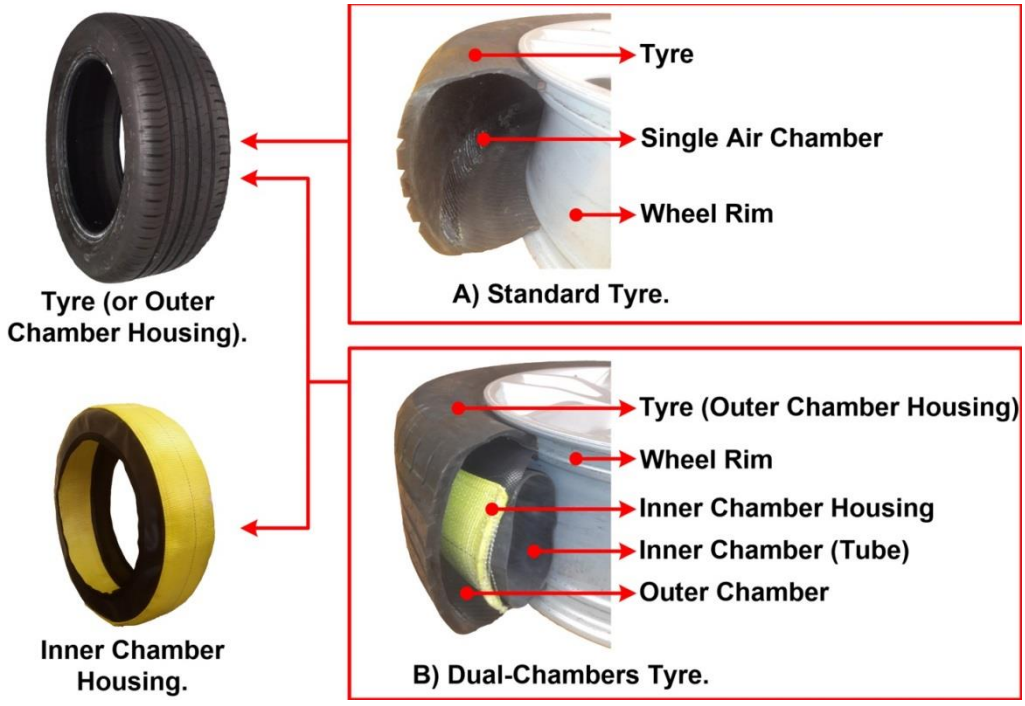


Figure 3.2 “Standard” and “Dual Chamber” Tyres [30]

Due to industrial confidentiality, neither the material properties nor the material specimens of the investigated tyre were readily available from the tyre manufacturer in which it had to be obtained through reverse engineering. To facilitate that, in accordance with ASTM D412-15a [181], ISO 4664-1 [182], ASTM D885/D885M [183] and other scholarly works [5, 7], the required material samples were extracted manually from an actual tyre product identical to that of the investigated tyre as shown in Figure 3.3. During extraction, care has been taken to ensure that at least three samples of each tyre component are obtained, which are of similar size, to ensure collected data precision (i.e. repeatability). Also, for the rubber components, the samples were to be straight and rectangular strips with its length at least ten times its width to ensure reliable results given the deformation mode to be subject to (i.e. tension) and the type of testing machine to be tested on (i.e. large, power-driven and constant-rate-of-extension operation).

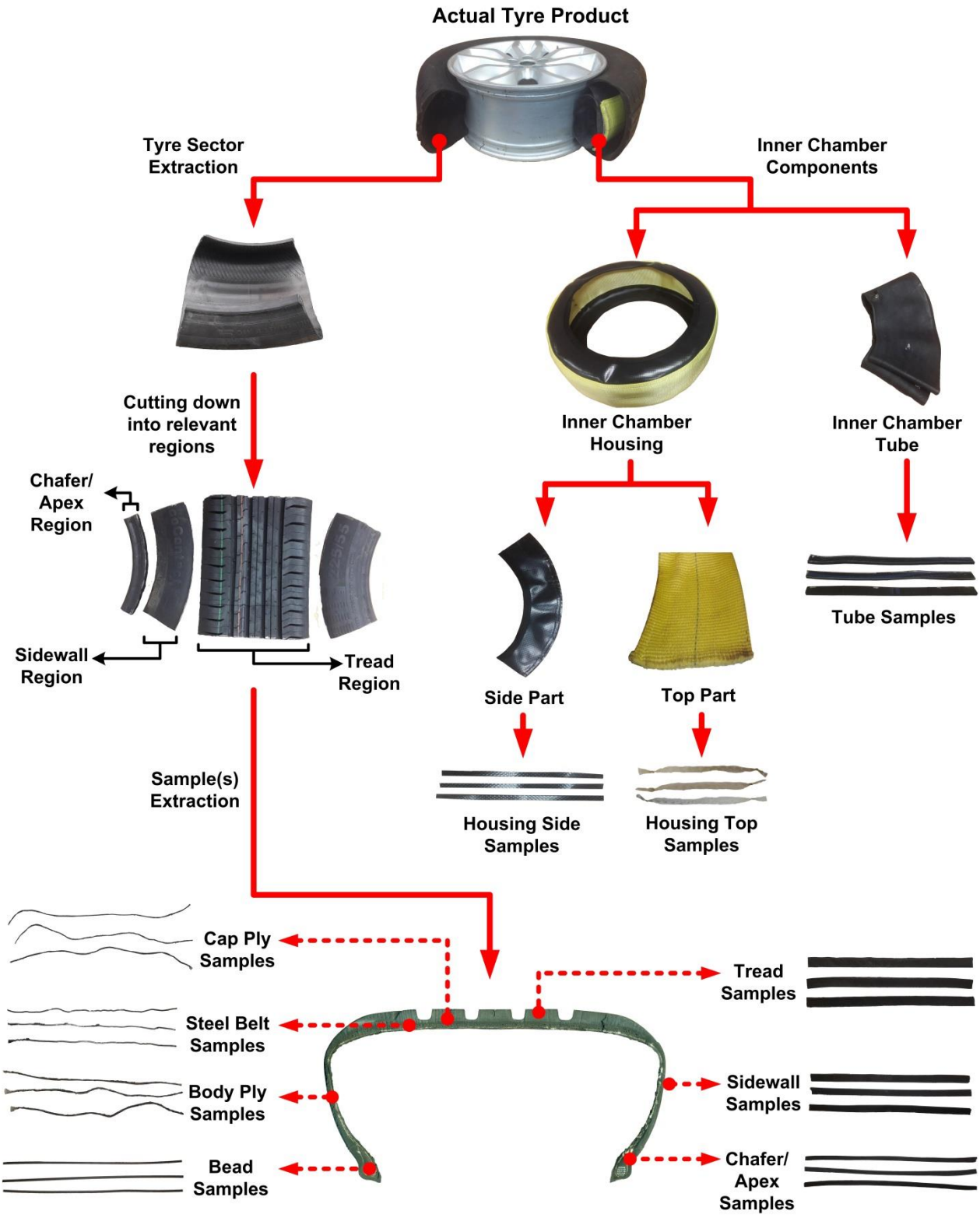


Figure 3.3 Material Sample(s) Extraction from Investigated Tyre(s)

As shown in Figure 3.3, fundamentally, the tyre is made-up of complex rubber and reinforcement components. To model the mechanical response of the tyre using FE, the hyperelastic and viscoelastic properties of the rubber components are needed to be considered along with the elastic properties of the reinforcement components [5, 7, 184, 185]. This is to be able to simulate the non-destructive and reversible deformation behaviour under quasi-static and dynamic conditions which are the scope of this research project.

The acquisition of the relevant material properties for both “standard” and “dual chamber” tyres is covered in this chapter. A third empirical tyre prototype, called “prototype 0.5”, made of five inner-chambers, which is used to additionally validate the author’s FE approach of modelling multi-chamber tyre(s), is not covered in this chapter. This is because of confidentiality reasons since it is a prototype designed and made by an external third party (i.e. Fusion Innovation) [140, 186]. However, the process followed by the author to gain the necessary material properties for the FE input for this prototype is similar to that covered in this chapter.

The material acquisition work done by the author in this chapter, as the main owner and contributor, was published as per a publication plan for this research project work. The related publications can be referred to through [29, 30, 187].

3.2 DATA ACCURACY AND PRECISION

With any experimental work, there is always bound to be both systematic and random errors during data collection. Nevertheless, good experimental equipment and practice can minimise those errors to within negligible levels [188]. In this research, for material testing, the systematic errors are addressed by ensuring to have measuring equipment of proper accuracy, performing the necessary calibration work to the equipment, and conducting the experimental measurement work altogether as per the international testing standards. For example, for rubber material testing, two RLT z-load cells are used of 50 N and 500 N load capacities respectively with a full-scale accuracy of 0.03% for both. Those load cells were calibrated using standard weights in accordance with ASTM E4-16 standard [189]. To evaluate the cells' accuracy, the load cells were used to perform the exact material testing as that intended for the actual main work, detailed in the next sections, following the relevant testing standards in which the reading error was calculated from the obtained experimental data using Eq. (3.1) and evaluated against ASTM D412-15a standard [181].

$$\text{Reading Error } (\%) = \frac{(\text{Full Scale Error (FS)}) \times (\text{Load Cell Capacity})}{\text{Force Measurement}} \times 100 \qquad (3.1)$$

An example of such reading error evaluation is Figure 3.4 for the 500 N load cell readings of a tread sample and Figure 3.5 for the 50 N load cell readings of each of a sidewall sample and an apex/chafer sample.

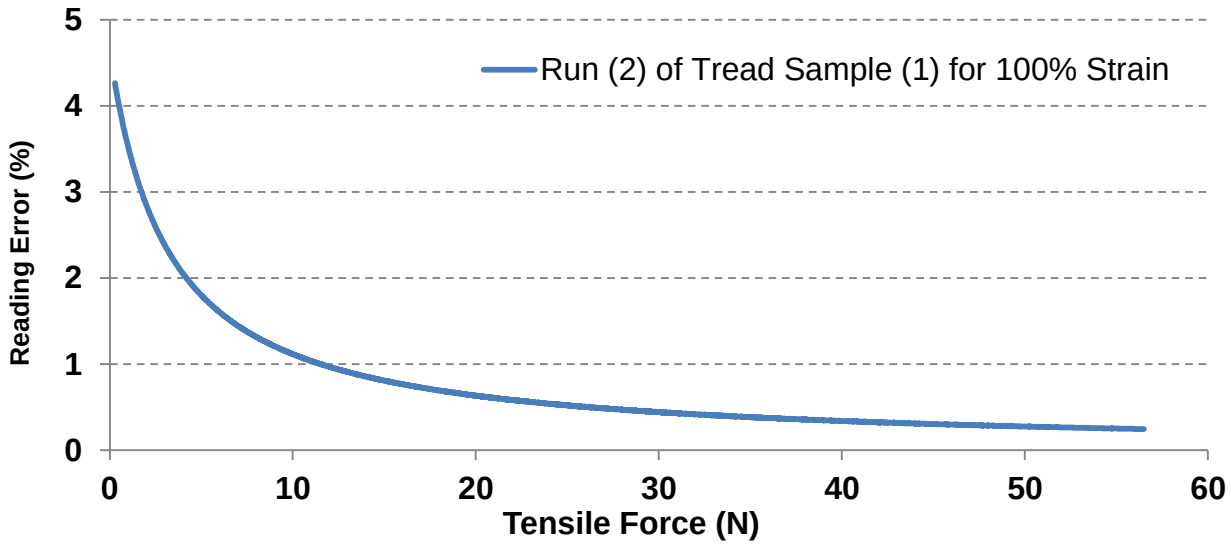


Figure 3.4 Reading Error (%) for a Tensile Test using 500 N Load Cell

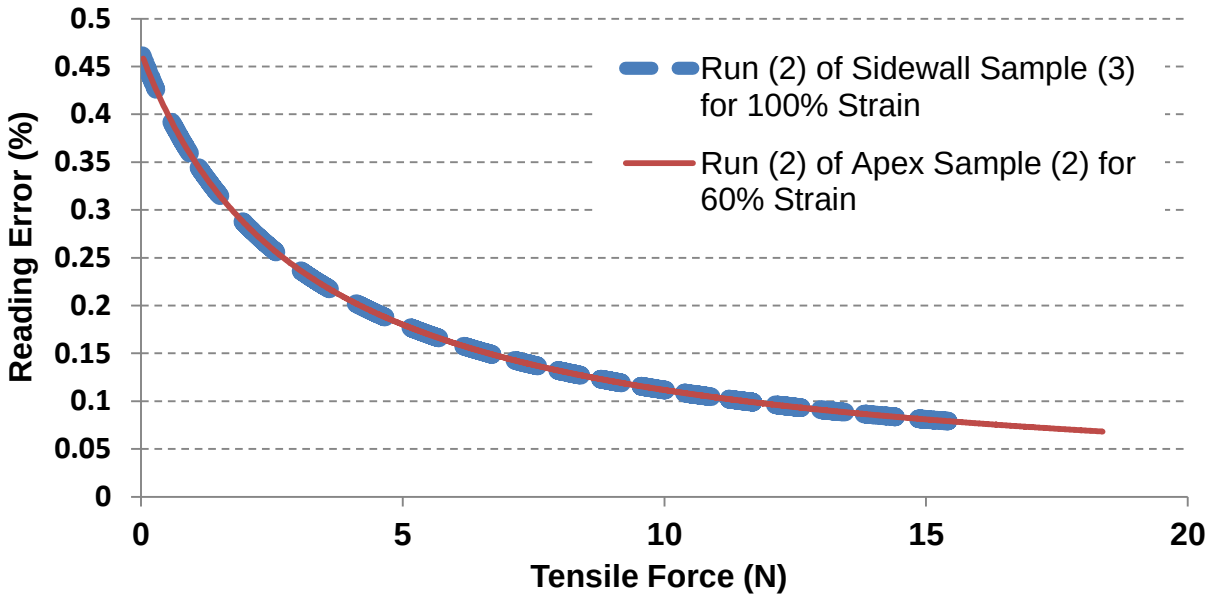


Figure 3.5 Reading Error (%) for a Tensile Test using 50 N Load Cell

According to ASTM D412-15a and ISO 5893 standards, in Figure 3.4 and Figure 3.5, both the 50 N and the 500 N load cells show proper measuring accuracy for all tyre

samples. This is because the reading error at the smallest force is far below the allowable error limit of 10% while the remainder of the error trend is below 2% which is the allowable limit for at least between 20% and 100% of the force measurement range [181, 190].

As for random errors, several practices were followed to improve data reading precision. Foremost, the same experimental measurement was repeated several times and an averaged value of all the measurements done was taken as the final reading. This was done by having at least three similar samples of each tyre component (i.e. tread, sidewall, and apex/chafer), testing each of those samples at least three times for the same measurement, and then taking the average for all the measurements done for all the samples of each tyre part [191]. Another practice was to apply consistent testing procedures as per the relevant testing standards under the same testing conditions. Furthermore, the extracted material samples for each tyre component were shaped and sized similar to each other following ASTM D412-15a standard and other scholarly works [5, 7].

To assess the measurement precision or level of random errors, uncertainty analysis of all the same repeated measurements was performed by calculating the standard deviation of those measurements from their mean value. An example of such analysis is the relative uncertainty calculated in Figure 3.6 using Eq. (3.2) for all the measurement runs of each tyre component [192].

$$\text{Relative Uncertainty (\%)} = \frac{\text{Uncertainty}}{\text{Mean Measure}} \times 100 = \frac{\text{Standard Deviation}}{\text{Mean Force}} \times 100 \qquad (3.2)$$

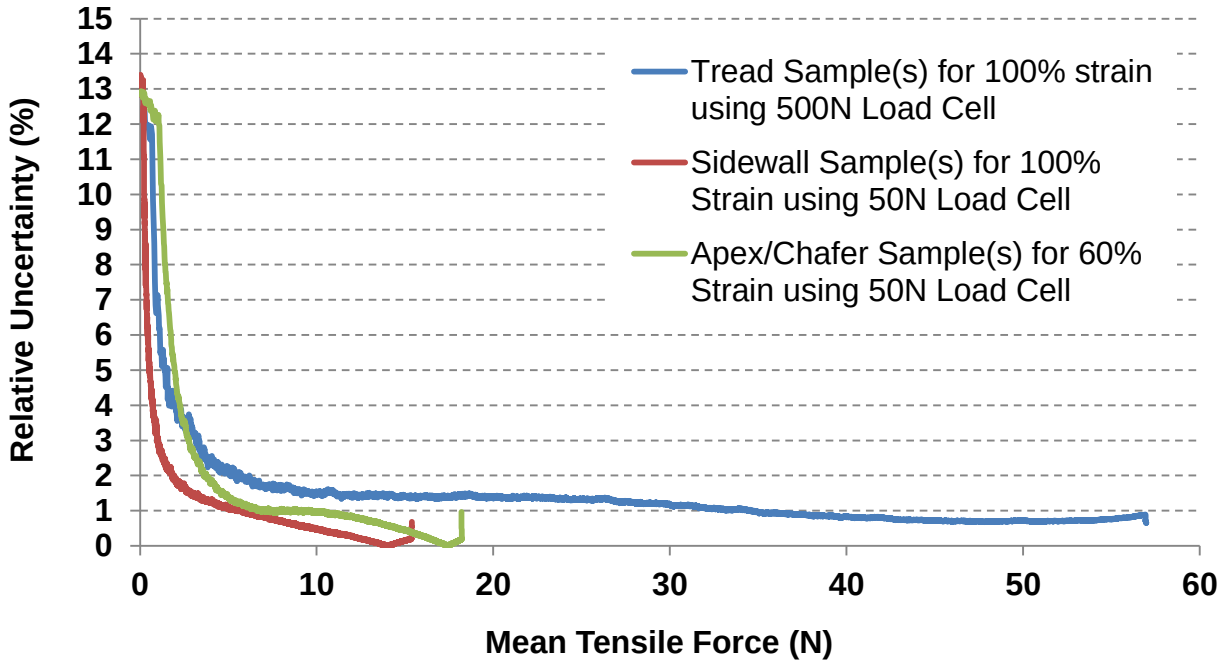


Figure 3.6 Relative Uncertainty Analysis

According to ISO 5893 and 7500-1 standards, the experimental measurement work done on tyre rubber materials has an acceptable random error level since its relative uncertainty falls below 2% which is the maximum allowable level of the relative repeatability error for at least between 20% and 100% of the force measurement range [190, 193].

3.3 RUBBER COMPONENTS

Due to the limited resources available and the difficulty involved in extracting the required material samples, only the core rubber components of the tyre, which constitute the tyre behaviour, were possible to extract and they are the tread, the sidewall and the apex/chafer as seen in Figure 3.3. This is in addition to the tube of the inner chamber of the tyre.

3.3.1 Hyperelasticity

The hyperelasticity property represents the elastic response (i.e. energy restored) of the viscoelastic rubber [194]. It describes the time-independent, instantaneous, non-linear and elastic deformational behaviour of rubber for finite-strain applications especially large strains [42, 194, 195]. This behaviour is accompanied with the consideration of rubber as an isotropic and nearly incompressible material. The rubber is approximated as an isotropic since almost the same mechanical properties are observed regardless of the orientation at its un-deformed state, small deformations and under monotonic loadings [185, 194, 195]. As for the incompressibility, this is due to the rubber exhibition of negligible volumetric changes during deformation as its bulk modulus is 10,000-100,000 greater than its Young and shear moduli [42, 195, 196]. There are certain cases where the rubber behaviour can be primarily described by hyperelasticity alone like quasi-static loadings and shorter under-loading intervals where the dissipative input is insignificant [42, 185].

To capture the real tyre elastic response, the nominal stress-strain experimental data were obtained for the different rubber components (i.e. tread, sidewall, apex/chafer and inner chamber tube) through conducting a simple uniaxial tensile test at 100% strain level using an Instron universal testing machine with sensitive Z-load cells as shown in Figure 3.7. This is except for the apex/chafer sample which was required to be stretched to just 60% since it is less flexible and harder than the other samples to fulfil its role of stabilising the structure around the tyre's bead.

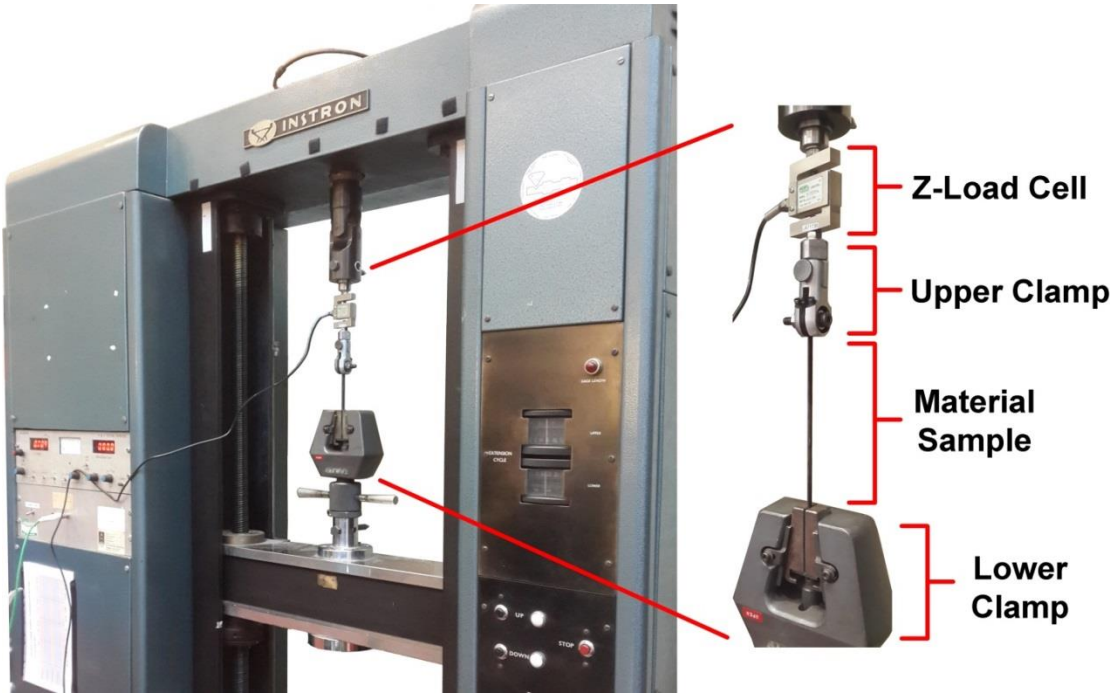


Figure 3.7 Instron Testing Machine with Z-Load Cell

According to both ASTM D412−15a [181] and ISO 23529 [197], first, the prepared material samples were thermal conditioned at their loose state at a test temperature of 23 ± 2 °C for at least three hours to reach thermal equilibrium close to that of common

practice. After thermal conditioning, the material samples were mechanically conditioned to remove “stress softening” (i.e. Mullins effect) in order to obtain consistent, reproducible and equilibrium stress-strain results [195, 198]. In the mechanical conditioning, the rubber samples were stretched to 100% strain at 50 mm/min for ten loading/unloading cycles in line with Yang [5] and Wei [7]. This is with exception of having the apex/chafer conditioned at 60% strain instead of 100% strain. After each full loading/unloading cycle, the rubber samples were left to relax for at least ten times the preceding loading period before starting the next loading/unloading cycle to allow for complete recovery from the viscoelastic effects [198]. Once the mechanical conditioning is done, the rubber samples were removed from the testing machine’s clamps and left to relax for one hour [5].

For the main test, the rubber samples were stretched to 100% strain (i.e. 60% for apex/chafer) at 50 mm/min and 23 ± 2 °C while recording force-displacement data using Z-load cells of 500N for the tread samples and 50N for the sidewall, apex/chafer and inner chamber tube samples. For each sample, this process was repeated at least three times and an average was taken out of the collected data to ensure precise measurement. During such a process, after each loading/unloading cycle, the samples were left to relax for at least ten times the preceding loading period. After the main test, as per ISO 37 [191], the collected data were finalised by converting the measured force to the nominal stress using Eq. (3.3) and the elongation to the nominal strain using Eq. (3.4).

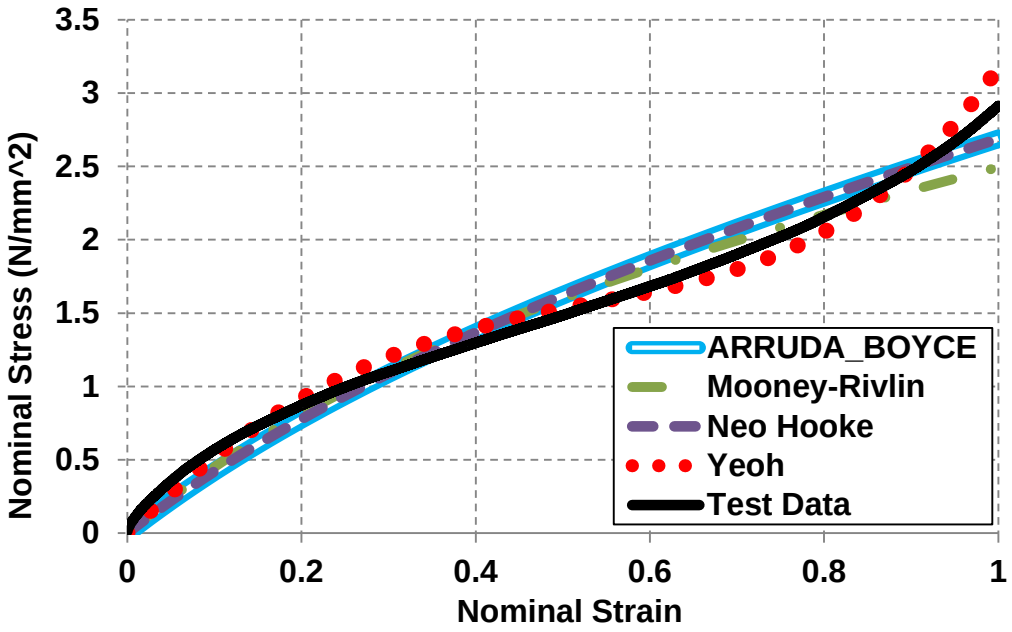
$$\sigma = F_T/A_0 \tag{3.3}$$

$$\varepsilon = \delta/L_0 \tag{3.4}$$

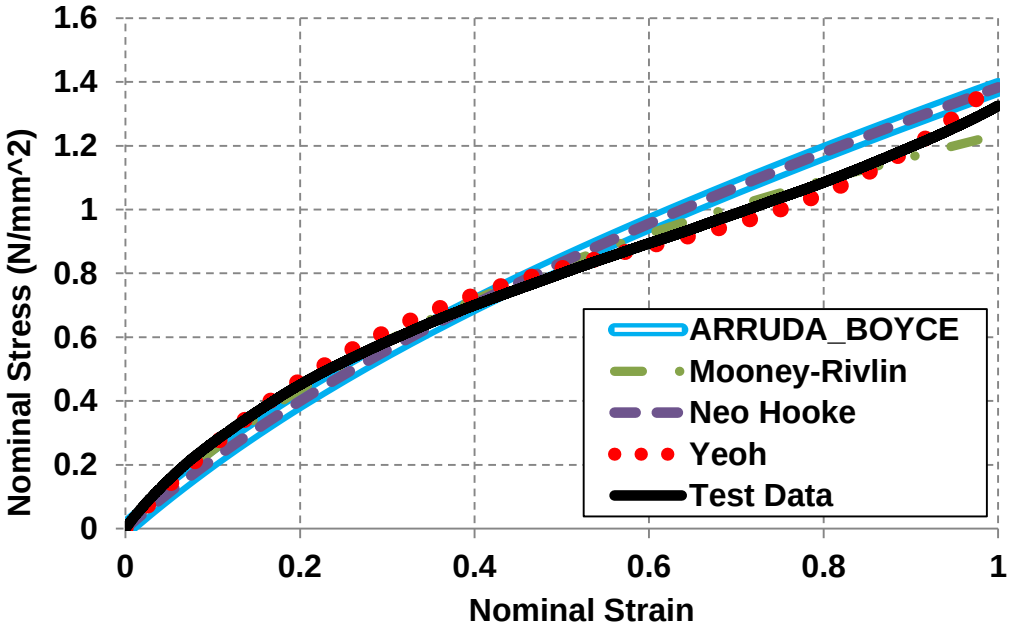
To represent the rubber hyperelasticity of the tyre in FE, several potential strain energy functions were computed and evaluated through “least-squares curve-fitting” against the obtained experimental stress-strain data using the material evaluation option available in Abaqus 6.13-1. During the fitting, the “relative error” (E_R) in nominal stress responses between the potential hyperelastic function(s) and the experimental data is assessed in which the best fit function would have the least relative error [194, 195]:

$$E_R = \sum_{i=1}^{n} (1 - T_i^{th} / T_i^{test})^2 \tag{3.5}$$

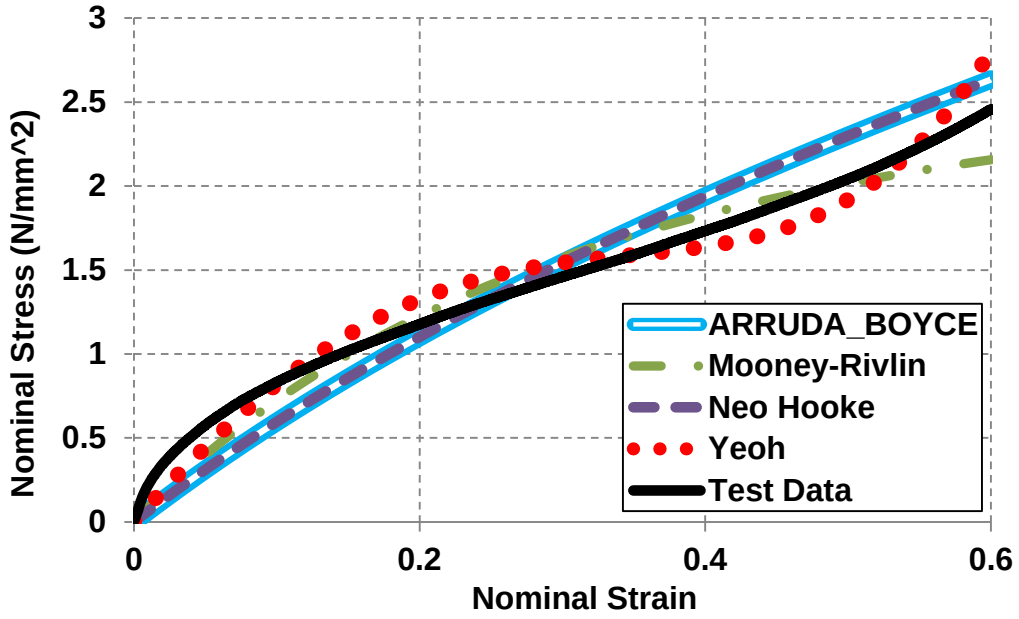
Using Abaqus, several stress-strain response curves were produced using the potential strain energy functions against the test data to determine the best fit function as seen in Figure 3.8 for each rubber component:


3.5
3
2.5
2
1.5
1
0.5
0
0
0.2
0.4
0.6
0.8
1
Nominal Stress (N/mm^2)
Nominal Strain
ARRUDA_BOYCE
Mooney-Rivlin
Neo Hooke
Yeoh
Test Data

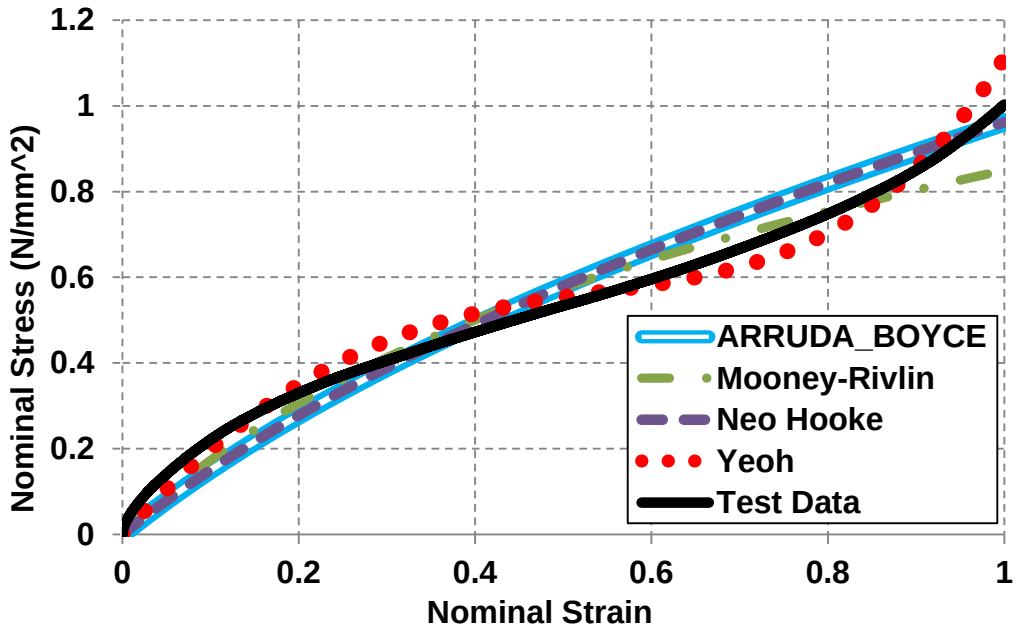
(a)


1.6
1.4
1.2
1
0.8
0.6
0.4
0.2
0
0
0.2
0.4
0.6
0.8
1
Nominal Stress (N/mm^2)
Nominal Strain
ARRUDA_BOYCE
Mooney-Rivlin
Neo Hooke
Yeoh
Test Data

(b)



(c)



(d)

Figure 3.8 Fitting of Various Strain Energy Functions against Experimental Data for (a) Tread, (b) Sidewall, (c) Apex/Chafer, and (d) Inner Chamber Tube

According to Drucker stability criterion [194] and the fitting error in Figure 3.8, Yeoh material model is chosen as the best function to represent the hyperelasticity over the other functions for all the rubber components. This is because Yeoh function is found to have a close data-fit, applicable with the other deformational modes, and have low testing cost. Yeoh is a phenomenological constitutive model, based on continuum mechanics, of a reduced polynomial form of the following cubic strain energy function of the first deviatoric strain invariants [7, 194, 195]:

$$U_Y = C_{10}(\bar{I_1} - 3) + C_{20}(\bar{I_1} - 3)^2 + C_{30}(\bar{I_1} - 3)^3 + \frac{1}{D_1}(J^{el} - 1)^2 + \frac{1}{D_2}(J^{el} - 1)^4 + \frac{1}{D_3}(J^{el} - 1)^6 \quad (3.6)$$

So, from Abaqus, the following long-term Yeoh hyperelastic material coefficients were obtained in Table 3.1:

Table 3.1 Yeoh Coefficients for Rubber Components

Rubber Part	**Yeoh Model Parameters**		
	C10	**C20**	**C30**
Tread	0.964	-0.285	0.0901
Sidewall	0.480	-0.105	0.0286
Apex/Chafer	1.57	-1.38	0.923
Inner chamber Tube	0.370	-0.125	0.0374

To account for incompressibility, the rubber was redefined as nearly incompressible, not as fully incompressible, for the FE code to work efficiently especially the Abaqus/Explicit [42, 194]. For this reason, the "D_1" coefficient, that governs the compressibility, was changed from being fully incompressible (i.e. D_1=0) to a non-zero value by setting the rubber's Poisson ratio to be just below 0.5 for a nearly incompressible option [194]:

$$\mathrm{D_1} = \frac{2}{\mathrm{K_0}} = \frac{3\,(1-2\mathrm{v_p})}{\mu_0(1+\mathrm{v_p})} \tag{3.7}$$

Where,

$\mu_0 = 2\mathrm{C_{10}} =$ Initial Shear Modulus.

Here, the Poisson ratio (v_p) was approximated as 0.49 based on the common range for the filled vulcanised rubbers in the literature [199-201]. This would give the following "D_1" coefficients for the different rubber components in Table 3.2:

Table 3.2 Yeoh "D_1" Coefficients for Tyre Rubbers

Rubber Part	**Yeoh Model "D_1" Parameters**
Tread	0.0209
Sidewall	0.0419
Apex/Chafer	0.0128
Inner chamber Tube	0.0544

3.3.2 Viscoelasticity

Viscoelasticity is the delayed (strain) response to stress change due to rubber's viscosity (hysteresis) in terms of material resistance to deformation (i.e. contact and breakdown of molecules chain entanglements under loading) in the form of heat dissipation [42, 185, 195]. In other words, it is the time-dependent stress-strain behaviour under loading/unloading conditions that is responsible for phenomena like stress-relaxation and creep [5, 42, 195]. Due to hysteresis, unlike hyperelasticity, the loading and unloading stress-strain routes take dissimilar trails from each other [185]. Under real-world loading situations, rubber exhibits considerable viscoelasticity [42, 80]. Therefore, for more realistic FE modelling of the tyre, especially Rolling-Resistance, the viscoelasticity is crucial along with hyperelasticity [7, 40, 185, 195].

In practice, the tyre's rubber viscoelasticity is highly non-linear. Therefore, for this research project, a non-linear viscoelastic function (i.e. PRF) is used in FE modelling to represent the tyre's viscoelasticity. However, the approach used to obtain the non-linear viscoelastic function involves the usage of the linear viscoelastic function (i.e. prony series) as a starting benchmark to calibrate and compute the non-linear viscoelastic model coefficient as will be seen in details in the next few sections.

3.3.2.1 Linear Viscoelasticity

For linear viscoelasticity, Abaqus uses the prony series function to evaluate and model the time-domain viscoelastic material property. To calculate prony series coefficients, a "stress-relaxation test" was conducted for the same rubber samples used in

hyperelasticity property utilising the same test machine in Figure 3.7. Prior to the main test, the rubber samples were thermally and mechanically conditioned then left to rest similar to the way it was done for the hyperelastic property. For the relaxation test, according to ASTM E328−13 [202], ISO 6914 [203] and Yang [5], each sample was uniaxially stretched at 100 mm/min to a strain level of 50% of sample's original length and held fixed at that position for 2000 seconds at 23 ± 2 °C during which the force change over that time was recorded. After the test is completed, the recorded force is converted to nominal stress using Eq. (3.3) as in the hyperelastic property test. Such a relaxation test was repeated three times for each sample and the stress-relaxation data collected were averaged.

To import the experimental data to Abaqus for material model fitting, the recorded "stress-relaxation data" ($\sigma(\mathrm{t})$) was converted into "normalised shear relaxation moduli" ($g(t)$) using the following equations, for small strains, respectively [204]:

$$\mathrm{E(t)} = \frac{\mathrm{F_T(t)/A_0}}{\varepsilon} = \frac{\sigma(\mathrm{t})}{\varepsilon} \tag{3.8}$$

$$\mathrm{G(t)} = \frac{\mathrm{E(t)}}{2(1+\mathrm{v_p})} \tag{3.9}$$

$$g(t) = \frac{\mathrm{G(t)}}{\mathrm{G(0)}} \tag{3.10}$$

A further term needed for Abaqus material evaluation is the “normalised long-term shear relaxation modulus” ($g(\infty)$). This term was determined through conducting an independent “non-linear least-squares-fit regression” analysis from that of Abaqus. The independent regression analysis was used to compute and build-up the following ($\mathrm{E_m(t)}$) material model to fit the Young modulus ($\mathrm{E_{Exp}(t)}$) obtained from the experimental stress data [205]:

$$\mathrm{E_m(t)} = \mathrm{E_\infty} + \sum_{\mathrm{i=1}}^{\mathrm{N}} \mathrm{E_i e^{-t/\tau_i}} \tag{3.11}$$

This is in order to determine the ($\mathrm{E_\infty}$) and from which then to determine the ($g(\infty)$) through using Eq. (3.9) to calculate ($\mathrm{G}(\infty)$) and ($\mathrm{G}(0)$) separately and then Eq. (3.10) to calculate ($g(\infty)$). To proceed with Abaqus, the experimental data in terms of the “normalised shear relaxation moduli” (($g(\infty) = \mathrm{G}(\infty)/\mathrm{G}(0)) \leq g(t) \leq (g(0) = 1)$) and the relaxation time ($0 < \mathrm{t} < \infty$) along with the computed “long-term normalised shear relaxation modulus” ($g(\infty)$) were imported into Abaqus material evaluation tool. The previous hyperelastic material data were imported too in conjunction with the viscoelastic data as its elastic response. As a final set-up for a good material-fitting, the allowable average root-mean-square error was set at ~ 0.001 and the maximum number of prony series terms (N) was set at $\leq \mathrm{logarithmic\ decades} = \log_{10}(\mathrm{t_{max}}/\mathrm{t_{min}})$, where ($\mathrm{t_{max}}$) and ($\mathrm{t_{min}}$) are the maximum and minimum experimental test time respectively [195, 204].

Having the required input data, Abaqus evaluation tool was used to calculate and fit the "prony series expansion of the dimensionless relaxation modulus" in Eq. (3.12) against the experimental data using a non-linear least-squares-fit procedure to reduce the fitting error and reach convergence with the lowest (N) possible within the given error tolerance [204]:

$$g(t) = 1 - \sum_{\mathrm{i}=1}^{\mathrm{N}} \overline{g_\iota}(1 - \mathrm{e}^{-\mathrm{t}/\tau_\mathrm{i}}) \tag{3.12}$$

The computed prony series coefficients ($\overline{g_\iota}$, τ_i) are given in Table 3.3 for all the rubber samples:

Table 3.3 Prony Coefficients for Tyre Rubbers

Rubber Part	**Prony Model Parameters**							
	$\overline{g_1}$	τ_1	$\overline{g_2}$	τ_2	$\overline{g_3}$	τ_3	$\overline{g_4}$	τ_4
Tread	0.0328	12.58	0.0358	88.42	0.0370	651.45		
Sidewall	0.0445	56.69	0.0352	932.71				
Apex	0.0298	11.48	0.0381	88.34	0.0394	781.59		
Inner chamber Tube	0.0488	0.87	0.0756	11.42	0.0740	70.51	0.0796	594.95

3.3.2.2 Non-Linear Viscoelasticity

As indicated earlier, the “Parallel Rheological Framework” approach is implemented to describe the tyre’s rubber non-linear viscoelasticity. For a non-destructive and recoverable deformation, the PRF function consists of a pure elastic network and several viscoelastic networks joined with each other in parallel as seen by Figure 3.9.

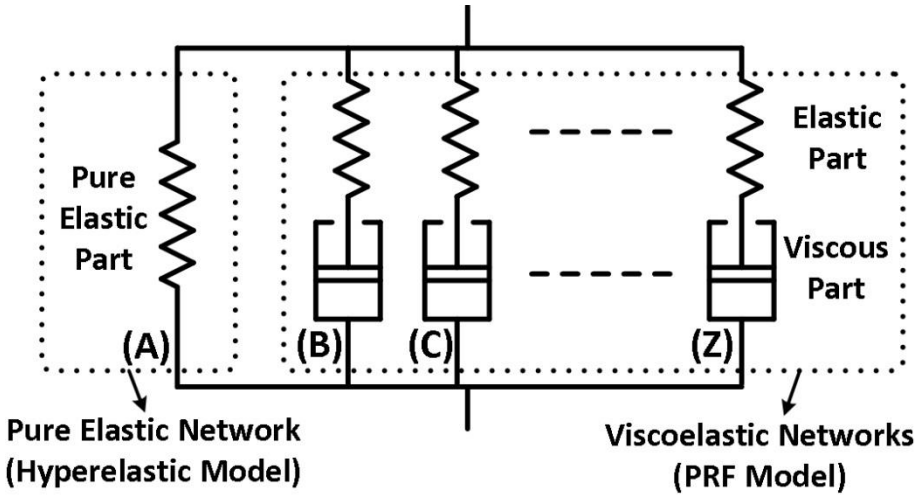


Figure 3.9 PRF Model [206]

The pure elastic network is described via the Yeoh hyperelastic function, developed in the previous section, to demonstrate the non-linear elastic response of the tyre and stop the stress from falling into complete relaxation in the PRF model. For the viscoelastic networks, the deformational response of each network is split into two parts; an “elastic” one and the other is “viscous”. The “elastic” section is determined using a scaled version of the same Yeoh hyperelastic function depending on each network’s stiffness level with respect to the overall material response. As for the “viscous” part, the viscosity is

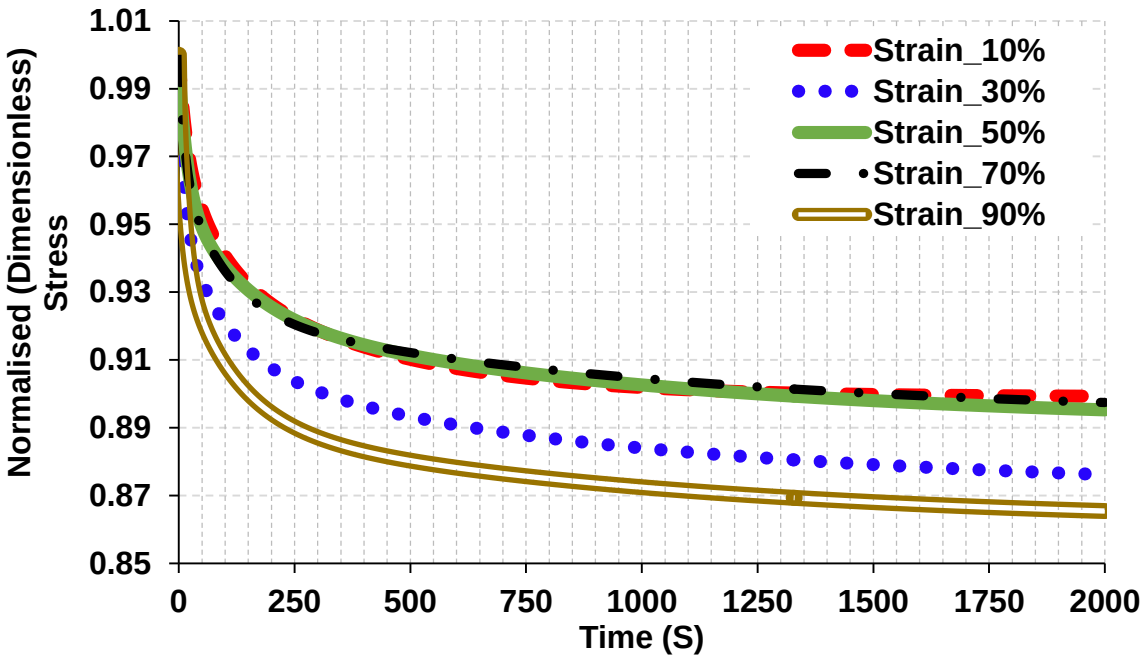
specified through both the “flow rule” in Eq. (3.13) and the “evolution law” represented by power-law strain hardening model in Eq. (3.14) below [206]:

$$D^{cr} = \frac{3}{2\bar{q}}\dot{\bar{\varepsilon}}^{cr}\bar{\sigma} = \frac{3}{2\tilde{q}}\dot{\bar{\varepsilon}}^{cr}\bar{T} \tag{3.13}$$

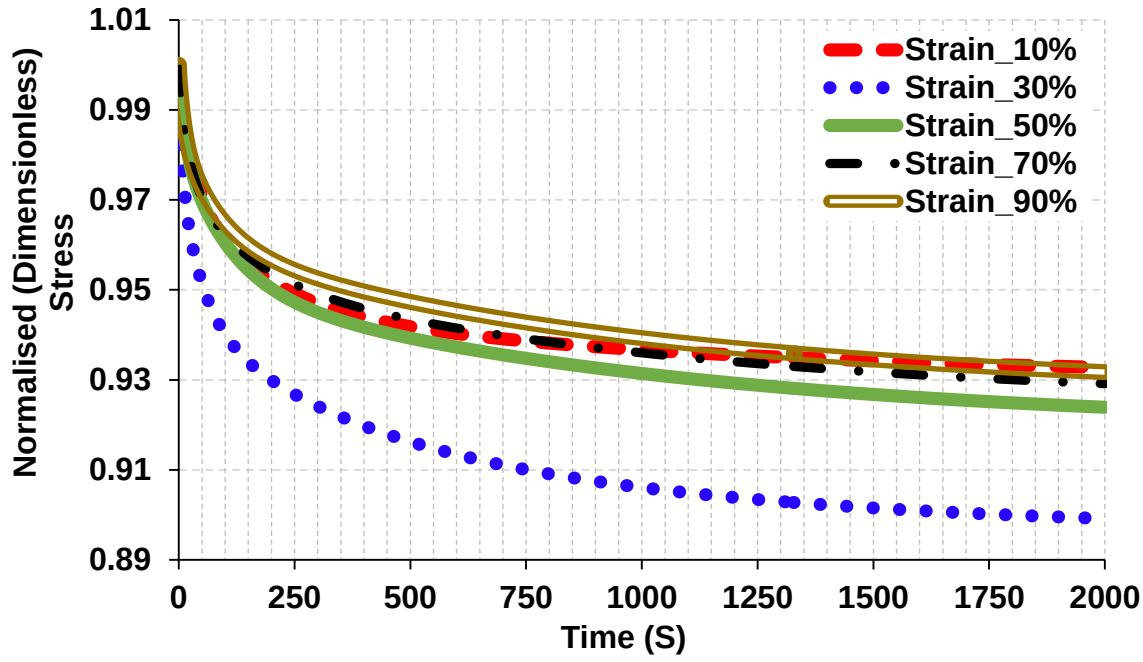
$$\dot{\bar{\varepsilon}}^{cr} = \left(A\tilde{q}^{n}[(m+1)\bar{\varepsilon}^{cr}]^{m}\right)^{\frac{1}{m+1}} \tag{3.14}$$

The PRF model coefficients were calibrated against a set of stress-relaxation experimental data for each rubber sample taken at different strain levels to account for the non-linearity. The same “stress-relaxation experimental test”, as that in section 3.3.2.1, was repeated for the same rubber samples but at different strain levels of 10%, 30%, 50%, 70% and 90% respectively for each of tread, sidewall and inner chamber tube samples whereas the Apex sample was tested at 10%, 30%, 40%, 50% and 60% strain levels respectively. Care was taken to allow enough rest time for the samples after each loading test before starting the next test (i.e. rest time = 10 x “previous loading time”) to avoid stress-softening effects [198].

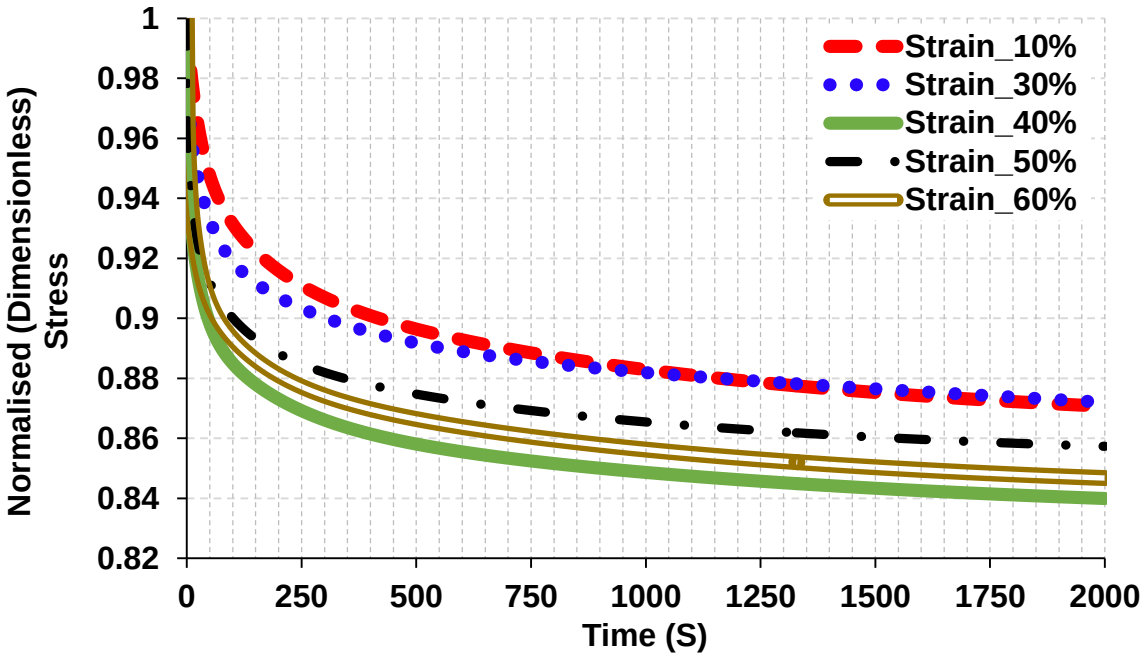
The obtained normalised stress-relaxation test data for all the rubber samples are shown in Figure 3.10. Based on the normalised experimental data, it is clear that each rubber sample is of non-linear viscoelasticity nature since its relaxation rate is not the same at different strains.


Normalised (Dimensionless) Stress
1.01
0.99
0.97
0.95
0.93
0.91
0.89
0.87
0.85
0
250
500
750
1000
1250
1500
1750
2000
Time (S)
Strain_10%
Strain_30%
Strain_50%
Strain_70%
Strain_90%

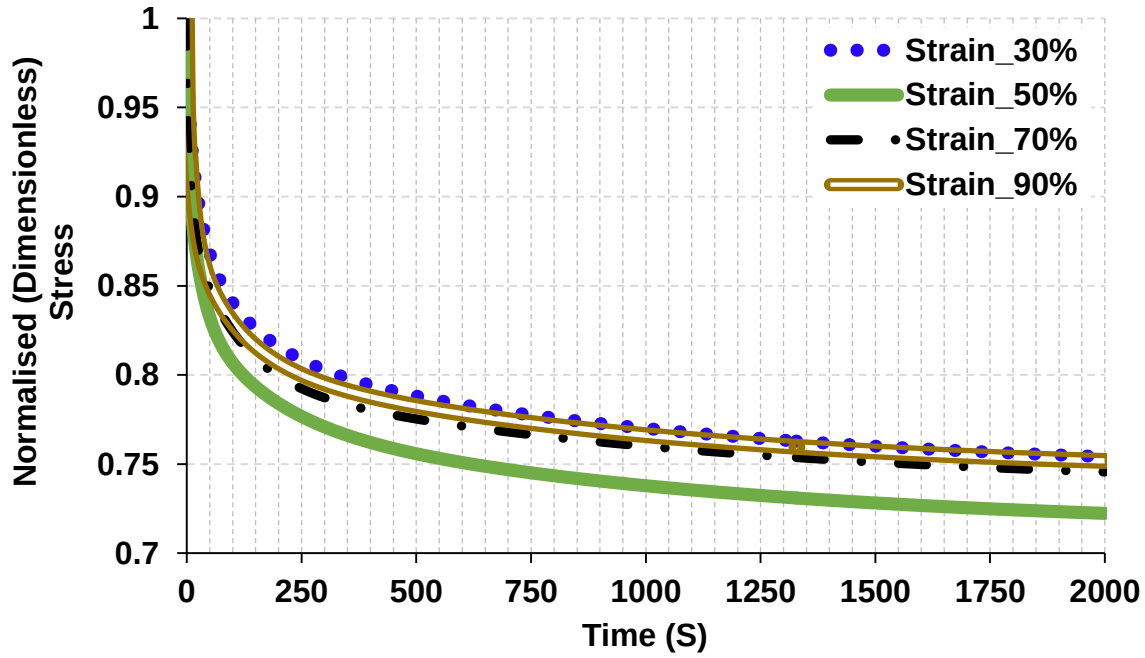
(a)


Normalised (Dimensionless) Stress
1.01
0.99
0.97
0.95
0.93
0.91
0.89
0
250
500
750
1000
1250
1500
1750
2000
Time (S)
Strain_10%
Strain_30%
Strain_50%
Strain_70%
Strain_90%

(b)



(c)



(d)

Figure 3.10 Normalised Stress Relaxation Test Data for (a) Tread, (b) Sidewall, (c) Apex/Chafer, and (d) Inner Chamber Tube

To fit the PRF model against the obtained experimental data, a calibration model was built using Isight 5.9.4, as seen in Figure 3.11, to optimise and re-compute the stiffness ratios (SR) of the viscoelastic networks, Yeoh hyperelastic coefficients (C_{i0}) in Eq. (3.6), and PRF model coefficients (A, n, and m) in Eq. (3.14) [40, 207].

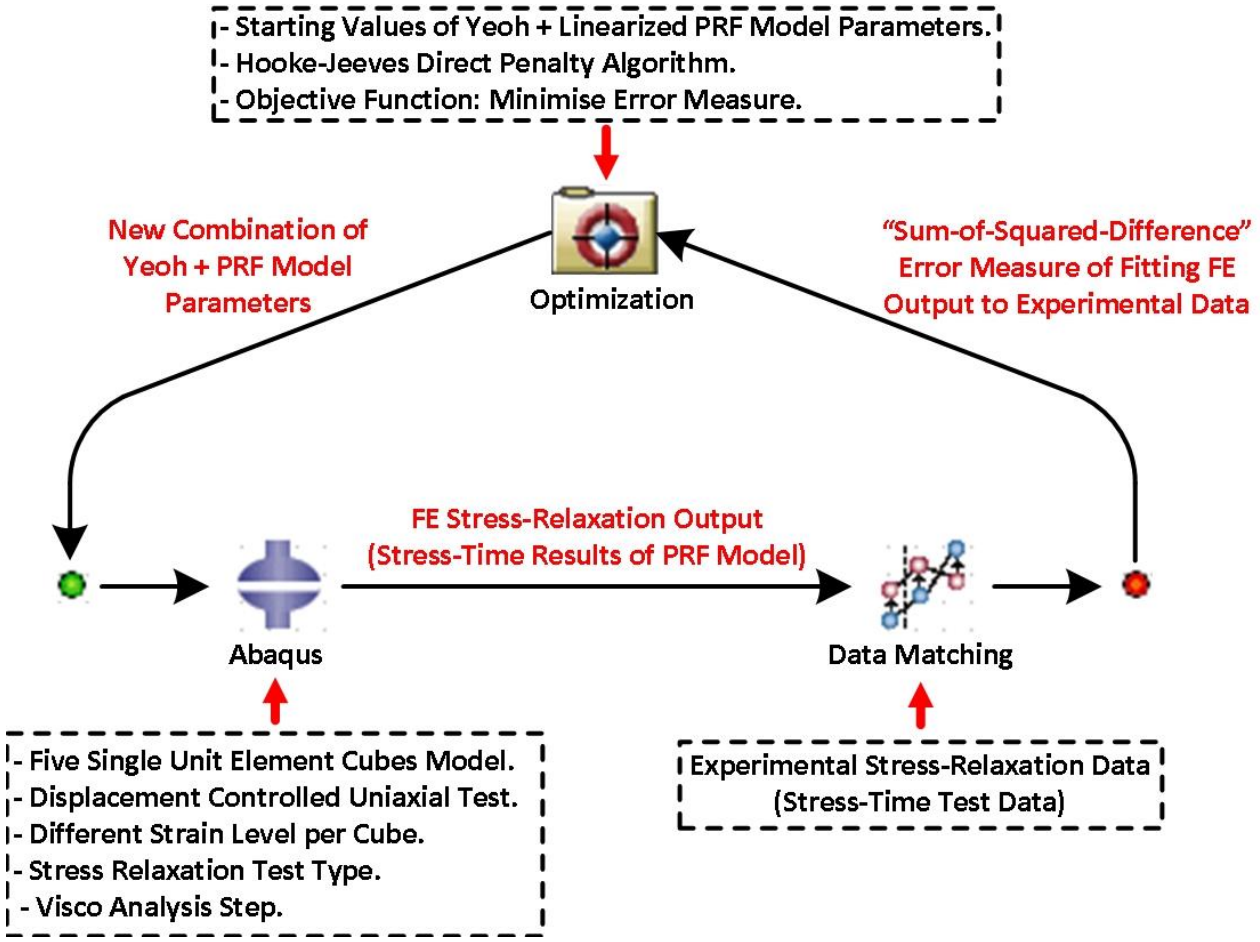


Figure 3.11 Isight Optimisation Model [29]

The Isight model set-up contained the following three components:

A) “Abaqus” Component:

This component contains an Abaqus FE model of five single unit element cubes as shown in Figure 3.12. Each cube represents a different strain level experienced by the rubber sample respectively corresponding to the experimental stress-relaxation test conducted. A single unit element cube is used instead of the real geometry of the rubber sample experimentally tested to reduce the computational costs greatly [208, 209]. The purpose of the Abaqus component in the Isight model is to use a given set of Yeoh and PRF coefficients as the “input variables” for the material property of the cubes to predict each cube’s stress-relaxation history as the “FE output variables” which to compare with the corresponding experimental data later.

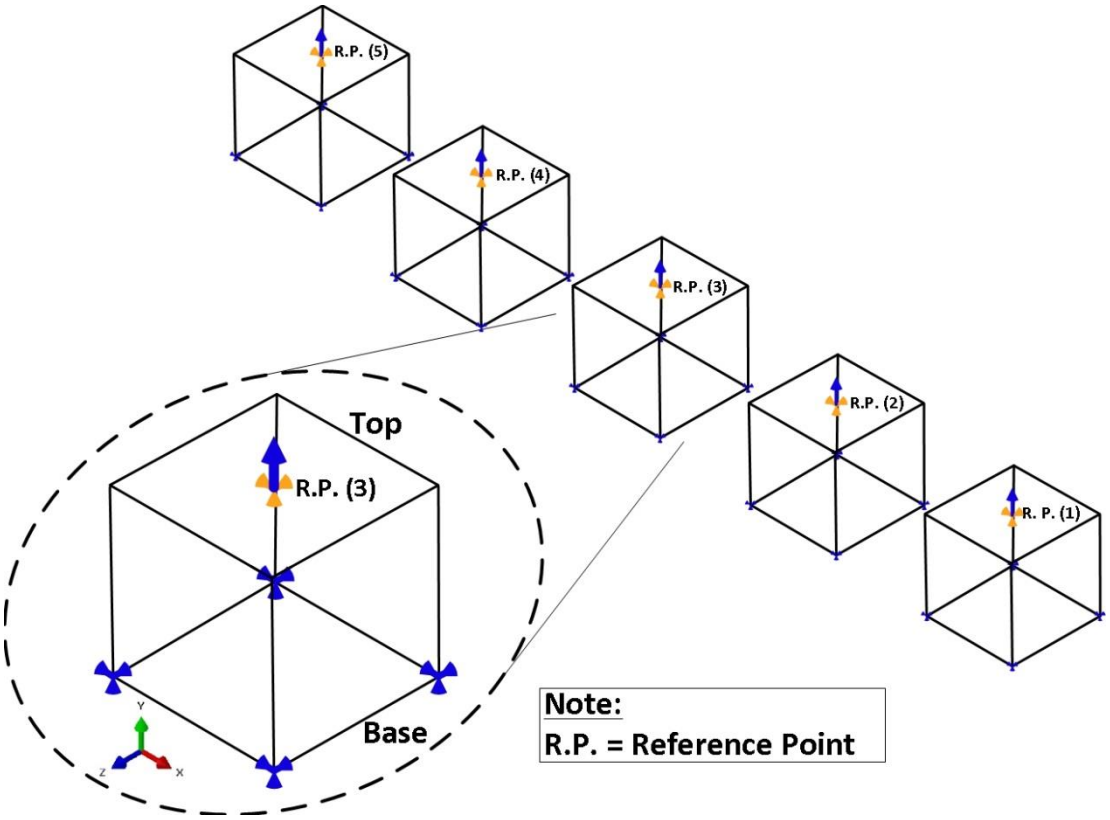


Figure 3.12 Single-Unit Element Cubes 3D FE Model

However, to begin the Isight optimisation process through Abaqus component, start-up values of the Yeoh and PRF coefficients are needed. For Yeoh coefficients, those were obtained from Table 3.1 in section 3.3.1 of rubber hyperelasticity property. As for the PRF coefficients, a linearised PRF version was possible to obtain from the prony series coefficients calculated previously in Table 3.3 using the following conversion equations [210]:

$$\mathrm{SR_i} = \mathrm{g_i} \tag{3.15}$$

$$A_i = \frac{1}{6 \times g_i \times \tau_i \times C10} \tag{3.16}$$

Whenever the PRF model is in the linear form, its material constants “m” and “n” are taken as m=0 and n=1 in Eq. (3.14). With that, the linearised PRF model coefficients were obtained for all the rubber samples and an example of that is shown in Table 3.4 for the tread sample below.

Table 3.4 Linearised PRF Model Parameters for Tread

Hyperelastic (Yeoh Model) Parameters		**Power Law Strain Hardening Linearised PRF Model Parameters**	
C10	0.964	m	0
		n	1
Linear Viscoelastic (Prony Series) Parameters		SR(i)=g(i)	
		A(i)=1/(6*g(i)* τ_i*C10)	
g1	0.0328	SR1	0.0328
τ_1	12.58	A1	0.419
g2	0.0358	SR2	0.0358
τ_2	88.42	A2	0.0545
g3	0.0370	SR3	0.0370
τ_3	651.45	A3	0.00717

Adopting the obtained linearised PRF coefficients for the viscoelastic model and Yeoh coefficients in Table 3.1 and Table 3.2 for the hyperelastic model as starting-up inputs, the set-up of the cube FE model was done in a way in which each cube was constrained at its base nodes with respect to the vertical direction and all the

rotational axes only. In addition, each cube's top nodes were structurally-distributed coupled with a reference point created at its top centre. Utilizing a "visco" analysis step, each cube was subjected to a uniaxial displacement-driven tension at its top reference point in the upward direction at different strain levels (e.g. 10%, 30%, 50%, 70% and 90%) respectively and held fixed at that strain-level for a simulation time of 2000 seconds. Since unit cubes are being used, the "force" outputs at each cube's reference point were treated as the "stress" outputs in the simulation. The "stress-time" results were requested at each cube's reference point as the model FE simulation outputs. An example of those FE outputs in comparison to the relevant stress-time experimental data is shown in Figure 3.13 for the tread sample.

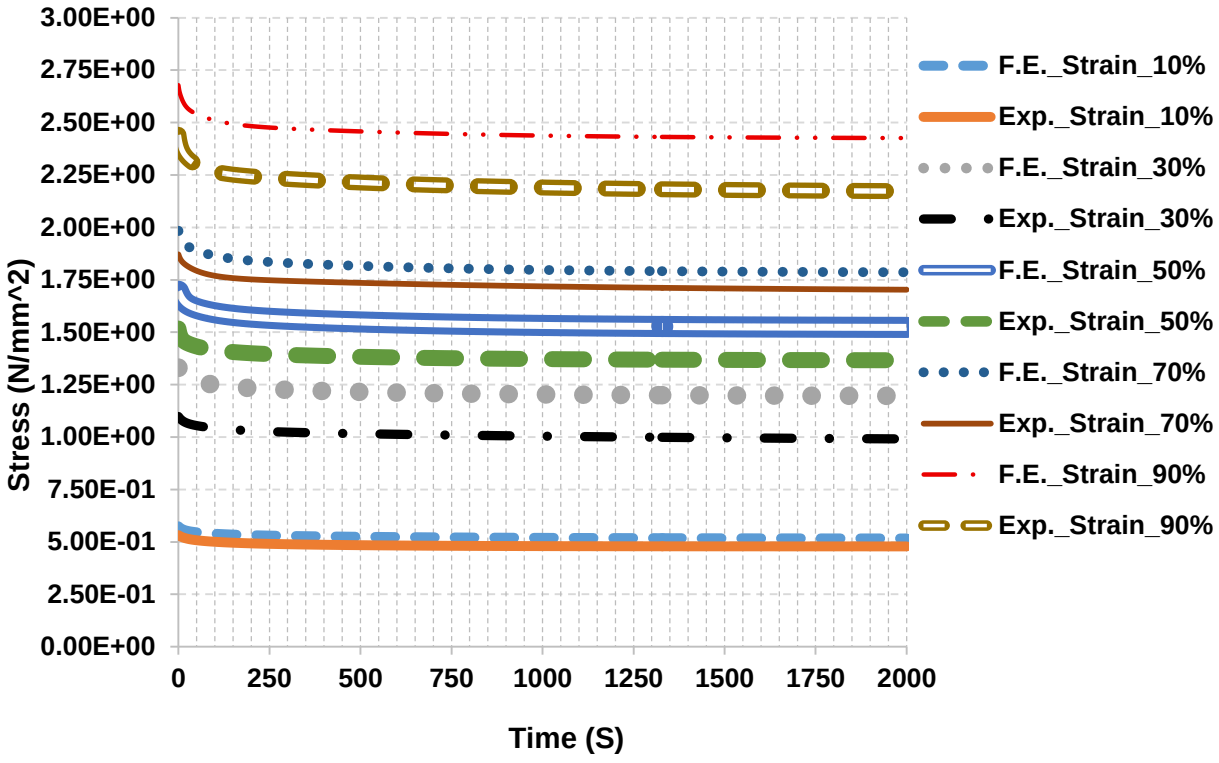


Figure 3.13 Tread Stress-Time Results of Linearised PRF Model and Test Data

There is an obvious difference between the FE outputs and the experimental ones because the PRF is in the linear form in which its modelling effects are the same as that of the Prony series model. With Isight optimization model in Figure 3.11, this difference is eliminated and the PRF model is fitted and converted to its non-linear form which is appropriate to describe the rubber non-linear viscoelasticity.

B) "Data Matching" Component:

In this component, the FE simulation stress-relaxation outputs from Abaqus cube model were fitted and compared against their relevant experimental stress-relaxation data using "sum-of-squared-difference" as the fitting error measure.

C) "Optimisation" Component:

Here, the Hooke-Jeeves direct penalty algorithm was selected to optimise both Yeoh and PRF coefficients against the "objective" of minimising the "sum-of-squared-difference" error measure received from the "data matching" component. Based on the fitting error received from "data matching", the "optimisation" component would send a new combination of Yeoh and PRF coefficients to "Abaqus" component to run and produce new stress-relaxation FE outputs until the fitting error is negligible. The Hooke-Jeeves procedure was set to run for 4000 evaluation iterations with a relative step size of 0.5 and allowable maximum failed runs of 4000. This is to allow the optimisation procedure to execute an effective exploration for the best fit solution.

The Isight optimisation process was repeated as many times as needed until a “sum-of-squared-difference” fitting error of nearly zero was reached. Figure 3.14 shows an example of the fitted FE stress-relaxation outputs against their corresponding experimental results after the Isight optimisation is finalised for the tread sample.

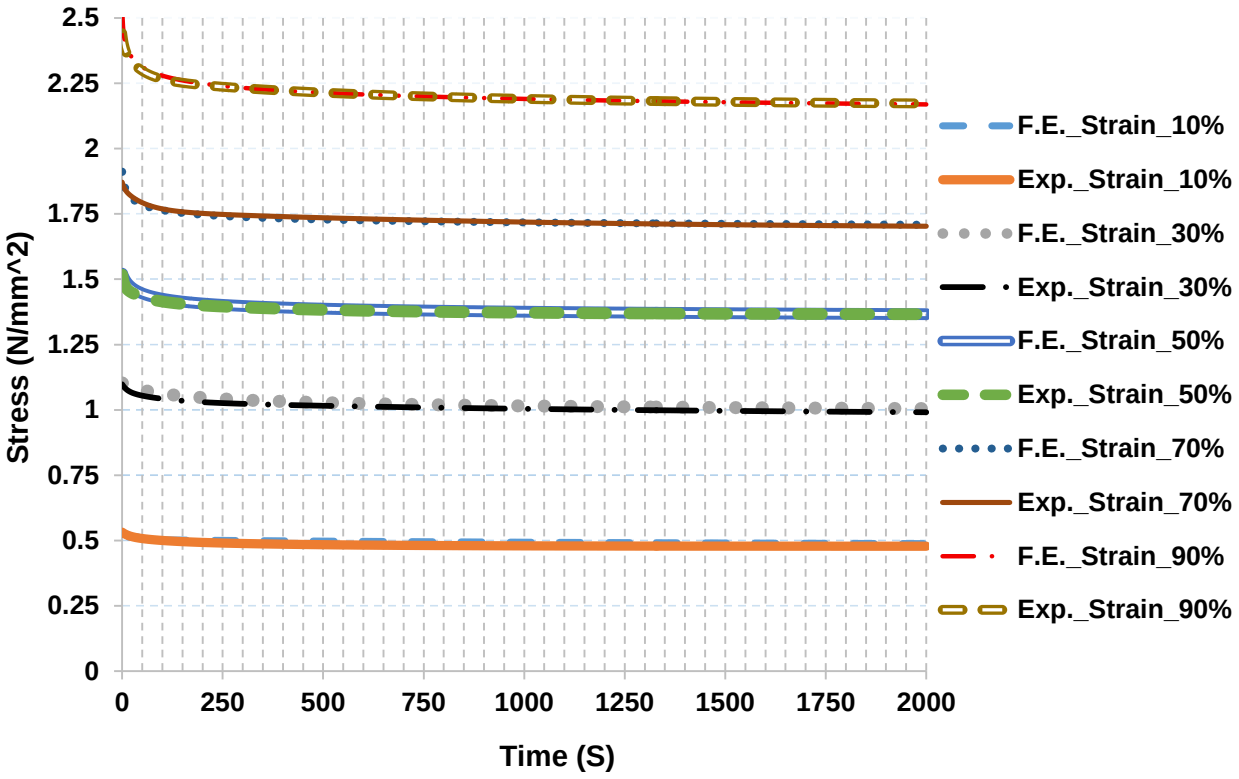


Figure 3.14 Tread Stress-Time Results of Optimised PRF Model and Test Data [29]

The following Table 3.5 shows the final optimised Yeoh and PRF coefficients for all the rubber samples:

Table 3.5 Optimised Yeoh and PRF Model Coefficients for all Rubbers

Material Model Parameters		Tyre Rubber Component(s)			Inner Chamber
		Tread	**Sidewall**	**Apex**	**Tube**
Yeoh	**C10**	0.641	0.386	0.789	0.221
	C20	-0.0738	-0.0346	-0.155	-0.0299
	C30	0.0315	0.00950	0.152	0.00924
PRF	**SR1**	0.396	0.123	0.000110	0.0358
	SR2	0.0306	0	0.394	0.0843
	SR3	0.00740		0.0361	0.124
	SR4				0.0387
	A1	3.869	0.755	0.163	26.662
	n1	4.044	2.715	1.050	1.0859
	m1	-0.650	-0.132	-0.0112	-0.0316
	A2	0.304	0.0381	1.499	0.803
	n2	2.769	1.223	6.496	1.132
	m2	-0.00720	-0.330	-0.348	-0.105
	A3	0.364		0.0488	0.0956
	n3	1.213		3.142	1.0635
	m3	-0.000357		-0.000439	-0.313
	A4				0.0270
	n4				1.0815
	m4				-0.0822

Based on the optimised material coefficients, Yeoh's "D1" coefficients were re-calculated for all the rubber samples using Eq. (3.7) similar to how it was done in section 3.3.1 to maintain tyre's nearly incompressibility in FE modelling. The re-calculated Yeoh's "D1" coefficients are indicated below in Table 3.6:

Table 3.6 Yeoh "D1" Coefficients for all Rubbers (Re-Calculated)

Rubber Part	Yeoh Model "D_1" Parameters
Tread	0.0314
Sidewall	0.0522
Apex/Chafer	0.0255
Inner Chamber Tube	0.0911

3.3.3 Density

As a part of the essential material properties to define for tyre FE modelling, the density for all the rubber components was specified at 1200 kg/m3. This was based on the past investigative research done by the vehicle dynamic group in University of Birmingham which concluded that the density for the different rubber components of the tyre is found very close to 1200 kg/m3 commonly [5, 7]. Other literature gave the same finding [211, 212].

3.4 REINFORCEMENT COMPONENTS

For the tyre, the reinforcements are the embedded cords and plies inside the tyre rubbers used to give the tyre the strength and endurance to withstand various loading conditions while retaining its shape. As shown in Figure 3.3, all the reinforcement components for the tyre were extracted. This involved extracting fibre samples of the polyester carcass and polyamide cap plies and steel samples of the belt and bead cords. In addition, fabric and polyvinyl-chloride (PVC) samples of the top and the side of the inner chamber housing respectively were extracted.

3.4.1 Elasticity

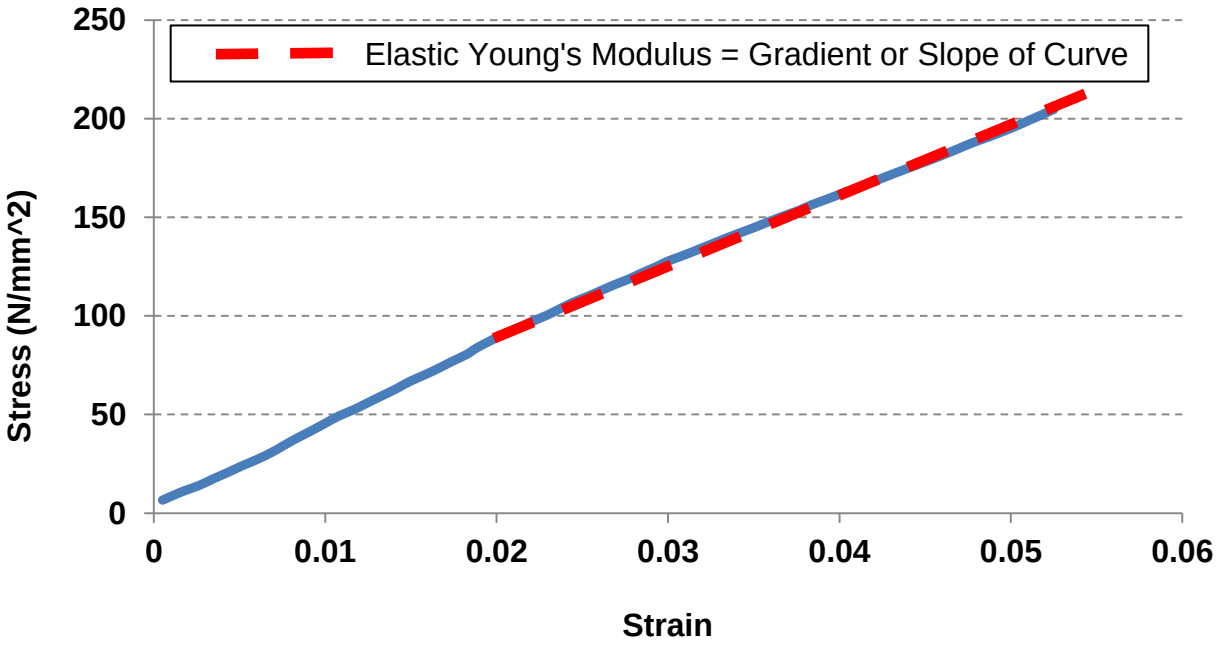
The reinforcements' behaviour is treated as isotropic and linear elastic of negligible viscoelasticity since they undergo only small and reversible deformations during normal tyre operations [5, 7, 195]. Based on that, the elastic Young's modulus was calculated for all the reinforcement components by subjecting each reinforcement sample to a uniaxial tensile test in accordance with ASTM D1776/D1776M−16 [213], ASTM D885/D885M−10a [183], ASTM D2969−04 [214] and Wei [7] work.

For the fibre and fabric samples, according to ASTM D1776/D1776M−16, no mechanical conditioning was needed to prepare the samples for testing. However, thermal conditioning was required in which the samples were left exposed at their loose state at 20 ± 2 °C for at least two hours (except for polyamide samples which were conditioned for 16 hours). According to ASTM D885/D885M−10a, for the main tensile test of the fibre/fabric samples, the Instron machine of constant-rate-of-extension type with a 50 N load cell, as shown in Figure 3.7, was used. Before the main test, each sample was pre-tensioned marginally to ensure it is in a straight upright position ready for the main tension test.

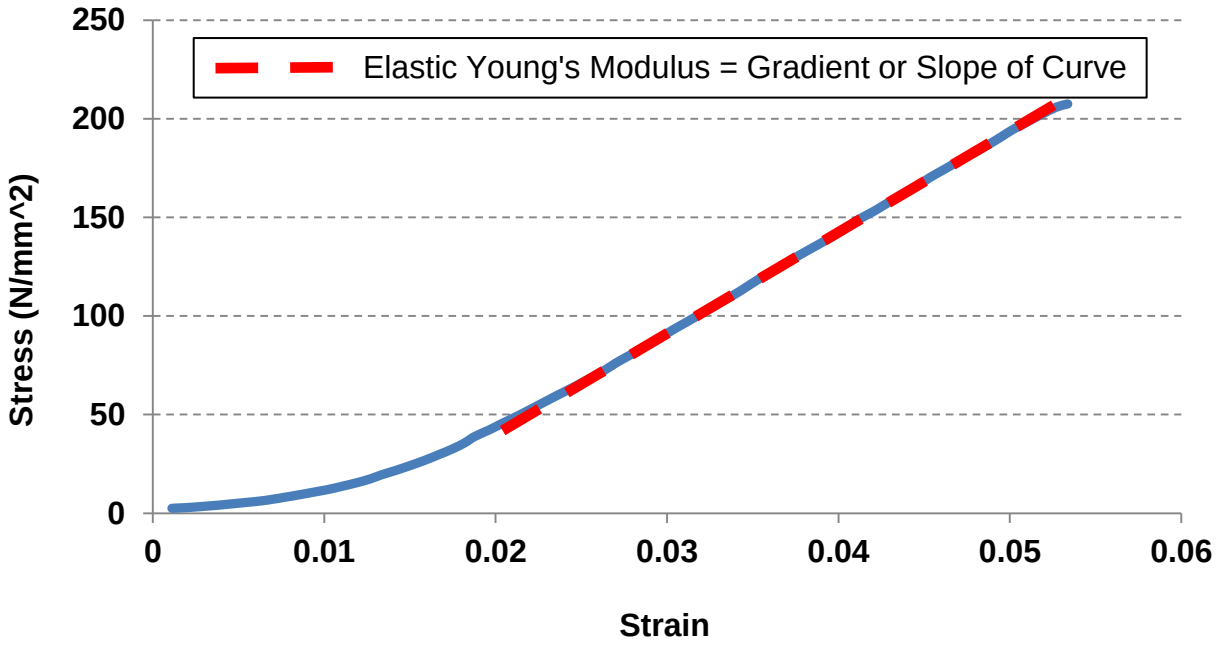
In the main test, each sample was stretched uniaxially up to ~5% strain at 20 ± 2 °C at a travel rate in mm/min of 50% of the nominal gage length of the tested sample. During the test, the generated tensile force and the travelled displacement in tension direction were recorded and converted later to the nominal stress using Eq. (3.3) and the nominal strain using Eq. (3.4) respectively. Based on that, the elastic Young's modulus was

calculated from the gradient of the nominal stress-strain relationship at the elastic region as seen in Figure 3.15 or using Eq. (3.17) alternatively. This tensile test was repeated three times for each sample and an average of the calculated Young's moduli was obtained.

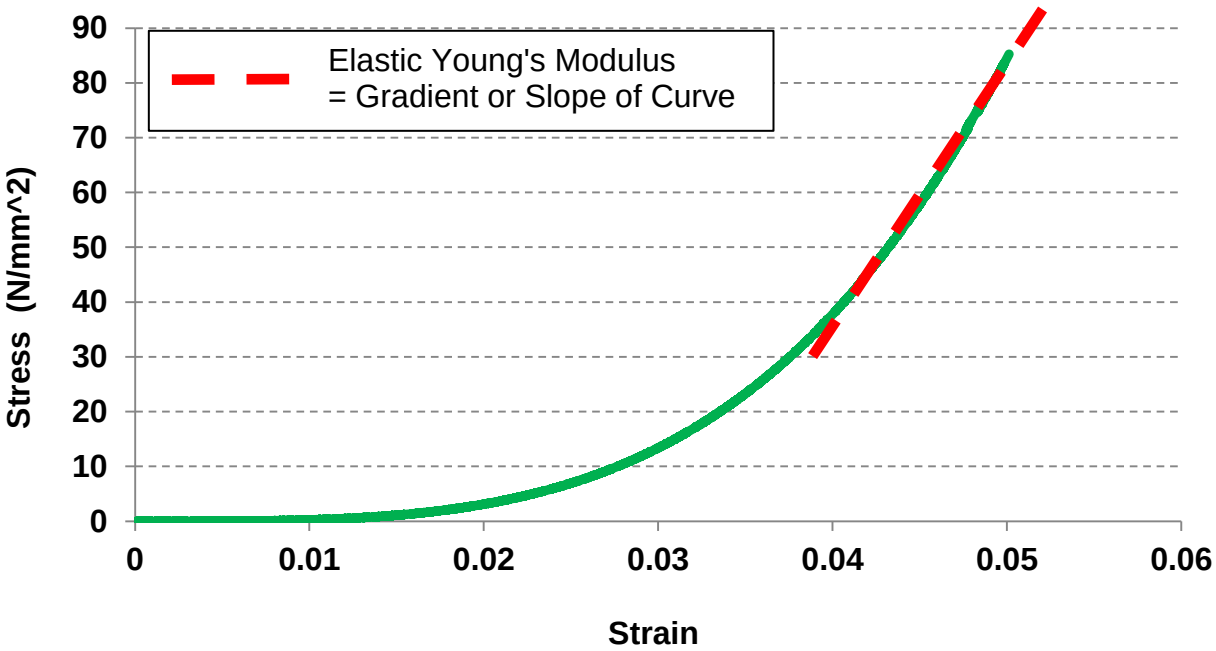
$$E = \frac{\Delta\sigma}{\Delta\epsilon} \tag{3.17}$$



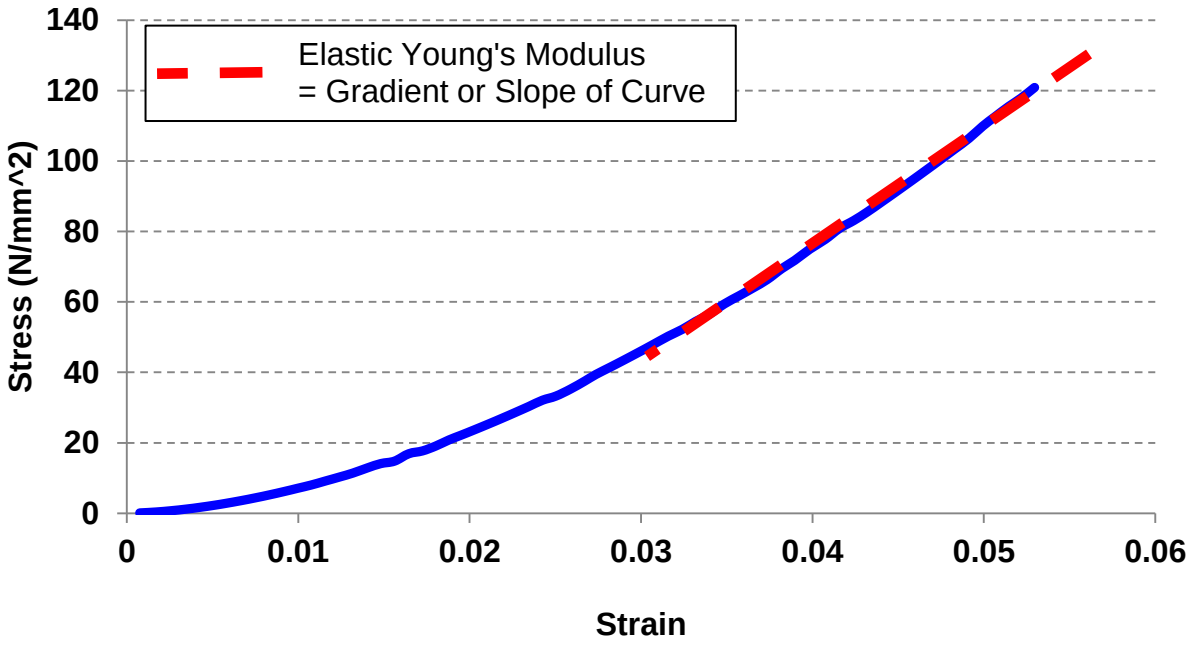
(a)


Elastic Young's Modulus = Gradient or Slope of Curve
Stress (N/mm^2)
250
200
150
100
50
0
0
0.01
0.02
0.03
0.04
0.05
0.06
Strain

(b)


Elastic Young's Modulus
= Gradient or Slope of Curve
Stress (N/mm^2)
90
80
70
60
50
40
30
20
10
0
0
0.01
0.02
0.03
0.04
0.05
0.06
Strain

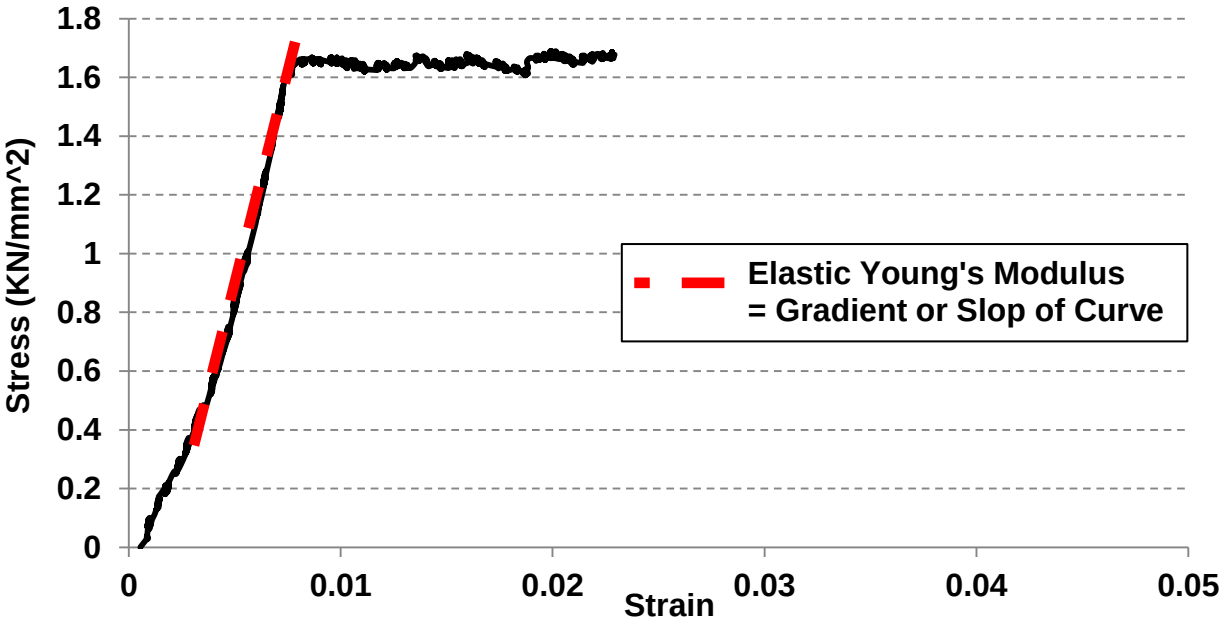
(c)



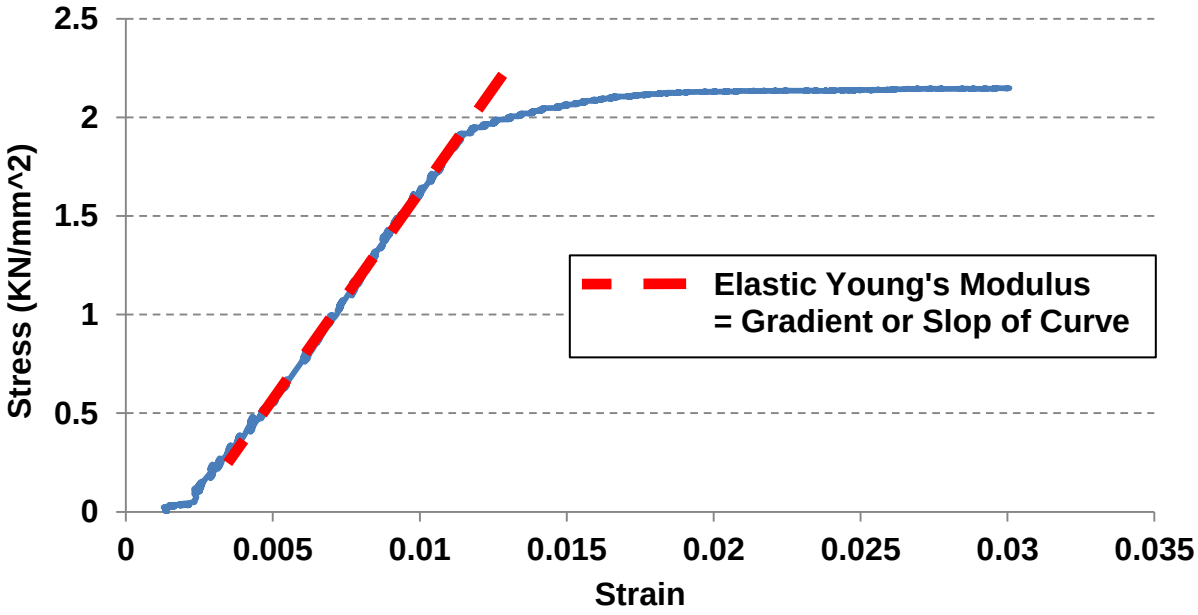
(d)

Figure 3.15 Experimental Stress-Strain Data for (a) Cap Ply, (b) Carcass (Body) Ply, (c) Inner Chamber Housing Top, and (d) Inner Chamber Housing Side

As for the steel samples, according to ASTM D2969−04 and Wei [7] work, no conditioning is required to be done. Prior to the tensile test, the steel samples were pre-tensioned at 1% of the full-scale force to ensure the samples are in an upright position ready for the tensile test. At the tensile test, the samples were stretched up to ~2% strain at 20 ± 2 °C at a travel rate in mm/min of 5-10% of the nominal gage length of the tested sample. During the test, the tensile force and the travelled displacement were recorded, converted later and averaged, the same way as the fibre/fabric samples case, to calculate the elastic Young's modulus as seen in Figure 3.16. For testing the steel samples, the Instron machine with a 2 KN load cell was used as shown in Figure 3.17.



(a)



(b)

Figure 3.16 Experimental Stress-Strain Data for (a) Steel Belt and (b) Bead

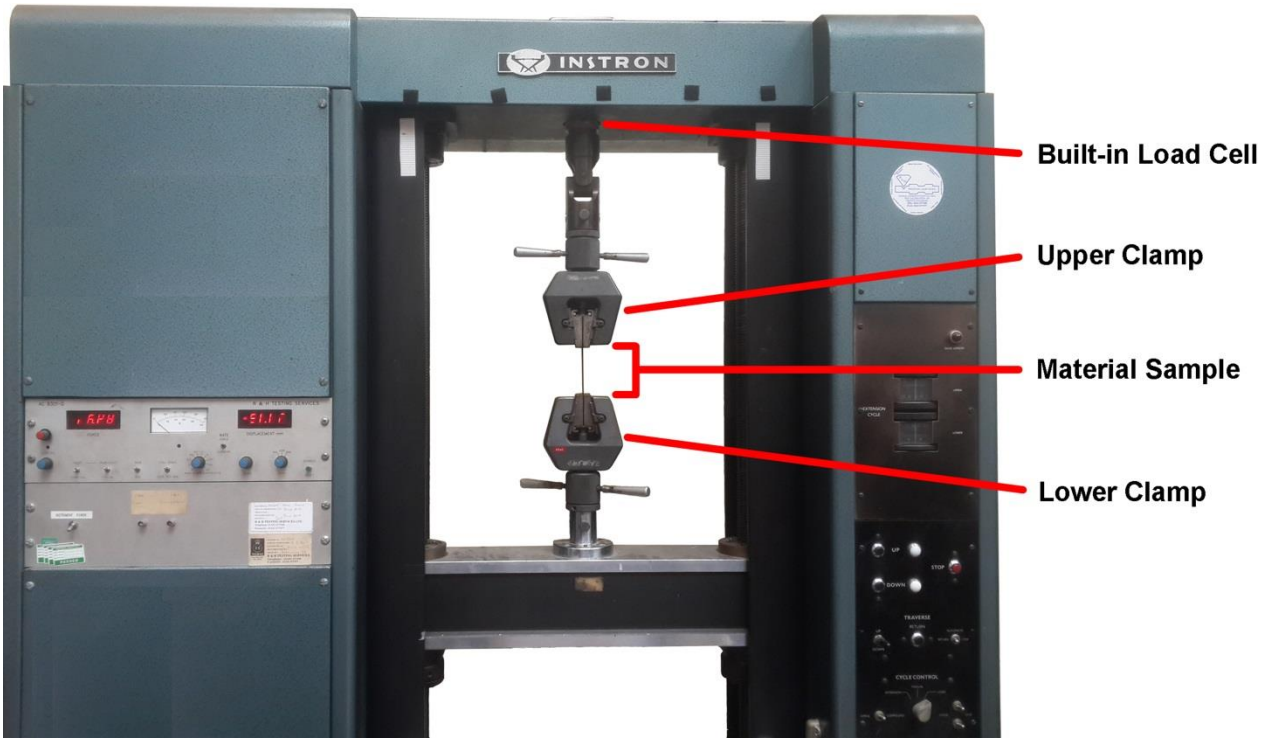


Figure 3.17 Instron Machine with 2 KN Load Cell

The final elastic Young's moduli calculated from the uniaxial tensile testing for all the reinforcement components are shown in Table 3.7 below:

Table 3.7 Finalised Elastic Young's Moduli for all Reinforcements

Reinforcements	Young's Modulus (MPa)
Steel Belt	200000
Bead	200000
Carcass (Body) Ply	5000
Cap Ply	3400
Inner Chamber Housing Top	4400
Inner Chamber Housing Side	3140

To account for the compressibility of the reinforcements in FE modelling, the Poisson ratio (v_p) was specified at ~0.3 for all the reinforcements since it is the common compressibility level found for most tyre reinforcements according to the relevant literature [5, 7, 201].

3.4.2 Lay-up Structure

The lay-up of the reinforcements within the tyre (rubber) structure was necessary to include in the tyre FE modelling since it helps in determining and constituting the tyre's overall strength and flexibility to a great extent. To identify the required lay-up settings of the reinforcements, the cross-sectional area of the reinforcing cord/string, the spacing between the cords/strings, and the angle of cord/string orientation inside the tyre (rubber) structure are necessary to specify for each reinforcement component (i.e. steel-belt, bead, carcass, and cap-ply).

For the cross-sectional area, according to ASTM D2969-04 [214], a micrometer with ~0.01 mm precision was used to measure the diameter at three different locations along each reinforcing cord/string length and take the average of those readings as shown in Figure 3.18 for example. This procedure was repeated at least three times for all the reinforcement samples of the tyre. Overall average measurement is taken of all the samples of each reinforcement component. Based on the cord's diameter measurement, the circular cross-sectional area was calculated using the following Eq. (3.18):

$$A_R = \pi \times {r_R}^2 \tag{3.18}$$



Figure 3.18 Cord Diameter Measurement using Precision Micrometer

As for the spacing between the cords and their orientation angle, an “image processing” technique was applied to measure those lay-up settings, as indicated in Figure 3.19, similar to that of Wei [7].

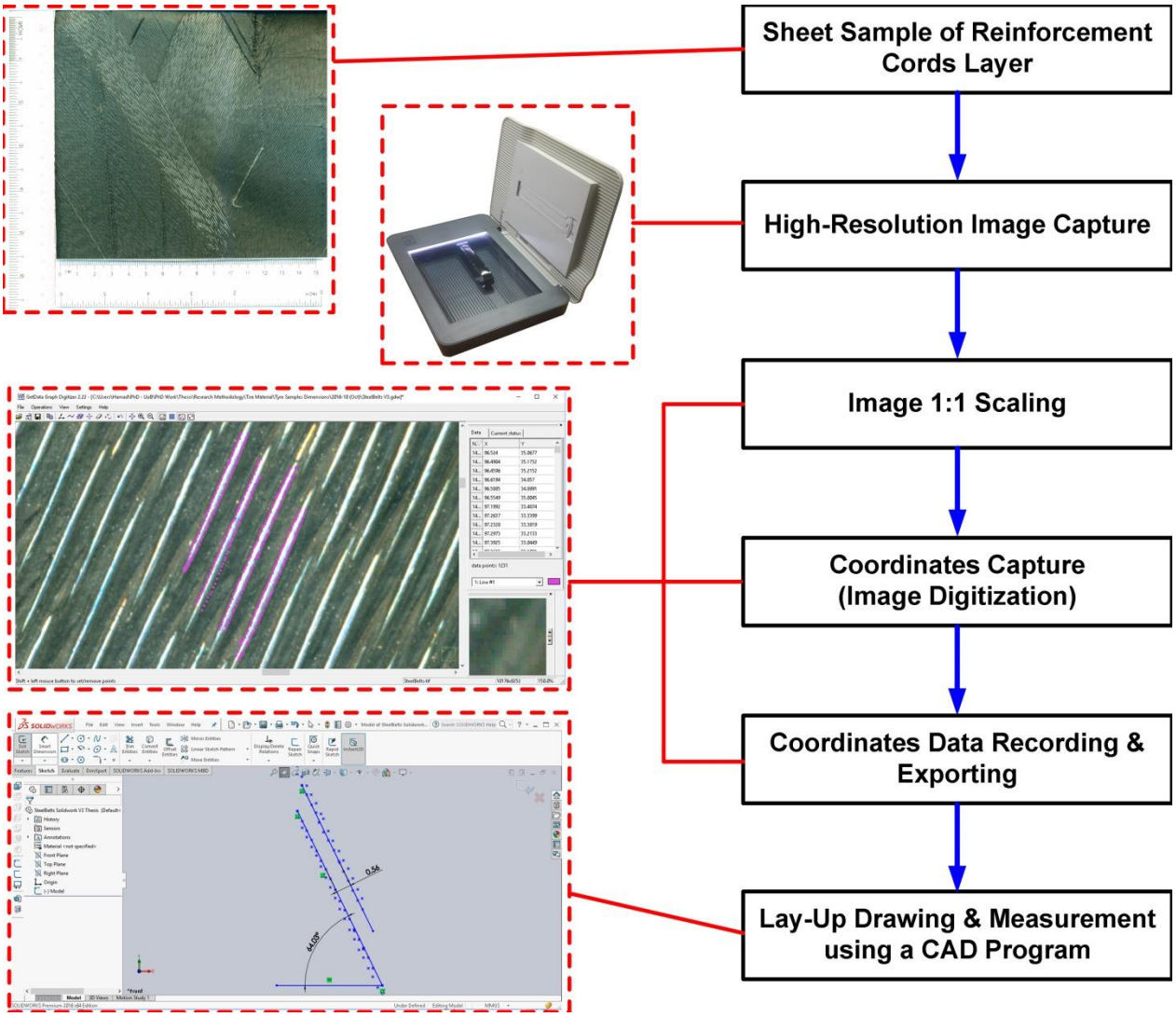


Figure 3.19 Image Processing Technique for Reinforcement Lay-Up Capture

In preparation for “image processing”, the relevant cord/string sheet layer for each reinforcement component was extracted from the tyre and cleaned-up until the cords lay-up was visible. A high-resolution image of each cord/string sheet layer was captured and imported to a processing computer in a picture format using a 1200 ppi resolution scanner. Using “GetData Graph Digitizer” software, the scanned image was scaled to

1:1 actual size and the relevant cords coordinates, indicating the spacing and the orientation angle, were captured. Those cords coordinates were exported later to a CAD program (i.e. SolidWorks) as coordinate points data to draw-up the cords lay-up and measure both the relevant spacing and orientation angle at three different locations for an average measurement. The obtained spacing and orientation angle for all the reinforcements are shown in Figure 3.20. Based on that, the finalised lay-up settings of all the tyre reinforcements for the FE input were acquired and are indicated in Table 3.8 below.

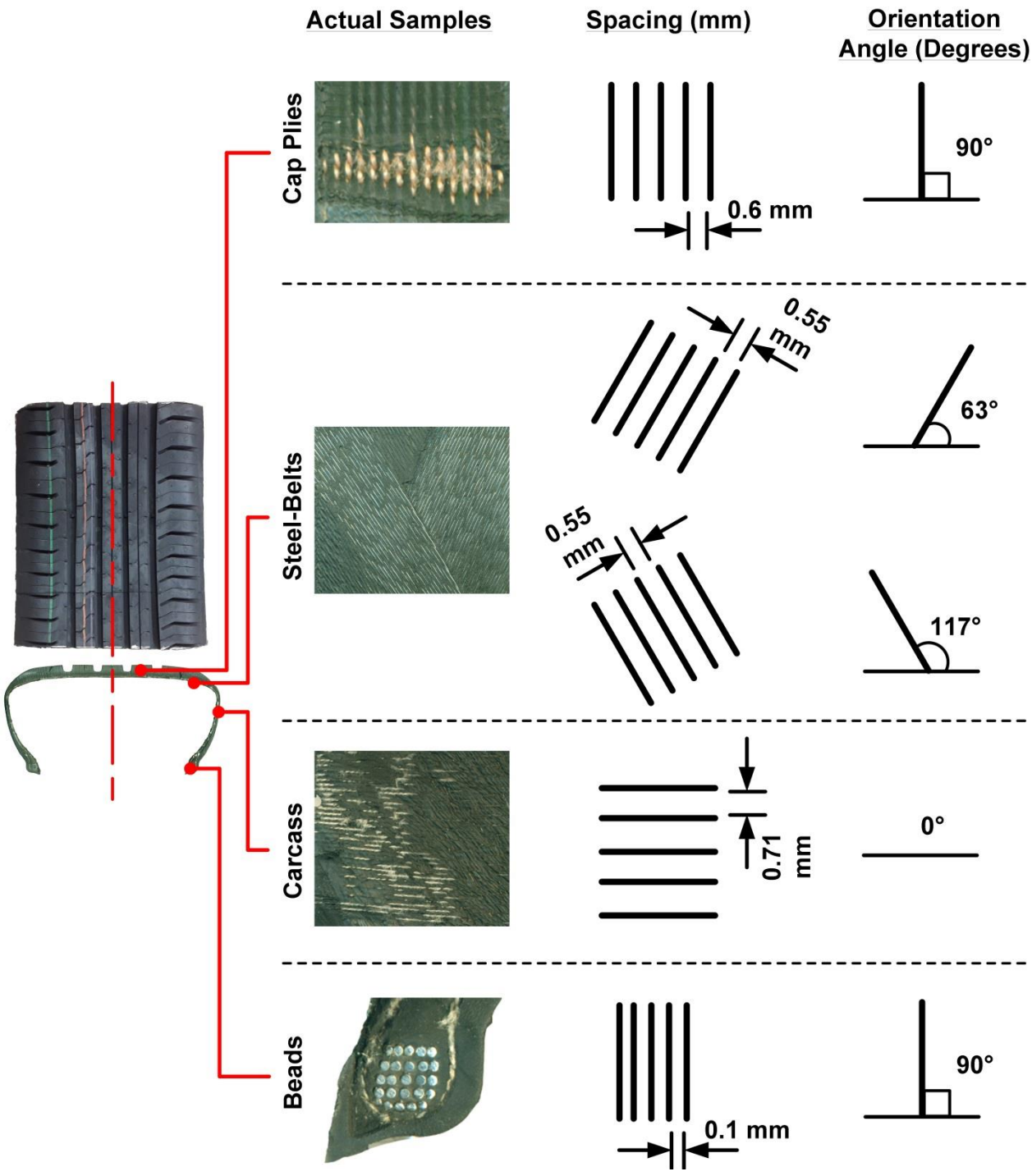


Figure 3.20 Cords Spacing and Orientation

Table 3.8 Lay-Up Settings for all Tyre Reinforcements

Reinforcements	Area-per-Bar ($\mathbf{mm^2}$)	Spacing ($\mathbf{mm}$)	Orientation Angle (Degree)
Cap-Plies	0.075	0.6	90
Body-Plies (CarCass)	0.11	0.71	0
Steel-Belt 1	0.125	0.55	63
Steel-Belt 2	0.125	0.55	117
Beads	1	0.1	90

3.4.3 Density

According to the relevant literature, the density of the reinforcements was specified as follows in Table 3.9 [5, 7, 200, 212]:

Table 3.9 Reinforcements' Density

Reinforcements	Density ($\mathbf{Kg/m^3}$)
Cap-Plies	1300
Body-Plies (Carcass)	1500
Steel-Belts	7800
Beads	7800
Inner Chamber Housing Top	1400
Inner Chamber Housing Side	1450

3.5 SUMMARY

In this chapter, the acquisition process of the necessary material properties for tyre FE modelling was explained. The acquisition procedure involved fitting the relevant material functions against their corresponding experimental test data using Abaqus evaluation

and Isight optimisation tools accordingly. Since only the reversible deformation of the tyre is of interest, the hyperelastic and viscoelastic properties of the tyre rubbers and the elasticity of the tyre reinforcements were measured and captured. Uniaxial tensile testing was performed for both tyre rubbers and reinforcements to measure their hyperelastic and elastic responses respectively. Stress relaxation test was conducted for the tyre rubber viscoelasticity. Other material properties like the density and the Poisson ratio were possible to obtain from the relevant literature resources.

The reinforcement's lay-up within the tyre (rubber) structure was captured in terms of the cross-sectional area of rebar cords using a precision micrometer, the spacing between the cords and the cords orientation angle using an image processing technique. Given the limited resources and information accessibility, the required material samples for experimental testing were manually extracted from an identical actual tyre to the investigated one. To ensure the accuracy and precision of measurements, the testing equipment and procedures applied were according to ASTM and ISO standards along with established scholarly works.

CHAPTER (4): DEVELOPMENT AND VALIDATION OF FINITE ELEMENT MODEL FOR STANDARD TYRE

4.1 INTRODUCTION

FE solution is growingly replacing the time-consuming and costly experimental approach as a cost-effective, time-saving and reasonable alternative for predicting the tyre performance under most contact/driving conditions and for designing tyres [66, 67, 215, 216]. However, for the FE solution to yield correct outputs, the input data of the tyre FE model are necessary to be provided in an accurate and detailed format [72, 215]. Mainly, these input data are the “material properties” and the “tyre geometry” [5]. A leading and widely used FE code for tyre analysis and design is Abaqus due to its non-linear capabilities, rebar feature, and handling of complex problems [66, 217].

This chapter uses the material properties data obtained in the previous chapter as one of the main inputs to develop an accurate and a working 3D FE model of the 225/55 R17 standard tyre (i.e. baseline design) using Abaqus 6.13-1 as per this research project objective(s). As indicated in chapter (3), the standard tyre is a conventional tyre that has a single chamber design as shown in Figure 4.1. The development process involved capturing a detailed 2D profile image of the actual tyre, transforming the captured image into a CAD drawing, creating an FE geometry from the CAD drawing, setting-up the FE model, refining model’s mesh and validating the FE model against experimental tests as seen in Figure 4.2. The FE development work done by the author in this chapter, as the

main owner and contributor, was published as per a publication plan for this research. The related publications can be referred to through [29, 30, 187].

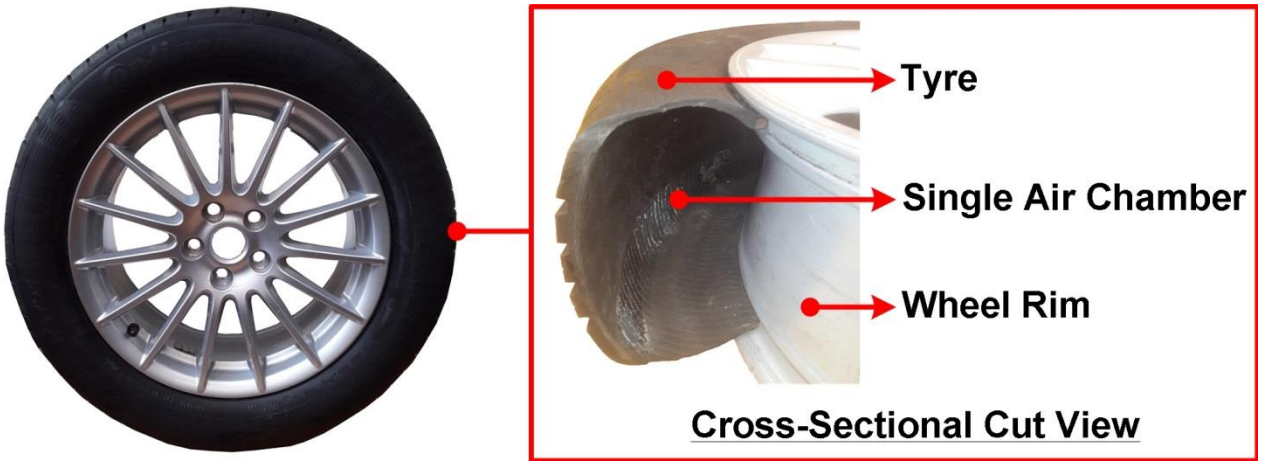


Figure 4.1 Standard (Baseline) Tyre

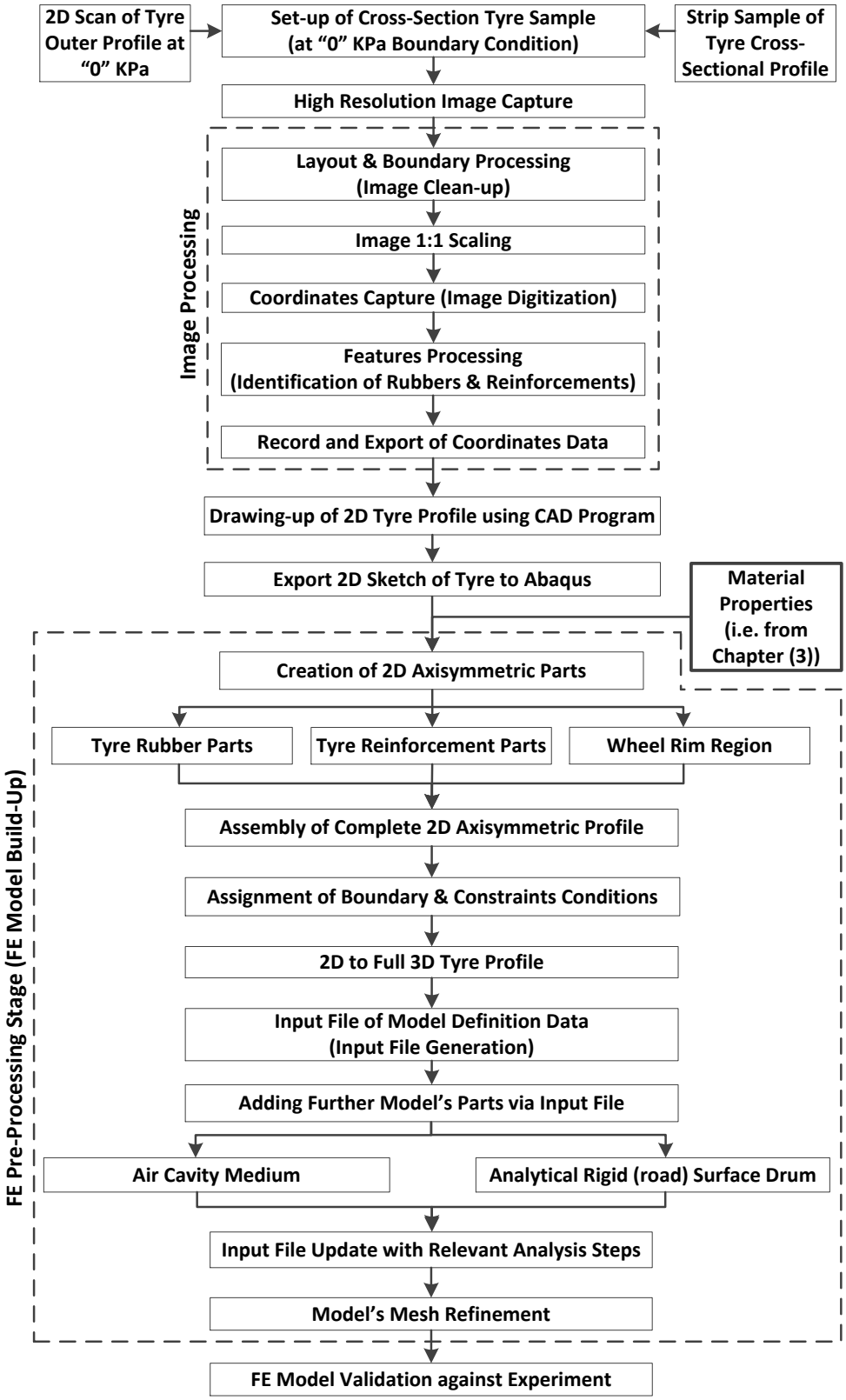


Figure 4.2 Tyre FE Model Development

4.2 GEOMETRICAL FEATURES CAPTURE

As highlighted earlier, it is necessary to have an accurate and detailed representation of the actual tyre geometry in FE modelling to help in ensuring the correct simulation of the given contact/rolling problem. However, due to commercial confidentiality, such tyre geometry was not readily available. Therefore, an alternative approach was implemented to capture the actual tyre geometry empirically as indicated in Figure 4.2 and similar to Yang [5] and Wei [7] which involves the processing of a high-resolution image of a 2D cross-sectional profile sample of the tyre.

In this “image-processing” approach, firstly, a clean-cut strip sample of the full cross-sectional profile of the tyre, in the lateral direction, was extracted manually from the actual tyre in which the embedded reinforcement layers were visible to see in the sample as shown in Figure 4.3. To capture an image of this strip sample that replicates closely the actual tyre profile mounted on wheel-rim at “0” KPa inflation, the extracted strip sample was required to be positioned exactly similar to that of the actual tyre profile. For this purpose, the 2D coordinates of the actual tyre outer profile (i.e. mounted on wheel-rim at “0” KPa) were captured through 3D laser scanning using “Faro Edge ScanArm” to adopt as a reference guideline through which to set-up the strip sample at an equivalent position to that of the actual tyre. This is by using a board with a 1:1 print of the outer profile based on which to fit the strip sample.

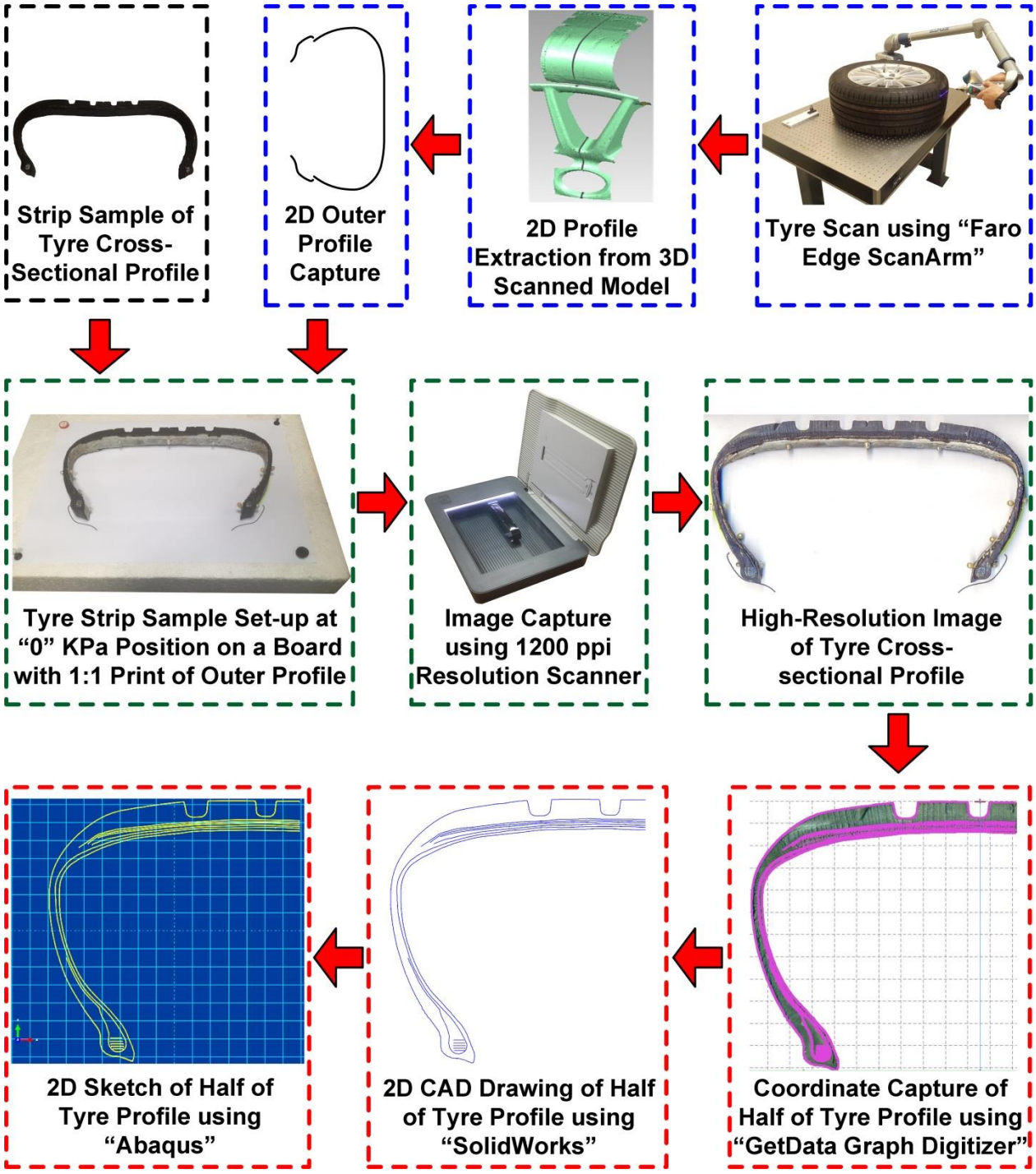


Figure 4.3 Image Capturing and Processing for Cross-Sectional Tyre Profile

Similar to the image processing procedure in section 3.4.2, a high-resolution image of the strip sample of the tyre cross-section at “0” KPa was captured and imported to a processing computer using a 1200 ppi resolution scanner as seen in Figure 4.3. The imported 2D tyre image was treated with “adobe photoshop” to extract only the tyre profile excluding irrelevant surroundings in the image. Later, the treated image was exported to the “GetData Graph Digitizer” to scale it 1:1 and extract the coordinates of all the rubber and reinforcement components of one half of the tyre profile since it has a symmetrical profile about its centreline. Those coordinate points were exported to “SolidWorks” to create a detailed 2D and half CAD drawing of the symmetrical cross-sectional tyre profile to use later as a sketch input to generate the different tyre parts in Abaqus as seen in the next sections.

4.3 FE MODEL SET-UP

4.3.1 2D Axisymmetric Modelling

After setting up the material properties and the rebar lay-ups obtained in the previous chapter in Abaqus model tree, the first stage of tyre modelling was to create a detailed 2D axisymmetric FE model of the tyre (i.e. to include reinforcements details) which to be used to create a 3D version of the tyre model later. To create the 2D axisymmetric model, the 2D CAD drawings of SolidWorks acquired from image processing in section 4.2 were imported to Abaqus/CAE as the geometry input for different axisymmetric tyre parts. In Abaqus/CAE, the sketch of the half tyre profile was mirrored about its symmetry axis to obtain the full 2D profile of the tyre cross-section. The 2D axisymmetric model

was created and partitioned to its sub-parts as seen in Figure 4.4 below for the standard tyre.

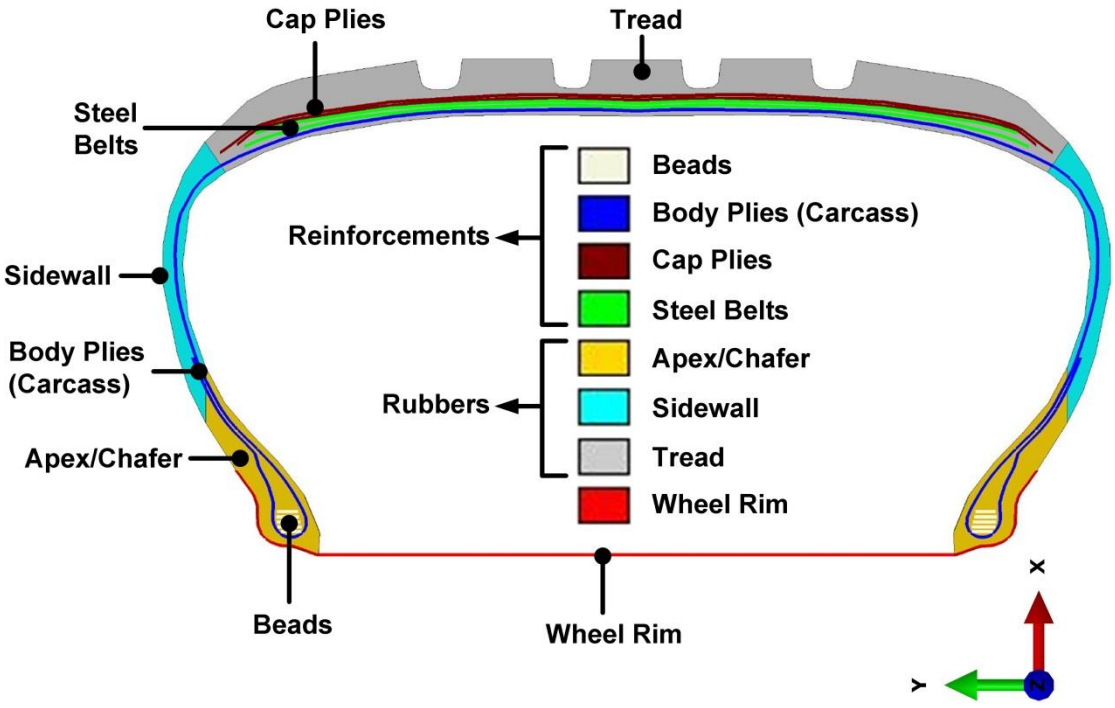


Figure 4.4 2D Axisymmetric Model of Standard Tyre

4.3.1.1 Rubber and Wheel-Rim Components

Given the tyre structure complexity and the usage of explicit dynamic solver to run the whole tyre analysis (i.e. see section 4.3.3 for more details), the rubber components in the 2D axisymmetric tyre model were modelled as deformable and twistable shell parts with reduced-integration bilinear axisymmetric quadrilateral solid elements (CGAX4R) similar to Bekakos *et al.* [218]. This is since linear-order reduced integration decreases "simulation time" particularly for 3D modelling, is robust for "large strain" applications, and prevents "shear (volumetric) locking" (i.e. over-stiffen response) by offering constant

volumetric strain across the element especially as the rubber response is nearly incompressible [219, 220]. Furthermore, with proper meshing, the quadrilateral (i.e. hexahedral in the 3D model) elements have a better convergence rate and can provide an accurate solution with lower costs [219]. The relevant material properties from the model tree database were assigned to each rubber component.

Nevertheless, the linear-order reduced integration elements may suffer from “hourglassing” (i.e. Non-physical (zero energy) modes) during deformation which could influence solution accuracy. To reduce the hourglassing effect greatly in the tyre model, the enhanced hourglass control algorithm was used for the rubber elements accompanied with reasonably fine meshing (i.e. see section 4.4.3 for greater details). Also, a groove-less tread profile was used, as shown in Figure 4.5, to distribute the loading or contact-patch over more elements to help in minimising hourglassing by avoiding concentrated or point loading/contact which works on exciting hourglassing modes [219-221]. This is since tread grooves have a negligible impact on tyre’s rolling-resistance, which is the main performance measure in this research project [8, 30, 67, 77].

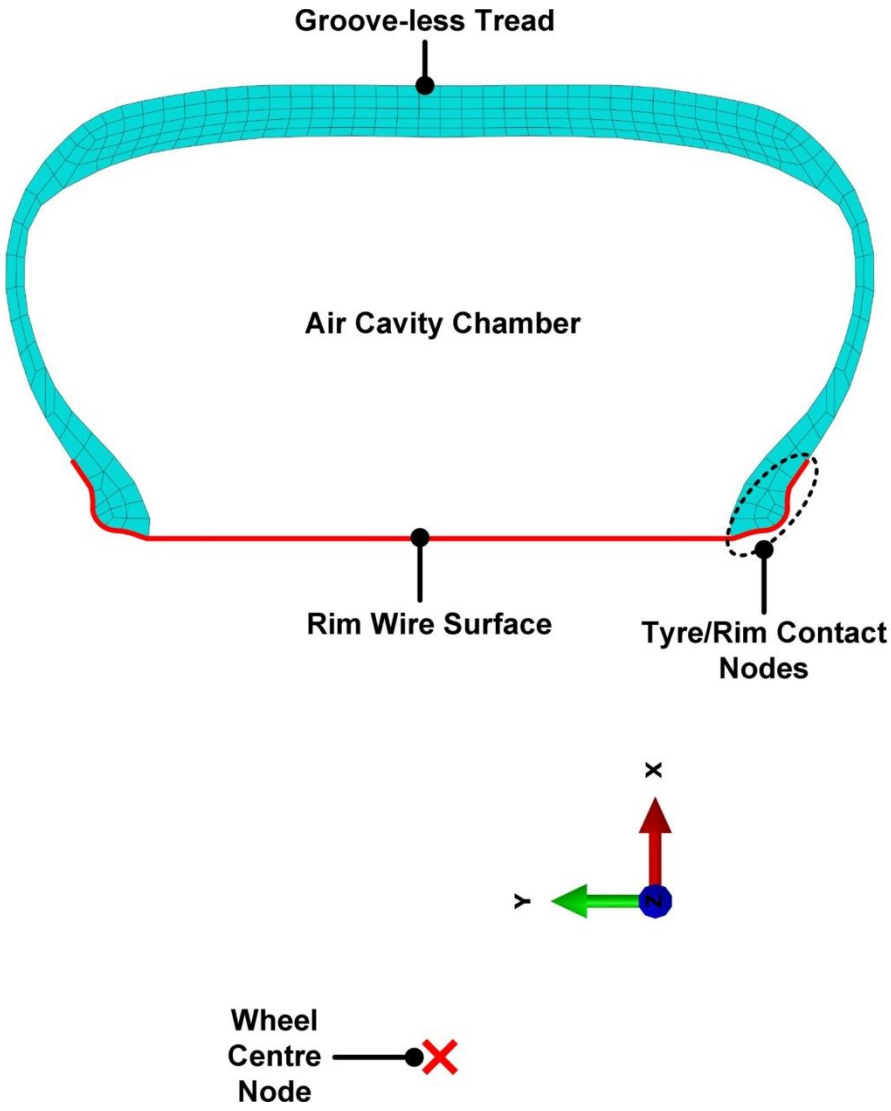


Figure 4.5 Groove-Less Tyre Rubber Profile with Fine Mesh and Wheel-Rim Assembly

As seen in Figure 4.5, the tyre wheel-rim was modelled by a rigid body definition using "tie" constraint function that contains and links the "wheel centre node", the "tyre/rim contact nodes", and the "rim wire surface" (i.e. modelled using SFMGAX1 element) altogether to form the wheel-rim assembly. The wheel-rim assembly was treated as a rigid part that is non-deformable since it exhibits almost no to very tiny and negligible

strains in practice during normal operation. Point-mass and rotary-inertia elements were coupled to the wheel centre to represent the wheel-rim's weight (8 Kg) and rotational inertia (0.249 Kg.m^2) respectively in Abaqus/Explicit.

Unlike the actual (asymmetric) rim, the wheel-rim was drawn as a simplified symmetric rim profile made of nodes and wire surfaces to minimise the model complexity and the required computational costs. Furthermore, the wheel-rim is assumed to have no or negligible impact on tyre performance, especially rolling-resistance, agreeing with others work [64, 67, 74, 77]. This is because only steady-state free-rolling conditions are investigated in this research, as indicated in section 1.3 of chapter (1), where wheel-rim rotational inertia has almost no impact [24]. Also, according to the aim of this research project, the wheel-rim assembly, in the tyre structural designing that was done, remained the same without any changes whether in the geometry or the physical properties in all the design versions.

4.3.1.2 Reinforcement Components

Given its shape and lay-up nature, the tyre's cord reinforcements were represented as deformable and twistable wire rebar layers with linear axisymmetric surface elements (SFMGAX1). The relevant material properties and rebar characteristics (i.e. rebar area, spacing between cords, and cord orientation angle) from the model tree database were assigned to each reinforcement component. The cord reinforcements were added to the axisymmetric tyre model as embedded regions inside the relevant rubber bodies as the host. Similar modellings of tyre reinforcements are Yang *et al.* [222] and Wei *et al.* [223].

4.3.2 3D Modelling of 2D Profile, Air Cavity and Road

Using the “symmetric model generation” and “symmetric results transfer” procedures available in Abaqus/Standard, the 2D axisymmetric tyre model was revolved 360° to create the full 3D tyre model as shown in Figure 4.6. During such a process, the elements of the rubber and reinforcement components were transformed to its corresponding 3D version; hexahedral (brick) solid elements (C3D8R) and quadrilateral surface elements (SFM3D4R) respectively. Also, an “input” file was generated comprising the model definition data. This “input” file was updated to include the necessary material properties for all the tyre components and to create other model’s parts and required simulation steps to run the tyre analysis as will be indicated next.

The full 3D tyre model was chosen over the 2D tyre model in order to be able to investigate the complete tyre design and its performance in-depth in a manner similar to that in practice and in line with this research goal. This is since the main work of this research involves introducing new structural designs to the standard design along the entire tyre circumference. With such 3D model, a visual on the performance of the entire tyre structure during rolling is possible to investigate its deformational response including vibratory oscillations in relation to the total energy dissipation and other driving performances such as cushioning and cornering. This would involve not only the tyre footprint but the outer circumference of the whole tyre as will be seen in section 4.5.4.

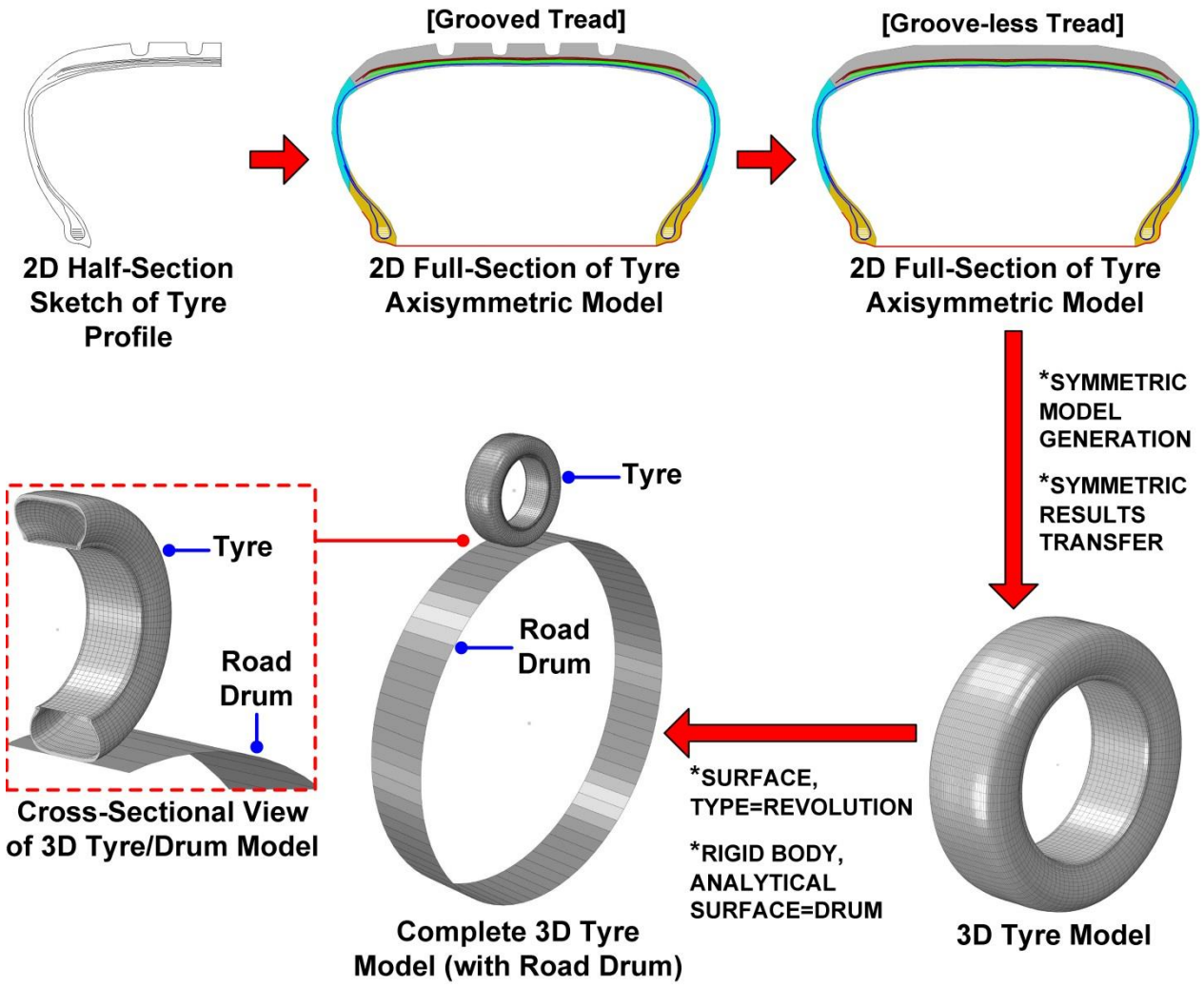


Figure 4.6 2D to 3D Tyre Model Development

To account for the trapped air inside the tyre's cavity, the conventional approach followed by many researchers was to apply uniform pressure load on the tyre's inner-liner (i.e. internal surface) to simulate tyre inflation only [224-227]. However, this method is found ineffective in accounting for the air response across the whole cavity and the air/tyre interaction during deformation since it considers the tyre cavity as a void with no

link or relation to the tyre's structure especially if there is more than one cavity chamber inside the tyre [30].

In this research project, an alternative solution was used to account for the cavity air behaviour more realistically in relation to the tyre structure. This solution was the "fluid cavity capability" provided by Abaqus. The fluid cavity capability is used to couple the deformation of tyre structure with the pressure and volume of its cavity air. The capability has two approaches available to create the cavity air volume (i.e. a surface-based approach and an element-based one). The "surface-based" approach was chosen in this research as it has better functionality, is easier to implement, is more suitable for 3D modelling, and requires lower computational costs [185, 228].

To model tyre's cavity air using "surface-based fluid cavity capability", the "air cavity boundary" was specified through a closed-loop (element-supported) surface definition and a "cavity reference node" was created at the wheel-hub centre for each air chamber in the tyre. Based on both the "air cavity boundary" and the "cavity reference node", Abaqus would construct and compute internally the air cavity volume(s) of the tyre using fluid volume elements (F3D4) [228]. The air medium inside the tyre cavities was assumed to behave as a compressible ideal gas [229-231]. Based on which, the air properties, as an ideal gas, were included in the model "input" file in terms of the molecular weight and the universal gas constant. Furthermore, the gas temperature was specified at 25 °C based on the assumption of isothermal behaviour corresponding to

that of the experimental testing done for tyre's rolling-resistance as will be seen in section 4.5.2.2. Similar work was done by Behroozi [185].

The tyre's cavity air was treated as an ideal gas because it agrees with the main assumptions for the kinetic theory of ideal gases. First, the intermolecular forces created from air molecules collision with each other inside the cavity chamber are insignificant in contrast with the tyre forces in action. Next, the air molecules have point masses that are too small in comparison to how far each molecule is apart from the other in which the overall volume of all molecules would be trivial with respect to the volume of the tyre cavity. Moreover, under normal working conditions, tyres operate at inflation pressures and temperatures that conform to the ideal gas laws [232].

As shown in Figure 4.6, to model the contact road surface, the model input file was updated with a 3D analytical (rotational) surface definition accompanied with rigid body definition to create an analytical rigid surface drum with 360° revolution and its reference node using ARSR elements. At drum's reference node, the drum was assigned an estimated mass and rotational inertia in order to run the explicit analysis procedure of the tyre model as will be seen later. An analytical rigid road drum, with a smooth and flat surface, was modelled to match the corresponding drum used in the experimental testing in section 4.5.1 which is taken as nearly non-deformable in practice. This is besides reducing the tyre model complexity and computational costs.

4.3.3 Simulation (Analysis) Steps

To run the full 3D tyre model for the targeted rolling analyses, Abaqus/Explicit solver was used to run the entire tyre analysis. There were several reasons to choose Abaqus/Explicit solver only over Abaqus/Standard and also over the coupled use of both Abaqus/Standard and Abaqus/Explicit together to run the complete tyre analysis. Firstly, unlike the Abaqus/Standard, Abaqus/Explicit is found to have the capability to handle, efficiently, non-linear and large deformational dynamic problems, including quasi-static, with complex contact conditions [56, 233-237]. This involves 3D problems with large rotations and discontinuities whether in contact or due to material wrinkling [56, 235]. All of these aspects are found commonly in the 3D tyre analysis, which is a highly non-linear FE problem whether it was for the geometry, the material response, or the contact boundaries [56].

Apart from that, Abaqus/Explicit offers an economical solution of the dynamic rolling simulations and avoids the non-convergence issues of the analysis in comparison with the Abaqus/Standard [56, 235, 238]. This is because Abaqus/Explicit uses a central-difference integration approach to directly compute the dependent (targeted) variables at a later time using known quantities at the current time without the need for any iterations or convergence checks since such computation is done over many sufficiently small time increments that would ensure the solution advances gradually and stays on track [56, 234, 235]. On the other hand, Abaqus/Standard uses Hilber-Hughes-Taylor integration approach to determine the dependent variables at the current time through solving a coupled set of equations several times (iteratively) until a solution is converged for each

time increment [56, 234, 239]. Such an approach would require significant computational resources. Due to that, Abaqus/Standard is more suited to use for static and steady-state rolling problems [56, 224].

Although Abaqus/Explicit uses a large number of time increments, the Abaqus/Explicit gives an inexpensive solution for dynamic rolling problems since each increment requires neither iterations nor simultaneous equations to solve in comparison to Abaqus/Standard [235, 240]. Regardless, it seems proper to use Abaqus/standard to run the quasi-static tyre analyses (i.e. tyre inflation and vertical loading) and then to transfer the results to Abaqus/Explicit to run the part of the dynamic rolling analysis as a more efficient computational approach as seen in others' work [241-244]. This is since using Abaqus/Explicit to run the quasi-static tyre processes for its normal time period is computationally unrealistic as it would require an unreasonably very small size of the time increment and an enormous number of increments [236].

However, for this research project, the coupled usage of both Abaqus/Standard and Abaqus/Explicit to run the complete tyre analysis, as suggested above, was not possible. This is because the PRF material module used to represent the tyre viscoelasticity in the tyre FE model is not compatible with the "steady-state transport" and the "import" features of the result transfer procedure between Abaqus/Standard and Abaqus/Explicit. Nandi *et al.* [40] outlined the same finding. To be able to use Abaqus/Explicit for the quasi-static tyre analyses and obtain an economical solution in this research, the simulation speed of the quasi-static processes (i.e. tyre inflation and

vertical loading) were artificially increased by reducing the total step time of each process in which the dynamic effects are eliminated [40, 236].

Therefore, with Abaqus/Explicit as the solver for the entire tyre analysis, the tyre model input file was updated with three simulation steps in order to run the complete tyre analysis of steady-state free rolling either in straight-line or at a slip angle as shown in Figure 4.7. In these simulation steps, the time increment was set below the stability limit of the central-difference operator to ensure a stable solution. For the first step, the tyre was inflated quasi-statically by applying the targeted inflation air pressure at the relevant cavity reference node. In the second step, a general contact definition was created to account for the complicated contact and any discontinuities between the tyre and the road drum with a coulomb (constant) friction coefficient of 0.75 during rolling similar to that of the experimental set-up in section 4.5.1 in which free-rolling conditions are used [245-248]. This step involved bringing the tyre into initial contact with the drum and then vertically loading the tyre against the drum quasi-statically by applying the prescribed vertical load at the wheel reference node (RP2).

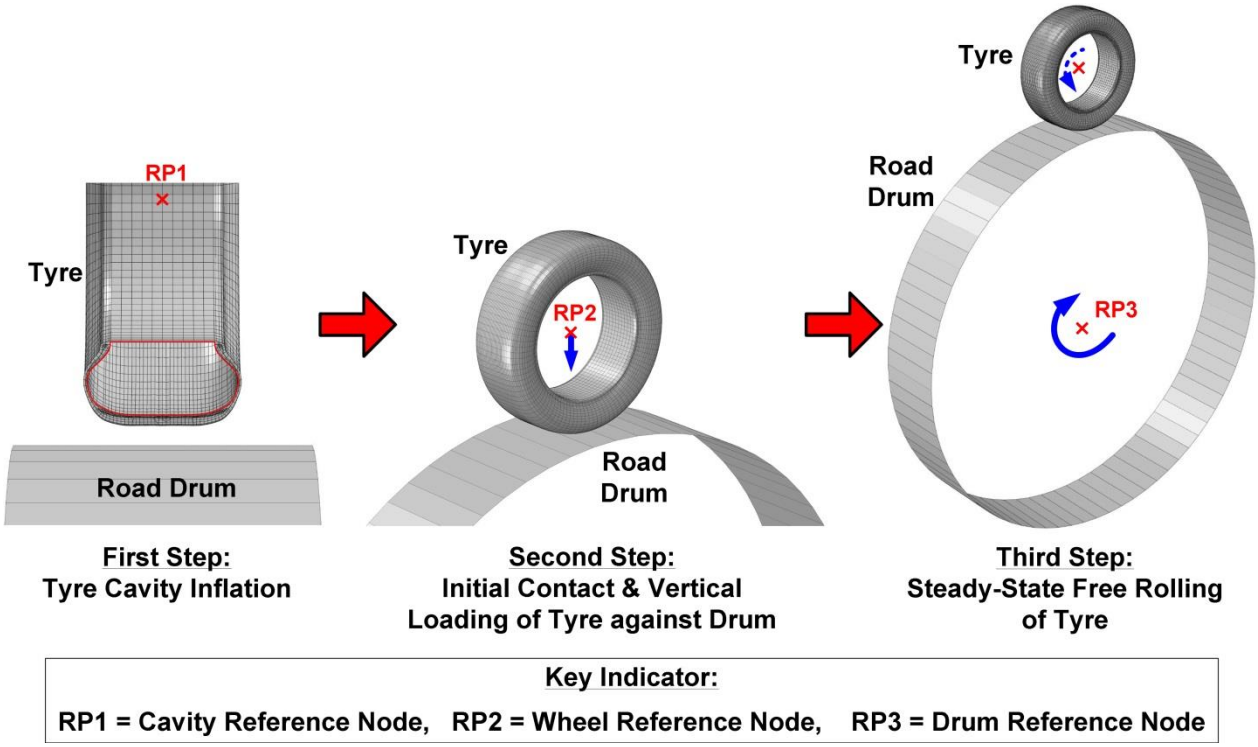


Figure 4.7 FE Simulation Steps for Complete Tyre Analysis

For the third step, the tyre was contact-driven by the road drum for steady-state free rolling around its wheel reference node (RP2) in a straight-line at a targeted constant speed. This is through rotating the road drum at the relevant angular velocity around its reference node (RP3) for at least three seconds to ensure reaching a steady-state rolling. In this step, a small amount of viscous contact damping was used to minimise the numerical noises in Abaqus/Explicit solution without influencing the physical rolling process. This was done by introducing a contact-damping property within the general contact definition of the tyre/drum with a unitless damping coefficient (0.03) as a fraction of the tyre critical damping computed internally by Abaqus/Explicit solver at the contact-patch during analysis [249]. For cornering simulation, the same simulation steps, as in

straight-line rolling, were used with the exception of changing the orientation of the road drum to lie at an angle relative to the tyre's longitudinal axis corresponding to the targeted cornering slip angle as seen in Figure 4.8.

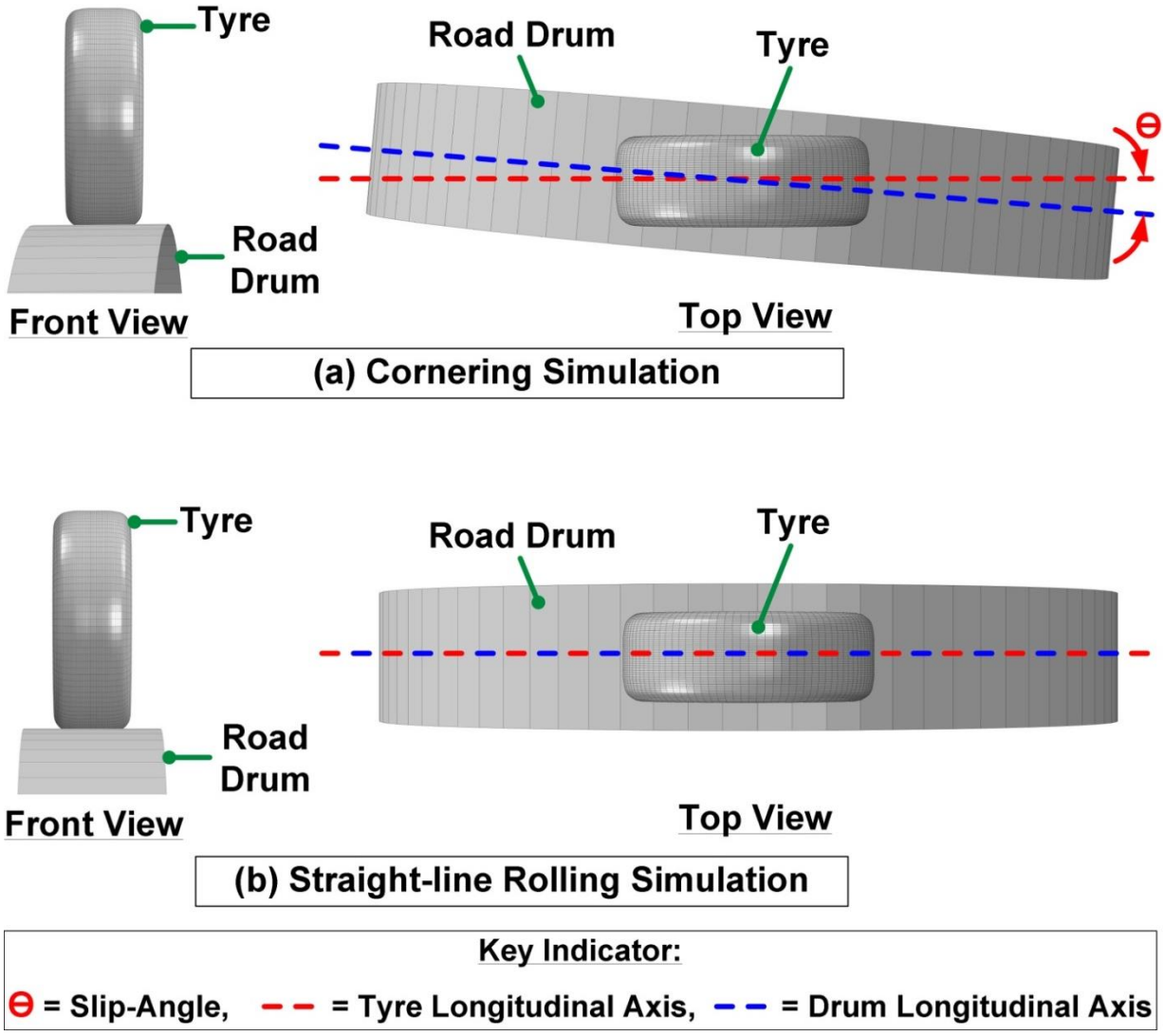


Figure 4.8 Tyre/Drum Model Orientation for (a) Cornering and (b) Straight-Line Rolling

To further minimise from the solution noises, Abaqus/Explicit analysis was run in “double precision” mode for more precise numerical roundoff of the FE results given the size and the nature of the FE tyre model [250, 251]. Furthermore, for the FE post-processing stage, the FE solution outputs were treated using low-pass (finite impulse response) filtration whenever it was needed to remove the numerical noises [252].

4.4 MESH REFINEMENT

To have a working FE model that yields the correct tyre response, a fine element mesh of the FE tyre model is required in terms of shape and density in which a mesh-independent, consistent and accurate FE solution is obtainable with no convergence problems and with the minimum computational costs possible. For this purpose, the following mesh refinement analyses were done in which a uniform 3D meshing was used across the entire tyre circumferentially since the tyre is being modelled explicitly:

4.4.1 Shape Quality

An “element shape quality” analysis was performed on the 2D axisymmetric tyre model (i.e. as the cross-sectional interface of the 3D tyre model) using the mesh verification tool available in Abaqus/CAE. In the analysis, the quality of the model’s element shape was assessed through its aspect ratio (i.e. ratio of the longest to the lowest side of an element) and internal angles [253]. According to the default criteria of Abaqus [253], the element shape is of good quality if the aspect ratio is below 10 (i.e. no large aspect ratios) and each internal angle falls between 10 and 160 degrees (i.e. no extreme corner angles).

The mesh quality analysis showed that the standard tyre profile, shown in Figure 4.5, had a good shape quality since the worst aspect ratio was found no more than 5.1 whereas the corner angles had a minimum of 25 and a maximum of 150.5 degrees in the model in which the average minimum angle was 72 and the average maximum was 108 degrees. The mesh refinement was more focused toward the tread region since it has the largest mass entity and is the only part that is in contact with the road; experiencing most of the deformation in the model. Although further mesh refinement is possible, the current fine meshing was used since a balance was needed to be achieved between the mesh refinement level and the computational efficiency [5].

4.4.2 Sensitivity Analysis

A “mesh convergence evaluation” was conducted on the entire 3D tyre model to determine the appropriate mesh density circumferentially that would provide mesh-independent, consistent and accurate FE outputs using minimum computational resources [254]. For this purpose, the 3D model of the standard tyre was subjected to a quasi-static footprint analysis at a common vertical load of 4000 N and a reference inflation pressure of 220 KPa using different mesh densities from coarse to fine similar to Yang [5]. The maximum pressure at the tyre contact-patch was assessed as the FE output and the CPU time was recorded as shown in Figure 4.9 using four CPU processors with 20 GB memory to run the 3D model analysis. The FE output of the maximum contact pressure was chosen since it is closely related to the tyre’s grip,

inflation pressure, vertical loading and hence rolling-resistance which are all of interest and to be investigated in this research work later in the next chapters.

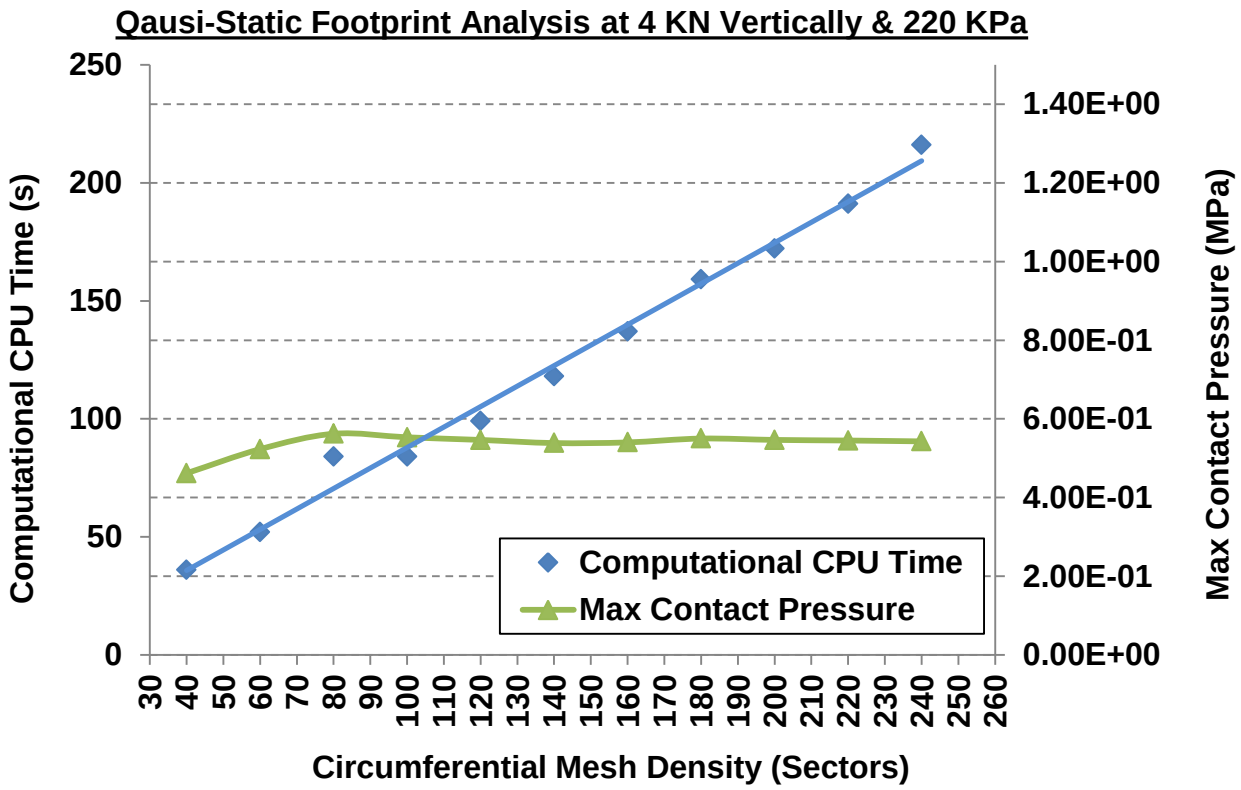


Figure 4.9 Mesh Convergence Analysis for 3D Standard Tyre Model

According to the convergence results in Figure 4.9, the 3D tyre model starts to yield consistent FE output at a mesh density of 140 sectors circumferentially and above whereas the CPU time incurred a linear increase with the increase of mesh density. The mesh density of 140 sectors would be a proper choice for the 3D tyre model due to its accurate FE output and reasonable computational cost compared to other mesh densities. However, for this research work, the best mesh density for the tyre model was

found to be 200 sectors despite the higher computational cost incurred as will be explained in section 4.4.3 next.

4.4.3 Energy Outputs Analysis

A further assessment for the validity of the simulation response of the 3D tyre model was to examine the model's energy outputs, in particular, the "total energy (ETOTAL)" and the "artificial strain energy (ALLAE)" [235]. For the "total energy" (ETOTAL), the total energy of the 3D tyre model was readily obtained as an FE history output from Abaqus/Explicit analysis in which it is represented in the FE model by the following energy balance equation [255]:

$$\mathrm{ETOTAL} = \mathrm{ALLKE} + \mathrm{ALLIE} + \mathrm{ALLVD} + \mathrm{ALLFD} - \mathrm{ALLWK} - \mathrm{ALLPW} \approx \mathrm{Constant} \qquad (4.1)$$

The total energy of a valid FE model should be "zero" for static analyses and approximately "constant" at non-zero value with an allowable error of ~1% for dynamic analyses [235, 244, 256]. Such a trend of total energy confirms that the external energies are balanced out by the kinetic and internal energies in the tyre model in which the model solution is physically following the principle of conservation of energy [257, 258]. The ETOTAL output for the standard tyre model was assessed for the economical option of tyre mesh density of 140 sectors circumferentially and found to show nearly zero at quasi-static analyses (i.e. tyre inflation and vertical loading) and almost a constant profile but with more than 1% deviation at the dynamic rolling stage as seen in

Figure 4.10. However, with mesh refinement of 200 sectors circumferentially, the standard tyre model was found to yield almost zero ETOTAL at the quasi-static stage of tyre simulation and nearly constant profile with ~1% error at the dynamic stage indicating that the model is complying with the conservation law of energy. A similar finding was reached by Zuo *et al.* [244].

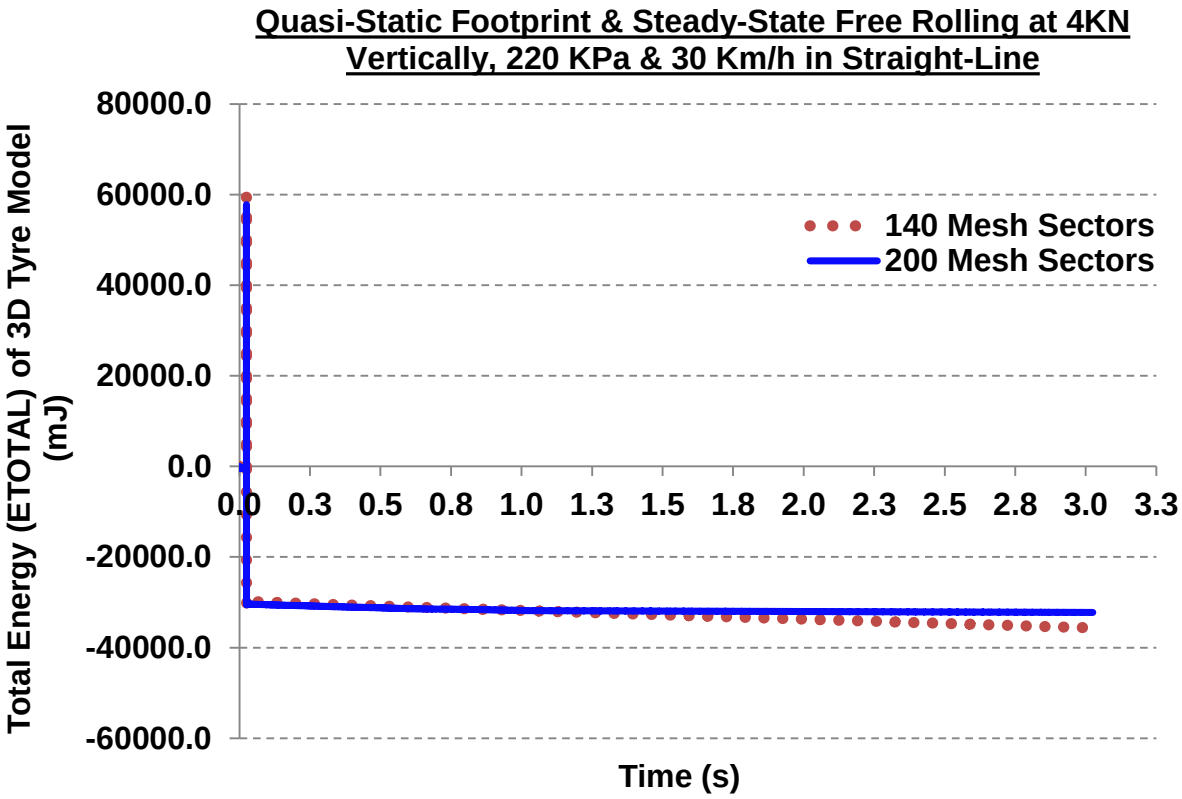


Figure 4.10 Total Energy (ETOTAL) for 3D Standard Tyre Model

As for the “artificial strain energy” (ALLAE), it is important for the 3D tyre model to have low ALLAE throughout the tyre simulation in order to ensure that the tyre has a good mesh quality and is being simulated physically in a proper way with no instabilities

influencing the solution accuracy such as excessive hourglassing effects as discussed previously [221, 259, 260]. To verify the level of the artificial strain energy, the ratio of the artificial strain energy (ALLAE) to the total strain energy (ALLIE) is assessed in which the ALLAE is considered to be low if the ratio was below 10% as a general rule [221, 244, 258]. For the 3D standard tyre model, the ALLAE/ALLIE was found to start with a ratio of above 10% and then fall below it at a later time toward the middle of tyre simulation for the mesh density case of 140 sectors as indicated in Figure 4.11. For a more stable model, a mesh refinement of 200 sectors was found to yield ALLAE/ALLIE below 10%; indicating negligible hourglassing effects and the model is physically simulating the tyre rolling process correctly. Zuo *et al.* [244] showed a similar conclusion in their work.

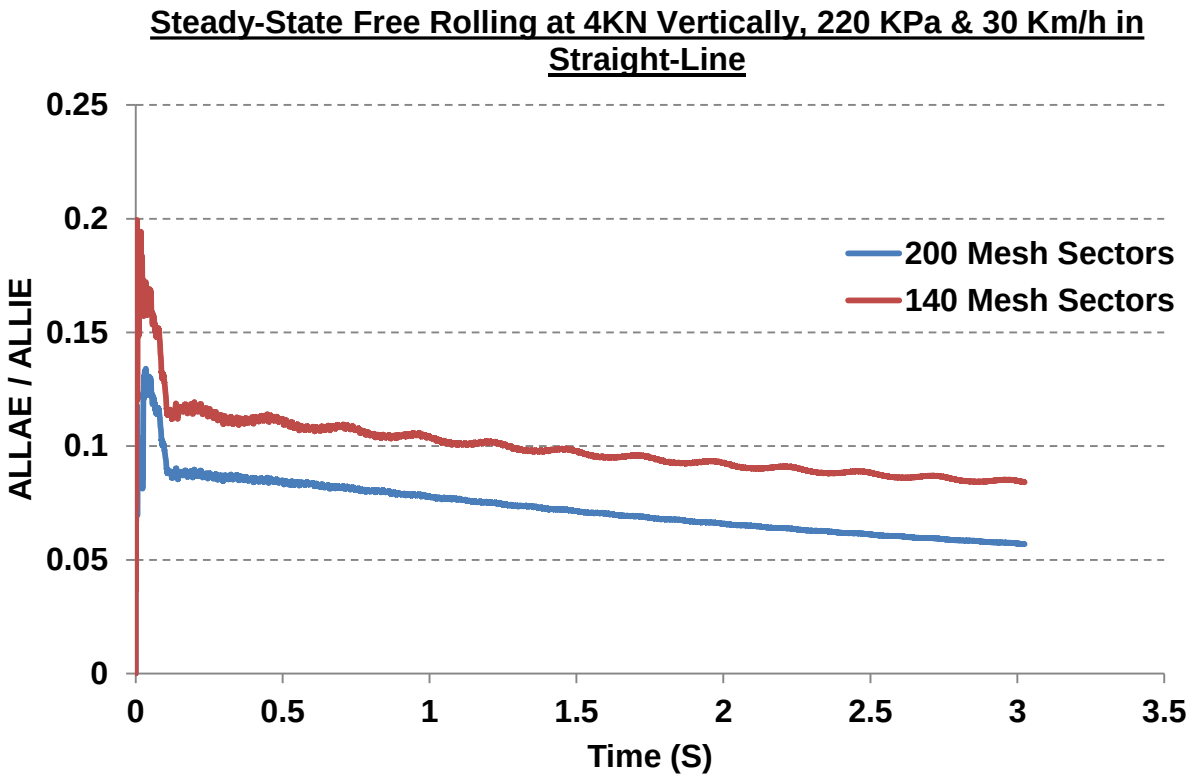


Figure 4.11 ALLAE/ALLIE Ratio for 3D Standard Tyre Model

Therefore, based on the previous energy outputs of the standard tyre model (i.e. base model for tyre designing), a tyre mesh density of 200 sectors circumferentially was adopted to run the tyre simulations properly.

4.5 FE MODEL VALIDATION

Apart from validating the FE model is functioning correctly in section 4.4, the 3D FE model of the standard tyre was required to be validated for yielding the same tyre response as that of the actual tyre it is simulating in practice. This is to ensure having a working FE model capable of producing FE results that are to be trusted and relied upon

as true especially for designing purposes. The best way to carry-out such validation was to conduct the tyre tests of interest numerically using the FE tyre model and compare the results with their corresponding experimental tests for similarity as illustrated in the next sections.

4.5.1 Validation (Experimental) Tool

According to the literature survey done in section 2.3.2.2, the best experimental method chosen for FE validation was the in-door testing using the laboratory tyre/drum rig with respect to this research aim and objectives. For this research, a “tri-axial electro-hydraulic tyre/drum rig” was used to conduct the majority of the experimental tests. The tyre/drum rig can perform a variety of static and dynamic rolling tests (e.g. footprint, vertical stiffness, straight-line rolling and cornering). The test rig has three axes of operation (i.e. vertical, longitudinal and lateral) and two test configurations (i.e. “straight-line rolling” and “cornering”) as shown in Figure 4.12 and Figure 4.13 respectively.

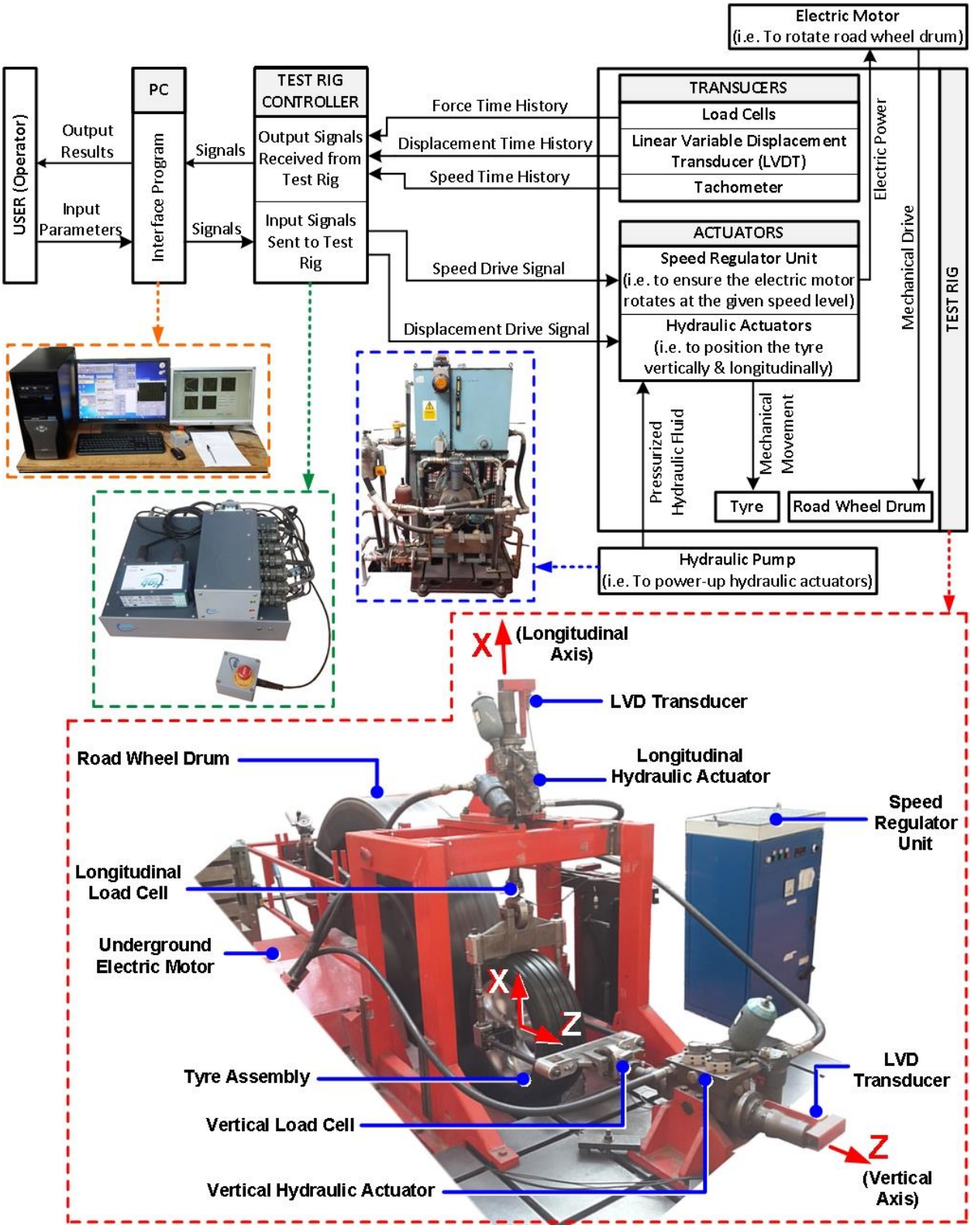


Figure 4.12 “Straight-Line Rolling” Set-Up of Tri-Axial Electro-Hydraulic Tyre/Drum Rig

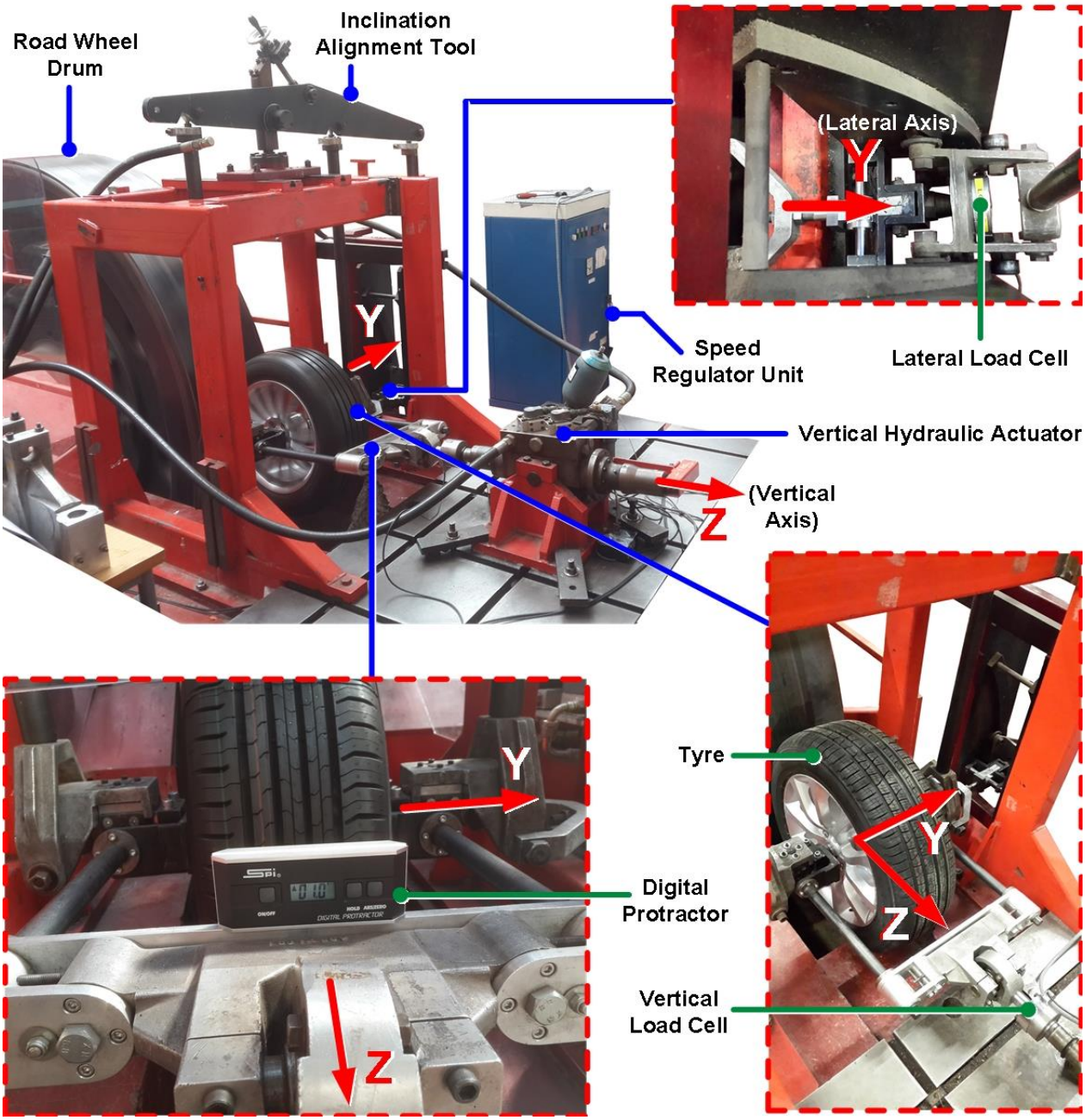


Figure 4.13 “Cornering” Set-Up of Tri-Axial Electro-Hydraulic Tyre/Drum Rig

The tyre/drum rig operates through a set of transducers (i.e. tachometer, LVDT and load cells) and actuators (i.e. speed regulator unit and hydraulic actuators) that are controlled

by a PC with a controller unit and powered by an electrical motor and a hydraulic pump. Through the PC with the controller unit, a 2.44 metres diameter drum of a smooth-and-even steel surface, representing the road in the test rig, was belt-driven by the electrical motor at a given rolling velocity. In the test rig, the position of the tyre unit was controlled vertically or both vertically and longitudinally by hydraulic actuator arms (i.e. powered by the hydraulic pump) via the PC with the controller unit based on the current tyre's coordinates supplied by LVDT transducers. This is to re-align the tyre with respect to the road drum, bring the tyre into initial contact with the road drum, and push the tyre against the road drum at a given vertical load. Generally, the main experimental readings that can be obtained from the tyre/drum rig are the force measurements at the tyre's wheel spindle using bi-directional pancake load cells of 0.5 tonne capacity with ±0.05% reading (accuracy) error in the vertical, longitudinal and lateral directions respectively.

Besides the tyre/drum rig, another experimental tool used for FE validation was "Faro Edge ScanArm" which is a 3D laser scanner probe with an accuracy of ±25 μm as seen in Figure 4.14. Faro scanner was used with a PC equipped with a 3D CAD program to scan and capture the outer tyre profile at different inflation pressures with respect to the tyre wheel centre as a reference and import the scanned profile as a 3D CAD model made of numerous coordinate points.

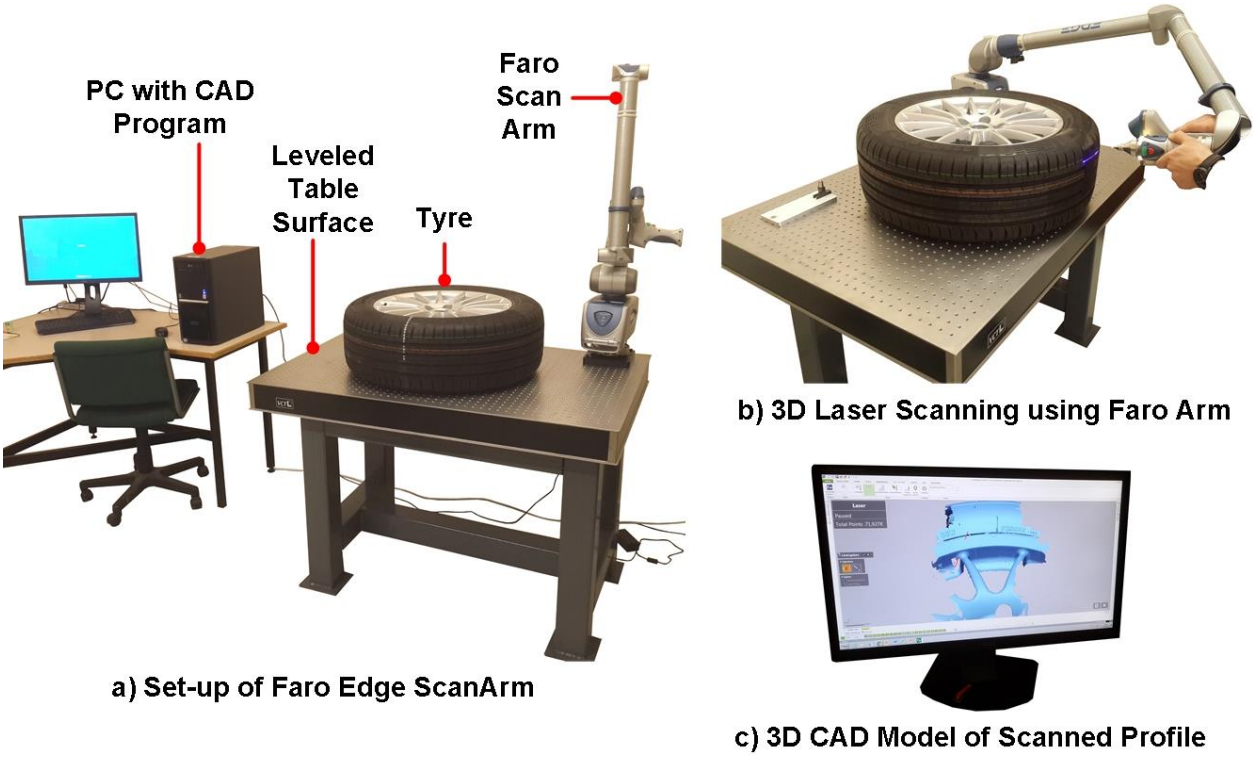


Figure 4.14 Experimental Set-Up of Faro Edge ScanArm

4.5.2 Validation Scope

The FE model of the standard tyre was validated by measuring a set of tyre properties that are directly related to this research aim, objectives and scope in sections 1.2 and 1.3 respectively. Both static and dynamic tyre properties were used in the validation which the FE tyre model is required to predict in order to able to evaluate the different tyre structural designs (i.e. multi-chamber tyre designs) later with respect to the core rolling-resistance and other fundamental driving requirements in line with this research aim and scope. Those static and dynamic tyre properties are highlighted in sections 4.5.2.1 and 4.5.2.2 respectively.

Besides ensuring the accuracy and precision of FE model in sections 4.3 and 4.4, prior to conducting the main validation tests, the experimental set-ups for FE validation (i.e. Faro Scanner and Tyre/Drum Rig) were assessed for their accuracy (i.e. systematic error) and precision (i.e. random error) as per the relevant assessment standards similar to that of section 3.2. For example, the longitudinal load cell of the tyre/drum rig was checked to have up-to-date calibration and the proper accuracy for the rolling-resistance test (i.e. reading error of ±0.5 N) according to ISO 18164:2005 [261]. Also, under the same tyre testing conditions with a minimum of three measurements, the repeatability (i.e. precision) of the rolling-resistance force readings of the load cell was evaluated and found to have an acceptable standard deviation of rolling-resistance coefficient measurements of ≤ 0.075 N/KN in agreement with ISO 28580:2009 [262].

All the FE and experimental runs for both static and dynamic properties validations were conducted at ~25 °C, assuming an isothermal equilibrium. Furthermore, to ensure and maintain the precision of the experimental readings, each experimental run of the same testing conditions was repeated at least three times to obtain an averaged measurement. For the “tyre/drum rig”, prior to conducting the experiments, the tyre has been dynamically balanced using a wheel balancer machine as seen in Figure 4.15 to ensure a stable run and then fitted to the tyre/drum rig and re-aligned properly with the centres of the road drum, the hydraulic actuator(s) and the load cells for correct experimental measurements.

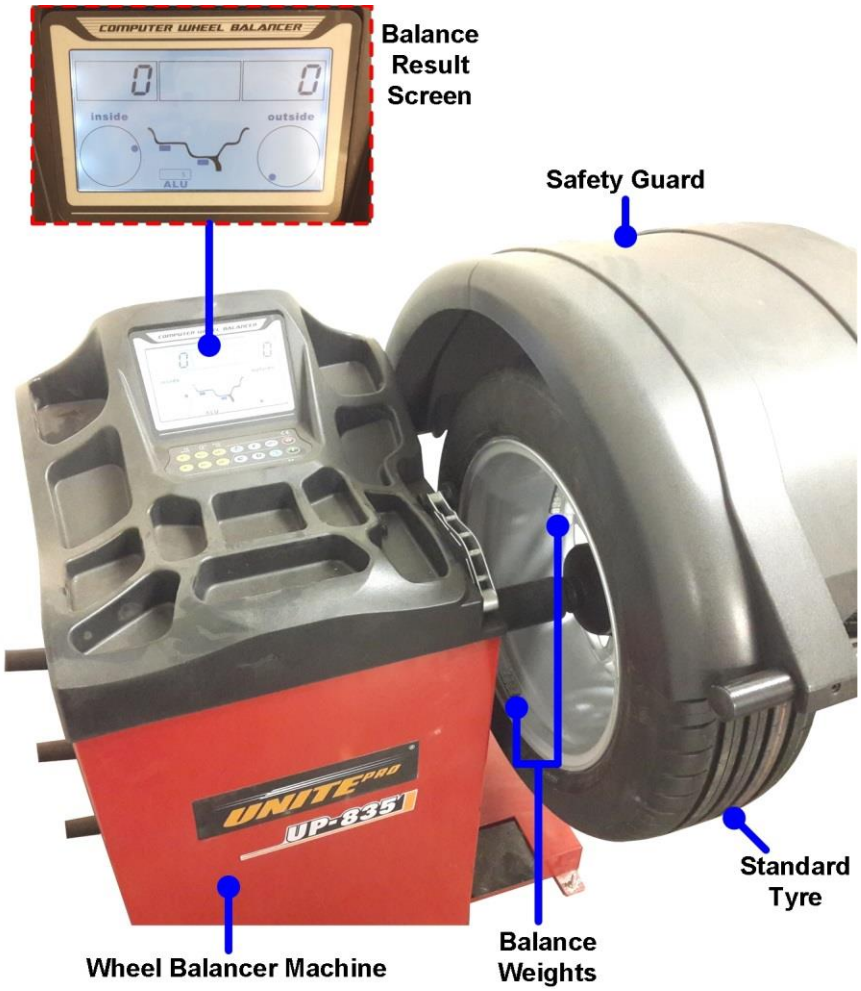


Figure 4.15 Mass Balancing of Standard Tyre/Wheel Assembly using Wheel Balancer

4.5.2.1 Assessment of Static Tyre Properties

As the first stage of FE validation, three quasi-static properties of the tyre were assessed both numerically and experimentally due to their close relation to the rolling-resistance, grip and mechanical comfort (cushioning). Those properties are the tyre's inflation, vertical (radial) stiffness and footprint area [30] as illustrated below:

A) Inflation Validation:

For the “inflation” validation, the geometrical changes in the outer tyre profile were measured at the tread centre and the outermost point of the sidewall of the tyre as a result of inflating the tyre’s cavity with different inflation pressures respectively as indicated in Table 4.1. A wide range of inflation pressure was used to evaluate the capability of the FE model to predict tyre deformation since it is a non-contact test and there is no risk of damaging the tyre at low pressure whereas the maximum pressure applied falls within the operating range of the standard tyre.

Table 4.1 Testing Settings for Inflation Validation of Standard Tyre

Test Number	Inflation Pressure (KPa)
1	0
2	160
3	200
4	240
5	280

In FE, the inflation step was simulated in the 3D FE model of the standard tyre using Abaqus 6.13-1 as indicated in section 4.3.3. Since the tyre has a symmetrical profile circumferentially, the relevant nodal displacements in the inflation direction were requested as a field output from a reference node at the tread centre and another at the sidewall outermost. Experimentally, for the actual tyre, similar to FE, the Faro ScanArm was used to scan and capture the geometrical change at a specific sector of the outer tyre profile for comparison purposes as seen in Figure 4.14. From the scanned CAD profile, the coordinates of the tread centre and the outermost sidewall point were

extracted at the given tested inflation and compared with that of “0” KPa profile as a benchmark for displacement in the inflation direction.

B) Vertical Stiffness Validation:

For the “vertical (radial) stiffness” validation, the tyre was brought into initial contact with the road drum and then pushed against the road surface quasi-statically in the vertical direction for a given vertical displacement while recording the time-history of the normal reaction force at the tyre centre or wheel spindle for different inflation settings as indicated in Table 4.2. More practical inflation settings were used for the stiffness validation to prevent damaging the tyre since it involves contact with the road drum whereas 220 KPa was chosen as the reference inflation pressure for the standard tyre given its specifications. The tyre’s stiffness was computed from the relationship slope of the normal reaction force recorded against the corresponding vertical displacement travelled by the tyre during contact.

Table 4.2 Testing Settings for Stiffness Validation of Standard Tyre

Test Number	Inflation Pressure (KPa)	Vertical Displacement or Deflection (mm)
1	180	24
2	200	
3	220	
4	240	
5	260	

In FE, the vertical stiffness modelling of the tyre was conducted by applying the inflation and contact simulation steps (i.e. first and second steps) indicated in section 4.3.3. Since an Abaqus/Explicit solver is used to run the FE simulation, the time-history record of the vertical reaction force had some numerical noises which were treated through linear regression. For the corresponding experimental part, the vertical stiffness validation was performed using the “tri-axial electro-hydraulic tyre/drum rig” shown in Figure 4.12.

C) Footprint Validation:

As for the “footprint area” validation, two sets of validation tests were conducted by bringing the tyre into initial contact with the road drum and then vertically loading the tyre against the drum quasi-statically to a targeted level in which the total area of the contact-patch was computed once the tyre has reached full contact with the road drum. One set involved testing the tyre at fixed inflation but different vertical loadings respectively, whereas the other set had the opposite testing conditions as seen in Table 4.3. In the first test set, the inflation was made fixed at 220 KPa since it was the normal inflation level for the standard tyre as indicated earlier while the second test had the vertical loading made constant at 4000 N since it is found to be within the common range of operating loads for such tyre category.

Table 4.3 Testing Settings for Footprint Validation of Standard Tyre

Test Set	Run Number	Inflation Pressure (KPa)	Vertical Load (N)
1	1	220	1000
	2		2000
	3		3000
	4		4000
2	1	180	4000
	2	200	
	3	220	
	4	240	
	5	260	

Similar to stiffness modelling, in FE, the footprint modelling of the tyre was performed by applying the inflation and contact simulation steps (i.e. first and second steps) indicated in section 4.3.3. With Abaqus/Explicit solver, the available option to calculate the total area in contact between the tyre and the road drum was to request the “CAREA” history output. A contour visualisation of the contact-patch area is not available in Abaqus/Explicit solver. However, a contour plot of the contact pressure distribution (i.e. via CPRESS field output) was possible to use as a general approximation of the actual footprint profile of the tyre [222, 263, 264]. For the experimental counterpart, the “tri-axial electro-hydraulic tyre/drum rig” was used again to carry-out the footprint tests in which the tyre footprint area was captured by having the related contact surface of the tyre sprayed with black-ink beforehand and imprinted against a white A4-paper attached on the road drum surface. Later, the imprint of the tyre footprint was image scanned into a PC and processed digitally to capture the footprint outline on 1:1 scale and calculate the contact patch area from the captured closed-loop outline as seen in Figure 4.16.

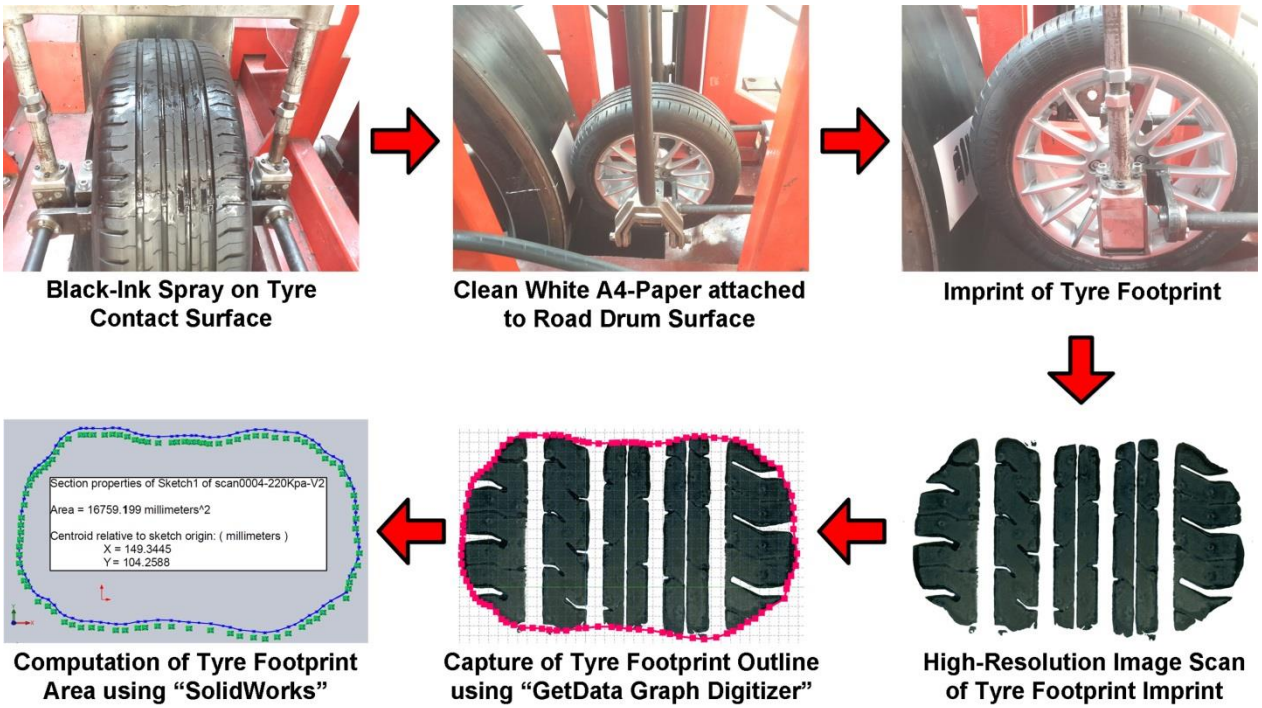


Figure 4.16 Experimental Capture Process of Tyre Footprint Area

In this section, the validation procedures adopted for the tyre static properties were similar to that done by both Yang [5] and Wei [7].

4.5.2.2 Assessment of Dynamic Tyre Properties

For the second stage of FE validation, three dynamic properties of the tyre were validated and they are the tyre's non-uniformity, rolling-resistance and cornering as indicated next:

A) Non-Uniformity Validation:

In the “tyre’s non-uniformity” validation, the variations in the vertical (radial) and lateral forces at the tyre’s centre or wheel spindle were measured while the tyre is in full contact with the road drum and free-rolling at a steady-state in a straight-line on smooth flat surface for the rolling conditions listed in Table 4.4 respectively. The reason for conducting the non-uniformity validation at a constant velocity is to be explained later in the rolling-resistance validation. The non-uniformity testing was conducted based on that of Michelin except for the testing conditions to suit this research scope [265].

Table 4.4 Rolling Conditions for Non-Uniformity and Rolling-Resistance Validations of Standard Tyre

Test Set	Run Number	Inflation Pressure (KPa)	Vertical Load (N)	Rolling Velocity (Km/h)
1	1	220	1000	30
	2		2000	
	3		3000	
	4		4000	
2	1	180	4000	
	2	200		
	3	220		
	4	240		
	5	260		

Normally, the non-uniformity test is conducted to assess the newly made tyres for any manufacturing flaws or imperfections resulting in undesirable non-uniformities in the tyre’s structure during rolling and hence leading to uncomfortable or unstable rolling ride [266]. Nevertheless, for this research project, the manufacturing flaws are considered negligible or non-existent since the actual tyre (i.e. standard tyre) investigated is a new

and an approved end-product, whereas the developed FE tyre model is of perfect symmetrical geometry and even mass distribution about its rotational axis. In that regard, the non-uniformity test can be used as an indicator of the deformational variations in the tyre's profile during rolling due to the tyre's structural design and characteristics [30]. This is since the tyre is free-rolling at a steady-state and on a smooth flat surface which makes the contribution of traction, braking and road roughness negligible on the tyre profile stability during rolling leaving the tyre structural design as the main contributor.

In FE, the non-uniformity test was conducted by applying all the simulation steps indicated in section 4.3.3 respectively for a free-rolling at a steady-state in a straight-line in which the history outputs for the vertical and lateral reaction forces at the tyre centre node (RP2) were extracted once the tyre has reached the steady-state rolling of fixed velocity. The corresponding experiment was performed using the "cornering configuration" of the tyre/drum rig in Figure 4.13. This is in order to be able to measure both the vertical and lateral forces at the tyre wheel spindle when the tyre is free-rolling at a steady-state of a constant velocity in which the inclination alignment tool with the digital protractor was used to set the tyre rolling in a straight-line (i.e. 0° slip angle). In line with ISO 18164:2005 [261], prior to the main test, the tyre was thermally conditioned for three hours at ~25 °C and then had a warm-up run for 30 minutes for the first testing conditions and 10 minutes for each subsequent testing conditions. For both the FE and

experimental outputs, a low-pass (finite impulse response) filtration was applied whenever it was necessary to eliminate noises from the recorded data.

B) Rolling-Resistance Validation:

For the “rolling-resistance” validation, the same rolling conditions as that of the non-uniformity validation were used as seen in Table 4.4. In this research project, the rolling-resistance is described as the “energy lost per unit distance travelled” by the tyre because it is found to be a more comprehensive definition and valid for a broader range of applications including complex and highly non-linear contact problems as indicated previously in section 2.3 [65, 67, 68]. The core rolling-resistance caused by the internal losses of the tyre structure (i.e. mechanical hysteresis) was chosen to be assessed only without including other contributing factors. This is in order to be able to independently evaluate the impact of the tyre structural design on the rolling-resistance in accordance with this research aim and scope in chapter (1). In this context, the tyre was tested for rolling-resistance under steady-state and free-rolling conditions of fixed rolling velocity in a straight-line path on a smooth, even and non-deformable road surface. This is to eliminate or significantly minimise to a negligible level the effects of traction, braking and road surface roughness on the tyre’s rolling-resistance [245, 267-269].

Furthermore, the tyre was set to roll at a constant low velocity of 30 Km/h only to exclude the impact of aerodynamic drag on the tyre’s rolling-resistance [20, 21, 30]. This is since increasing the rolling velocity above 30 Km/h would lead to the aerodynamic drag to grow and begin to add more rolling-resistance to the tyre gradually where this

influence shoots up sharply at 120 Km/h with the formation of standing waves in the tyre [8, 85]. As for 30 Km/h and below, the rolling velocity is concluded to have no influence on the tyre's rolling-resistance [8, 20, 23, 83, 85]. Such experimental set-up would make the rolling-resistance dependent primarily on the tyre's structural deformation (i.e. mechanical hysteresis due to viscoelasticity) which can count up to 95% of the total rolling-resistance of the tyre under the given rolling conditions [8, 10, 20, 152].

In the FE solution, the same simulation steps as that of the non-uniformity validation were applied to have the tyre reaches a free-rolling at a steady-state in a straight-line and a constant rolling velocity. For computational efficiency, a proposed method was introduced to compute the rolling-resistance according to the "hysteresis damping ratio" produced by the entire tyre and the "work done by the vertically loaded tyre at the contact-patch" as shown in Figure 4.17 [187]. In this method, after the tyre reaches a steady-state under the prescribed rolling conditions, the "hysteresis damping ratio" (HR) of the entire tyre structure was possible to determine from the gradient of the time history outputs of the dissipated energy (ALLCD) over the total strain energy (ALLIE) of the tyre. Given the FE model captures the entire tyre geometry in great detail, the ALLCD/ALLIE ratio encompasses the hysteresis damping due to any structural deformations developed in the complete tyre geometry or its dimensional profile during rolling including the contact-patch. Nevertheless, the ALLCD/ALLIE ratio excludes the input of the road drum and only considers the input of the complete tyre structure.

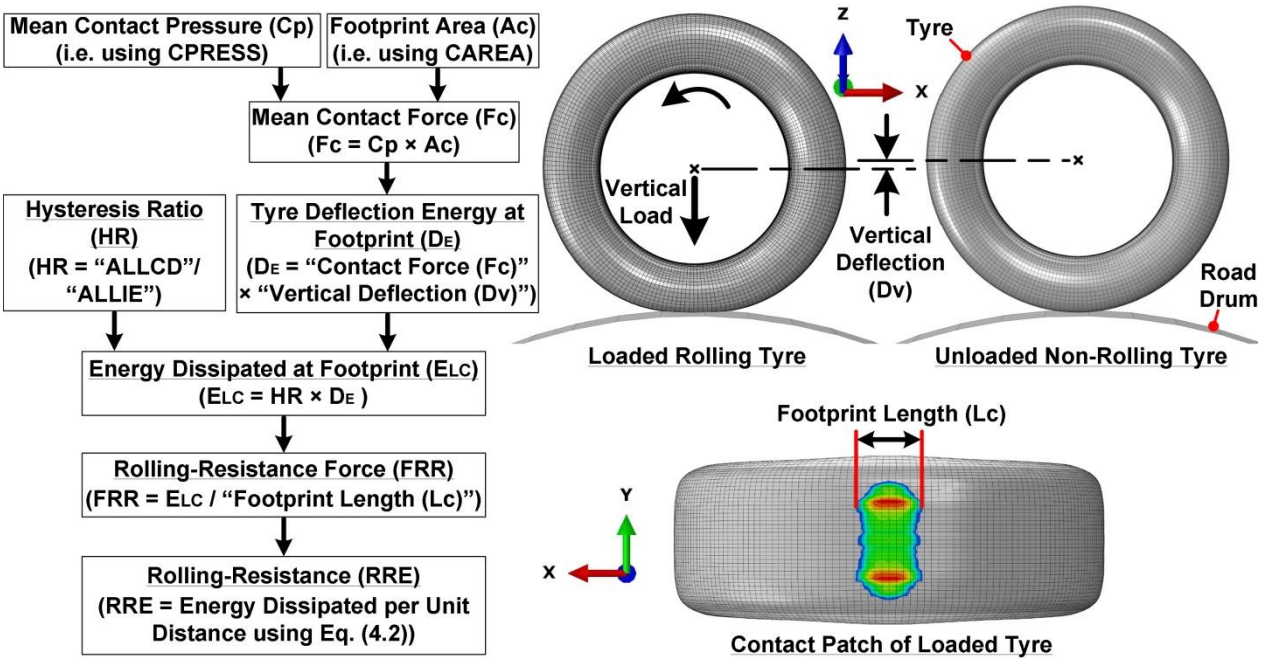


Figure 4.17 Rolling-Resistance Computation in FE Simulation [187]

Under the given rolling conditions, the dominant and governing deformational work that gives rise to the rolling-resistance in the tyre would be the tyre deformation at the contact-patch under vertical loading during rolling [270]. Based on that, the energy needed to deform the tyre vertically against the road drum (i.e. deflection energy (D_E)) was possible to determine through the work done during such process which can be found from the product of the mean of the normal contact force (F_C) at the contact-patch against the vertical deflection travelled by the tyre (D_V). To specify the amount of energy lost during such deformation at the contact-patch (E_{LC}), the "hysteresis ratio" (HR) was multiplied by the "deflection energy" (D_E). From that, it was possible to compute the "rolling-resistance force" (F_{RR}) by dividing up the "energy lost at the contact-patch" (E_{LC}) over the "length of the contact-patch" (L_C). As per ISO 18164:2005 for tyre/drum contact

[261], the rolling-resistance of the tyre (RRE), as the energy dissipated per unit distance travelled, was determined from the "rolling-resistance force" (F_{RR}) using Eq. (4.2):

$$\mathrm{RRE} = \mathrm{F_{RR}} \,.\left(1 + \frac{\mathrm{R_L}}{\mathrm{R_D}}\right) \tag{4.2}$$

In the experimental part, the rolling-resistance testing was conducted using the "straight-line rolling" configuration of the tyre/drum rig in Figure 4.12 as per ISO 18164:2005 [261] except for the testing conditions to meet this research aim and scope. Similar to the non-uniformity test, thermal conditioning followed by warm-up runs were performed for the tyre prior to the main test(s). Also, prior to the main test, a skim load test was conducted where the tyre rolled at the velocity and inflation pressure to be tested at in the main test but with a very light vertical load of ~100 N to maintain tyre's contact with road drum without slippage. The skim load test was used to measure and exclude the parasitic losses, which involves the frictional losses of the tyre/drum contact, from the tyre's rolling-resistance measurements [261]. During the main test, the longitudinal force (i.e. rolling-resistance force) was measured at the wheel spindle when the tyre was free-rolling at a steady-state of a constant velocity. The measured force was converted to the rolling-resistance as the energy lost per unit distance using Eq. (4.2).

C) Cornering Validation:

As for "cornering" validation, the lateral forces were measured at the tyre centre or wheel spindle as the tyre was in full contact with the road drum and free-rolling in a steady-

state of a constant velocity for different slip angles respectively as indicated in Table 4.5. A rolling velocity of 10 Km/h was chosen since the velocity has a negligible impact on the cornering forces for the given slip angles and rolling conditions [271, 272]. This is in addition to improve the FE computational efficiency.

Table 4.5 Rolling Settings for Cornering Validation of Standard Tyre

Test Number	Slip Angle (Degrees)	Inflation Pressure (KPa)	Vertical Load (N)	Rolling Velocity (Km/h)
1	1	220	4000	10
2	2			
3	3			
4	4			
5	5			

The FE solution for cornering was obtained applying the relevant simulation steps in section 4.3.3. For the experimental counterpart, the cornering set-up of the tyre/drum rig in Figure 4.13 was used to set the tyre at different slip angles using the “inclination alignment tool” and the “digital protractor” provided in which the lateral forces were possible to measure utilising the lateral load cell available.

4.5.3 Static Validation and Analysis

4.5.3.1 Geometrical Inflation Analysis

As per the inflation validation in section 4.5.2.1, the FE outputs show a good agreement with its experimental counterpart as seen in Figure 4.18 and Figure 4.19 for the displacements induced by inflation in the tread centre and sidewall outmost points

respectively. This indicates the capability of the FE model to predict the deformations in the tyre profile close to that in practice.

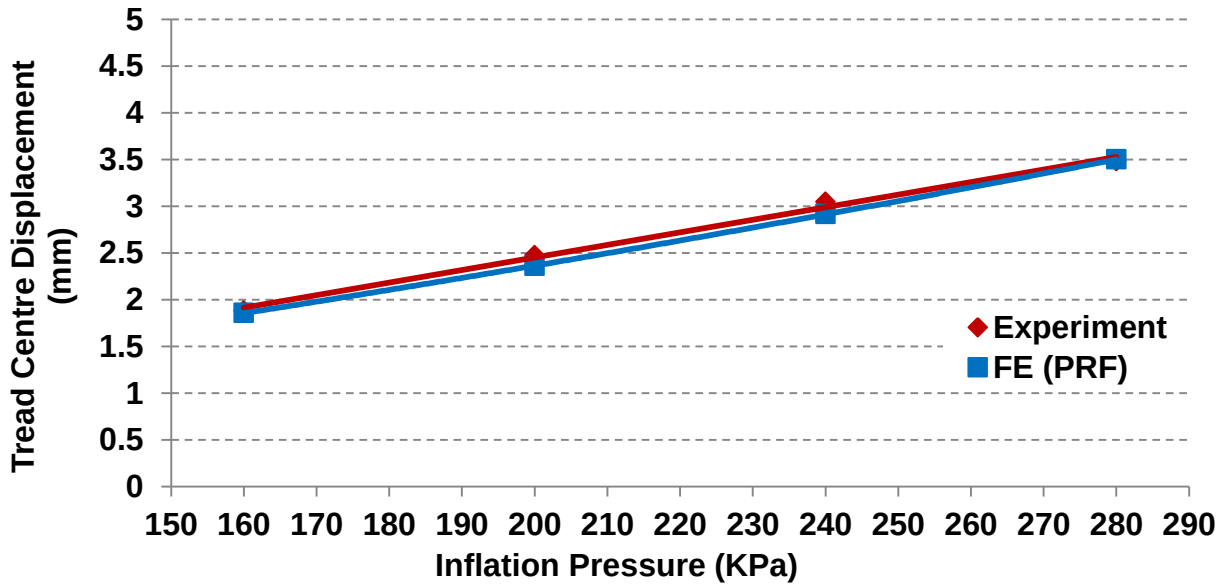


Figure 4.18 Tread Centre Displacement due to Inflation

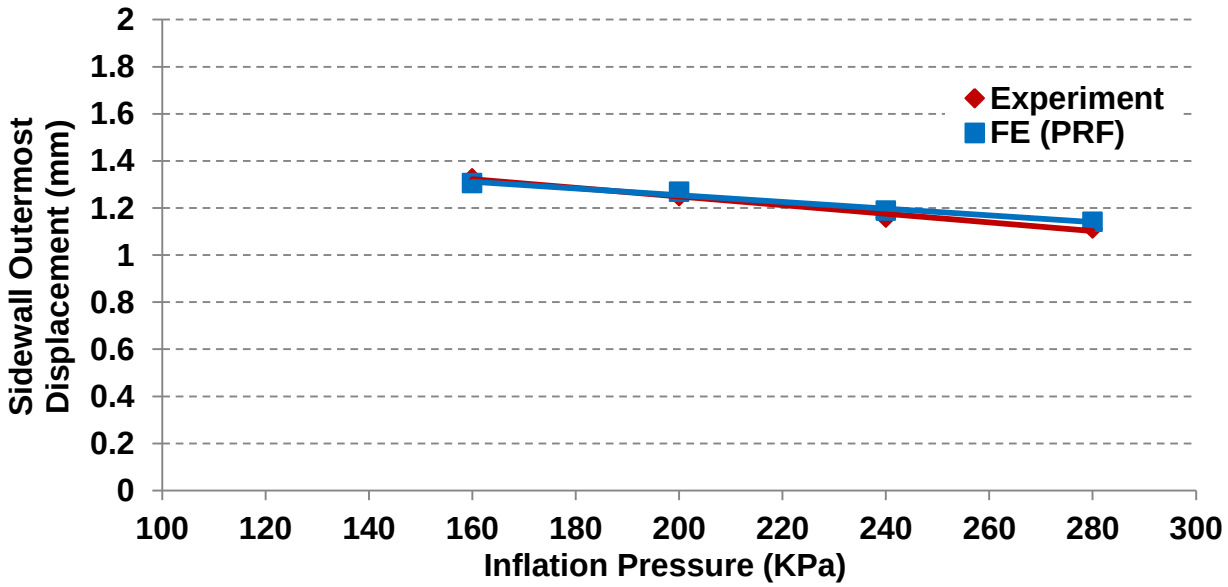
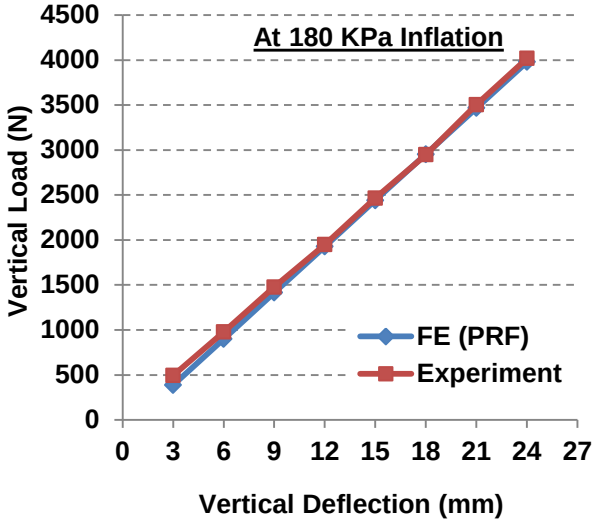


Figure 4.19 Sidewall Outermost Displacement due to Inflation

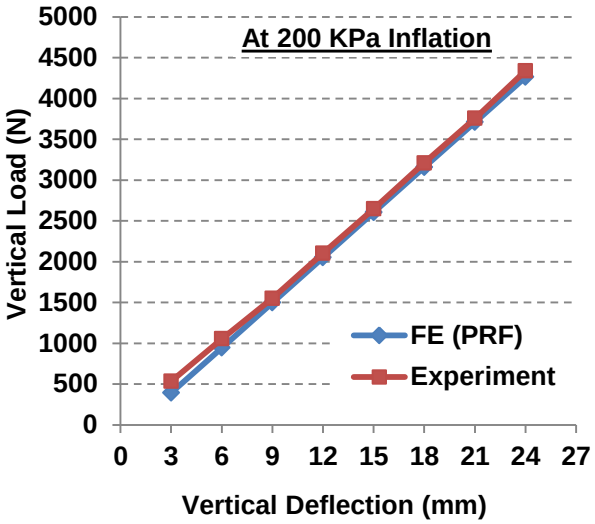
With the increase of the inflation pressure, the inflation results illustrate that the tread would be pushed outward whereas the sidewall would be pulled inward a little to accommodate a taller and thinner tyre profile. This is because increasing the inflation pressure would mean more air molecules accumulated inside the tyre cavity and compressed against each other and the cavity boundaries leading to pushing the (thick and hard) tread part outward which in turn would cause pulling the (flexible and thin) sidewalls inward slightly. Similar findings are reached by Yang [5] and Wei [7].

4.5.3.2 Vertical Stiffness Analysis

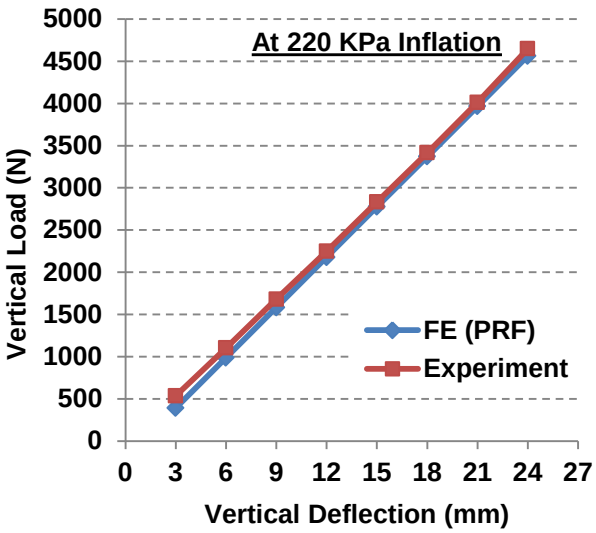
For the vertical stiffness validation in section 4.5.2.1, a close similarity is observed between the FE and the experimental results as shown in Figure 4.20, in which the tyre's vertical stiffness is represented by the gradient of the relationship between the vertical load and the vertical deflection of the tyre. This gives another indication on the FE model capability to simulate the deformational behaviour of the tyre correctly as a result of contact with the road surface as that of reality.


At 180 KPa Inflation
Vertical Load (N)
4500
4000
3500
3000
2500
2000
1500
1000
500
0
0 3 6 9 12 15 18 21 24 27
Vertical Deflection (mm)
FE (PRF)
Experiment

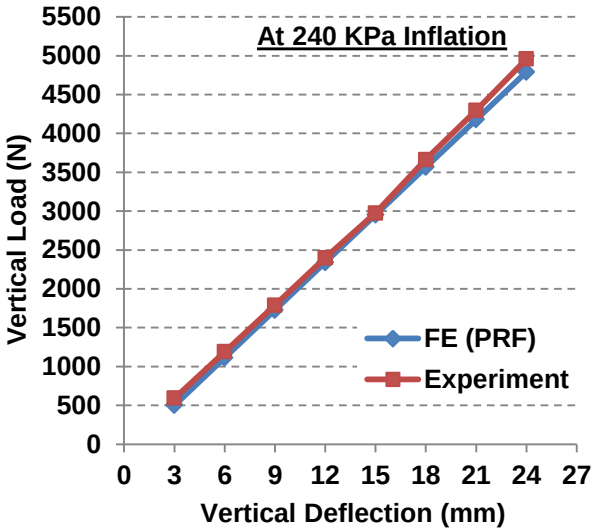
(a)


At 200 KPa Inflation
Vertical Load (N)
5000
4500
4000
3500
3000
2500
2000
1500
1000
500
0
0 3 6 9 12 15 18 21 24 27
Vertical Deflection (mm)
FE (PRF)
Experiment

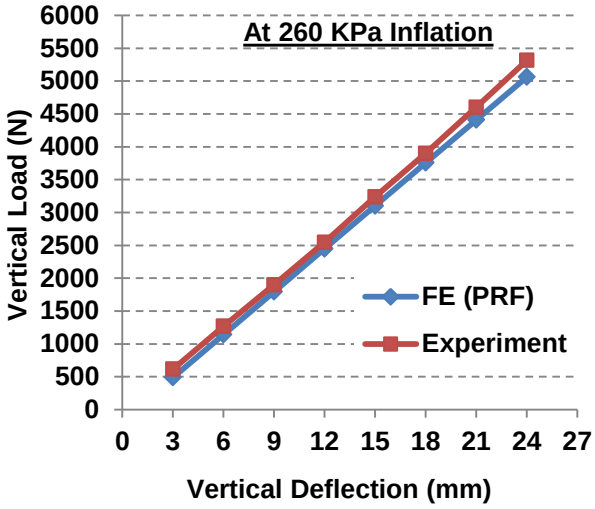
(b)


At 220 KPa Inflation
Vertical Load (N)
5000
4500
4000
3500
3000
2500
2000
1500
1000
500
0
0 3 6 9 12 15 18 21 24 27
Vertical Deflection (mm)
FE (PRF)
Experiment

(c)


At 240 KPa Inflation
Vertical Load (N)
5500
5000
4500
4000
3500
3000
2500
2000
1500
1000
500
0
0 3 6 9 12 15 18 21 24 27
Vertical Deflection (mm)
FE (PRF)
Experiment

(d)



(e)

Figure 4.20 Tyre Vertical Stiffness at (a) 180 KPa, (b) 200 KPa, (c) 220 KPa, (d) 240 KPa and (e) 260 KPa

In Figure 4.20, it is noticeable that the higher the inflation pressure the stiffer the tyre will become due to the tyre's air cavity becoming denser with more air molecules to fill-out space and lesser room to be further compressed. Lee *et al.* [273], Yang [5] and Wei [7] shared the same findings.

4.5.3.3 Footprint Analysis

The footprint validation, in section 4.5.2.1, yielded a fair agreement between the FE outputs and its corresponding experimental results as seen in Figure 4.21 and Figure 4.22 respectively. This provides further evidence of the FE model capability to compute the tyre structural deformation properly in terms of the contact interface between the tyre and the road in relation to practice.

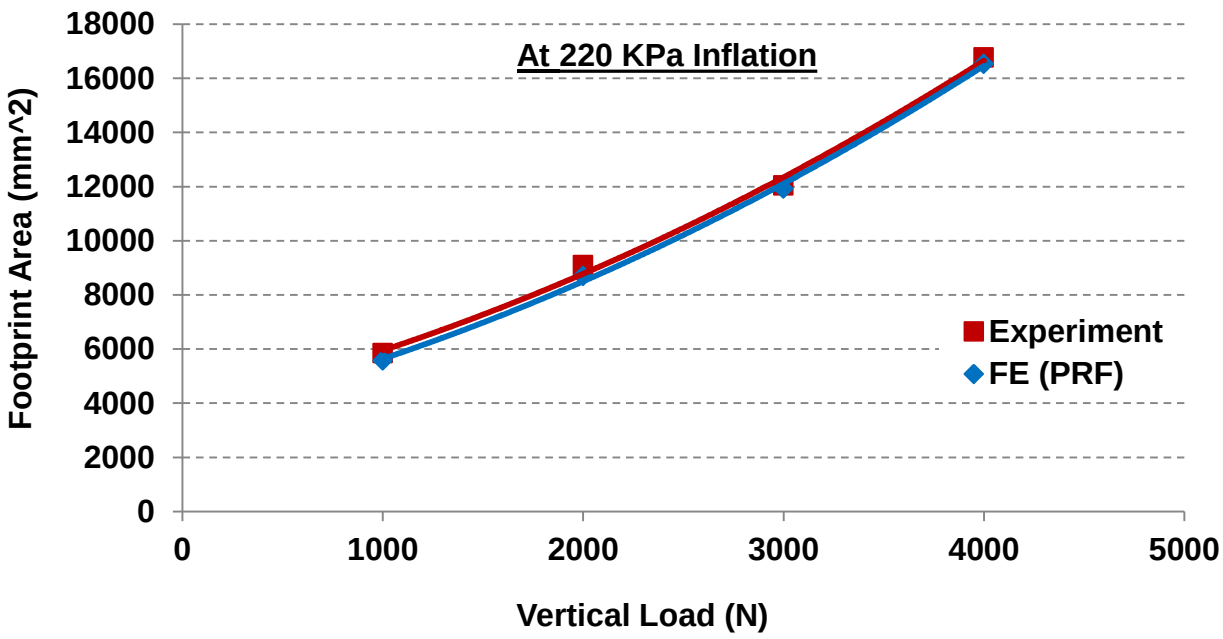


Figure 4.21 Footprint Area under Different Vertical Loads [30]

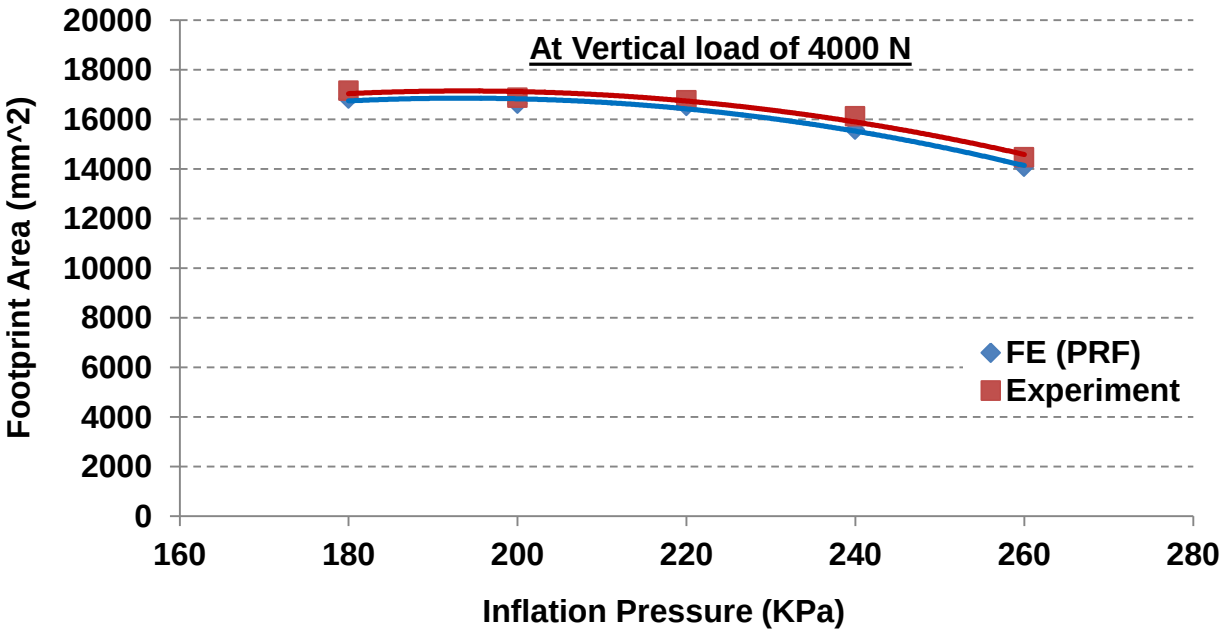


Figure 4.22 Footprint Area under Different Inflation Pressures

In Figure 4.21, the footprint area is almost linearly proportional to the vertical load since increasing the vertical loading would lead to greater tyre structural deformation at the contact interface with the road given the tyre structure flexibility and the inflation air compressibility. As for Figure 4.22, the footprint area is nearly inversely proportional to the inflation pressure. For example, increasing the inflation pressure would mean more air molecules to resist and withstand the vertical loading on the tyre; making the tyre stiffer as indicated in section 4.5.3.2 and less prone to deformation at the contact-patch and vice versa. Similar outcomes were reached by Yang *et al.* [222], Stallmann and Els [274], Hoever [54], and Hernandez *et al.* [275]. Furthermore, an example of the FE model ability to predict the footprint profile closely to that of the actual footprint through the contact pressure distribution using CPRESS field output can be seen in Figure 4.23. Each of Yang *et al.* [222], Kumar *et al.* [264] and Vayalat [263] showed a similar outcome.

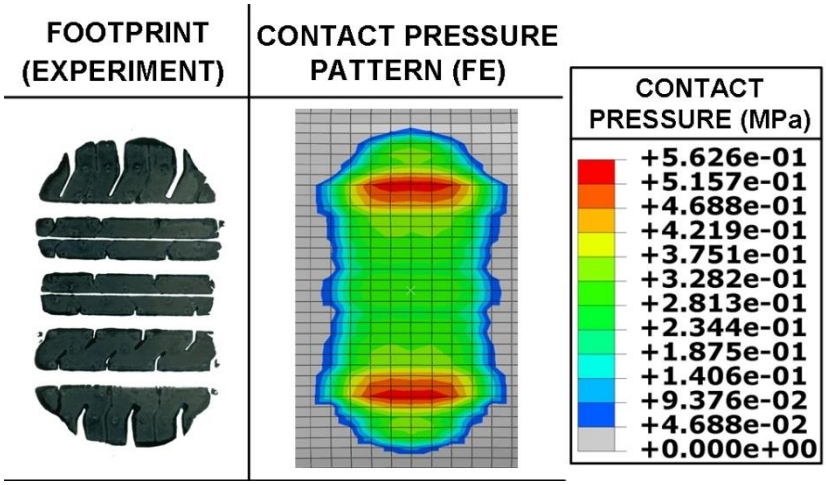


Figure 4.23 Footprint Profile at 220 KPa Inflation and 4000 N Vertical Load [30]

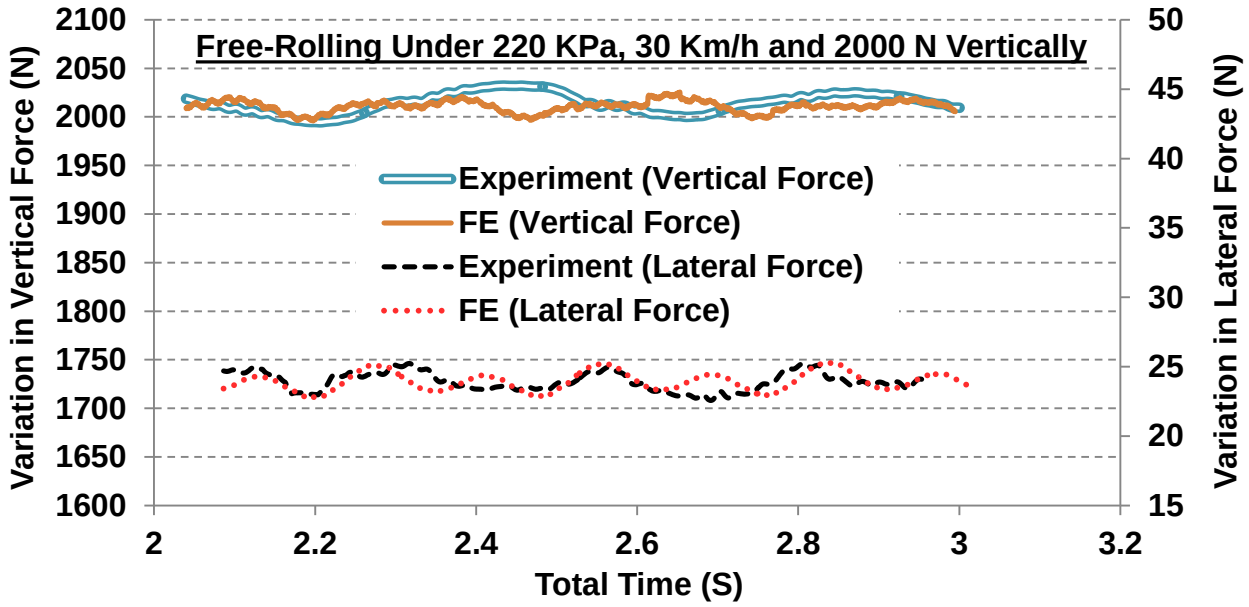
4.5.4 Dynamic Validation and Analysis

4.5.4.1 Non-Uniformity Analysis

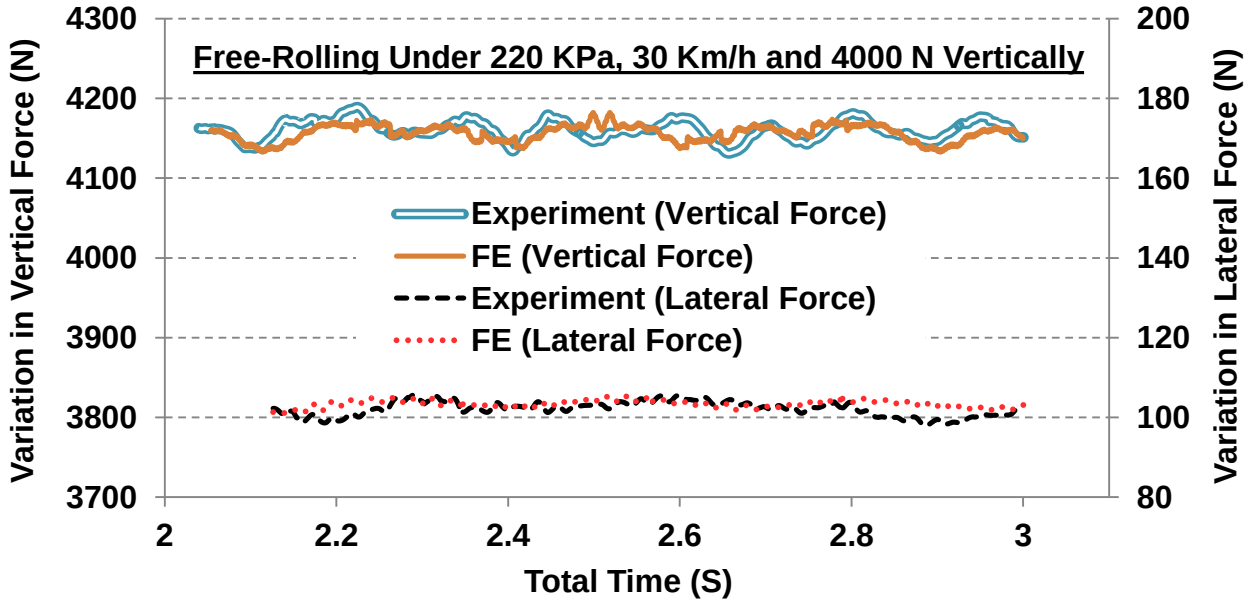
In the non-uniformity validation in section 4.5.2.2, a reasonable match can be found between the FE and its experimental counterpart for the radial and lateral non-uniformities in the tyre as shown in Table 4.6. The non-uniformities in the tyre were expressed in terms of the variations in the respective forces by taking the standard deviation of the force history record during rolling. Examples on the history record of force variations are seen in Figure 4.24.

Table 4.6 Radial and Lateral Non-Uniformities of Standard Tyre

Test Set	Run	Inflation Pressure (KPa)	Vertical Load (N)	Radial Non-Uniformity		Lateral Non-Uniformity		Rolling Velocity (Km/h)
				Variations in Vertical Force (N)		Variations in Lateral Force (N)		
				Experiment	FE	Experiment	FE	
1	1	220	1000	4.749	4.626	0.510	0.351	30
	2		2000	10.440	8.842	0.660	0.654	
	3		3000	17.485	16.441	1.173	0.880	
	4		4000	23.022	21.819	2.347	1.908	
2	1	180	4000	30.358	28.939	2.916	2.742	
	2	200		27.4767	25.217	2.526	2.298	
	3	220		23.022	21.819	2.347	1.908	
	4	240		21.263	21.144	1.923	1.790	
	5	260		18.841	19.999	1.742	1.675	



(a)



(b)

Figure 4.24 History of Radial and Lateral Forces of Standard Tyre at (a) 2000 N and (b) 4000 N Vertical Loads

The validation results indicate the ability of the FE model to adequately simulate the deformational response of the tyre profile circumferentially during rolling in comparison to that in practice. This is despite the slight differences between the FE and the experimental outputs which may be attributed to the marginal manufacturing imperfections in the actual tyre construction [30]. From Table 4.6, it is noticeable that increasing the vertical loading on the tyre would lead to more non-uniformities in the tyre profile during rolling especially radially. This is since the higher the vertical load, the greater (more violent) the tyre deformation at the contact-patch and its subsequent reflexes across the tyre circumferentially as a result of the peristaltic pumping effect. Nevertheless, increasing the inflation pressure of the tyre would help in decreasing the non-uniformities in the tyre structure during rolling since this would make the tyre stiffer and less deformable as indicated earlier in both sections 4.5.3.2 and 4.5.3.3.

4.5.4.2 Rolling-Resistance Analysis

For the rolling-resistance validation in section 4.5.2.2, a good agreement was achieved between the FE and its corresponding experimental results of the rolling-resistance calculated as the energy lost per unit distance as seen in Figure 4.25 and Figure 4.26 respectively. Such validation shows the ability of the FE model to properly predict the rolling-resistance, due to the internal losses in the tyre structure, compared to practice for a variety of rolling conditions.

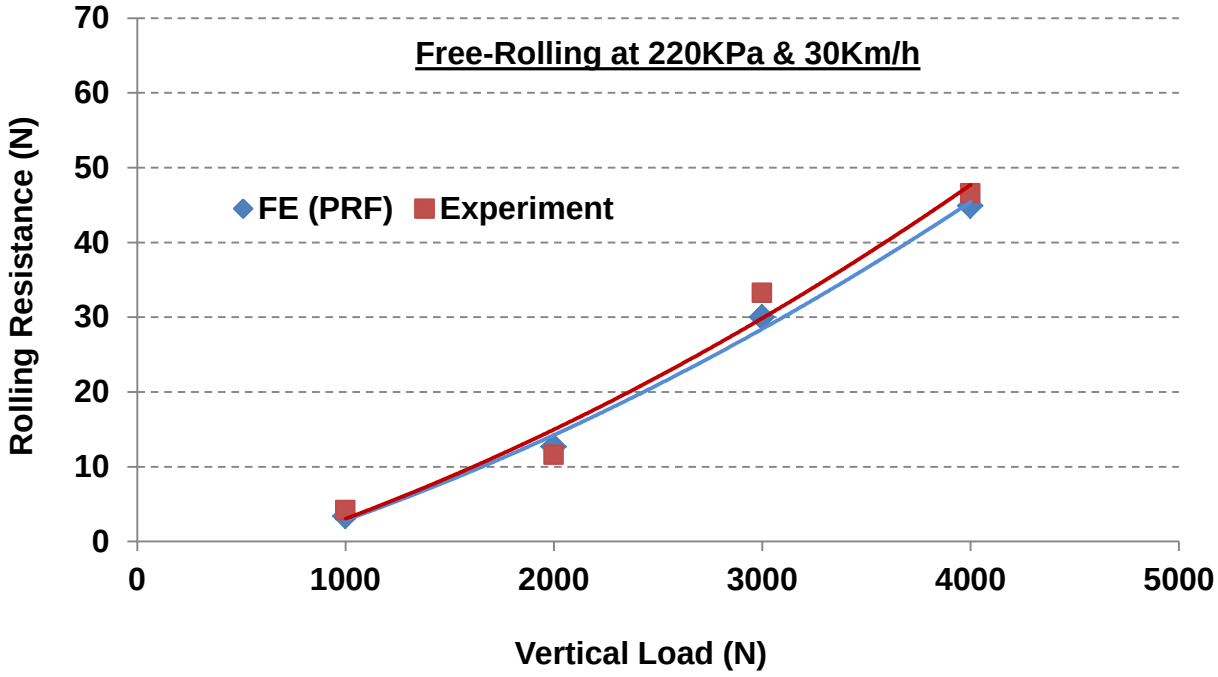


Figure 4.25 Rolling-Resistance under Different Vertical Loads for Standard Tyre [187]

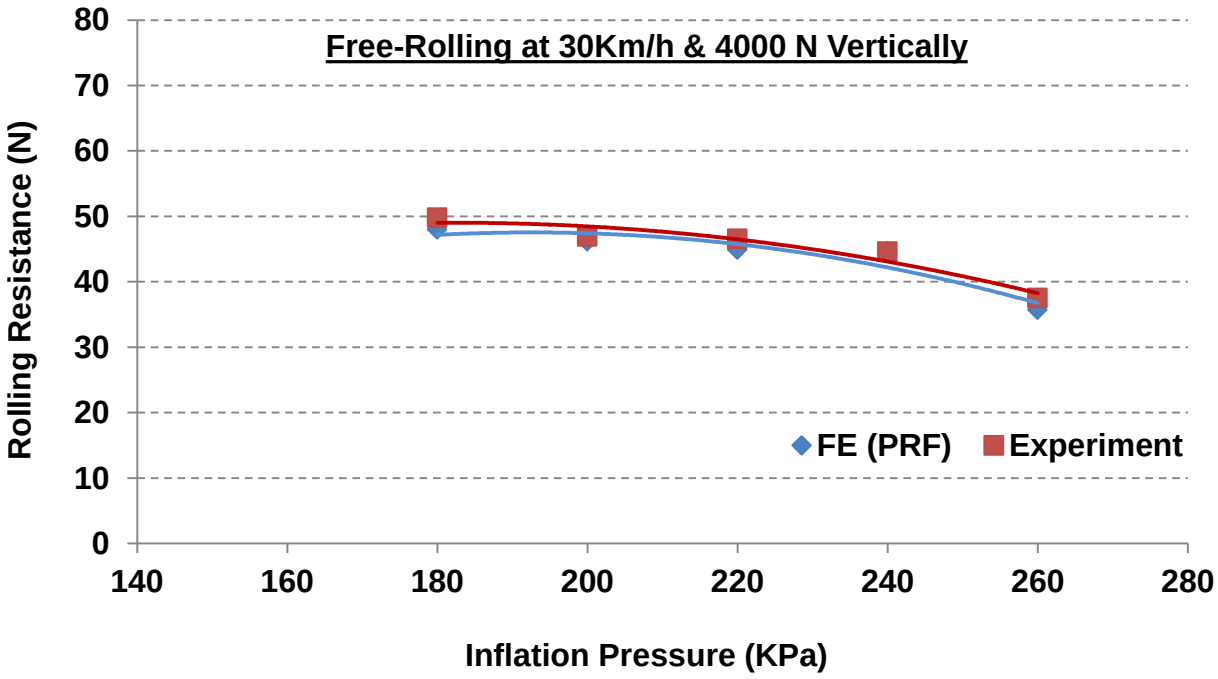


Figure 4.26 Rolling-Resistance under Different Inflations for Standard Tyre [187]

Under different vertical loads, in Figure 4.25, the rolling-resistance exhibits a nearly linear proportionality with the vertical load. This is because more vertical loading on the tyre would mean deflecting the tyre further vertically causing greater deformation of the tyre structure at the contact patch, as indicated in sections 4.5.3.2 and 4.5.3.3, and thus further hysteresis damping losses during rolling. At different inflation pressures, in Figure 4.26, the rolling-resistance displays an almost inverse proportionality with the inflation pressure. This is because a higher inflation pressure would make the tyre stiffer and less deformable, as indicated in sections 4.5.3.2 and 4.5.3.3, leading to lower mechanical hysteresis damping during rolling. Similar findings are reached by Hernandez *et al.* [64], Shida *et al.* [72], Ebbott *et al.* [70], Hall and Moreland [12], and Narasimha Rao *et al.* [276].

Furthermore, the FE model provides a logical and sensible contribution share of each relevant tyre component to the total energy dissipation of the tyre structure using ALLCD output, as shown in Figure 4.27 for example, in relation to the literature [64, 71, 277]. This is in which the tread region is the sole dominant contributor to the energy loss in the tyre structure due to its high viscoelasticity for tyre gripping and cushioning since it is the only part in direct contact with the road. Compared to the tread, the other tyre parts (i.e. sidewall and chafer/apex) provide small to marginal contribution to the energy losses in the tyre structure during rolling.

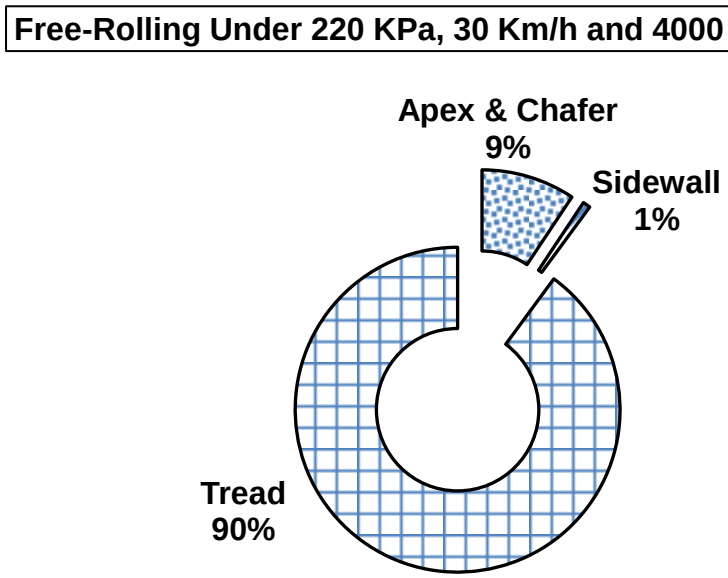


Figure 4.27 Contribution to Energy Dissipation (ALLCD (%)) by Region for Standard Tyre

4.5.4.3 Cornering Analysis

In cornering validation as per section 4.5.2.2, the FE model shows a close match to the relevant experimental results of cornering (lateral) forces at different slip angles as shown in Figure 4.28. This indicates the capability of the FE model to simulate the deformational mechanism at the tyre contact-patch that is responsible for generating the cornering forces in line with that of practice.

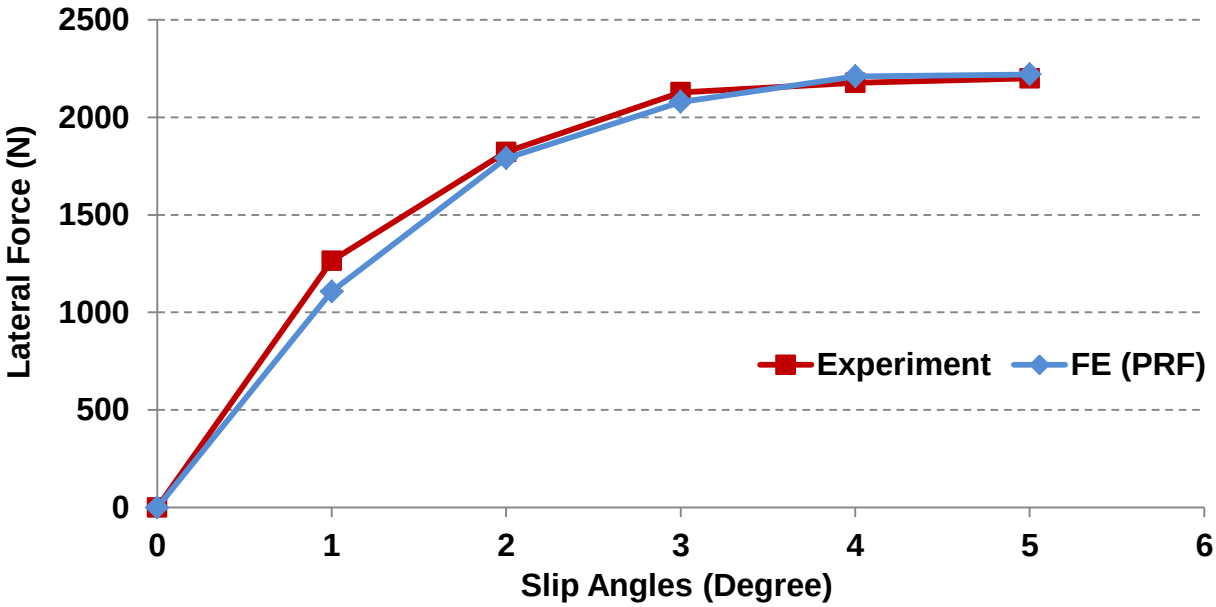


Figure 4.28 Cornering Performance for Standard Tyre

According to Figure 4.28, the standard tyre displays two distinctive responses over the given different slip angles. Under 3° slip angle, the cornering force is almost linearly proportional to small slip angles in which it is dependent on the spring-like side deformation of the contact-patch and the adhesive contact between the tyre and the road [278]. However, at 3° slip angle and above, the cornering force starts to stabilise and become independent of the slip angles as the tyre begins to slide and lose its adhesion with the road [279, 280]. Similar outcomes are given by Wei [7], Yang [5] and Parisouz [281].

4.6 SUMMARY

This chapter illustrated the development of an operational (full) 3D tyre model in Abaqus FE code for the standard tyre. A proved image capturing and processing technique was

used to obtain a detailed 2D drawing profile of the cross-sectional tyre geometry including the embedded reinforcements. Based on the captured 2D tyre profile, a 2D axisymmetric tyre model was developed in Abaqus/CAE using the relevant material properties obtained from chapter (3) to specify all rubber and reinforcement components of the tyre. The wheel assembly was introduced as a rigid body with a simplified geometry for computational efficiency. The full 2D axisymmetric model was revolved to create a full 3D tyre model. The model's input file was updated to introduce a cavity air medium as an ideal gas, a road drum as an analytical rigid surface, and the necessary simulation steps to run the complete tyre analysis. Abaqus/Explicit solver was used to run the tyre analysis given the nature of simulation and the tyre's model complexity.

Several mesh refinement assessments were performed to ensure the tyre model yields a consistent, accurate and valid solution response with no numerical instabilities. To have a fully validated FE tyre model ready for tyre designing and testing, the FE model was validated against the relevant experiments for several static and dynamic tyre properties related to rolling-resistance and other driving requirements in which a method was proposed to calculate the rolling-resistance based on tyre's hysteresis ratio. The validation results demonstrated the capability of the FE model to simulate the deformation and dissipation processes of the standard tyre during rolling correctly compared to practice. This is despite the marginal differences between the FE and the experiments in some of the results which may be referred due to not including the tread grooving and reinforcement viscoelasticity in FE solution, the numerical noises in the Abaqus/Explicit procedure, and tolerable manufacturing imperfections in the actual tyre.

CHAPTER (5): DEVELOPMENT AND VALIDATION OF FINITE ELEMENT MODEL FOR DUAL-CHAMBER TYRE

5.1 INTRODUCTION

Having a validated and working FE model for the standard tyre in chapter (4), the next targeted stage would be to structurally develop potential multi-chamber solutions in line with this research topic. However, prior to that, further validation would be needed for the developed FE model to ensure its capability to account for the interaction between the cavity air and the surrounding tyre structure especially for the case of a multi-chamber tyre. For this purpose, in this chapter, two basic experimental prototypes of multi-chamber tyre solutions were used to validate the FE modelling approach proposed by the author for the same static and dynamic tyre properties in chapter (4).

The first prototype involved transforming the standard tyre from containing a single cavity chamber into comprising concentric and annular dual chambers (i.e. dual-chamber tyre solution). This is by inserting an inner bead-lock chamber, provided by Coyote [137], inside the main cavity chamber of the standard tyre as seen in Figure 5.1.

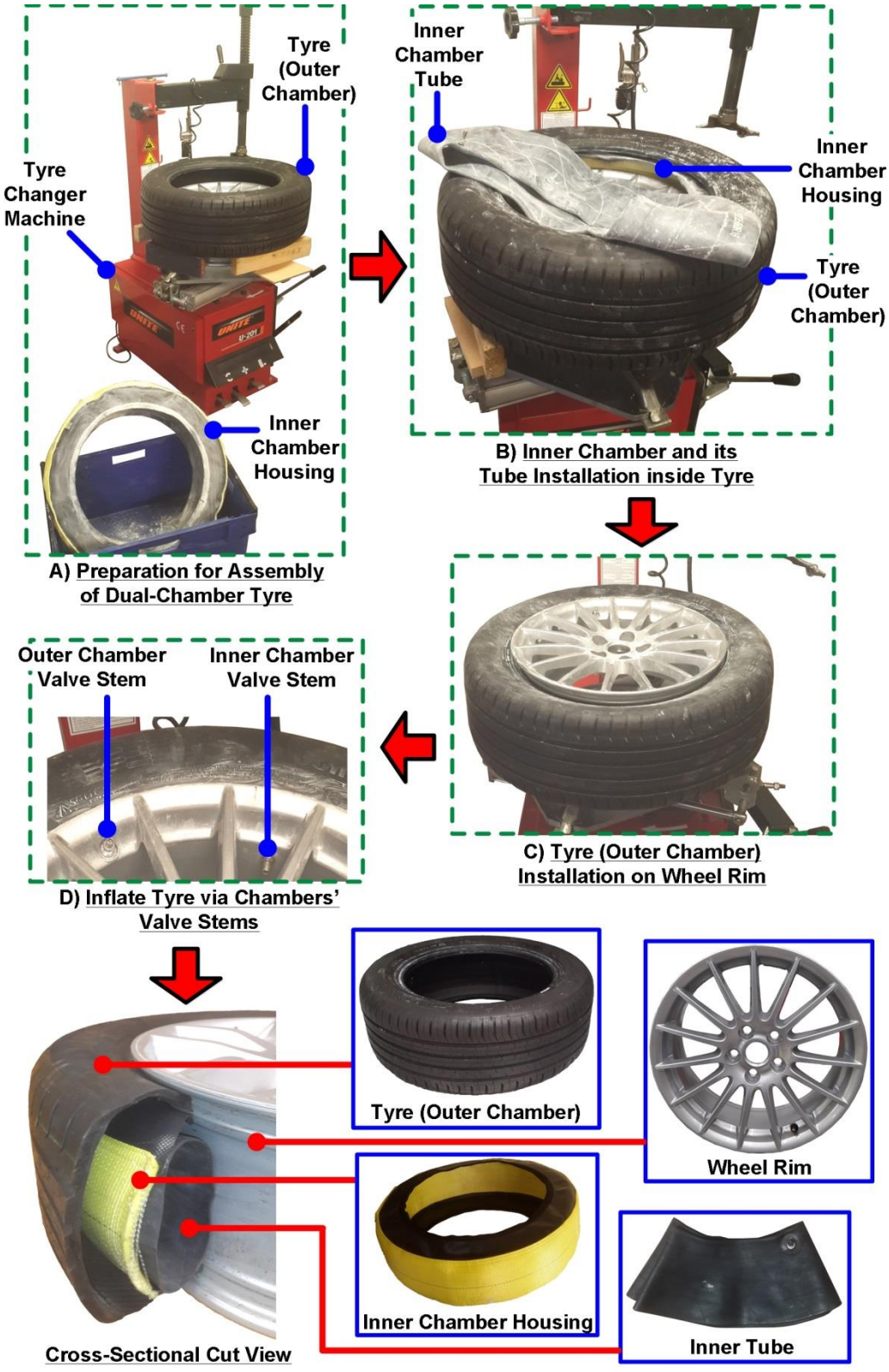


Figure 5.1 Experimental Prototype of Dual-Chamber Tyre

For the second prototype, it is a five chambers tyre solution (i.e. prototype 0.5) which have multiple inner tubes fitted inside 205/50 ZR15 tyre to form each chamber in addition to the main chamber of the tyre as shown in Figure A.0.7 in appendix (B). This basic solution was developed and manufactured as a part of “InterjetRR IDP12” project run by Fusion Innovation in collaboration with the University of Birmingham [186]. The author assisted in testing prototype 0.5 in the University testing facilities and gained permission from Fusion Innovation, as seen in appendix (C), to use the experimental data to further validate the author’s FE modelling approach of the multi-chamber solution.

Mainly, this chapter covers the FE model development and validation of the “dual-chamber” tyre in which “prototype 0.5” is briefly discussed in section 5.4 with the relevant FE validation is shown in appendix (B) since it is a design that belongs to Fusion Innovation and has confidentiality restrictions. In this chapter, the work done by the author with regard to the dual-chamber tyre solution, as the main owner and contributor, was published as per a publication plan for this research and it can be found in [30].

5.2 FE MODEL SET-UP AND REFINEMENT

Fundamentally, the “dual-chamber tyre” is the same as the “standard tyre” with the exception of the inner chamber housing and its inner tube as shown in Figure 3.2. Based on that, the developed and validated FE model of the standard tyre in chapter (4)

was modified to include the dual-chamber solution. To incorporate the geometry of the inner chamber housing and its tube to the FE model, a similar procedure to the one in section 4.2 was done to capture the geometry of the inner chamber housing of the dual-chamber tyre as indicated in Figure 5.2.

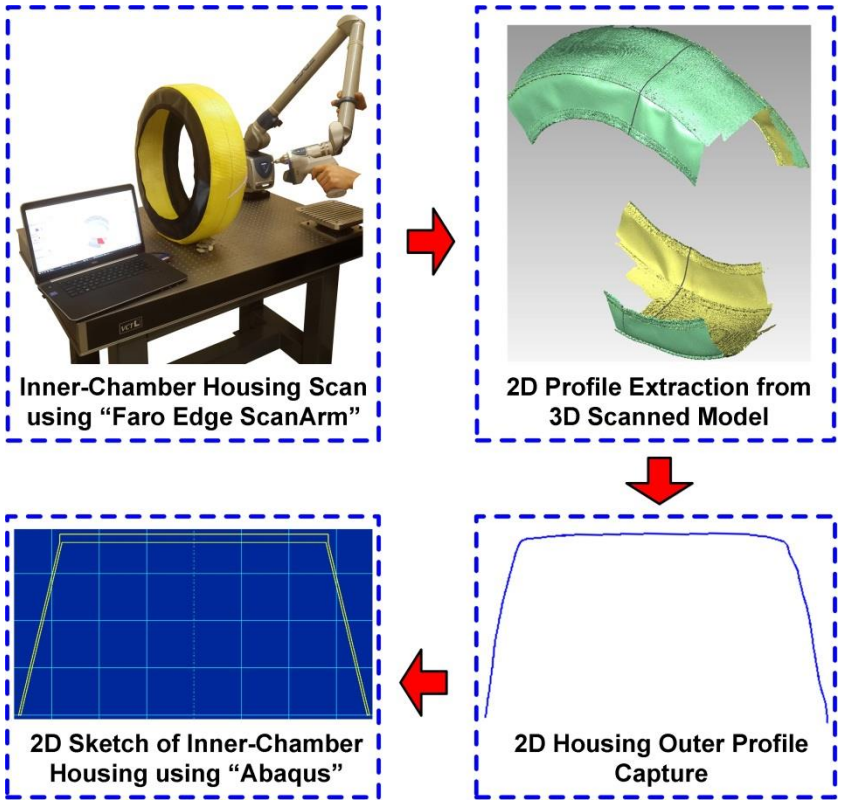


Figure 5.2 Outer Profile Capture of Inner Chamber Housing of Dual-Chamber Tyre

Furthermore, the relevant material properties for the inner chamber housing and its tube in chapter (3) were added to the FE model tree. The 2D axisymmetric model had the inner chamber housing partitioned from its tube as adjacent but two separate parts as seen in Figure 5.3 in which both parts were modelled as deformable and twistable shell

parts with CGAX4R solid elements given their geometry and set-up. The lower ends of the inner chamber housing and its tube were set fixed to the wheel-rim using a “tie” constraint definition since there will be a tight fit with negligible movement between their interfaces in practice after chamber inflation.

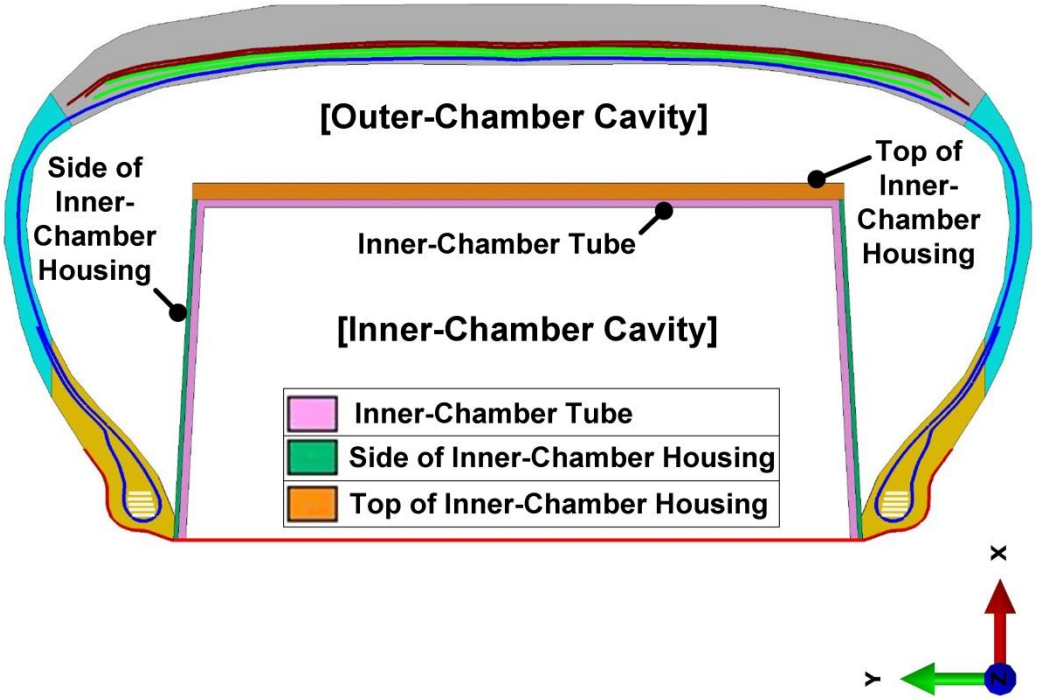


Figure 5.3 2D Axisymmetric Model of Dual-Chamber Tyre

The 3D modelling procedure of the 2D tyre profile with the road drum was similar to that of the standard tyre in chapter (4). The same goes for the analysis (simulation) steps used to run the 3D FE model of the “dual-chamber” tyre shown in Figure 5.4. In the 3D model, the air cavity was modelled in a similar way to that of the standard tyre in chapter (4) but with using two separate surface-based cavity definitions to model the air cavity and its inflation of the inner chamber and the outer chamber independently. As in

chapter (4), the same mesh refinement analyses were done for the FE model of the "dual-chamber" tyre in which the model gave close outcomes to that of the standard tyre since they share the same baseline design and hence a tyre mesh density of 200 sectors circumferentially was chosen to run the FE solution properly.

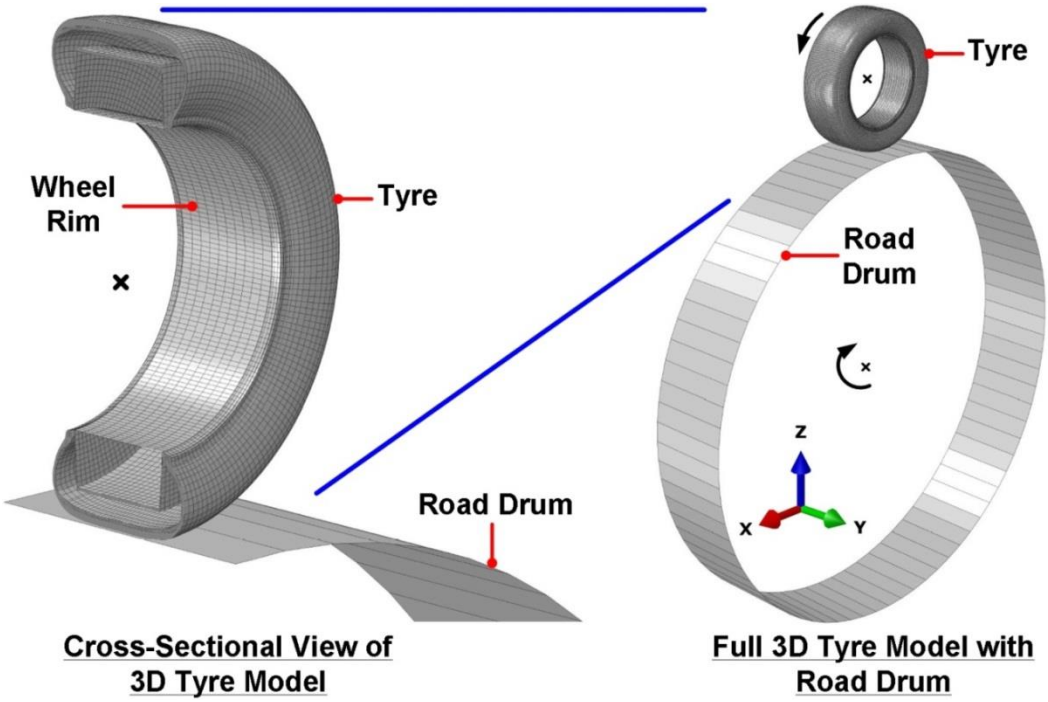


Figure 5.4 3D Model of Dual-Chamber Tyre

5.3 FE MODEL VALIDATION

5.3.1 Validation Scope

Prior to conducting the experimental testing, the "dual-chamber" tyre was dynamically balanced using a wheel balancer machine as seen in Figure 5.5 to ensure stable rolling around its axis during testing. The FE model of the "dual-chamber" tyre was validated against the same experimental tests and equipment as that in section 4.5 in chapter (4)

using the Faro scanner for the geometrical inflation validation and the tri-axial electro-hydraulic tyre/drum rig for the rest of all validation tests as shown in Figure 5.6 and Figure 5.7 respectively. This is to verify that the FE model is capable of simulating the multi-chamber tyre solution correctly for the targeted tyre characteristics compared to practice. However, the inner chamber used in the “dual-chamber” tyre was not tailored especially for the investigated tyre (i.e. standard tyre) since it came in a standardised commercial size for 17-inch wheel tyres in general. This has placed some restrictions on the range of testing conditions that the “dual-chamber” tyre can be subjected to without causing damage of the tyre’s chambers due to severe contact during rolling. The restricted testing conditions are indicated in the next section.

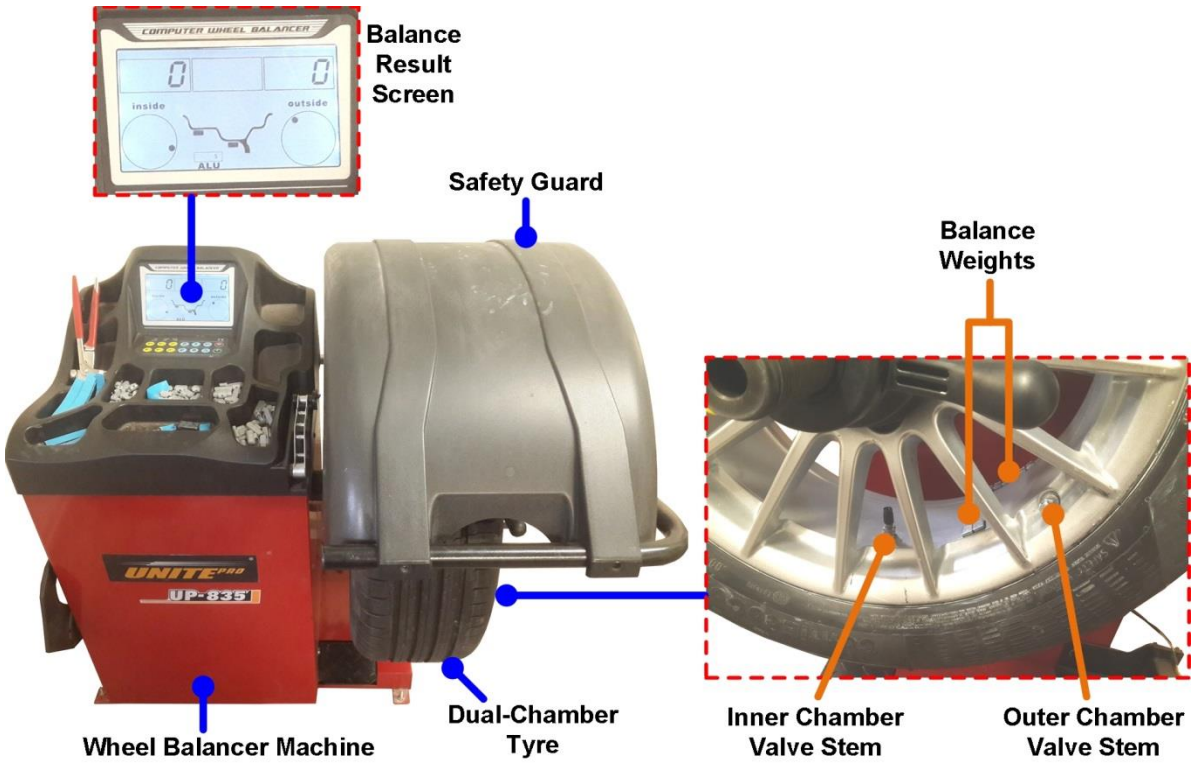


Figure 5.5 Mass Balancing of Dual-Chamber Tyre/Wheel Assembly

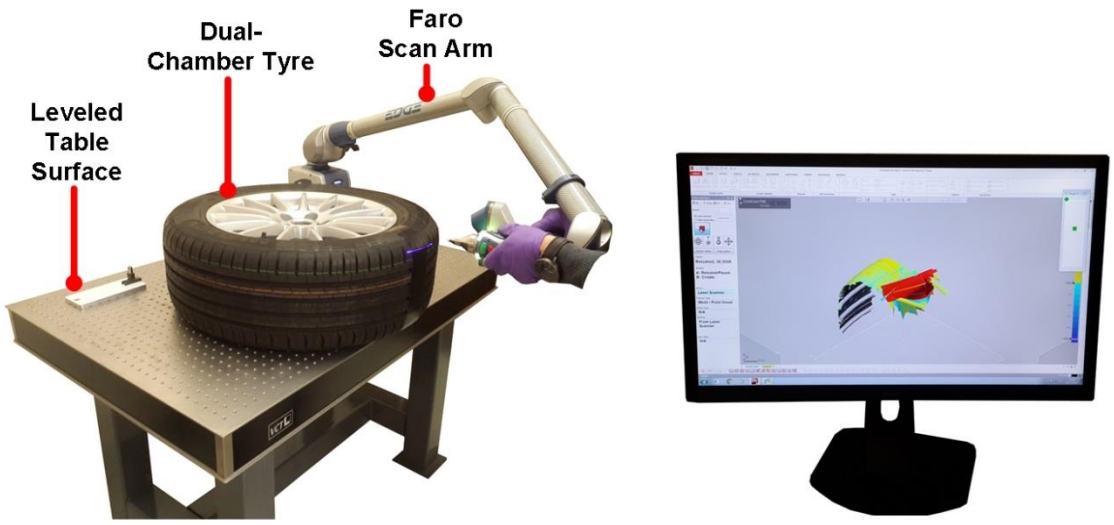
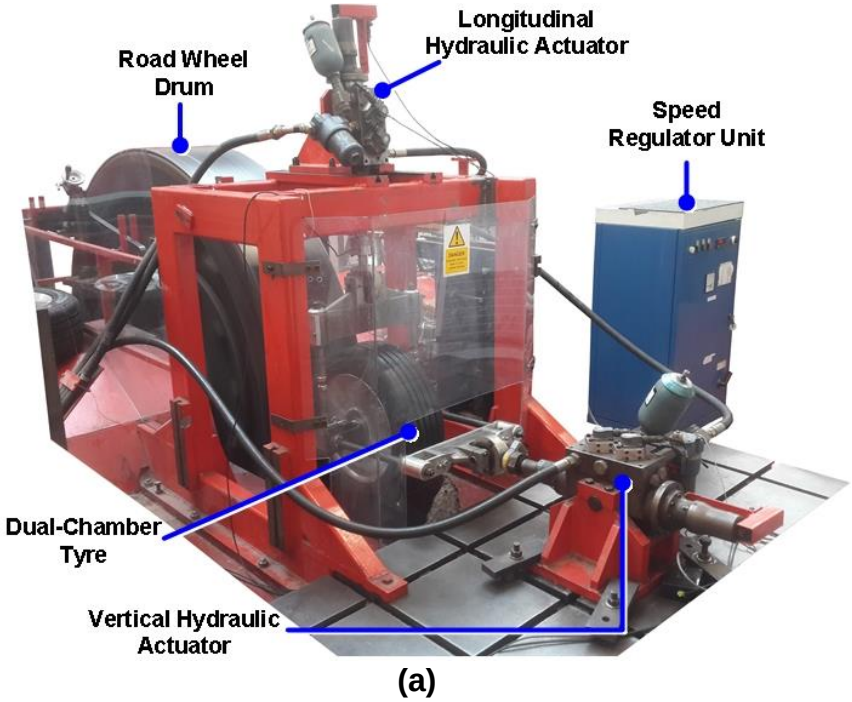


Figure 5.6 Experimental Set-Up for Inflation Validation of Dual-Chamber Tyre



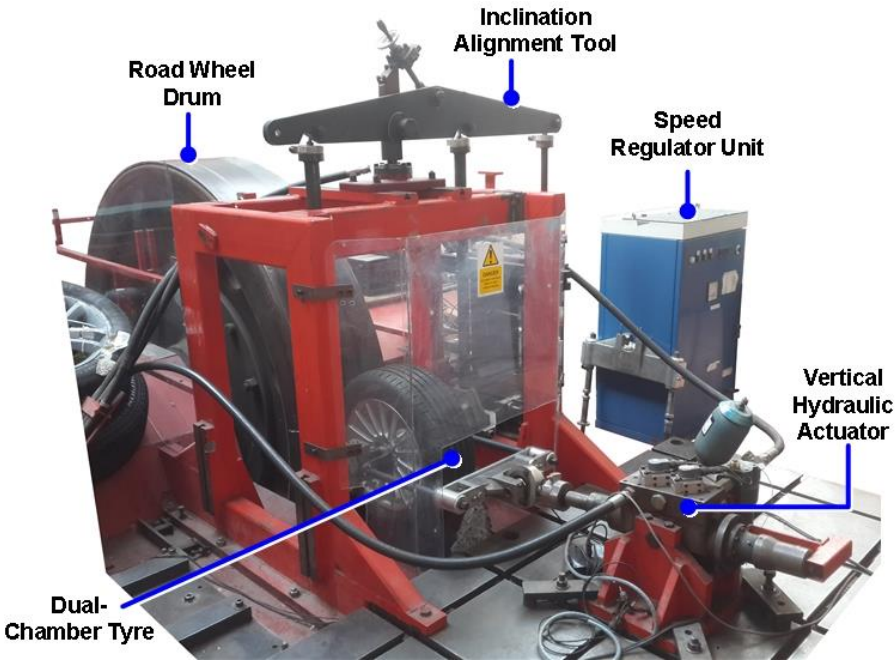


Figure 5.7 Experimental Set-Up of Dual-Chamber Tyre for (a) Vertical Stiffness, Footprint and Rolling-Resistance and (b) for Cornering and Non-Uniformity Validations

5.3.2 Static Validation and Analysis

5.3.2.1 Geometrical Inflation Analysis

For the inflation validation, as seen in Table 5.1, the inner chamber was set constant at higher inflation to secure the mounting of the tyre's beads and uphold the outer chamber. The outer chamber was set at different inflation pressures respectively in which it was put at a minimum of 180 KPa to prevent an internal clash between the chambers and at a maximum of 240 KPa to avoid causing wrinklings in the inner chamber [137].

Table 5.1 Testing Conditions for Inflation Validation of Dual-Chamber Tyre

Test Number	Dual-Chamber Tyre (KPa)	
	Inner Chamber	Outer Chamber
1	280	180
2	280	200
3	280	220
4	280	240
5	260	220
6	300	220

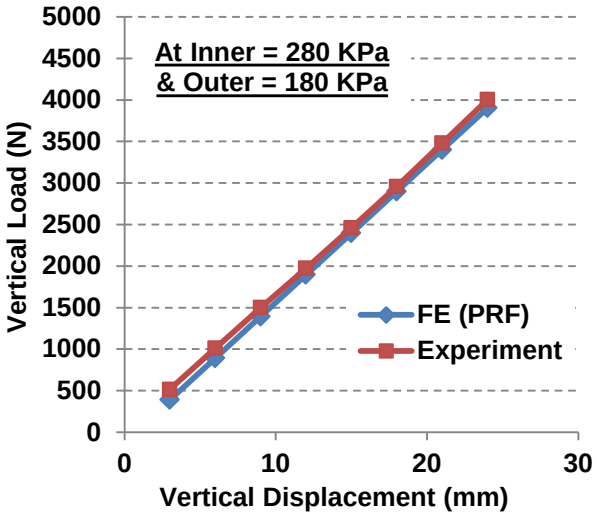
As shown in Table 5.2, a fair agreement is found between the FE and its experimental counterpart for inflation validation of the dual-chamber tyre. This is despite the slight differences which may be attributed to the marginal profile non-uniformity of the actual tyre circumferentially. The dual-chamber tyre exhibits similar behaviour to the standard tyre with regard to the tread and sidewall movements during inflation at different pressures. The dual-chamber tyre shows close profile change under inflation to that of the standard tyre especially for the tread region if the inflation of the outer chamber is set at the same level as that of the standard tyre. This is since in this case the outer chamber of the dual-chamber tyre has an identical structure with the same inflation pressure applied to its inner-liner as the standard tyre in which the inner chamber did not play a noticeable role given the set-up of the chambers, the cavity air compressibility and the inflation process occurring quasi-statically.

Table 5.2 Displacement of Tread Centre and Sidewall Outermost due to Inflation [30]

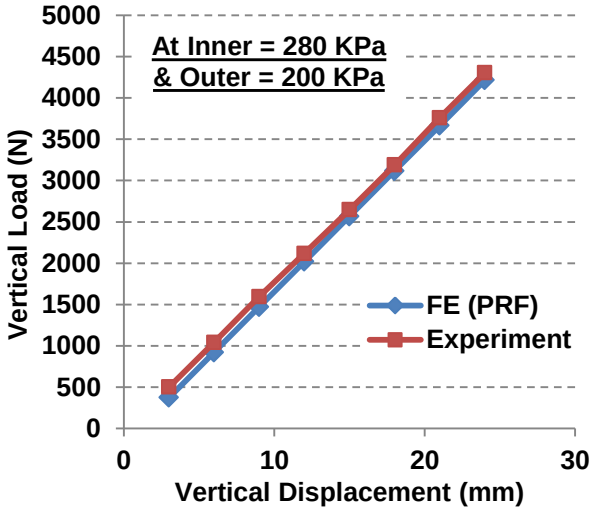
Test Number	Inflation Pressure (KPa)		Tread Centre (mm)		Sidewall Outermost (mm)	
	Inner Chamber	Outer Chamber	FE	Experiment	FE	Experiment
1	280	180	2.105	2.585	1.139	1.185
2	280	200	2.362	2.796	1.081	1.119
3	280	220	2.632	3.047	1.060	1.108
4	280	240	2.914	3.190	1.063	1.071
5	260	220	2.632	2.914	1.060	1.088
6	300	220	2.632	2.909	1.060	1.113

5.3.2.2 Vertical Stiffness Analysis

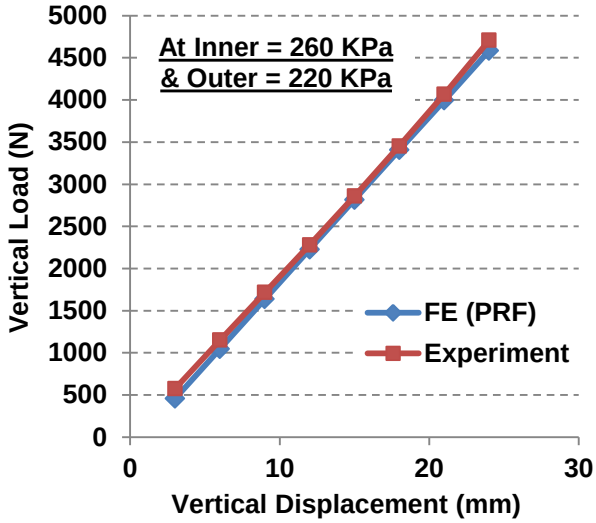
Under the same inflation settings as in Table 5.1, the “dual-chamber” tyre was subjected to a maximum of vertical deflection of 24 mm to avoid direct contact between the chambers inside the tyre. In Figure 5.8, the FE model shows a good match with its corresponding experimental results for the vertical stiffness property. The dual-chamber tyre displays a similar stiffness performance as that of the standard tyre in Figure 4.20 for the cases where the inflation of the outer chamber of the dual-chamber tyre is the same as the standard tyre. This is because the deformation mainly occurs at the outer chamber only due to its direct contact with the road drum whereas the inner chamber has negligible deformational changes since it has physical contact with neither the road surface nor the outer chamber. Such a process makes changing the inflation pressure in the inner chamber have a little noticeable impact on the vertical stiffness unlike the outer chamber as seen in Figure 5.8 especially as the tyre deflection is quasi-statically done.


At Inner = 280 KPa
& Outer = 180 KPa
Vertical Load (N)
Vertical Displacement (mm)
FE (PRF)
Experiment
5000
4500
4000
3500
3000
2500
2000
1500
1000
500
0
0
10
20
30

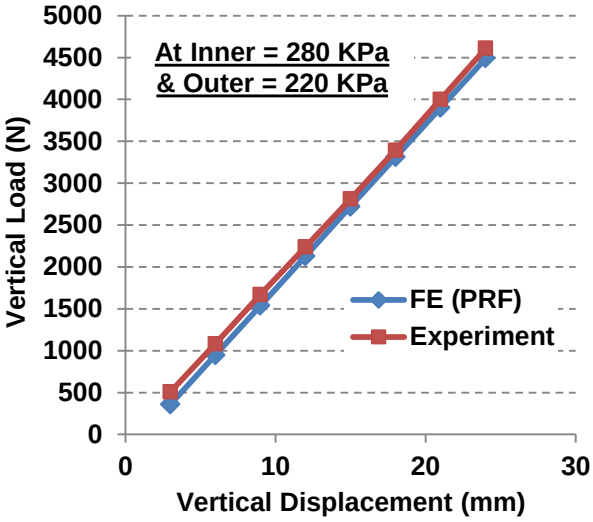
(a)


At Inner = 280 KPa
& Outer = 200 KPa
Vertical Load (N)
Vertical Displacement (mm)
FE (PRF)
Experiment
5000
4500
4000
3500
3000
2500
2000
1500
1000
500
0
0
10
20
30

(b)


At Inner = 260 KPa
& Outer = 220 KPa
Vertical Load (N)
Vertical Displacement (mm)
FE (PRF)
Experiment
5000
4500
4000
3500
3000
2500
2000
1500
1000
500
0
0
10
20
30

(c)


At Inner = 280 KPa
& Outer = 220 KPa
Vertical Load (N)
Vertical Displacement (mm)
FE (PRF)
Experiment
5000
4500
4000
3500
3000
2500
2000
1500
1000
500
0
0
10
20
30

(d)

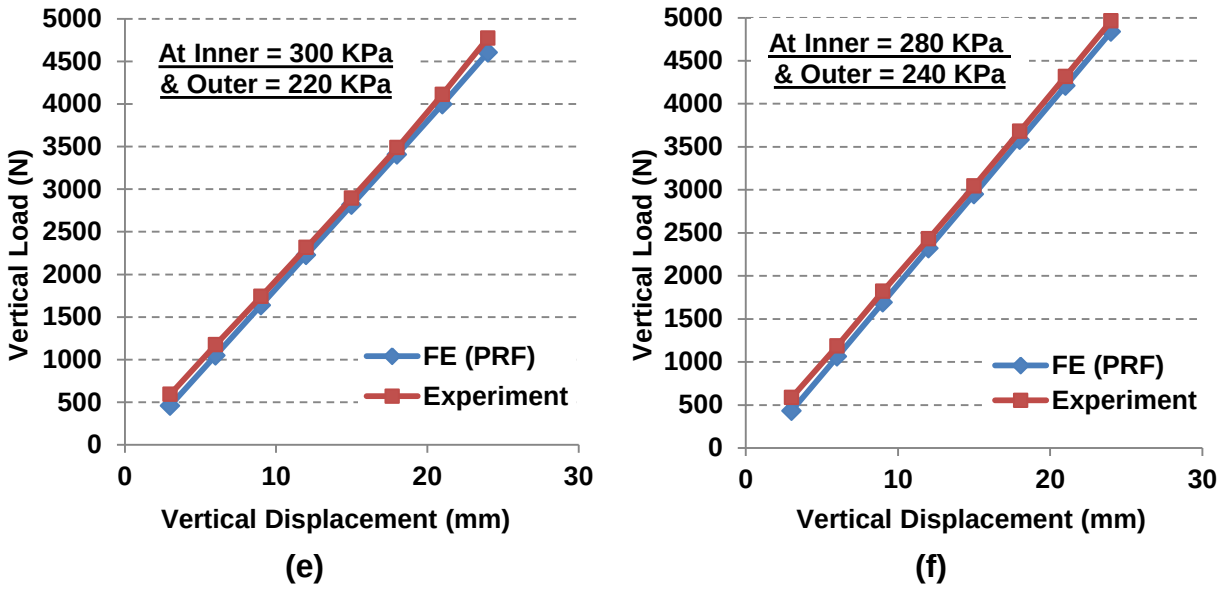


Figure 5.8 Vertical Stiffness of Dual-Chamber Tyre at (a) 280-180 KPa, (b) 280-200 KPa, (c) 260-220 KPa, (d) 280-220 KPa, (e) 300-220 KPa and (f) 280-240 KPa

5.3.2.3 Footprint Analysis

The footprint validation was conducted under two test sets as indicated in Table 5.3. A good agreement is found between the FE and its corresponding experiments for the footprint area of the dual-chamber tyre in Figure 5.9 and Figure 5.10 respectively. Similar to the stiffness validation, changing the inflation of the inner chamber has almost no impact on the footprint area, unlike the outer chamber.

Table 5.3 Testing Conditions for Footprint Validation of Dual-Chamber Tyre

Test Set	Run	Vertical Load (N)	Inflation Pressure (KPa)	
			Inner Chamber	Outer Chamber
1	1	1000	280	220
	2	2000		
	3	3000		
	4	4000		
2	1	4000	280	180
	2		280	200
	3		280	220
	4		280	240
	5		260	220
	6		300	220

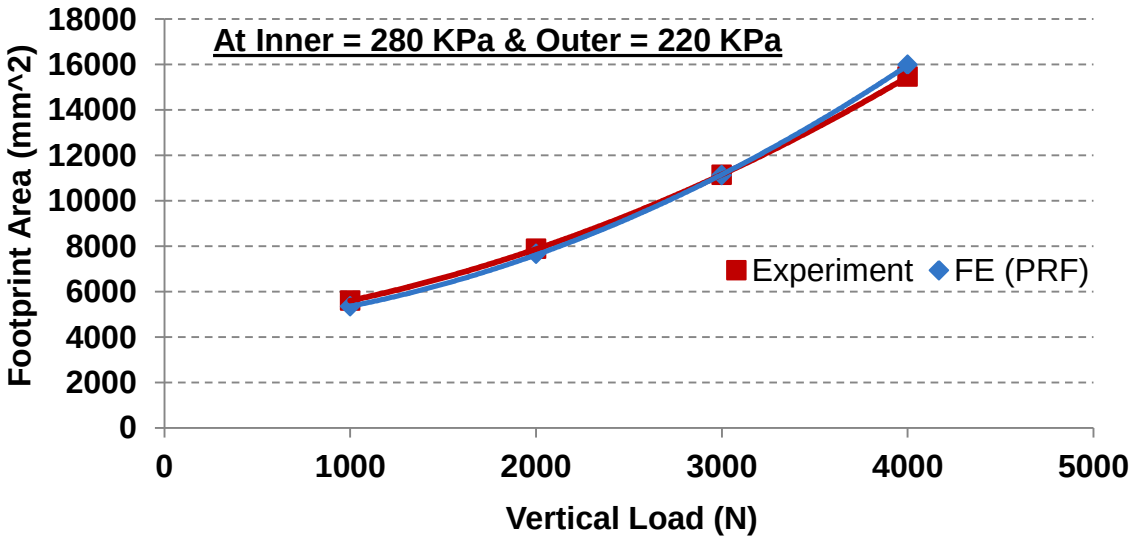


Figure 5.9 Footprint Area under Different Vertical Loading [30]

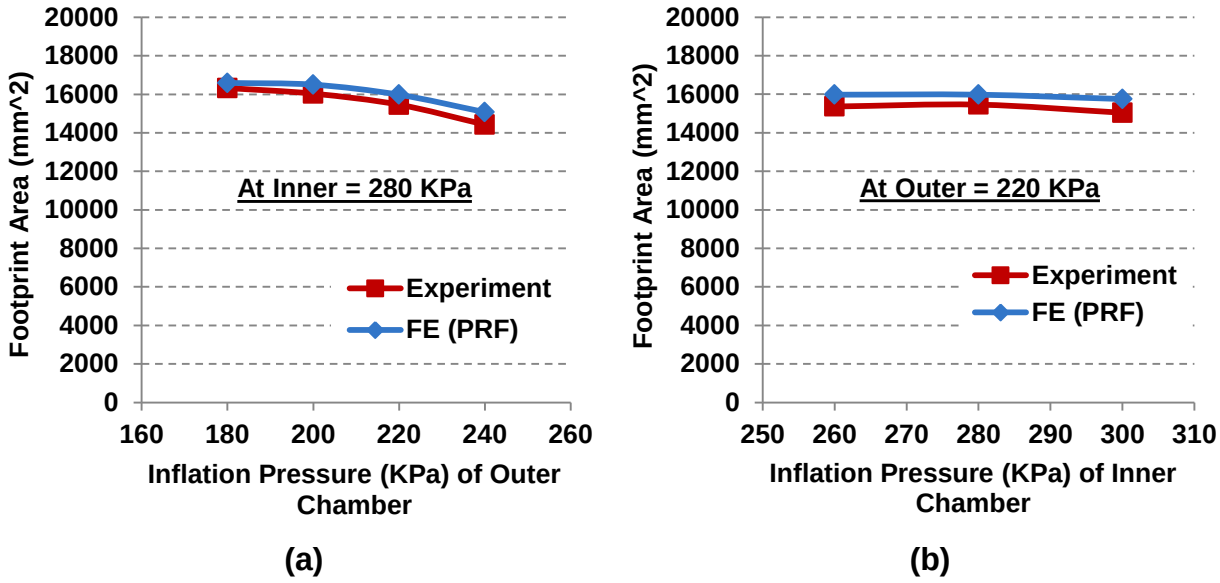


Figure 5.10 Footprint Area under Different Inflation Pressures of (a) Outer Chamber and (b) Inner Chamber

In contrast with the “standard tyre” in section 4.5.3.3 for similar testing conditions, the “dual-chamber” tyre shows slightly smaller footprint areas; leading to undermining the tyre’s grip. This is because the outer chamber of the dual-chamber tyre provides less space for the air molecules to move, re-collide, accumulate and reach saturation to build-up the pressure level to maintain the tyre shape more efficiently especially circumferentially where the loading is low or minimum at the contact-patch in which the air volume is much less compressed. Such a trend conforms with the kinetic theory of gases and can be seen in the footprint shape obtained for the “dual-chamber” tyre in comparison to the “standard” tyre in the example shown in Figure 5.11 in which the dual-chamber tyre had shorter outskirts of its footprint circumferentially. Furthermore, the inner chamber occupies a larger cavity space in the tyre that is negligibly deformed due

to its much higher inflation pressure and non-contact set-up, leaving the outer chamber with smaller space as indicated earlier.

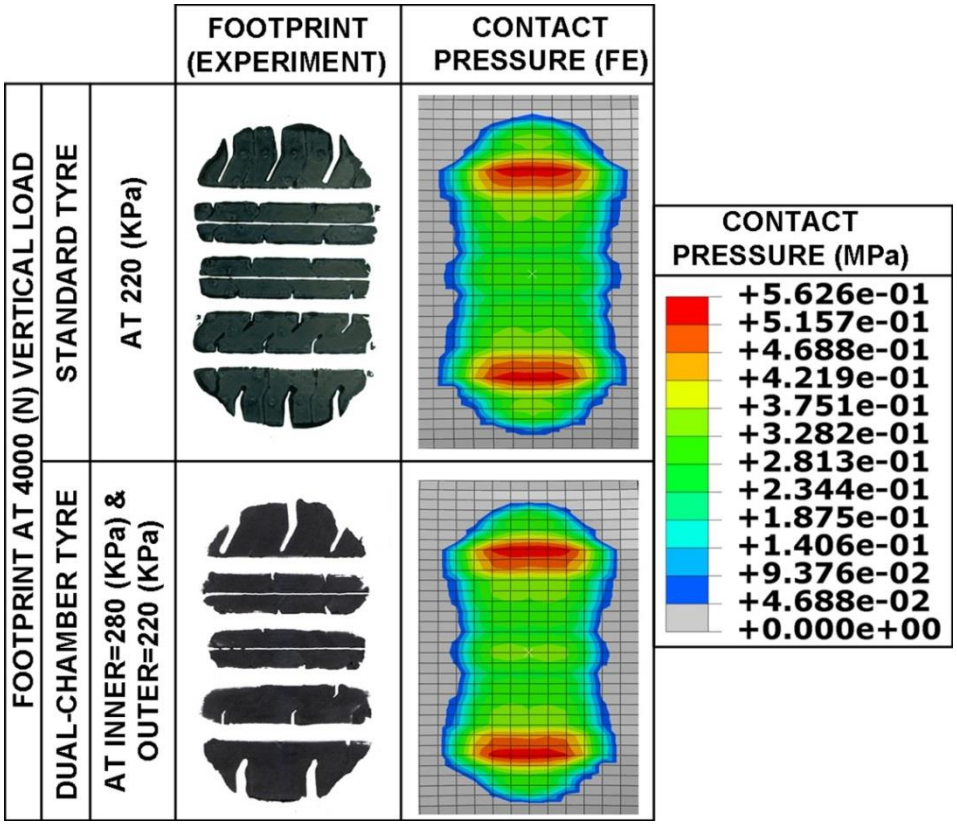


Figure 5.11 Footprint Profile for Dual-Chamber Tyre and Standard Tyre [30]

5.3.3 Dynamic Validation and Analysis

5.3.3.1 Non-Uniformity Analysis

For the same testing conditions as in Table 5.3, but for a free-rolling case at steady-state of a constant velocity of 30 Km/h in a straight-line, the FE solution shows a close match with its experimental counterpart as indicated in Table 5.4. Similar to the previous validations, altering the inflation of the inner chamber does not noticeably influence the

tyre's non-uniformity compared to the outer chamber. In comparison with the standard tyre in Table 4.6 under similar testing conditions, the dual-chamber tyre has more uniform rolling. According to the kinetic theory of gases, this is because the internal structural design of the dual-chamber tyre gives the outer chamber (i.e. that is in direct contact with the road) a smaller cavity volume for the confined air molecules to move inside, re-collide and rebuild-up the inflation pressure after passing the contact patch region during rolling. This is in which reducing the residual vibrational effect of the peristaltic pumping on the tyre structure circumferentially during rolling. As indicated previously, in the dual-chamber tyre, the inner chamber will maintain its shape with negligible changes during rolling which would also help to stabilise the profile of the outer chamber more efficiently after contact with the road.

Table 5.4 Non-Uniformity in Dual-Chamber Tyre during Rolling

Test Set	Run	Inflation Pressure (KPa)		Vertical Load (N)	Radial Non-Uniformity		Lateral Non-Uniformity	
					Variations in Vertical Force (N)		Variations in Lateral Force (N)	
		Inner	Outer		Experiment	FE	Experiment	FE
1	1	280	220	1000	4.327	4.117	0.569	0.473
	2			2000	7.749	6.827	0.607	0.677
	3			3000	10.553	10.485	0.954	0.851
	4			4000	12.280	11.334	1.645	1.420
2	1	280	180	3000	20.823	20.147	2.415	2.360
	2	280	200		16.722	16.069	1.865	1.633
	3	280	220		10.553	10.485	0.954	0.851
	4	280	240		6.113	7.377	0.766	0.701
	5	260	220		10.831	10.667	1.144	1.079
	6	300	220		10.257	10.485	1.121	0.912

5.3.3.2 Rolling-Resistance Analysis

Under the same testing conditions as the non-uniformity validation in section 5.3.3.1, the FE model exhibits a good agreement with its corresponding experiment for the rolling-resistance (i.e. as energy lost per unit distance) as shown in Figure 5.12 and Figure 5.13 respectively. As with the previous validations, mainly, changing the inflation of the inner chamber has a negligible effect on the rolling-resistance in contrast with the outer chamber since the inner chamber experiences almost no deformation during rolling due to its non-contact set-up and high inflation pressure.

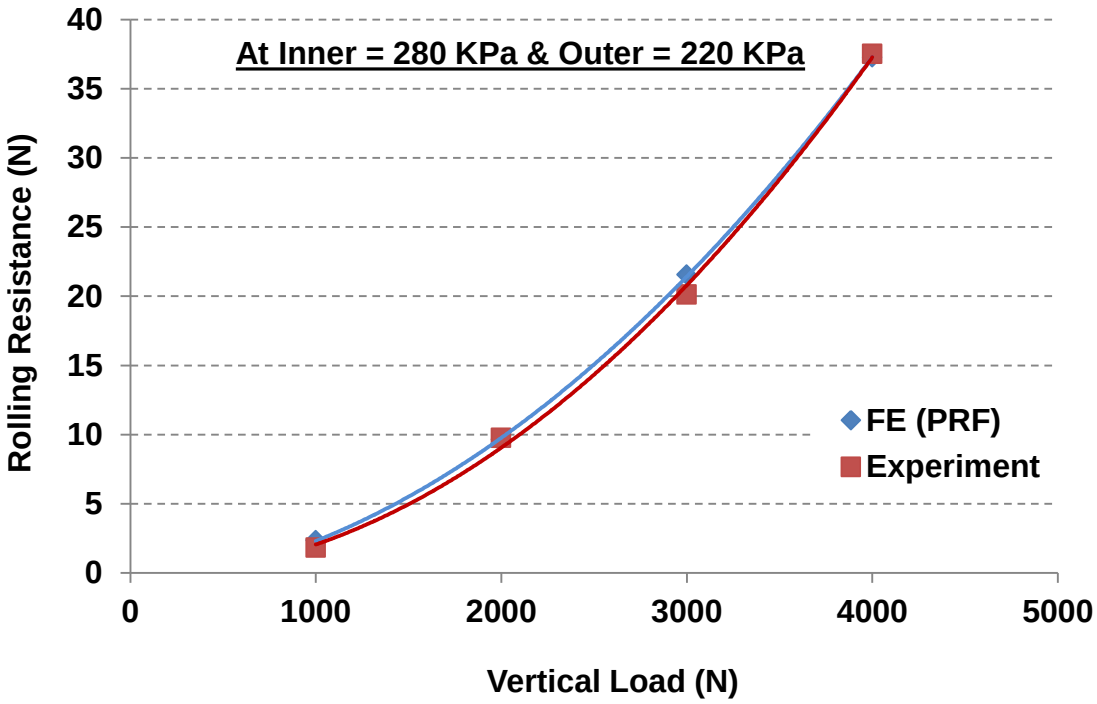


Figure 5.12 Rolling-Resistance at Different Vertical Loads for Dual-Chamber Tyre [30]

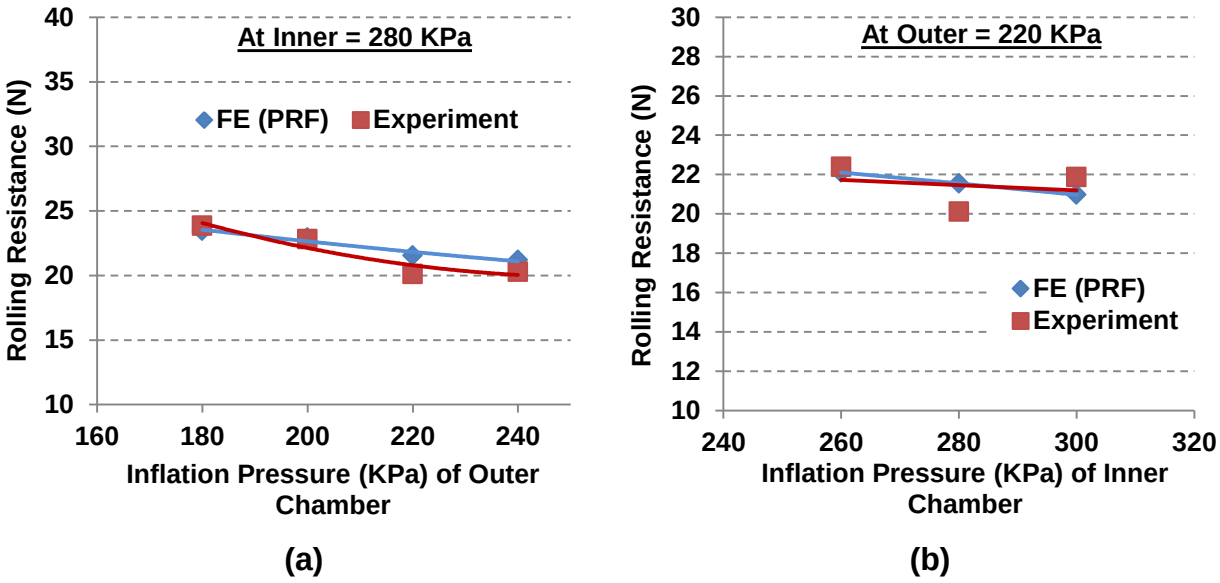


Figure 5.13 Rolling-Resistance under Different Inflations of (a) Outer Chamber and (b) Inner Chamber for Dual-Chamber Tyre

The dual-chamber tyre provides a lower rolling-resistance performance with a reduction of over 10% compared to that of the standard tyre in Figure 4.25 and Figure 4.26 respectively under similar testing conditions. Such performance is because the dual-chamber tyre is subjected to less deformation during rolling at the contact-patch, as it has a lower footprint area as indicated in section 5.3.2.3, and through its profile circumferentially since it has a lower radial non-uniformity as shown in section 5.3.3.1. This would lead to a lower hysteresis damping in the dual-chamber tyre and hence lower energy losses during rolling.

5.3.3.3 Cornering Analysis

The cornering validation was conducted under the testing conditions shown in Table 5.5 for both the dual-chamber tyre and the standard tyre for comparison purposes. For the dual-chamber tyre, a fair agreement between the FE solution and its corresponding experiment is seen in Figure 5.14. In contrast with the standard tyre, the dual-chamber tyre shows slightly lower cornering (lateral) forces which may be due to the marginal interference of the inner chamber with the tyre sidewall deformation during cornering. This may weaken the tyre's grip and stability slightly during cornering.

Table 5.5 Cornering Settings for Dual-Chamber Tyre and Standard Tyre

Test Number	Slip Angle (Degrees)	Inflation Pressure (KPa)			Vertical Load (N)	Rolling Velocity (Km/h)
		Dual-Chamber		Standard		
		Inner	Outer			
1	1	280	220	220	3000	10
2	2					
3	3					
4	4					
5	5					

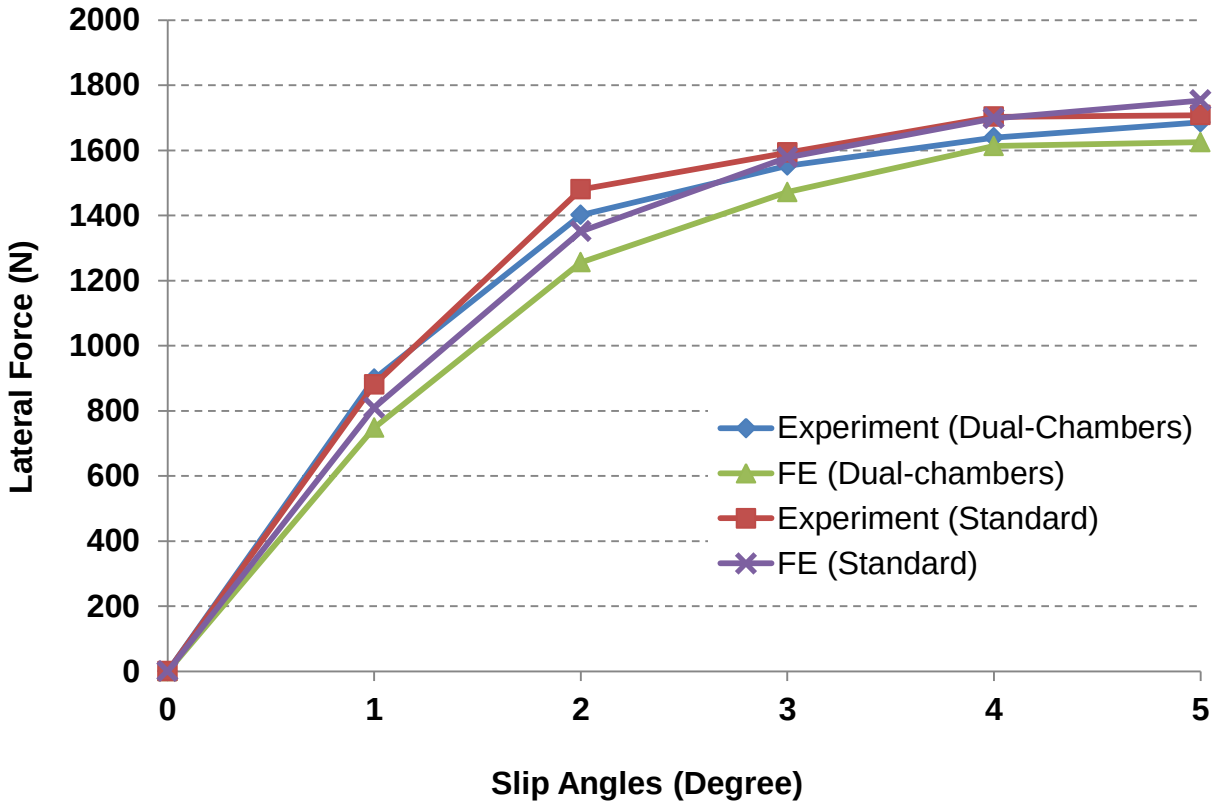


Figure 5.14 Cornering Performance for Dual-Chamber and Standard Tyres [30]

5.4 FE MODELLING AND VALIDATION OF FIVE CHAMBERS TYRE

Besides the “dual-chamber tyre”, as a further validation of the author’s FE approach for modelling the multi-chamber solution, the relevant experimental data of a “five-chamber tyre” (i.e. prototype 0.5 shown in Figure A.0.5 in appendix (B)) designed by an external party as a part of a confidential commercial project were used after gaining the required permission as shown in appendix (C). In relation to the experimental prototype 0.5, the author has developed a full 3D FE replica of the five-chamber tyre as seen in appendix (B) using the same methodologies as in chapters (3) and (4) to capture the needed material properties and geometrical features respectively. Also, the developed FE model

was mesh refined, assessed for energy output validity, and run for tyre simulation using the same relevant approaches as in chapter (4).

The testing and analysis of prototype 0.5 tyre performance in FE and its experimental counterpart were conducted in a similar way to that of chapter (4). According to appendix (B), the developed FE model of prototype 0.5 shows a good agreement with its corresponding experiment for different tyre characteristics. This indicates the validity and the applicability of the author's FE approach to model the multi-chamber tyre solution close to that of practice.

5.5 SUMMARY

This chapter covered the validation of the FE approach adopted to model the multi-chamber tyre solution as in practice. For this purpose, two experimental prototypes of multi-chamber tyres were used and tested for several static and dynamic tyre properties in FE and its experimental counterpart similar to the way done with the standard tyre in chapter (4). The first validation involved modifying and turning the "standard tyre" into a concentric and annular "dual-chamber" tyre by inserting an inner chamber housing with its tube inside the tyre. Likewise, the FE model of the dual-chamber tyre was an upgrade of the standard tyre's FE model by including the inner chamber housing and its tube as deformable and twistable solid elements in which their material properties were imported from chapter (3). The FE model of the dual-chamber tyre had a good agreement with its corresponding experiment for different tyre properties. The "dual-chamber" solution had

a rolling-resistance reduction of over 10% compared to that of the standard tyre but with trade-offs in terms of weaker grip and cornering stability.

The second validation involved using an experimental five-chamber tyre (i.e. prototype 0.5) owned by an external third party after obtaining usage permission. A full FE model of prototype 0.5 was developed following the same methodologies introduced in chapters (3) and (4) respectively. A close match was achieved between the FE solution and its experimental counterpart of prototype 0.5 for different tyre characteristics. Taken altogether, those validations indicate the credibility of the author's FE modelling approach used to simulate the multi-chamber tyre solution for rolling-resistance and other driving requirements in line with that of practice.

CHAPTER (6): PROTOTYPE DESIGNING, EVALUATION AND CHARACTERISATION

6.1 INTRODUCTION

Having developed and validated a working FE model capable of simulating multi-chamber tyre solution in chapters (4) and (5) respectively, this chapter uses the FE model of the standard tyre, as a baseline design, to structurally develop the single chamber design inside the standard tyre to include potential multi-chamber solutions for lower rolling-resistance without compromising other driving requirements. In this respect, in this chapter, the “total design” approach of Stuart Pugh [282] was implemented to reach a sub-optimum prototype design of the multi-chamber tyre solution that would be promising toward lowering rolling-resistance and meeting other driving, manufacturing and maintenance requirements. This serves as the first stage of design development out of two stages to develop the final design (i.e. optimum design in chapter (7)).

For this chapter, the adopted Pugh’s approach involved determining the essential design specifications to be met based on the relevant literature, generating potential multi-chamber designs, evaluating the different prototype designs according to the identified specifications against the standard tyre (i.e. baseline design), and selecting the best sub-optimum design for further development later in chapter (7). All the development work and investigations are done in this chapter using the validated FE tyre model(s)

from chapters (3) and (4). The work done by the author in this chapter, as the main owner and contributor, has been published and can be found in [30].

6.2 TARGETED DESIGN SPECIFICATIONS (PDS)

According to the relevant literature and tyre market [283-285], any conventional road tyre would be expected to have and fulfil a number of core characteristics and roles (i.e. design requirements) during its product life cycle. Mainly, these key design requirements fall under three main categories, and they are as follows:

A) Manufacturability:

- Feasible and achievable.
- Easy to manufacture.
- Cost-effective.

B) Driving performance:

- Grip.
- Handling.
- Fuel economy.
- Ride comfort.

C) Maintenance:

- Serviceable (e.g. Puncture repairable, easy to install on a wheel-rim and vice versa, and has reasonable servicing costs).
- Durability.

- Flat run handling.

In practice, such design requirements would require extensive and numerous different testings to be done on different operating conditions, indoor/outdoor and on/off-vehicle. However, given the research scope, the nature of development work and the available resources for this research project, several core design requirements were investigated on a limited range that is sufficient to provide in-depth insights, guidelines and a starting platform on the new research field of multi-chamber tyre solution for low rolling-resistance for prospective research and development works. Based on that, in line with this research aim, the potential multi-chamber designs were assessed using the validated FE model against the standard tyre, as the baseline, for the following core design requirements and criteria of the tyre:

a) Contact Grip:

In terms of tyre's grip, both the "footprint area" and the "contact pressure distribution" at the contact-patch were evaluated using CAREA and CPRESS outputs of the FE tyre model respectively similar to that in chapter (4). Such outputs were assessed because they are the core elements that represent the tyre's grip mechanism [269]. This is as the footprint area indicates the number of rubber-blocks interacting with the road surface at the contact-patch, through molecular adhesion, to generate friction and hence grip. While contact pressure points-out how deep the rubber-blocks are compressed down against the road surface minimising the void spots at the contact-patch. In general, a specific balance is required to be maintained between the

magnitudes of the footprint's contact pressure and its corresponding contact area to avoid destabilising the tyre's grip [286].

b) Cornering:

To assess the cornering performance for different tyre designs, the "cornering stiffness" was evaluated by determining the gradient of the cornering (lateral) forces against that of its corresponding slip angles at which the slip angles are close to zero where the cornering force is linearly proportional to the slip angle [5, 32]. This is because the cornering stiffness is a more comprehensive and accurate measure of the cornering property of the tyre especially for comparison purposes between different tyres [7, 32]. In addition to that, the "footprint area" at a given slip angle was assessed using CAREA output for more insights on the tyre stability and handling of turns [30].

c) Rolling-Resistance:

As the energy lost per unit distance travelled, the rolling-resistance due to the internal losses in the tyre (i.e. mechanical hysteresis damping) only was investigated to study the effect of the tyre structural design on the rolling-resistance as indicated previously in section 4.5.2.2 of chapter (4) in line with this research aim and objectives. As a comprehensive measure for comparison purposes, the "rolling-resistance coefficient" was assessed by taking the quotient of the rolling-resistance force over the normal force obtained from applying the calculation approach of the rolling-resistance in section 4.5.2.2 of chapter (4). Besides using the standard tyre as a benchmark in

evaluating the potential multi-chamber designs for rolling-resistance, another benchmark that can be used is the target level of rolling-resistance coefficient of 6.5 kg/tonne (or 0.0065) set by the vehicle manufacturers to meet Europe's 2021 emissions regulations [18]. However, this benchmark is not emphasised in this chapter until an optimum design is reached later in chapter (7).

d) Ride (Mechanical) Comfort:

For free-rolling on an ideally smooth and flat road surface, assuming negligible manufacturing imperfections in the tyre, the "tyre non-uniformity" can be utilized, as expressed in section 4.5.2.2 of chapter (4), to indicate the tyre's mechanical comfort. However, for an actual road, the vertical static stiffness of the tyre was evaluated as a more reliable indication of the tyre mechanical comfort (cushioning) [30]. This is by determining the slope of the history of the applied vertical load on the tyre over the resultant vertical deflection of the tyre structure as indicated in section 4.5.3.2 of chapter (4).

Nevertheless, it was still possible to use the "tyre non-uniformity" to indicate the deformational intensity of the tyre profile circumferentially during rolling due to the multi-chamber structural design adopted which can give insights on the stability and the energy dissipation of the adopted structural design in comparison to the baseline standard tyre [30].

e) Net Weight, Manufacturability and Maintenance:

Although the net weight and the manufacturability of the tyre are out of this research scope as indicated in section 1.3 of chapter (1), careful consideration and care were given in selecting the best multi-chamber design for low rolling-resistance and other driving requirements to ensure its simplicity, practicality and conciseness. This is by looking for a design with fewer structural parts and simple layout configuration of the following attributes:

- Is possible to make using existing manufacturing technologies.
- Gives sufficient room to uninstall/install from/on the wheel-rim and to perform puncture repairs.
- Has more than one chamber to maintain rolling and compensate for any failed chamber in case of run-flat scenario.
- Maintains airtight seal and proper mounting on the wheel-rim.
- Maintains a stable profile during normal operation.

With such design, if there were an increase in weight, it would be of a small magnitude that can be compensated by a corresponding weight reduction in either the wheel-rim, the vehicle or both.

Therefore, based on the targeted design specifications mentioned earlier, the proposed multi-chamber designs were assessed through FE modelling for a lower rolling-resistance than that of the standard tyre and for either similar or better performance in

terms of grip, cornering and mechanical comfort (cushioning) compared to that of the standard tyre. In addition to the simplicity and the practicality of the design, the best design in meeting such criteria was chosen as the sub-optimum multi-chamber design in this chapter to be further improved later for the optimum design in chapter (7) as the second stage of design development.

6.3 DESIGN CONCEPTS GENERATION

6.3.1 Global Behaviour of Tyre Cavity Air

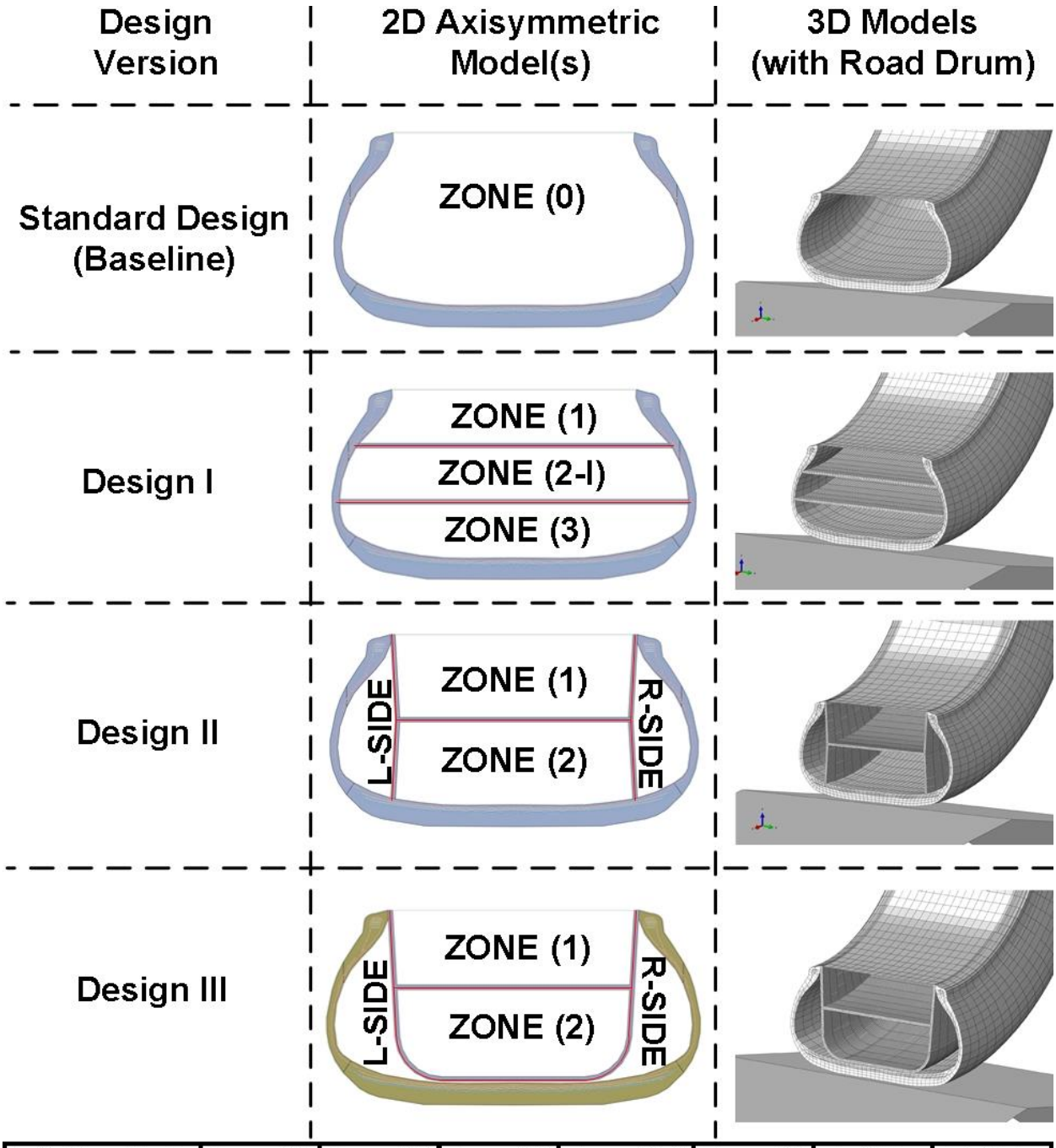
As per the kinetic theory of gases, the pneumatic medium inside the tyre cavity is formed-up from numerous very small molecules which are spread randomly and distant from each other in a case of constant, rapid and arbitrary movement and collision against each other and the cavity walls. This collision between the air molecules and the cavity walls is what leads to pneumatic pressure formulation inside the cavity. Such characteristics allow the cavity air to expand and fill out the entire cavity space inflating the tyre and when subjected to vertical loading to retract and be compressed down.

As a result of the peristaltic pumping effect during rolling, the standard tyre would have a large part of its cavity air subjected to continuous compression and re-expansion since it is made up of a single sizeable cavity space. From the standpoint of the air contribution, after passing the contact-patch region, the re-expansion process of the cavity air in order to restore and support the tyre profile would have some delay. This is because of the time consumed for the necessary air molecules to travel across the ample cavity space, re-collide at the cavity wall, re-stabilise and re-establish the pressure needed to

support the tyre profile. Such a delay would mean further deformation and destabilisation of the tyre profile circumferentially leading to greater hysteresis damping and hence energy dissipation.

6.3.2 Concepts of Multi-Chamber Solution

To minimise the delay in the recovery and stabilisation of the cavity air in the standard tyre, the multi-chamber solution can be used to trap or restrain the air molecules inside smaller cavity spaces limiting the travel time and the motion wildness of the air molecules through the cavity volume. Furthermore, with the multi-chamber option, the levels of air concentration for specific cavity regions in the tyre can be controlled and increased to strengthen the tyre's total stiffness and restrict the tread profile deformation. In that regard, three novel design concepts of multi-chamber tyre solution (i.e. Designs I, II and III) were generated as shown in Figure 6.1.



Inflation Mode	Zone (0)	Zone (1)	Zone (2)	Zone (2-I)	Zone (3)	L-Side	R-Side
Normal	220 KPa	320 KPa	220 KPa	280 KPa	220 KPa	220 KPa	220 KPa
Economy	280 KPa	320 KPa	280 KPa	280 KPa	245 KPa	220 KPa	220 KPa

Figure 6.1 Potential Designs I, II and III of Multi-Chamber Tyre Solution [30]

In Figure 6.1, the proposed designs were created on the basis to have different ways of linking the inner chambers to the core tyre construction (i.e. standard tyre structure) to evaluate their influence on the tyre driving response. Also, those design concepts were laid out in an attempt to satisfy the targeted design specifications indicated in section 6.2 along with the following safety and functional pre-requisites:

- Includes a beadlock chamber (i.e. zone 1 chamber) with the utmost inflation pressure in the tyre to strengthen tyre's beads mounting on the wheel-rim, back-up the succeeding chambers, and keep the tyre rolling during run-flat.
- To have a minimum of 35 KPa difference in the inflation of the chambers placed adjacent to each other vertically in which the beadlock chamber next to the wheel-rim would have the utmost pressure followed by lower pressure chambers respectively. This is to prevent excessive wrinklings and distortions in the structure of the inner chambers that would undermine the rolling stability [137].
- Avoids a completely straight and perpendicular inner chamber walls that are directly linked to the tyre tread in order to prevent a constantly stiffer tyre at the cost of ride comfort.
- Avoids small and complicated structure of the inner chambers, which can negatively affect the design's integrity, manufacturability, operation and housing.

To improve the capability of the multi-chamber tyre solution in addressing the different driving requirements, the multi-chamber tyre is to have two interchangeable inflation

modes (i.e. normal and economy) either manually or automatically using existing inflation technologies as will be indicated later in chapter (8). Each inflation mode has its application scope depending on the driving/road conditions at hand. For the normal inflation mode, the multi-chamber tyre will be inflated at such mode to carry-out the conventional and day-to-day operational driving requirements, in which tyre's grip and cushioning are essential, such as traction, braking, cornering, and rolling over road surfaces with different hardness and roughness.

As seen in Figure 6.1, the normal mode includes inflating the cavity chambers (i.e. zones 2, 3, L-Side and R-Side), that is directly responsible for maintaining the tread contour, at similar pressure level to that of the standard tyre to compare the different designs against each other and assess the effect of the structural design of inner chambers on the tyre performance. For greater radial stiffness and hence further reduced rolling-resistance, the economy inflation mode is used whenever the tyre's grip and cushioning are not crucial in situations such as travelling in a straight and flat roadway with negligible traction and braking.

All multi-chamber designs were investigated under steady-state and free-rolling conditions similar to that of the standard tyre in chapter (4). Using FE modelling, all designs were subjected to two rolling tests respectively, straight-line rolling and cornering, for comparison purposes and to study the effect of structural design on the driving performance. In the straight-line rolling test, the tyre is set to roll under 4000 N vertical load, 30 Km/h rolling velocity and at two different inflation modes (i.e. normal and

economy) respectively as shown in Figure 6.1. In this respect, at normal inflation mode, the multi-chamber tyre designs were assessed for grip, rolling-resistance and mechanical comfort (cushioning). As for economy mode, the designs were evaluated for rolling-resistance mainly. For cornering evaluation, the tyre is positioned to free-roll at normal inflation mode and under 4000 N vertical load, 10 Km/h rolling velocity and different slip angles at 0°, 0.5°, 1.0° and 1.5° respectively for cornering stiffness assessment and at 3° for footprint area assessment.

6.3.3 FE Development of Inner Chambers

For all multi-chamber designs, the developed 2D FE model of the standard tyre in chapter (4) was used as the base (core) FE tyre model. This is in which the cavity domain in the FE model of the standard tyre was modified, updated and integrated with the relevant structural design of the inner chambers (i.e. designs I, II and III) respectively. In all the designs, the inner chambers were built from thin rubber walls with reinforcement plies implanted inside those walls in its middle cross-section as shown in Figure 6.1. The rubber walls were modelled as deformable and twistable shell parts with CGAX4R solid elements whereas the reinforcement plies were modelled as deformable and twistable wire rebar layers with SFMGAX1 surface elements similar to modelling the tyre's sidewall and carcass ply respectively in chapter (4).

Similarly, the rubber walls and its reinforcement plies were made from the same material properties as that of the sidewall and the carcass ply of the standard tyre respectively in chapter (3). This is since the sidewall material is of low energy dissipation properties

compared to other tyre rubber components as seen in Figure 4.27 in chapter (4) for example which would decrease greatly from the contribution of the inner chambers to the overall energy losses in the tyre. Furthermore, no other materials of lower dissipation properties for the inner chambers were looked for since the material role is out of the scope of this research project.

The inner wall reinforcements in all the designs have the same lay-up configuration as that of the standard tyre's carcass indicated in Table 3.8 of chapter (3). However, for each inner wall facing the tyre's tread in parallel, an extra layer of reinforcement was placed inside the wall throughout the tyre circumferentially with slightly different rebar lay-up orientation in which the layer is set at 90° angle to the tyre carcass with spacing between the plies of 0.55 mm. This is to provide the inner walls parallel to the tread with a more load-bearing capacity to enclose the cavity air and withstand the inflation pressure with the peristaltic pumping effect during rolling. Figure 6.2 shows an example on the lay-up of the inner wall reinforcements for design II in which the other designs have similar lay-up configuration.

The 3D modelling and analysis procedures for the developed 2D FE model of all the multi-chamber designs were done similar to that of the standard tyre in chapter (4) having the same tyre mesh density of 200 sectors circumferentially since all designs have the same base (core) tyre model and for comparison purposes too.

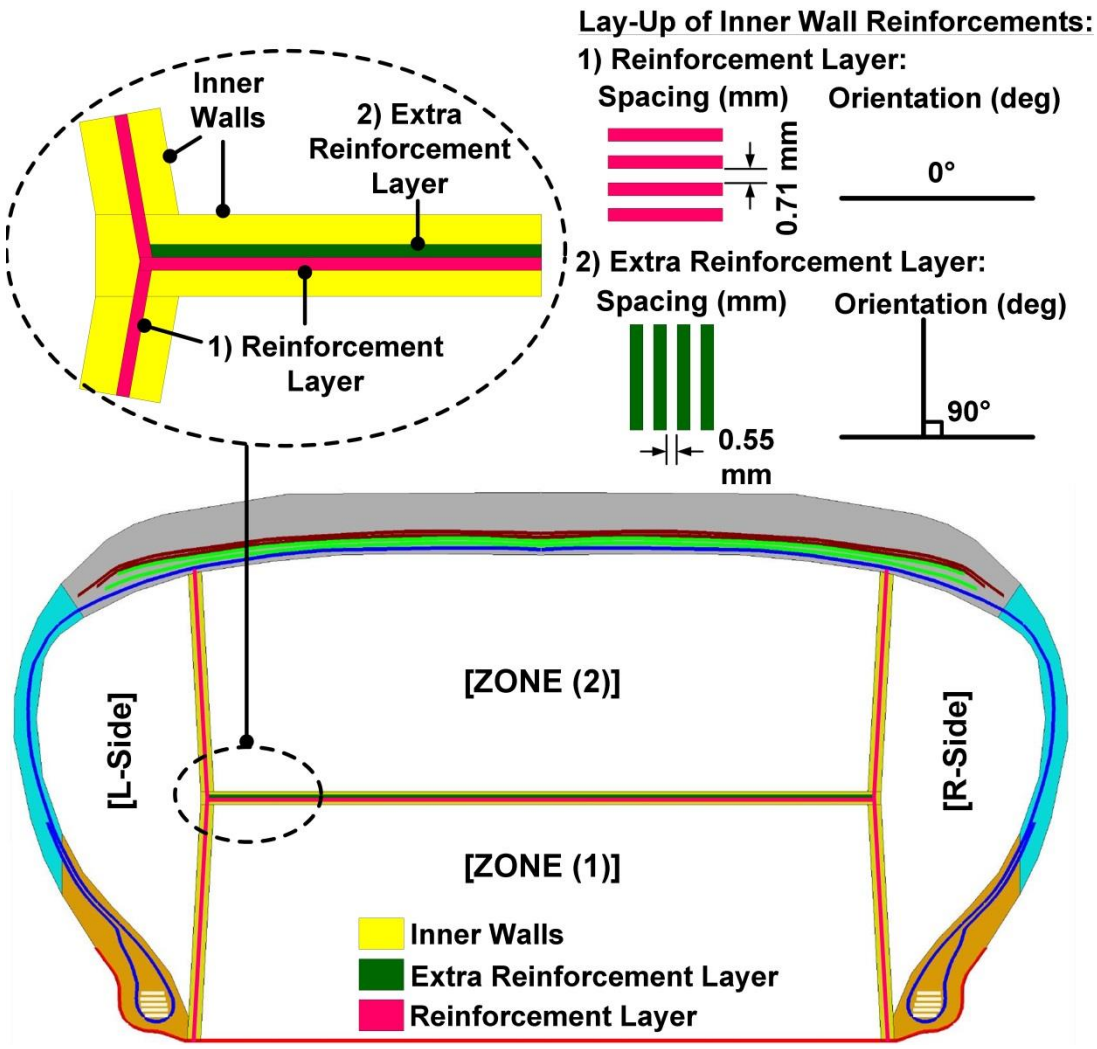
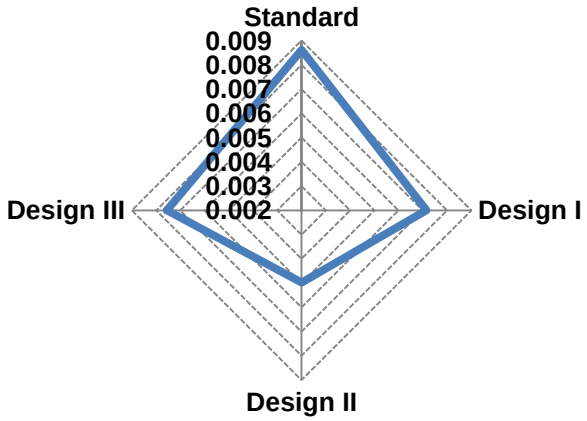


Figure 6.2 Lay-up Orientation of Inner Wall Reinforcements for Design II

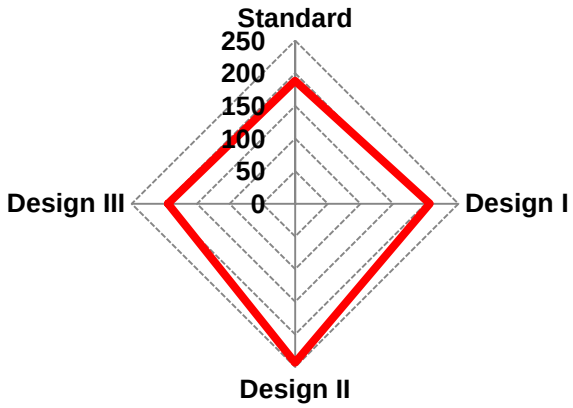
6.4 CONCEPTS EVALUATION

Under the straight-line free-rolling conditions indicated in section 6.3.2, “design II” shows the least rolling-resistance in contrast with the other designs with more than 40% decrease in resistance with respect to the standard tyre in both normal and economy modes as shown in Figure 6.3 and Figure 6.4 respectively. Design II had the utmost vertical stiffness, which made it experiences the least deformation in structure as

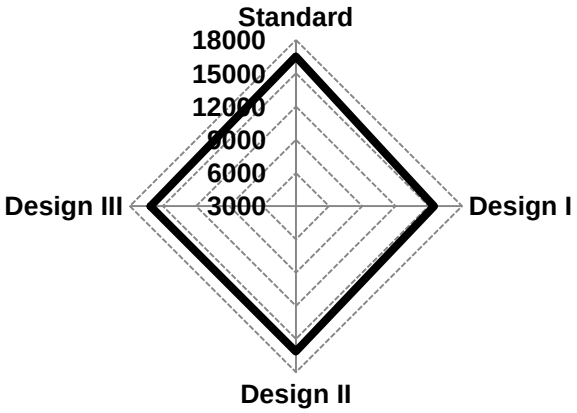
indicated in terms of profile radial non-uniformity in Figure 6.3 and Figure 6.4, tyre's vertical deflection and footprint width (i.e. tread's curvature) in Figure 6.5. According to the first law of thermodynamics and under the assumption of thermal equilibrium, lower deformation would require lower work to recover it and therefore lower energy dissipated in the tyre.



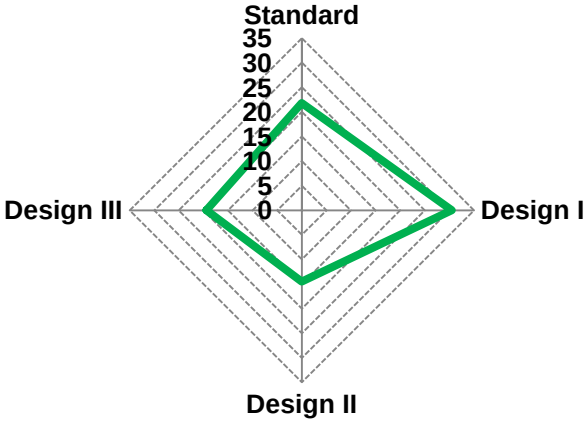
(a)



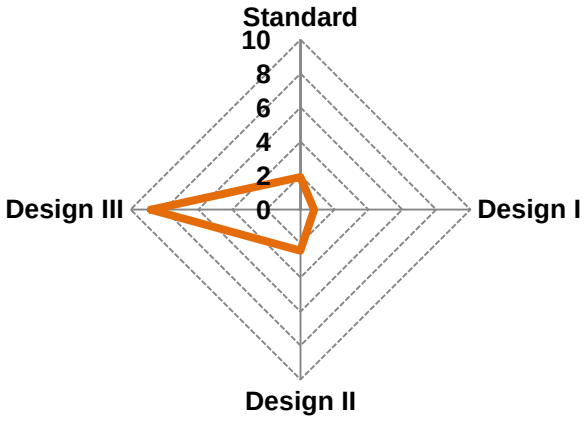
(b)



(c)

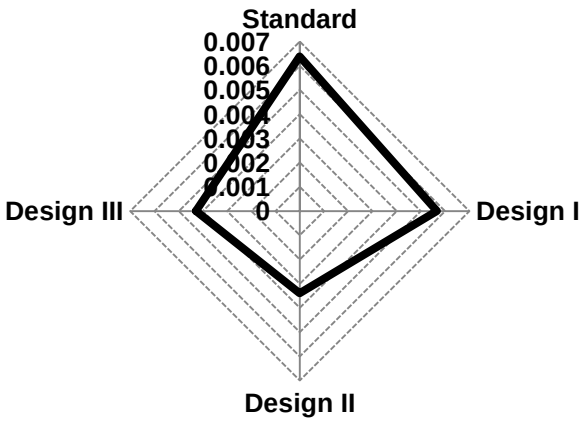


(d)

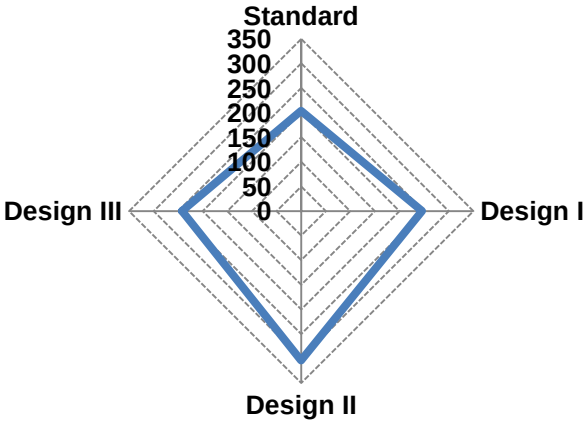


(e)

Figure 6.3 Performance of Designs I, II and III at Normal Inflation for (a) Rolling-Resistance Coefficient, (b) Static Vertical Stiffness (N/mm), (c) Footprint Area at Straight Rolling (mm^2), (d) Radial Non-Uniformity (N), (e) Lateral Non-Uniformity (N)



(a)



(b)

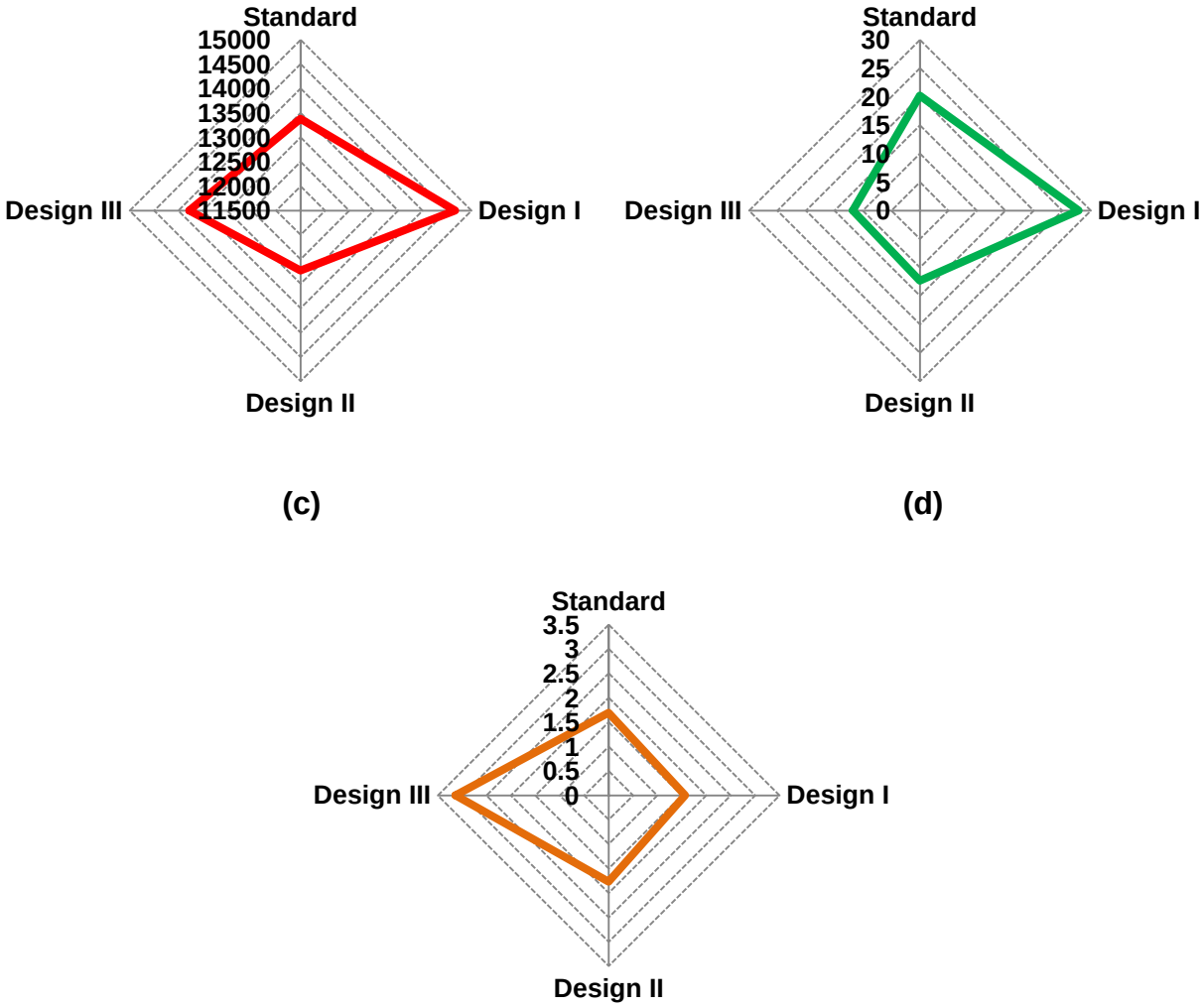


Figure 6.4 Performance of Designs I, II and III at Economy Inflation (a) Rolling-Resistance Coefficient, (b) Static Vertical Stiffness (N/mm), (c) Footprint Area at Straight Rolling (mm^2), (d) Radial Non-Uniformity (N), (e) Lateral Non-Uniformity (N)

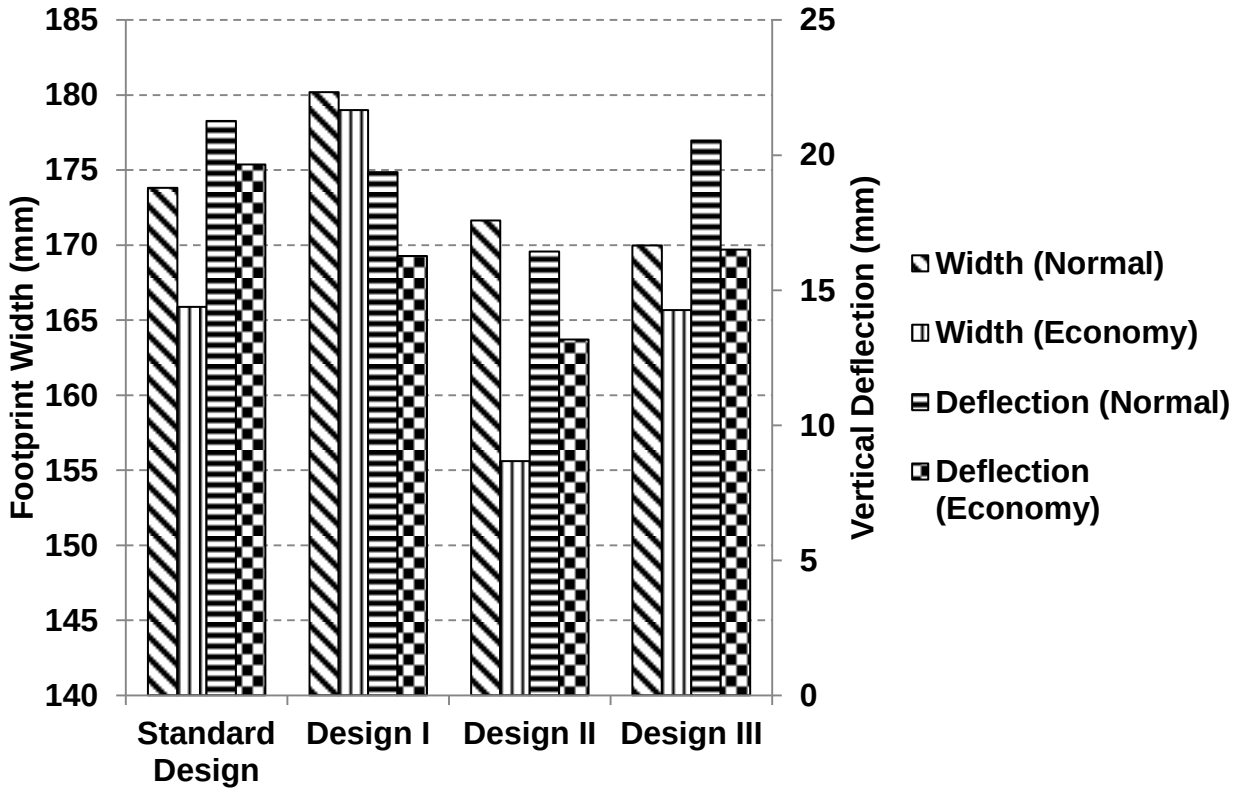


Figure 6.5 Vertical Deflection and Footprint Width of Designs I, II and III

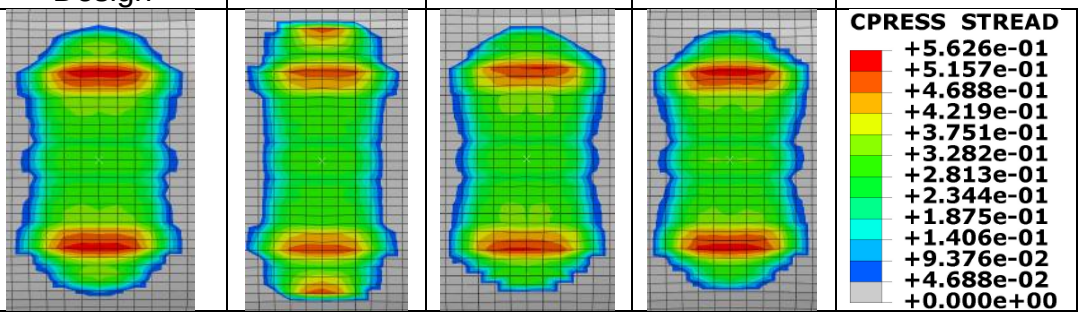
The apparent difference in the rolling-resistance between the multi-chamber designs can be attributed to the sort of structural support involved and the manner of employing the air volume to uphold the tyre profile. The enhanced stiffness and the reduced deformational level of design II were possible as a result of the usage of extra inner sidewalls to help the tyre's main sidewalls with holding out against the applied vertical load. Also, those inner sidewalls isolate the main sidewalls from the core air cavities (i.e. zones 1 and 2) in order to prevent disrupting and drawing away from the air volume responsible directly for supporting and upholding the tyre's tread contour. This is since the deformational side movements of the tyre's main sidewalls during rolling would

agitate and cause bulky movements of surrounding air volume agreeing with Schuring *et al.* [287].

However, for the inner sidewalls of design II, they are restrained in the middle by a lateral inner wall parallel to the tread as seen in Figure 6.2 to keep them in place, stabilise their motion and limit from the intensity and size of air movement. An obvious example on the effect and contribution of the multi-chamber designs is the assessment of “design II” against “design III” in Figure 6.3 at the normal mode in which they displayed largely different performance outputs despite having similar inflation across all the zones.

For the tyre’s grip, each of the footprint area and the contact pressure pattern were assessed at straight free-rolling and normal inflation mode, as seen in Figure 6.3 and Table 6.1 respectively. Designs II and III show close grip to the standard tyre’s since they have nearly similar footprint area, footprint profile and contact pressure distribution to that of the “standard tyre”. Nevertheless, for “design I”, an abnormal contact-patch profile, dissimilar contact pressure distribution and reduced footprint area are found leading to weakening and destabilising the tyre’s grip greatly. This can be referred due to the irregularity of the sidewalls profile and its inflexibility in “design I” which will be explained further later on.

Table 6.1 Contact Pressure Pattern of Designs I, II and III [30]

	Normal Mode			
	Standard Design	Design I	Design II	Design III
Contact Pressure (MPa)				

As for the non-uniformity of the tyre profile during rolling at normal and economy modes, “design I” shows the highest vibrational deformation radially with the “standard tyre” coming second whereas “design II” displays the lowest radial non-uniformity indicating a more stable rolling as shown in Figure 6.3 and Figure 6.4. Laterally, “design III” exhibits the utmost oscillation in sidewalls profile whereas the other designs show lower and nearly similar non-uniformity to each other at each of normal and economy modes. The apparent divergence in the non-uniformity response among the multi-chamber designs can be attributed to the stability of the inner chambers and their corresponding cavity air during rolling, the interaction of the inner chambers with the core tyre structure, and the flexibility of tyre’s sidewalls. For “design I”, the inner walls of its chambers are directly integrated with the tyre’s main sidewalls structurally which resulted in restricting tyre’s sidewalls movement, increasing sidewalls’ rigidity and having an irregular profile of the sidewalls during rolling as indicated in Figure 6.6. Such rigidity and irregularity of the tyre’s sidewalls led to unstable and vibratory rolling beside disrupting the cavity air noticeably which conforms with Schuring *et al.* [287].

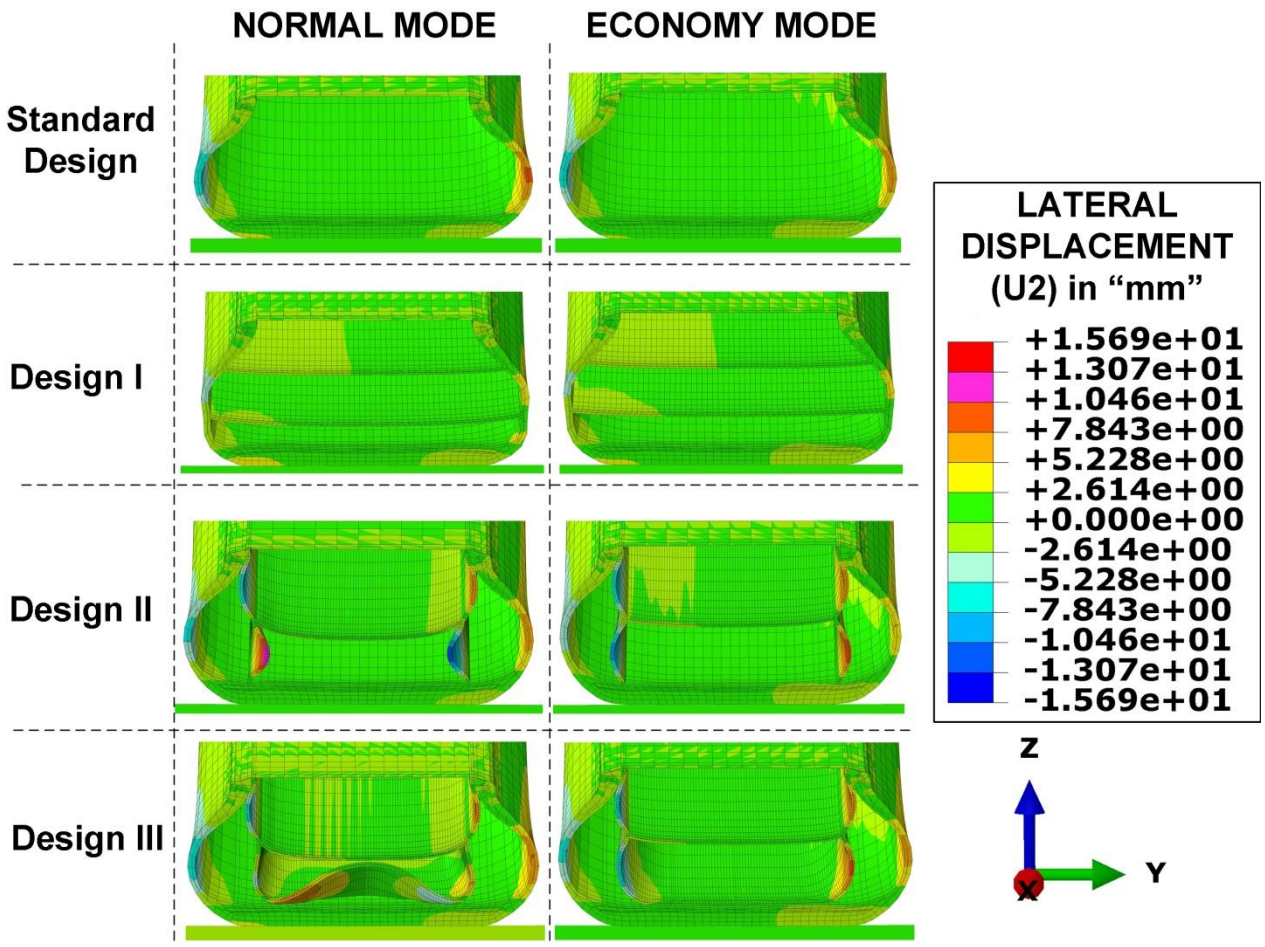


Figure 6.6 Tyre Deformation under Vertical Loading [30]

The "standard tyre" exhibits the most random and bulky movement of cavity air since it has a single and spacious cavity chamber promoting for such wild air movement as can be seen from the lateral displacement of the tyre's sidewall in Figure 6.6 and the tyre's vertical deflection in Figure 6.5 which are the greatest compared to the other designs. The same finding is highlighted by Schuring *et al.* [287]. As indicated previously, "design II" offers a multi-chamber solution that isolates the main tyre sidewalls from the core air

cavities (i.e. zones 1 and 2) which would help in preserving the core air volumes supporting the tread profile directly while keeping the flexibility and outline of the main sidewalls. Such solution minimises considerably the wildness of air volume movement inside the tyre because the air volume is confined into smaller and separate sub-volumes and the core air cavities are not largely affected by the curvy contour and movement of main sidewalls. This is since any air volume near and exposed to the main sidewalls would be excited and disrupted significantly by the sidewalls' curvy outline and deformational movement during rolling. Rae and Skinner [288] in addition to Schuring *et al.* [287] showed a similar finding.

For "design III", in its design set-up, it has a detachable cavity chamber (i.e. zone 2) close to the tread region to support the tread contour during rolling. This sort of set-up led to zone 2 chamber to incur excessive distortion in its profile with lateral slipping due to the arbitrary movement of air surrounding zone 2 induced by the peristaltic pumping during rolling, particularly for the normal inflation mode, as shown in Figure 6.3 and Figure 6.6. In return, such a set-up affected the overall stability of the tyre negatively during rolling.

In the assessment of tyre cushioning (i.e. mechanical comfort) at normal inflation, using tyre's vertical stiffness as seen in Figure 6.3, "design II" is found to have the stiffest structure (i.e. 243 N/mm) with the "standard tyre" having the lowest stiffness (i.e. 188 N/mm) whereas the other designs were slightly higher than the standard. While the other designs seem to have a satisfactory cushioning ability, "design II" would experience a

rougher ride to a degree. Based on the scope of tyre usage, “design II” may be of tolerable ride comfort because radial passenger car tyres usually come with about 200-220 N/mm of vertical stiffness [273, 289-291]. In the case, the ride (mechanical) comfort is emphasised, the tyre cushioning can be further improved by using a compatible car suspension to substitute for the lack in the required cushioning level, lowering inflation pressure as appropriate, and altering the structure of the inner chambers to include inner walls of less thickness or slightly changed layout.

As for cornering response, under the cornering testing conditions indicated in section 6.3.2, designs II and III display a close response to that of the standard tyre with small differences in terms of footprint area and cornering stiffness as shown in Figure 6.7 unlike “design I” which has lower cornering stiffness and larger footprint area. With such outputs, “design II” has the potential to keep the car’s stability in cornering and achieve close cornering performance to that of the standard tyre which can be further improved with the necessary structural modifications as appropriate. Although “design III” shows small differences with the standard tyre, it is unstable during cornering because of the excessive and irregular distortions in its zone 2 chamber across the tyre circumferentially, especially at the contact-patch region. In addition to the underperformance in cornering, “design I” also suffers from rolling instability during cornering due to its tyre’s sidewall rigidity and irregularity.

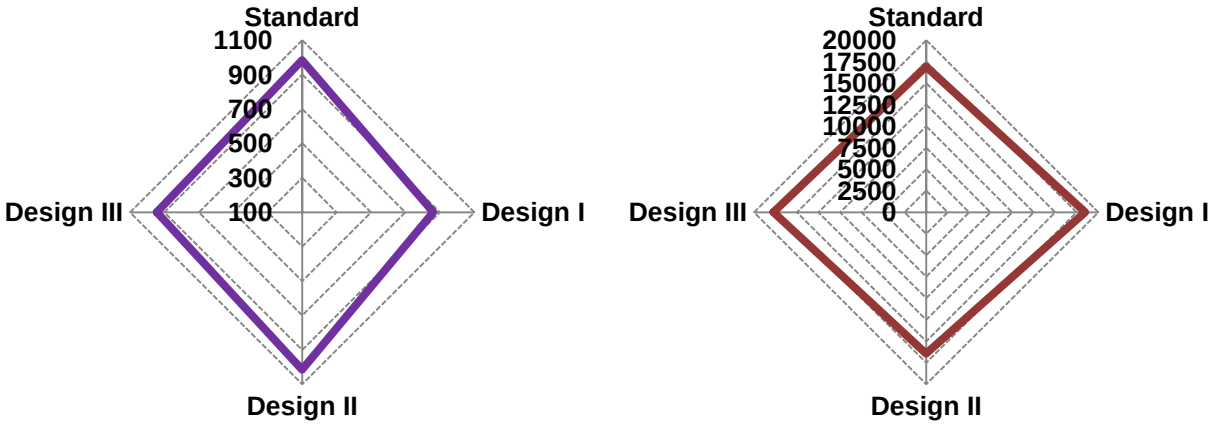


Figure 6.7 Cornering Performance of Designs I, II and III at Normal Inflation for (a) Cornering Stiffness (N/deg) and (b) Footprint Area (mm^2) at 3° Slip

6.5 BEST SUB-OPTIMUM DESIGN

Based on the evaluation of the designs in section 6.4, “design II” is found to be the best and most promising solution among the proposed multi-chamber designs. This is because “design II” offers the most energy-efficient solution to lower the rolling-resistance and provides a close performance of tyre’s grip and cornering to that of the standard tyre with small differences. Furthermore, “design II” has the most stable rolling profile among the other designs but at the cost of having the roughest ride comfort. Mainly, the other designs (i.e. designs I and III) suffer from rolling instability excited by the set-up of their inner chambers in relation to the core tyre structure. This is despite those designs providing slightly decreased rolling-resistance compared to the standard

tyre but still greater than that of “design II”. “Design I” shows the worst overall performance, especially in grip and cornering, in contrast with the other designs.

However, although “design II” has the best overall performance over the other designs, it still needs further development in design to address the driving requirements, in terms of grip, cornering and cushioning, more effectively. Altogether, “design II” is chosen as the best sub-optimum design in this chapter to be further improved in the next chapter for an optimum design for low rolling-resistance while meeting the other driving requirements satisfactorily (i.e. multi-purpose generalised solution).

6.6 SUMMARY

In this chapter, the initial designing and evaluation of several potential prototypes for the multi-chamber tyre solution were introduced using the “total design” approach of Stuart Pugh to identify simple, practical and most promising design for low rolling-resistance and meeting the other driving requirements as well. Three different designs of the multi-chamber tyre (i.e. designs I, II and III) were proposed in which each has a different way of structurally relating its inner chambers to the core (base) tyre construction (i.e. standard tyre construction) in order to study their structural effects on the tyre performance. Those proposed designs were developed using the validated FE model of the standard tyre from the previous chapters as the base FE tyre model. To add versatility to the function of the multi-chamber solution, the designs were set to include two interchangeable inflation modes, and they are a normal mode for various driving requirements and an economy mode for further reduced rolling-resistance. Using FE

modelling, the proposed multi-chamber designs were assessed against the standard tyre as the baseline for rolling-resistance, grip, cushioning and cornering performances. The evaluation of the different multi-chamber designs revealed the following main findings:

- At the contact-patch, the tyre's profile deformation and its flexibility can be influenced noticeably by how the inner chambers are structurally linked-up to the tyre, how the air volume is handled and exploited to support the tyre profile, and the level and distribution of air concentration across the tyre.
- Separating the air cavities directly connected to the sidewall and the tread from each other would considerably assist in stabilising the global air mass responsible for supporting the tread's outline while preserving the sidewall's profile and flexibility.
- After tyre deformation at the footprint, more rapid restoration of the cavity air volume is possible with a cavity chamber of smaller size.
- The oscillations and distortions of the tyre during rolling rely on how stable the inner chambers and their air volumes are inside the tyre, the uniformity of the tyre's shape and the rigidity of the tyre's sidewalls.

Based on the evaluation findings, "design II" was found to be the most promising solution among the other designs since it provides the lowest rolling-resistance with a decrease of over 40% and the most stable profile during rolling in addition to keeping a close performance with small differences only to that of the standard tyre in grip and

cornering. Despite that, “design II” had an undermined cushioning as a result. On the other hand, “designs I and III” were unstable during rolling and hence unsafe, especially “design I” which had weak gripping and cornering. With that, “design II” is selected as the best sub-optimum design over the other designs which requires further optimisation to obtain a tailored and well-balanced design for all driving requirements in terms of rolling-resistance, grip, cushioning and cornering. Such a requirement is to be covered in the next chapter.

CHAPTER (7): OPTIMUM MULTI-CHAMBER DESIGN FOR LOW ROLLING-RESISTANCE

7.1 INTRODUCTION

As a starting platform for a more developed and optimum design for low rolling-resistance, this chapter uses the initial promising and novel “design II”, that was reached in chapter (6), as a base design to create further advanced novel designs of multi-chamber tyre solution to evaluate and identify the optimum design. In this chapter, the targeted optimum design is a multi-purpose (comprehensive) design customised for low rolling-resistance and meeting other crucial driving requirements in terms of grip, cushioning and cornering satisfactorily. To reach such an optimum design, a parametric investigation was conducted using the “full-factorial design of experiments” (DoE) with the FE model of “design II” as the base model to develop and evaluate further designs for the best inner chamber design and to further optimise that best inner chamber design for the best cavity volume and inflation pressure settings.

All the multi-chamber designs were assessed at the same free-rolling testing conditions as that indicated in section 6.3.2 of chapter (6) but at normal inflation mode only unless otherwise stated to evaluate the designs for all the driving requirements as per that in section 6.2 of chapter (6) and for comparison purposes too. In the evaluation of the designs, since a multi-purpose design is targeted and for practicality, the “tyre’s grip” was given priority to ensure safety and obtaining the required rolling performance

followed respectively by “cornering” for control and stability during turns, “rolling-resistance” for fuel-saving and low CO2 emissions, and “cushioning” for mechanical ride comfort. The work done by the author in this chapter, as the main owner and contributor, has been published and can be found in [292].

7.2 EFFECT OF INNER CHAMBER DESIGN

7.2.1 Designing Constraints

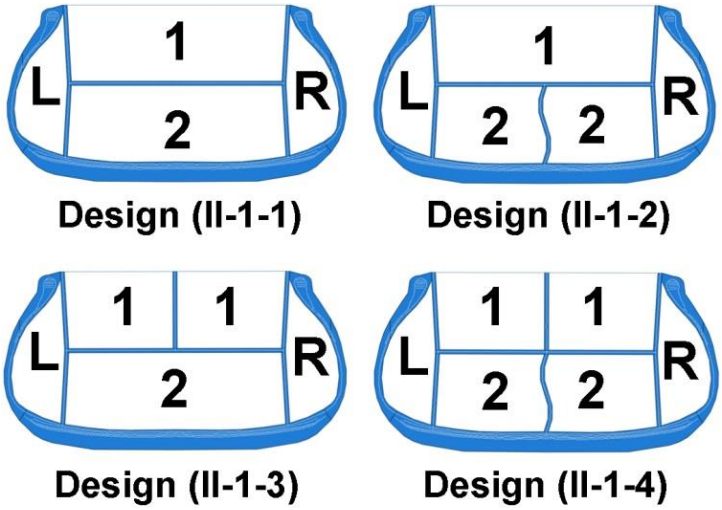
In addition to meeting the safety and functional pre-requisites in section 6.3.2, several design restrictions were to be satisfied in modifying “design II” as the base design for further developed designs in search for an optimum design that is valid and practical. Firstly, the re-designing of the inner chambers is to include just zones 1 and 2 excluding the side zones (R) and (L) to prevent interference with the flexibility of the main sidewalls of the tyre. Next, in zones 1 and 2 combined, the developed designs are to contain a maximum of two cavity chambers both radially and laterally to ensure simple, realistic and cost-effective designs. Moreover, for the cavity chambers laid next to each other laterally in either zone 1, zone 2 or both, the inflation pressure of those chambers is to be set at the same level to ensure a dynamically balanced tyre during rolling. Finally, in some of the designs, a curvy inner wall was added vertically in the middle of zone 2 to avoid the straight wall option in order to ensure a dynamically balanced tyre during rolling, include fewer chambers only and prevent a constantly stiffer tyre.

7.2.2 Finite Element Model Development

As per the design constraints in section 7.2.1, the full-factorial DoE in Table 7.1 with the developed FE model of “design II” from chapter (6), as the base model, were used to develop further advanced novel designs (i.e. II-1 designs). Four novel designs of multi-chamber tyre solution were developed comprising “design II” itself, which was renamed as “design II-1-1”, as shown in Figure 7.1. Those designs share the same geometrical and material features as that of the base design (i.e. design II or II-1-1) in the FE model for both the tyre and its inner chambers with the exception of the number, location and outline of the inner walls used to build-up the inner cavity chambers as seen in Figure 7.1.

Table 7.1 Full-Factorial DoE for Further Development of Design II

Number	Factors	Number of Inner Chambers (Levels of Factor)	
1	Zone 1	1	2
2	Zone 2	1	2



Inflation Mode	II-1 Design Zones			
	1	2	L	R
Normal (KPa)	320	220	220	220

Figure 7.1 II-1 Designs of Multi-Chamber Tyre Solution [292]

7.2.3 II-1 Designs Evaluation

At the normal inflation mode indicated in Figure 7.1 and using the same free-rolling testing conditions as in section 6.3.2, the II-1 designs (i.e. shown in Figure 7.1) were evaluated in which each design was found to have specific trade-offs in terms of the different driving requirements. For straight-line free-rolling at steady-state, the designs were tested under 4000 N vertical load, 30 Km/h rolling velocity and normal inflation in Figure 7.1 for tyre's grip, rolling-resistance and cushioning. With regard to the tyre's grip, the contact area and the contact pressure pattern of the tyre's contact-patch were evaluated as shown in Figure 7.2 and Table 7.2 respectively. For the area and profile of the contact-patch, each of designs "II-1-1" and "II-1-3" maintains a close match to the "standard tyre" while designs "II-1-2" and "II-1-4" display smaller profile. This outcome is

because of the additional vertical stiffness acquired by both designs “II-1-2” and “II-1-4” as a result of having an extra inner wall added vertically in their zone 2 which made the designs stiffer and hence less deformable at the footprint region.

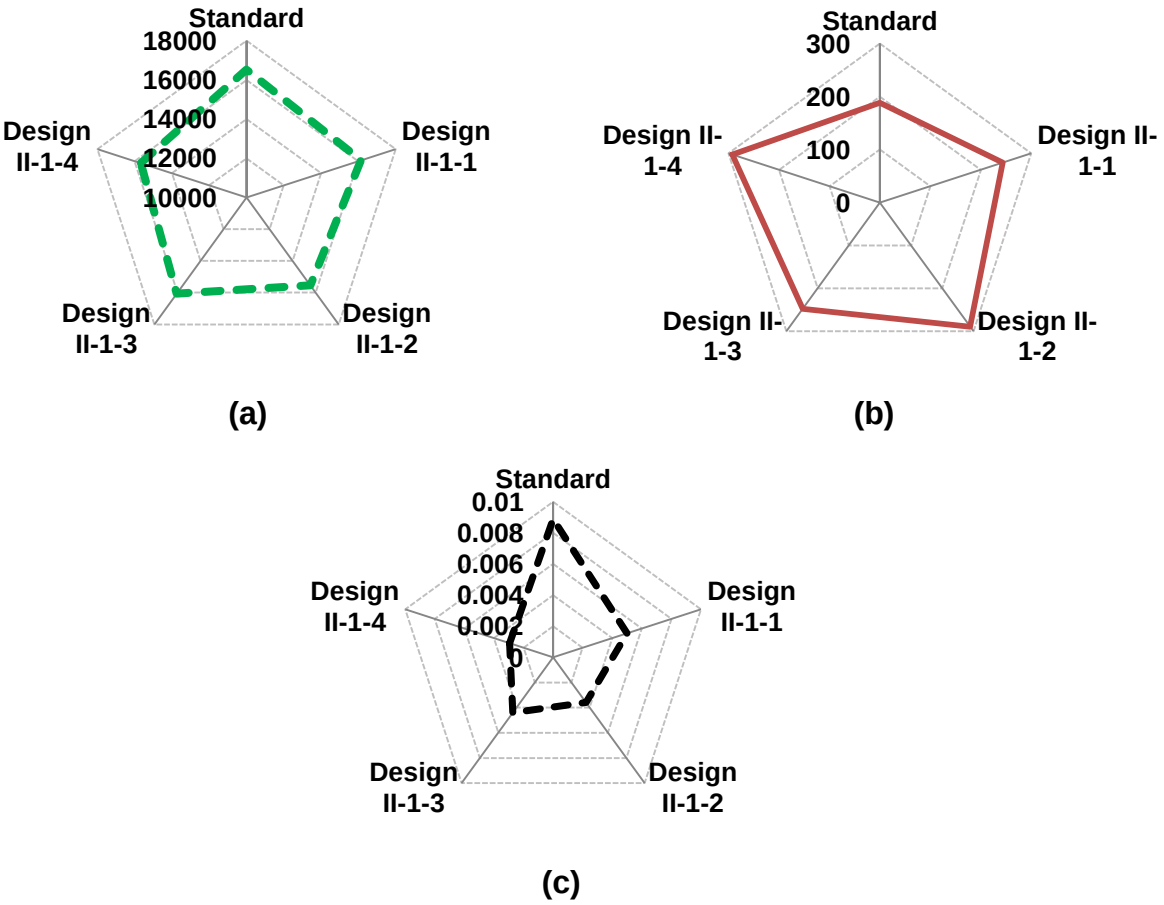
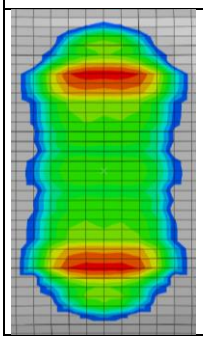
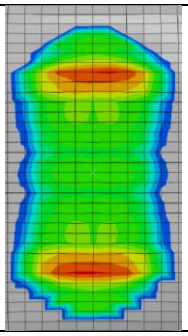
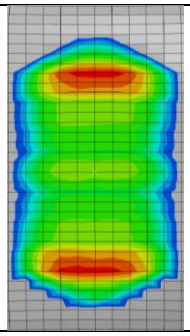
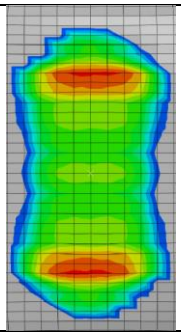
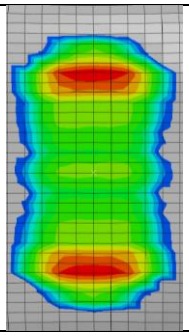
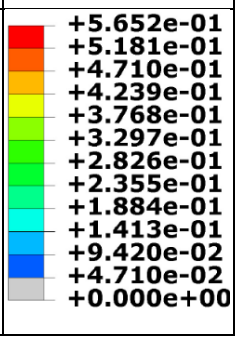


Figure 7.2 Straight-Line Free-Rolling Performance of II-1 Designs at Normal Inflation for (a) Footprint Area (mm^2), (b) Static Vertical Stiffness (N/mm) and (c) Rolling-Resistance Coefficient [292]

Table 7.2 Contact Pressure Distribution of II-1 Designs Contact-Patch [292]

Straight Free-Rolling at Normal Inflation Mode					
Standard	Design II-1-1	Design II-1-2	Design II-1-3	Design II-1-4	Contact-Pressure (MPa)
					

As for the contact pressure distribution, compared to “standard tyre”, both designs “II-1-1” and “II-1-3” show slightly dissimilar pressure pattern with weaker contact pressures, especially at the shoulders. This dissimilarity could be due to the intervention of the side inner walls of zone 2 with how the tread is usually vertically loaded in which the inner walls act more like a direct rigid linkage of vertical loading upon the tread at a loading point and orientation that are different from the case with the standard tyre. For designs “II-1-2” and “II-1-4”, such dissimilarity is reduced as a result of using a curvy inner wall vertically in the middle of zone 2 which served more as spring-like support of low rigidity and friendly orientation with respect to the tyre’s tread minimising the direct loading impact of the straight side inner walls of zone 2 on the tread.

The isolation of the cavity air into smaller and separate sub-volumes (chambers) in the II-1 designs, particularly in the direct route to upholding the tread outline, helped to maintain the majority of air volume to support the tyre’s tread at the contact-patch during

rolling and hence to minimise the deformation in the tyre's structure. This agrees with both the kinetic theory of ideal gases and the findings of the previous chapter. Furthermore, the usage of more inner walls vertically, particularly of the straight form or in zone 2, made II-1 designs stiffer vertically as can be seen in the cases of designs "II-1-2" and "II-1-4" in Figure 7.2 (b) since the inner walls would make the route of vertical loading across the tyre's structure to be more directly leading to the tread. Ji [293] highlighted a similar observation. Such increased stiffness led to lower deformational levels in the tyre, especially the tread curvature, and hence considerably lower rolling-resistance at the cost of poorer ride comfort as shown in Figure 7.2 (b) and (c) for designs "II-1-2" and "II-1-4" as an example.

For cornering, the II-1 designs were tested at steady-state free-rolling under 4000 N vertical load, 10 Km/h rolling velocity, normal inflation in Figure 7.1 and different slip angles at 0°, 0.5°, 1° and 1.5° respectively for cornering stiffness assessment and at 3° for footprint area assessment. As shown in Figure 7.3, II-1 designs show higher cornering stiffness compared to the standard tyre due to the additional lateral support given by the side inner walls of zone 2 to the tyre's main sidewalls during turning to offset the related opposite centrifugal forces. Despite that, all the II-1 designs exhibit smaller contact-patch area in relation to the standard tyre in which designs "II-1-1" and "II-1-4" are found to be smaller slightly. This can be attributed to the high vertical stiffness of the II-1 designs which made them less deformable at the contact-patch during rolling as indicated previously.

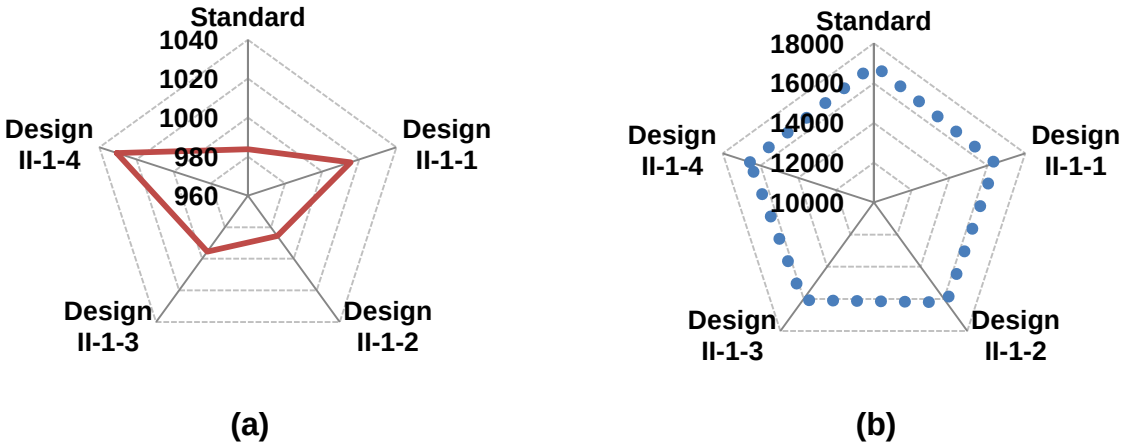


Figure 7.3 Cornering Performance of II-1 Designs at Normal Inflation for (a) Cornering Stiffness (N/deg) and (b) Footprint Area (mm^2) at 3° Slip [292]

In total, among the existing II-1 designs, there is no design yet that meets all the different driving requirements adequately. Based on that, more developments were carried out on the most promising solution among the II-1 designs and it was the II-1-1 design in order to arrive at a more satisfying design for the driving requirements. The developments involved mainly modifying the side inner walls of zone 2 that are of the straight form, which seem to cause the undermined performance of the design as indicated previously. In contrast with the rest of the II-1 designs, the II-1-1 design was selected because it provides the closest contact-patch area to the standard tyre's, the least ride roughness (i.e. best ride comfort), and the simplest layout with fewest components to manufacture.

An improved and more satisfying version of II-1-1 design was reached by transforming the outline and position of the side inner walls of zone 2 from a straight rigid-like to a

wavy spring-like to attain further elasticity and more supporting loading route toward the tread footprint. This improved version of II-1-1 design is shown in Figure 7.4 under the naming of “II-1-1B” design in which its rolling performance with respect to the diverse driving requirements is covered in the following section 7.3.

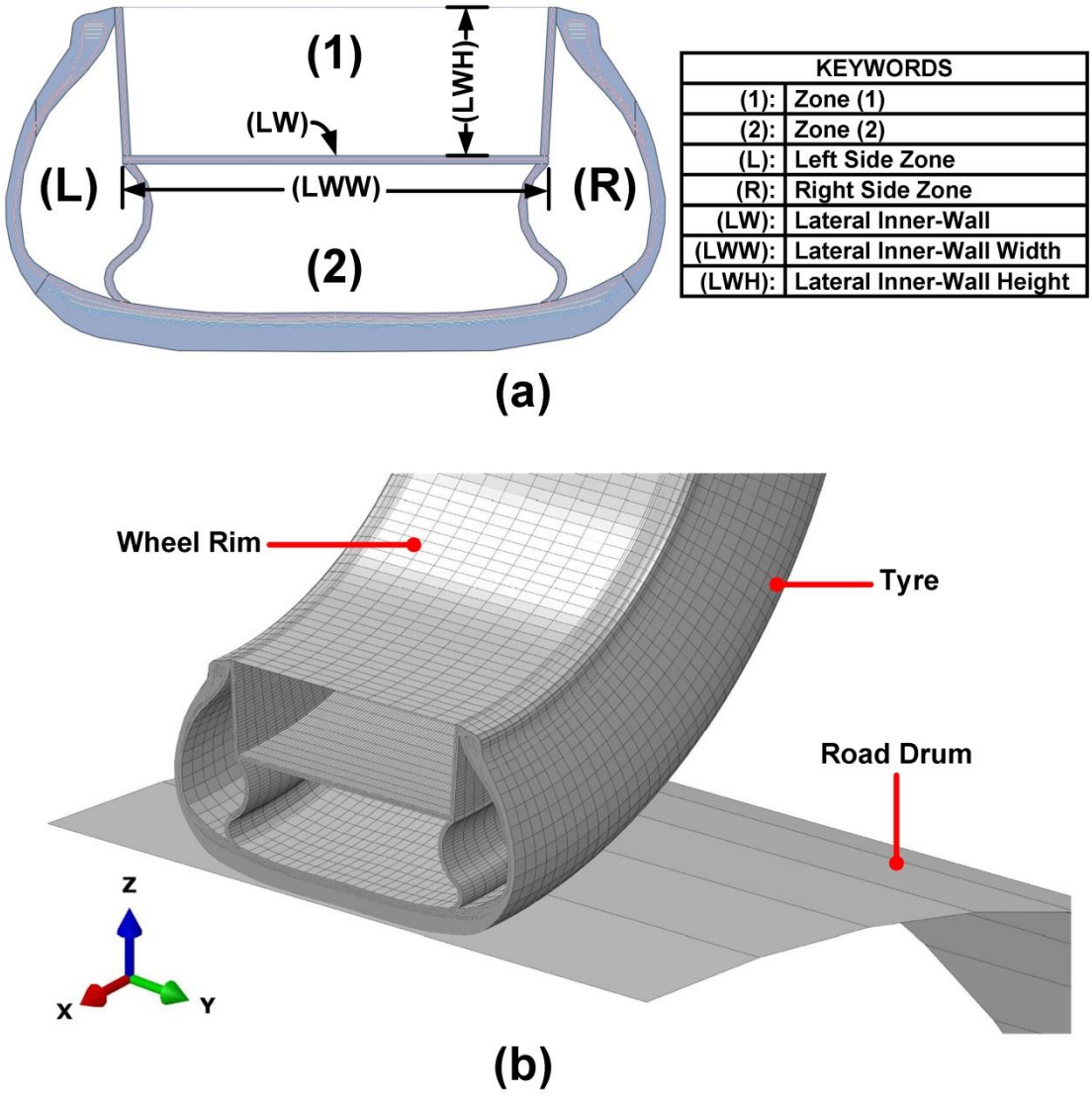


Figure 7.4 (a) 2D Axisymmetric and (b) 3D Cross-Sectional Models of II-1-1B Multi-Chamber Design [292]

7.3 EFFECT OF CAVITY VOLUME

Arriving at the best possible structural design of inner chambers (i.e. II-1-1B) based on the II-1 designs at the previous section 7.2.3, a further step toward a more optimum design was to investigate the II-1-1B design shown in Figure 7.4 for the best cavity volume settings of its inner chambers that would provide the best overall performance for the diverse driving requirements. This is in terms of lowering rolling-resistance while maintaining tyre's grip, cornering and cushioning satisfactorily compared to the standard (baseline) tyre. Using the full-factorial DoE in Table 7.3 and the FE model of the II-1-1B design in Figure 7.4, twenty-five various versions of cavity volume settings for the II-1-1B design were developed and assessed against the targeted driving requirements using the same rolling test conditions for straight-line rolling and cornering as in the previous section 7.2.3 for comparison purposes. The various versions of cavity volume settings were possible by changing the height and the width of the "lateral inner wall" (LW) of the II-1-1B design shown in Figure 7.4 accordingly which would lead to modifying the cavity volume of all the inner chambers. The changes in the height and the width of the LW were done within specific dimensional restraints as seen in Table 7.3 to preserve design practicality as indicated in sections 6.2 and 6.3.2 respectively.

Table 7.3 Full-Factorial DoE for Cavity Volume Settings of II-1-1B Design [292]

Number	Factor	Dimensional Constraints (mm)
1	Lateral Inner Wall Height (LWH)	30
		38
		45
		53
		60
2	Lateral Inner Wall Width (LWW)	110
		121
		132
		143
		154

For clarity and conciseness, samples of the evaluation results for the twenty-five versions of II-1-1B design, which represents the population's main outcomes, are shown and discussed in this section. This is in which the evaluation results for all the twenty-five volume versions of II-1-1B design are available in Table A.0.6 in appendix (D).

In terms of grip, the contact-patch area of the tyre is found to grow larger if the LW is getting wider while its height is set constant at any level above 38 mm or if the LW's height is increasing while its width is set at its maximum of 154 mm as shown in the example in Figure 7.5 (a) and (b). This can be attributed as a result of the local orientation axes of the side inner walls of each of zones 1 and 2 are moving nearer toward the direct route of tyre vertical loading when the LW is getting wider. Such behaviour would make the vertical loading to be transmitted further directly and greatly through the side inner walls to the tyre's tread causing more deformation at the contact-patch given the curvy profile of zone 2's side inner walls.

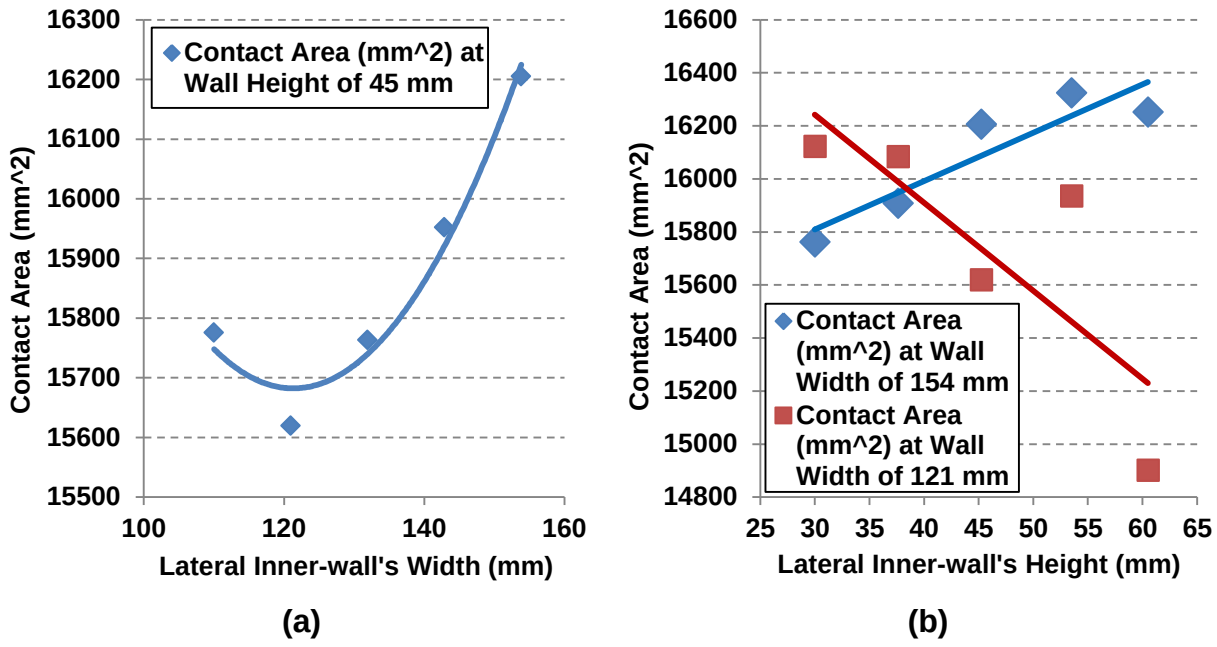
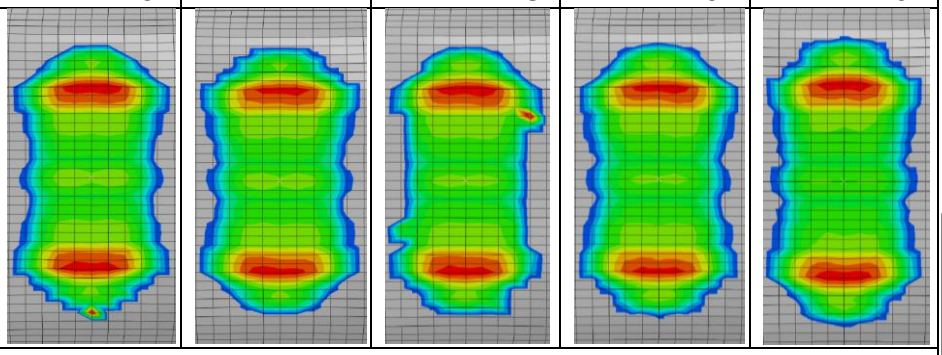
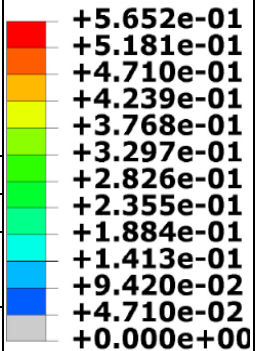
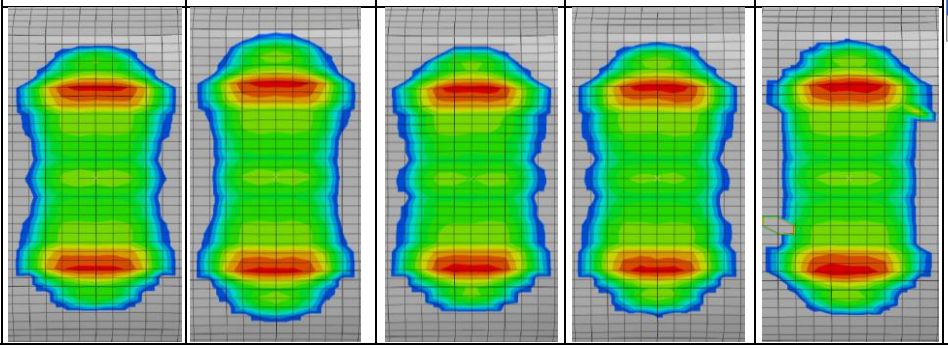


Figure 7.5 Effect of (a) Width and (b) Height of LW on Footprint Area at Straight Free-Rolling [292]

Nevertheless, the increase of LW's height shows an opposite effect on the tyre's contact-patch area if the LW's width is set constant at 132 mm or lower as shown in the example in Figure 7.5 (b). In addition to moving away from the direct route of vertical loading, based on Hooke's law of spring-like bodies and the kinetic theory of gases, under the indicated dimension set-up, the increase of LW's height would minimise the chamber size of zone 2 along with its side inner walls making them stiffer in the process. Due to such stiffness, lower deformational work of zone 2 chamber would be needed in order to uphold the tyre's tread against the applied vertical loading.

For the contact pressure pattern, as shown in the example in Table 7.4, narrowing the LW's width would lead to increasing the contact pressure at the tyre's contact-patch centre. This is because reducing the LW's width would cause shifting the orientation of the cavity volume in zones 1 and 2 further inward to the tyre's centreline in which the pressure/displacement work done by those volumes would be more focused at the tread's centre of the contact-patch during rolling. Moreover, increasing the LW's height would propagate and strengthen the maximum pressure spots at the shoulders of the tyre's contact-patch. This effect is because of the decrease in the size of zone 2 and its curvy side inner walls which led to reducing the flexibility of the walls and making the vertical loading transmission through the walls to the contact-patch shoulders more rigid-like, direct and greater. Such a feature helped in increasing the vertical stiffness of the tyre as a result of increasing the LW's height as shown in the example in Figure 7.6 (a) in which the LW's width shows no apparent influence over the vertical stiffness.

Table 7.4 Contact Pressure Distribution for Several II-1-1B Designs [292]

	Straight Free-Rolling at Normal Inflation Mode					Contact-Pressure (MPa)
At Wall's Height of 53 mm	Lateral Inner-Wall's Width (mm)					
	110	121	132	143	154	
	Design II-1-1B-16	Design II-1-1B-17	Design II-1-1B-18	Design II-1-1B-19	Design II-1-1B-20	
						
At Wall's Width of 143 mm	Lateral Inner-Wall's Height (mm)					
	30	38	45	53	60	
	Design II-1-1B-4	Design II-1-1B-9	Design II-1-1B-14	Design II-1-1B-19	Design II-1-1B-24	
						

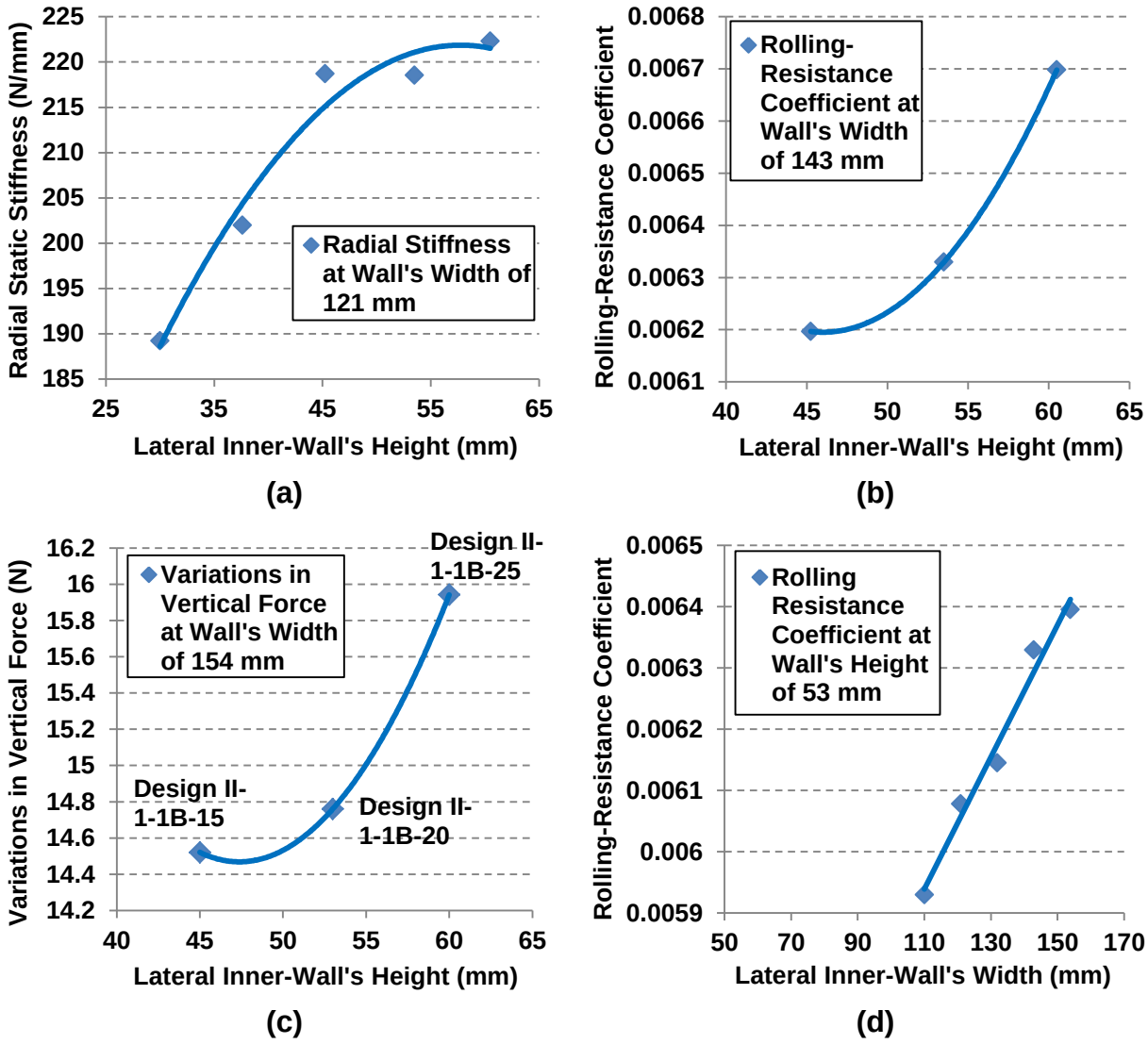


Figure 7.6 Influence of LW's Height on (a) Vertical Stiffness (N/mm), (b) Rolling-Resistance Coefficient and (c) Radial Non-Uniformity (N) and LW's Width on (d) Rolling-Resistance Coefficient during Straight Free-Rolling [292]

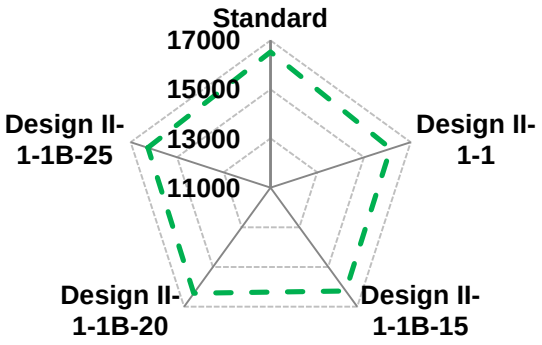
Regardless of the increased vertical stiffness, the increase in the LW's height from 45 mm and above is found to cause a slight increase of the tyre's rolling-resistance as seen in Figure 7.6 (b). This can be explained due to the small increase in the radial non-

uniformity of the tyre profile during rolling corresponding to the increase in the LW's height. Such an observation means that the tyre tread profile would be experiencing gradually higher flexing circumferentially during rolling and therefore a small increase in the rolling-resistance as the LW's height is increasing. The increase of tyre's radial non-uniformity can be attributed to the decrease of the chamber size of zone 2 and its curvy (spring-like) side inner walls with the increase of LW's height. This made the cavity chamber of zone 2 smaller, of lower resilience, more easily disrupted and incapable of preserving the tyre's tread outline in place more efficiently in front of the cyclic deformational oscillations circumferentially resulting from the peristaltic pumping action during rolling. Despite that, the II-1-1B designs still maintain a lower level of radial non-uniformity compared to the standard tyre which has non-uniformity of ~21.8 N.

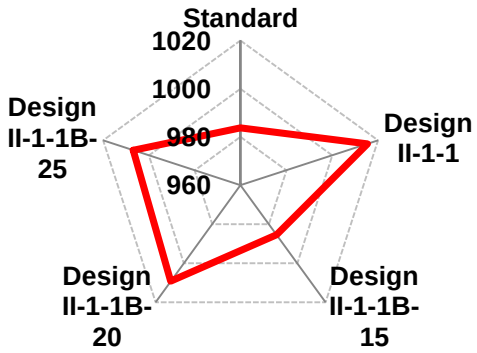
For the LW's height being constant at any level above 30 mm, the tyre's rolling-resistance is found to increase as the LW gets wider as shown in Figure 7.6 (d). A wider LW leads to a larger deformation at the contact-patch and hence a higher rolling-resistance because of the side inner walls of zones 1 and 2 are getting near the direct route of vertical loading of the tyre as indicated previously. This is in which the side inner walls would start to transfer the vertical load more directly to the tyre's tread and, with the curvy side walls of zone 2, the tread would start to deform and get into contact with the road more.

From the twenty-five volume versions of II-1-1B design, the most satisfying three designs with regard to the tyre's grip (i.e. as the top priority of design) were chosen for

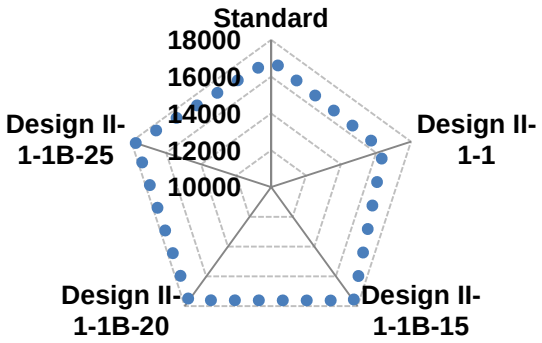
further assessment to determine the most balanced and fit design (i.e. multi-purpose design) for the diverse driving requirements. The chosen designs were II-1-1B-15, II-1-1B-20 and II-1-1B-25. As seen in Figure 7.7, the II-1-1B-20 design shows the most balanced performance for all the driving requirements in comparison with the standard tyre, the other designs and the rolling-resistance requirements in relation to Europe's 2021 emission regulations. This makes II-1-1B-20 design the best solution to adopt.



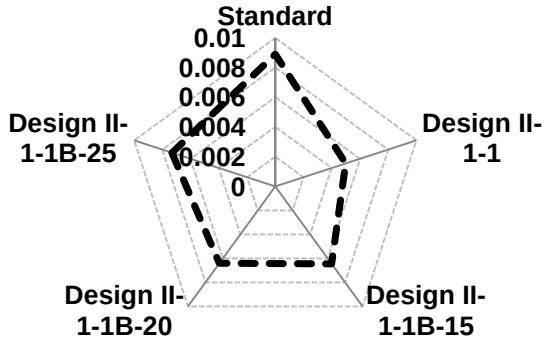
(a)



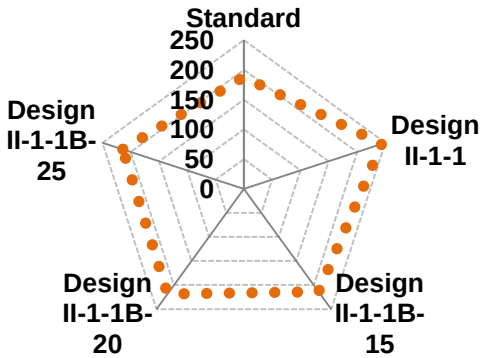
(b)



(c)



(d)



(e)

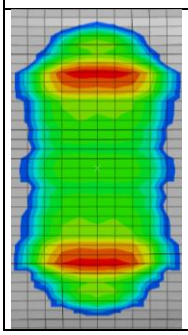
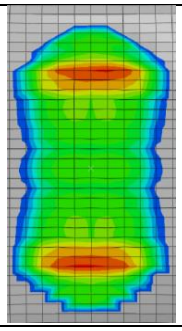
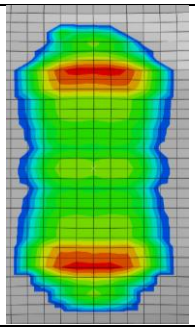
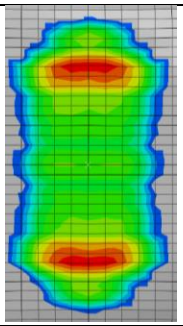
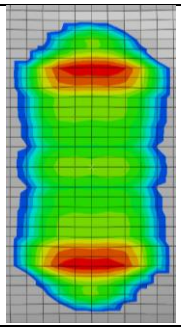
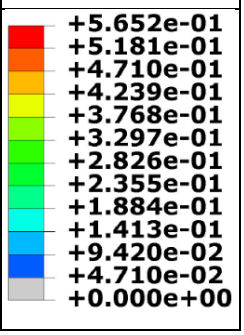
Design	Lateral Inner-Wall Dimensions	
	Height (mm)	Width (mm)
II-1-1B-15	45	154
II-1-1B-20	53	154
II-1-1B-25	60	154

Designs & its Dimensional Settings

Figure 7.7 Performance of II-1-1B Designs at Normal Inflation for (a) Footprint Area (mm^2) at Straight Rolling, (b) Cornering Stiffness (N/deg), (c) Footprint Area (mm^2) at 3° Slip, (d) Rolling-Resistance Coefficient and (e) Static Vertical Stiffness (N/mm) [292]

In terms of tyre's grip, II-1-1B-20 design exhibits similar profile and area of the contact-patch along with similar contact pressure distribution in relation to that of the standard tyre in which the other designs display an undermined grip as shown in Figure 7.7 (a) and Table 7.5 respectively. In cornering, each of II-1-1B-20 and II-1-1B-25 designs demonstrates better cornering performance than the standard tyre while II-1-1B-15 design gives a close level to that of the standard tyre as seen in Figure 7.7 (b) and (c). For the cornering stiffness, the use of the curvy side inner walls in zone 2 gives added lateral support and stability to the tyre's sidewalls in II-1-1B-20 and II-1-1B-25 designs in terms of an increased cornering stiffness to balance out the relevant opposite centrifugal forces during cornering. As for the footprint area during cornering, with the direct and firm holding provided by the almost undeformed chamber of zone 1, the chamber of zone 2 and its curvy (spring-like) side inner walls would offer further support to press-down and keep the tyre's tread in contact with the road surface resulting in secure and larger footing of the tyre.

Table 7.5 Contact Pressure Distribution for II-1-1B-15, II-1-1B-20 and II-1-1B-25 Designs

Straight Free-Rolling at Normal Inflation Mode					
Standard	Design II-1-1	Design II-1-1B-15	Design II-1-1B-20	Design II-1-1B-25	Contact-Pressure (MPa)
					

The rolling-resistance of each of II-1-1B-15, II-1-1B-20 and II-1-1B-25 designs is found to be lower than that of the standard tyre in which both II-1-1B-15 and II-1-1B-20 designs are almost similar and have the lowest rolling-resistance. In addition to using the standard tyre as a baseline, II-1-1B-15 and II-1-1B-20 designs show a rolling-resistance coefficient of 0.00646 and 0.00639 respectively as seen in Figure 7.7 (d) which satisfactorily meet the rolling-resistance requirement of 0.0065 set by the vehicle manufacturers in relation to Europe's 2021 emission regulations [18]. With regard to the tyre's ride (mechanical) comfort, all the three designs show an obvious increase in the vertical stiffness compared to that of the standard tyre in which II-1-1B-20 design has marginally higher stiffness than that of the other two designs as shown in Figure 7.7 (e). Nevertheless, the vertical stiffness of II-1-1B-20 design falls under the normal range for passenger car tyres and it is about 200-220 N/mm in which II-1-1B-20 design would have an acceptable level of ride comfort [30, 273, 289].

7.4 EFFECT OF INFLATION PRESSURE

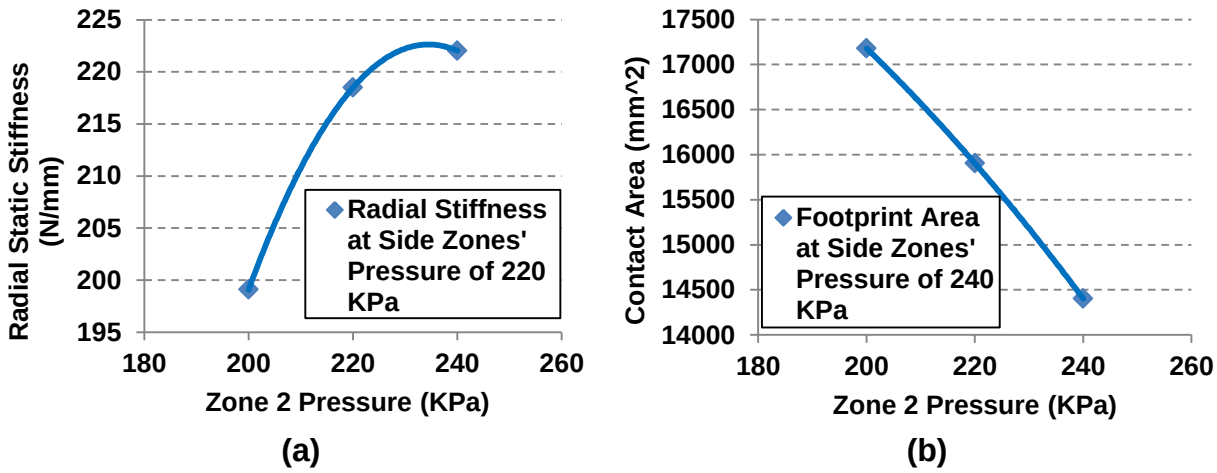
With the II-1-1B-20 design as the best inner chamber design with optimum cavity volume settings, the next further development was to investigate the II-1-1B-20 design for the best inflation settings that would allow for a more improved overall performance if possible. Several inflation constraints were needed to be met in order to carry out a proper investigation in addition to the constraints indicated previously in section 6.3.2. First, the inflation range to be investigated was specified close to the normal inflation mode in an effort to preserve the physical characteristics of the tyre under safe and appropriate operating conditions. Secondly, the chamber inflation of zone 1 was set constant with no changes to retain the stability of the design in terms of securing the seating of tyre's beads and supporting the other subsequent chambers. Thirdly, both side zones (L) and (R) were inflated at the same level of pressure to ensure a balanced rolling of the tyre.

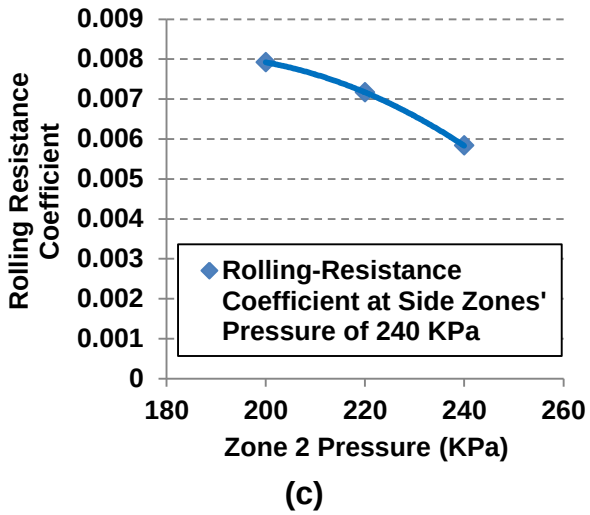
Implementing the full-factorial DoE in Table 7.6 using the FE tyre model of II-1-1B-20 design, nine various inflation settings of II-1-1B-20 design were developed and assessed against the different driving requirements under the same rolling test conditions for straight rolling and cornering as that of sections 7.2.3 and 7.3 unless otherwise stated. The complete evaluation results of those nine inflation settings of II-1-1B-20 design are available in Table A.0.7 in appendix (E). In this section, only samples of the population's main trends were used to avoid redundancy.

Table 7.6 Full-Factorial DoE for Inflation Settings of II-1-1B-20 Design [292]

Number	Factor	Pressure Levels (KPa)
1	Zone (2)	200
		220
		240
2	Side Zones (L) and (R)	200
		220
		240

Altering the inflation pressure of zone 2 of II-1-1B-20 design is found to show a noticeable effect on the physical attributes of the tyre while there is no apparent impact of the size zones (L) and (R). Since zone 2 is directly responsible for upholding the tyre's tread, the increase of zone 2's inflation causes enhancing the contact pressure at the contact-patch shoulders and boosting the vertical stiffness of the tyre which would decrease the contact-patch area in both straight rolling and cornering, in addition, to reduce the rolling resistance as shown in Figure 7.8. Nevertheless, the inflation of zone 2 is found to have no obvious influence on the cornering stiffness.

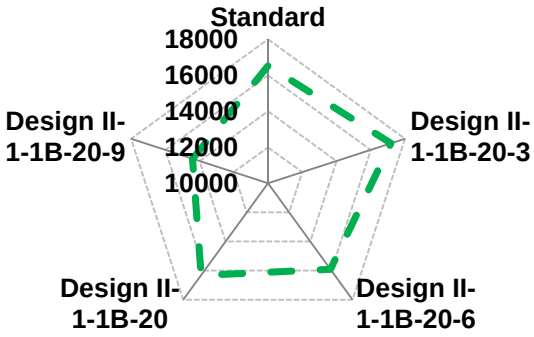




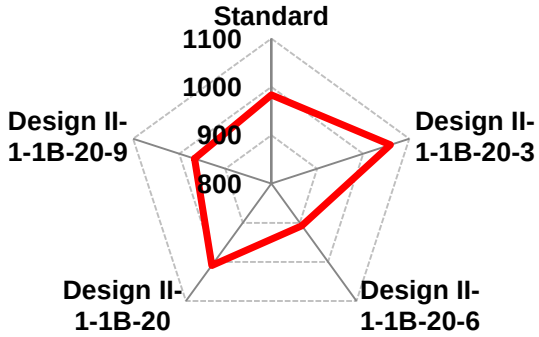
(c)

Figure 7.8 Effect of Zone 2's Inflation on (a) Vertical Stiffness (N/mm), (b) Contact-Patch Area (mm^2) and (c) Rolling-Resistance Coefficient at Straight Free-Rolling [292]

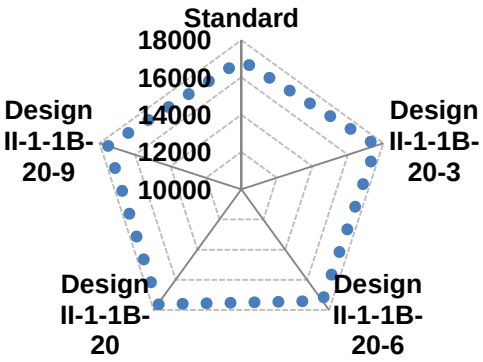
As shown in Figure 7.9 as an example, generally, any modifications to the inflation of zone 2, side zones ((L) and (R)) or both are found to cause trade-offs in the tyre's rolling performance for the various driving requirements. In this context, the normal inflation mode of II-1-1B-20 design is determined as the best inflation setting for an improved, satisfactory and balanced overall performance of the tyre since the II-1-1B-20 design was customised and developed at that mode to address the various driving requirements.



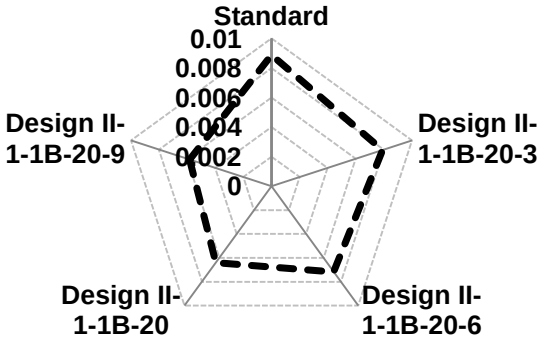
(a)



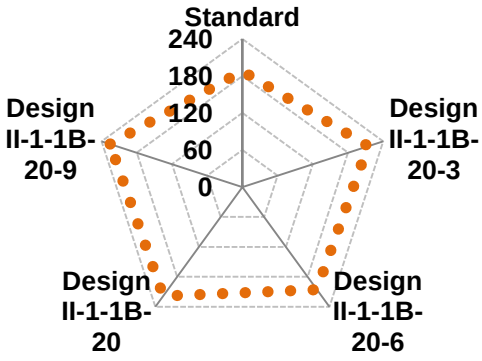
(b)



(c)



(d)



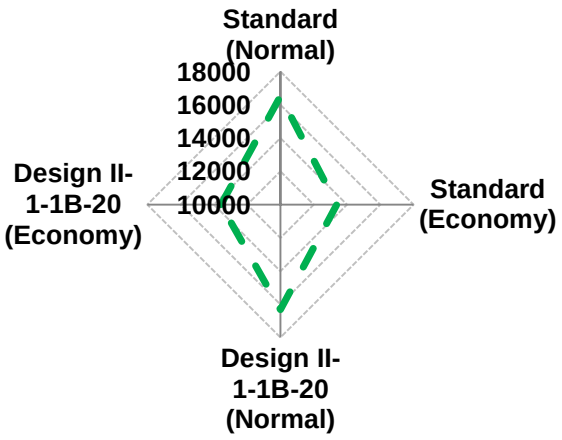
(e)

Design	Inflation Setting (KPa)		
	Zone 1	Zone 2	Zones (L) & (R)
Standard (220 KPa)	N/A	N/A	N/A
II-1-1B-20-3	320	200	240
II-1-1B-20-6	320	220	240
II-1-1B-20	320	220	220
II-1-1B-20-9	320	240	240
Designs & its Inflation Settings			

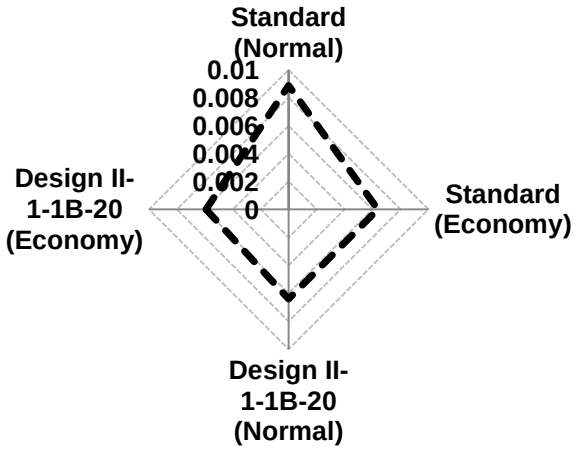
Figure 7.9 Performance of II-1-1B-20 Design at Different Inflations for (a) Footprint Area (mm^2) at Straight Rolling, (b) Cornering Stiffness (N/deg), (c) Footprint Area (mm^2) at 3° Slip, (d) Rolling-Resistance Coefficient and (e) Static Vertical Stiffness (N/mm) [292]

Regardless, as indicated in section 6.3.2 of chapter (6), II-1-1B-20 design can still be used under different inflation mode than that of the normal mode shown in Figure 7.1 and Figure 7.9 but within limited operational scope to achieve extended versatility of tyre functionality according to the given driving/road conditions at hand. As in section 6.3.2, the II-1-1B-20 design can be inflated at an “economy mode” as shown in Figure 7.10 in which only zone 2 inflation will be increased from 220 KPa at the normal mode to no more than 280 KPa in line with the design constraints in section 6.3.2 whereas the other zones will remain at their normal inflation mode. This would provide II-1-1B-20 design with an added vertical stiffness making it less deformable and hence having less rolling-resistance as seen in Figure 7.10. The economy mode would be suitable for usage in driving situations where tyre’s grip and cushioning are not emphasised such as travelling in straight and nearly flat roads with minimum traction and braking.

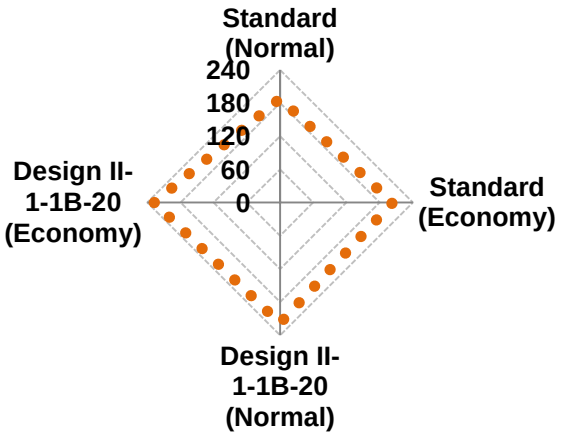
For driving situations where tyre’s grip and cushioning are necessary, like traction, braking, rolling on bumpy roadway and cornering, the II-1-1B-20 design will be set at the normal inflation mode by putting back zone 2’s inflation at 220 KPa as shown in Figure 7.10. Using the II-1-1B-20 design at the normal inflation mode, a further reduction in the rolling-resistance was possible by ~28% compared to that of the standard tyre at the normal inflation mode. As for the II-1-1B-20 design at the economy mode, a greater decrease in the rolling-resistance was reached by ~33% compared to the standard tyre at the normal mode and by ~7% compared to the standard tyre at the economy mode.



(a)



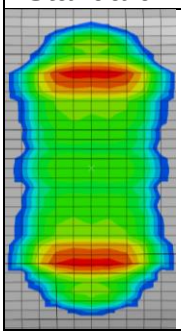
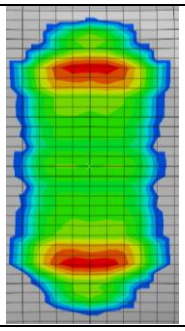
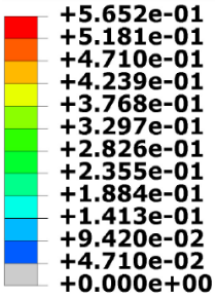
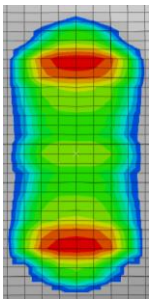
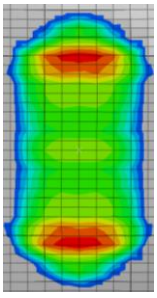
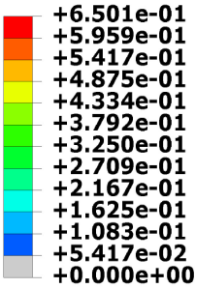
(b)



(c)

Mode	Design	Inflation Settings (KPa)		
		Zone 1	Zone 2	Zones (L) & (R)
Normal	Standard (220 KPa)	N/A	N/A	N/A
	II-1-1B-20	320	220	220
Economy	Standard (280 KPa)	N/A	N/A	N/A
	II-1-1B-20	320	280	220

Designs & its Inflation Settings

Normal Mode			Economy Mode		
Standard	II-1-1B-20	Pressure (MPa)	Standard	II-1-1B-20	Pressure (MPa)
					

(d)

Figure 7.10 Straight Free-Rolling Performance of II-1-1B-20 and Standard Designs at Normal and Economy Inflations for (a) Footprint Area (mm^2), (b) Rolling-Resistance Coefficient, (c) Vertical Stiffness (N/mm) and (d) Contact Pressure Pattern (MPa) [292]

7.5 OPTIMUM DESIGN VERSUS STANDARD DESIGN

A more comprehensive look on the overall performance of the reached optimum II-1-1B-20 design was done through comparing its performance against that of the standard (baseline) tyre over a wider range of operating conditions at the normal inflation mode to assess all the driving requirements. The comparison involved running the tyre at a straight-line free-rolling of a steady-state under normal inflation, 30 Km/h rolling velocity and different vertical loadings of 1000, 2000, 3000 and 4000 N respectively as seen in Figure 7.11 and Table 7.7. In addition, a cornering assessment was done under normal inflation, 10 Km/h rolling velocity, 4000 N vertical load and different slip angles of 1, 2, 3, 4 and 5 degrees respectively as shown in Figure 7.12.

In this section, the trends of the overall performance in the comparison conducted were in agreement with that done in the previous sections 7.3 and 7.4. The II-1-1B-20 design shows a reduced rolling-resistance due to its added vertical stiffness, an improved cornering roll, a matching grip and an acceptable mechanical comfort (cushioning) compared to the standard (baseline) tyre. As seen in Figure 7.11 (a), the gap in the rolling-resistance between the II-1-1B-20 design and the standard tyre becomes greater as the vertical loading increases. This is because of the role and involvement of the side inner walls of zones 1 and 2 in the direct path of vertical loading become more active and noticeable as the loading increases in terms of transferring the loading more directly to the contact-patch and withstanding the loading which gave an added vertical stiffness.

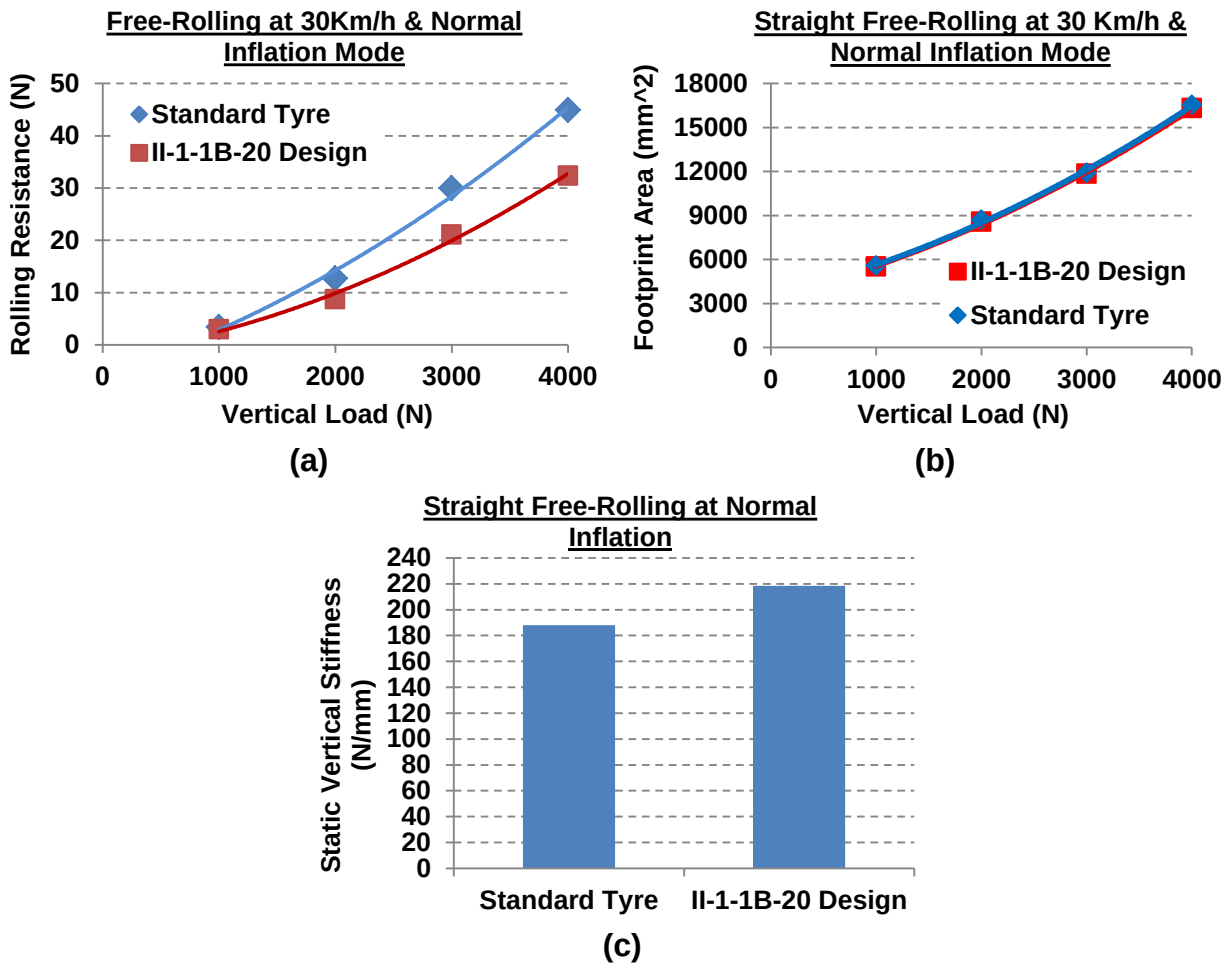
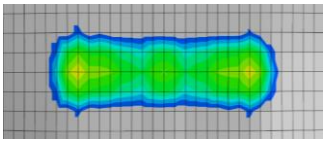
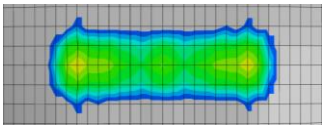
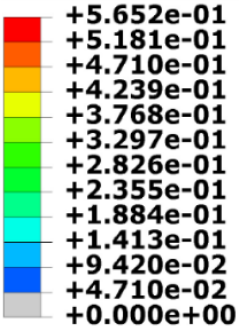
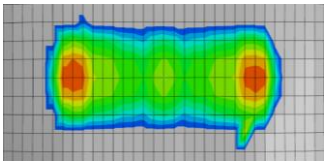
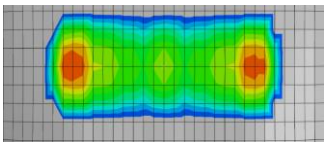
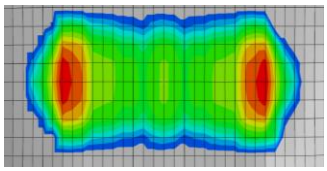
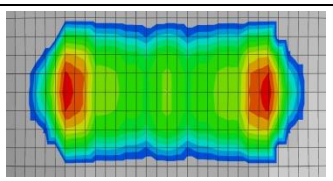
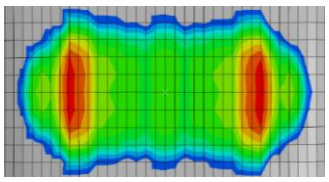
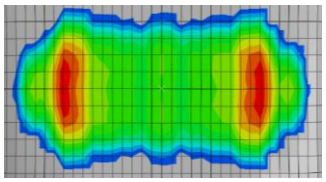


Figure 7.11 Straight Free-Rolling Performance of II-1-1B-20 Design under Different Vertical Loadings for (a) Rolling-Resistance (N) as Energy Lost per Unit Distance, (b) Footprint Area (mm^2) and (c) Vertical Stiffness (N/mm)

From the advantages of the II-1-1B-20 design over the standard tyre, the II-1-1B-20 design allows the tyre to retain its contact-patch grip in terms of profile, area and contact pressure despite having an increased vertical stiffness in comparison to that of the standard tyre as shown in Table 7.7 and Figure 7.11 (b) and (c). The reason behind that is the semi-complete isolation of the side regions (including main sidewalls) of the tyre

from its centre region (including the tyre tread) in the II-1-1B-20 design. Besides having the same base structure as the standard tyre, this was done by having the side zones (L) and (R) almost isolated from zones 1 and 2 in addition to being inflated at the same pressure as that of the standard tyre. This would allow the tyre sidewalls in the II-1-1B-20 design to be vertically loaded and get into contact with the road surface around the shoulders part almost the same way as the standard tyre.

Table 7.7 Contact Pressure Distribution of II-1-1B-20 Design under Different Vertical Loadings

Straight Free-Rolling at Normal Mode			
Vertical Load (N)	Standard	II-1-1B-20	Pressure (MPa)
1000			
2000			
3000			
4000			

Furthermore, both zones 1 and 2 with their side inner walls would make the added vertical stiffness acting more toward the tyre's tread centre without affecting the

sidewalls and their side zones (L) and (R) significantly. With the usage of the curvy (spring-like) side inner walls of zone 2 which are of a friendly and supportive orientation to the tyre tread, the added vertical stiffness would allow for a similar pattern of loading and contact pressure at the contact-patch to that of the standard tyre.

As indicated previously in sections 7.3 and 7.4, the usage of the side inner walls of zones 1 and 2 provided the II-1-1B-20 design with improved stability during cornering as shown in Figure 7.12 (a) and (b) in terms of greater counter lateral forces and larger footing respectively. The trend of the decrease of the footprint area with the increase in the slip angle goes in line with the findings of Wei *et al.* [294] and Haney [295].

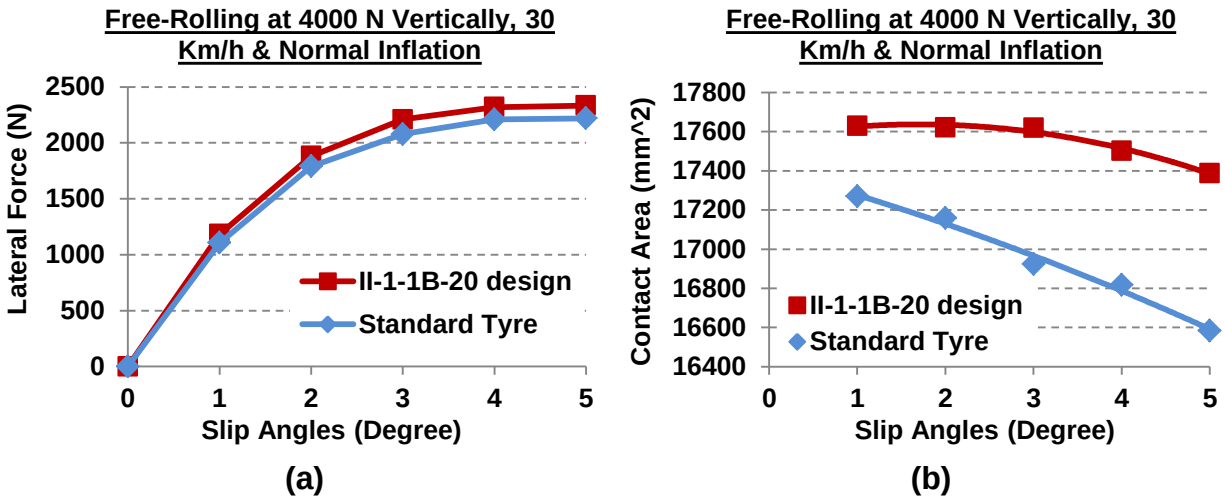


Figure 7.12 Cornering Performance of II-1-1B-20 Design at Different Slip Angles for (a) Lateral Force (N) and (b) Footprint Area (mm^2)

7.6 SUMMARY

This chapter covered the parametric investigation and development process of the sub-optimum (base) “design II” (i.e. obtained from chapter (6)) used to reach the optimum and multi-purpose design of II-1-1B-20 with the best cavity volume and inflation settings for low rolling-resistance and to meet the other key driving requirements satisfactorily. The multi-chamber design of II-1-1B-20 was concluded as the optimum solution to offer a balanced performance for the targeted driving requirements and achieve the aim of this research project successfully. This is because the II-1-1B-20 design was able to provide a reduction in rolling-resistance of ~28% while offering a similar tyre’s grip, a better cornering response and a satisfactory cushioning compared to that of the standard tyre at the normal inflation mode. In addition to that, the II-1-1B-20 design was able to meet the targeted requirement of the rolling-resistance coefficient of 0.0065 given by the vehicle manufacturers in response to Europe’s 2021 emission regulations.

The key characteristic of the II-1-1B-20 design was the isolation of the air volume inside the tyre into separate and smaller sub-volumes especially in the direct route of vertical loading of the tyre which led to the tyre’s sides (i.e. side zones (L) and (R)) being almost independent of the tyre’s central domain (i.e. zones 1 and 2). Such characteristic allowed the design to retain the same tyre’s footprint as that of the standard tyre while gaining an increased vertical stiffness. The II-1-1B-20 design had a simple overall layout with fewer chambers (i.e. four chambers) which involved the usage of curvy side inner walls in zone 2 that made the chamber of zone 2 to gain more elastic potential energy compared to the base “design II”. Those curvy inner walls of zone 2 have increased the

non-linear complexity of the tyre response which led to the inconsistency in the way of how the different cavity volume settings could affect the various driving requirements. Nevertheless, certain volumetric effects were apparent with regard to the rolling-resistance and it is the marginal increase in rolling-resistance with the decrease of zone 2's size and/or when the orientation axes of the side inner walls of zone 2 are getting nearer to the direct path of vertical loading.

The capability of the II-1-1B-20 design can be further extended by switching between its normal inflation mode and the economy mode according to the given driving/road conditions which involve changing the inflation pressure of zone 2 only while the other zones remain at the same pressure. At the normal mode, zone 2 is set at 220 KPa whenever the tyre's grip and cushioning are crucial. Otherwise, the economy mode can be used by inflating zone 2 at 280 KPa for increased vertical stiffness and hence lower rolling-resistance if the tyre to roll on a straight path with marginal traction and braking. A further decrease of the rolling-resistance by ~7% can be achieved by the II-1-1B-20 design at the economy mode in contrast to its normal mode.

CHAPTER (8): SUMMARY, CONCLUSION AND FUTURE RECOMMENDATIONS

This chapter summarises and concludes the overall work that has been done to accomplish this research project on “multi-chamber tyre solution for low rolling-resistance”. In addition, this chapter gives recommendations on future research work that can be done to further improve and expand the current research work for more insights and research findings.

8.1 SUMMARY AND CONCLUSION

In this study, an extensive survey of the existing literature on the tyre advances for low rolling-resistance revealed the crucial need and the urgency to reduce the tyre’s rolling-resistance to improve fuel economy and lower CO2 emissions for the welfare of the people and the environment considering the enormous amount of vehicles used globally. However, a major obstacle facing the reduction of the rolling-resistance is the persistent trade-offs with the other key performances of the tyre due to the complexity of tyre construction and operation. In this respect, the literature survey indicated that the multi-chamber tyre concept is a potential alternative solution to reduce the rolling-resistance considerably with negligible or no trade-offs. In addition, such a potential solution is found to have shallow coverage in the literature especially on the topic of rolling-resistance reduction with no actual applications yet. In that regard, the multi-chamber tyre concept is yet to be explored and investigated in-depth.

This research project introduced and investigated thoroughly a promising design of the multi-chamber tyre (i.e. II-1-1B-20) that can offer a reduction in rolling-resistance while maintaining the other key driving requirements of the tyre satisfactorily. In this project, a detailed, full and 3D finite element model capable of predicting the multi-chamber tyre solution was developed and validated against several experimental tyre prototypes (i.e. single chamber tyre, dual-chamber tyre and five chambers tyre) respectively for rolling-resistance, grip, cushioning and cornering. Using this validated FE tyre model as a base model, a variety of different novel multi-chamber designs were developed and evaluated for the optimum inner chamber design with the best cavity volume and inflation settings to provide an overall balanced performance of reducing rolling-resistance while maintaining tyre's grip, cushioning and cornering satisfactorily. Such a research project resulted in the following key research contributions:

A. The introduction of a new and efficient method to determine the core rolling-resistance of the tyre based on the "hysteresis damping ratio of the entire tyre" and the "work done by the tyre during its vertical deflection" computed from the outputs of the finite element tyre model which captures the rubber non-linear viscoelasticity using the parallel rheological framework. This method was published by the author in a technical paper through the Society of Automotive Engineers (SAE) [187].

B. The development of a finite element approach that is capable of simulating the "multi-chamber tyre" solution successfully. This approach involved coupling the deformation of tyre structure with the pressure and volume of its cavity air using the surface-based fluid cavity capability available in Abaqus 6.13-1 code. The approach is proven to be effective in accounting for the tyre/air interaction unlike the ineffective traditional method of only applying uniform pressure load on the tyre inner liner. Such an approach and findings were published by the author in a research paper through the SAE International Journal of Passenger Cars – Mechanical Systems [30].

C. The development of a genuine, simple and novel multi-chamber tyre design (i.e. II-1-1B-20) that is capable of reducing the rolling-resistance by ~28% while providing similar tyre's grip, satisfactory cushioning and improved cornering performance compared to the standard (baseline) tyre at the normal inflation mode. In addition, this novel design provides a rolling-resistance coefficient which meets that of the targeted requirement of vehicle manufactures (i.e. 0.0065) in response to Europe 2021 emission regulations. The key characteristic of this design is the isolation of cavity air inside the tyre into independent and smaller air sub-volumes especially in the direct path of vertical loading for an added vertical stiffness and between the tyre central domain (i.e. zones 1 and 2) and the tyre sides (i.e. side zones (L) and (R)) to retain the same tyre footprint. Such novel design and its evaluation were published by the author in a research paper

through the proceedings of the Institution of Mechanical Engineers (Part D: Journal of Automobile Engineering) [292].

D. The presentation of new and in-depth insights, findings and interpretations on the "multi-chamber tyre" solution for low rolling-resistance that help in enriching the current shallow literature. This involved the development and exploration of a range of different novel multi-chamber designs (i.e. designs I, II, III and II-1-1B) identifying their work mechanism, advantages and disadvantages. Those research findings can be used as a starting platform and guidelines for future research and development works. Such research findings were published by the author over two research papers through the SAE International Journal of Passenger Cars – Mechanical Systems and the proceedings of the Institution of Mechanical Engineers (Part D: Journal of Automobile Engineering) respectively [30, 292].

8.2 FUTURE RECOMMENDATIONS

As with any research project conducted, this research project was limited by its allocated time, funding and available resources and based on that this project had a specific scope of research and investigation which yielded meaningful research findings of novelty, magnitude and importance. This is especially since the tyre is a highly complex product which requires high costs to manufacture, test and investigate experimentally. In addition to that, the "multi-chamber tyre" solution is a relatively new subject with little findings in the literature and no substantial research works yet which means it has rich

research opportunities and infinite designing possibilities. With that said, further research work and improvements can be done to expand the current work reported in this research project with respect to the finite element tyre model, the experimental work and the “multi-chamber” design (i.e. II-1-1B-20). These improvements are as follows:

8.2.1 Improvements to Finite Element Tyre Model

Depending on the targeted application scope, the FE tyre model in this research project can be further developed but with caution to the balance between the model complexity and its incurred computational costs since the currently developed model is already complex and requires some computational resources to run. The contact behaviour can be predicted more accurately by finding a way to include the detailed tread grooves and patterns without causing undesirable hourglassing modes in the FE tyre model. Also, the computation of material response can be further improved by including the viscoelasticity properties of tyre’s reinforcements although it is of negligible effect.

The current PRF material definition adopted in the FE tyre model could be redefined based on frequency-based experimental data instead of strain-based (time domain) data to account more accurately for the speed effects on the tyre performance if it was of interest. Furthermore, if the temperature effect is to be accounted, similarly, the current material definition of the FE tyre model needs to be redefined based on the relevant temperature-dependent experimental data. In this research, the current FE tyre model can predict the global behaviour of the air cavity inside the tyre but not the local air behaviour in which the FE tyre model needs to be coupled with a CFD (i.e.

Computational Fluid Dynamics) analysis code in order to do so. This is to be able to investigate the role of cavity air on the tyre performance more accurately and in-depth for more effective designing of multi-chamber tyre solution and its control mechanisms.

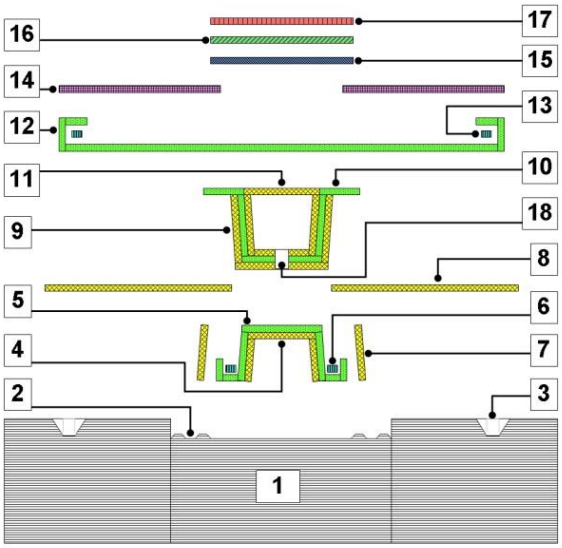
8.2.2 Improvements to Experimental Work

In this research project, the tri-axial electro-hydraulic tyre/drum rig used to examine the tyre prototypes for rolling-resistance had a limited operational range for tyre testing in which the tyre was limited to roll at low speeds and free-rolling conditions at one type of road surfaces only. Based on that, the test rig needs to be re-configured so it includes tyre testing at higher speeds, traction/braking conditions and different road roughness. This is in order to be able to examine the tyre further on rolling conditions that are closer to that of practice and to investigate the role of speed, road roughness and traction/braking on the effectiveness of the multi-chamber tyre solution.

8.2.3 Practicality Evaluation of Multi-Chamber Design

The optimum multi-chamber design (i.e. II-1-1B-20) developed in this research project needs to be further investigated for whether it is feasible to realise in practice and hence can be used in practical applications. Therefore, to evaluate the design manufacturability, a potential manufacturing method was proposed by the author in a research paper through the proceedings of the Institution of Mechanical Engineers (Part D: Journal of Automobile Engineering) [292]. The proposed manufacturing method needs to be evaluated and tested in practice if the proper resources were available. As shown in Figure 8.1, this manufacturing method suggests the usage of the conventional

“extrusion” and “calendering” processes applied currently in tyre manufacturing to produce the different tyre structural layers of II-1-1B-20 design respectively. To assemble those layers together, a tyre building drum is proposed to be modified as suggested in Figure 8.1. The relevant structural layers are assembled on the modified tyre building drum in the order and the way specified in the (A) to (F) procedures shown in Figure 8.1 respectively similar to the conventional building process in which a bonding film is added between the relevant layers when necessary to tie them.



Exploded Cross-sectional View of Tyre Structural Layers on Tyre Building Drum

1 Dynamic & Triple Tyre Building Drum(s).

2 & 3 Grooves for Beads Mounting.

7 , 8 & 9 Airtight Inner Liners for Side Zones.

6 & 13 Steel Beads.

4 Airtight Inner Liner for Zone (1).

5 , 10 & 12 Body Plies.

11 Airtight Inner Liner for Zone (2).

4 to 7 Inner chamber (Zone (1)).

9 to 11 Inner chamber (Zone (2)).

14 Sidewalls.

15 Steel Belts.

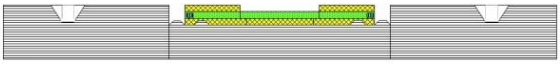
16 Cap Plies.

17 Tread.

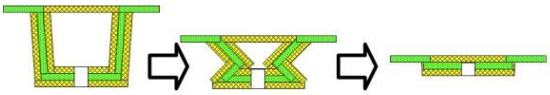
18 Inflation Hole.

Note:

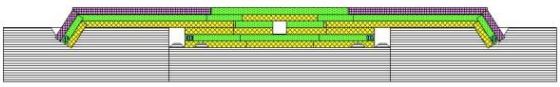
- The different tyre structural layers are possible to produce using the conventional "extrusion" & "calendering" processes.
- Procedures (A) to (F) are similar to that of the conventional building process where a bonding film is added between the relevant layers when necessary to tie them.
- After building phase, the tyre is cured to fuse the different tyre layers into one solid structure & give the tyre its physical properties.



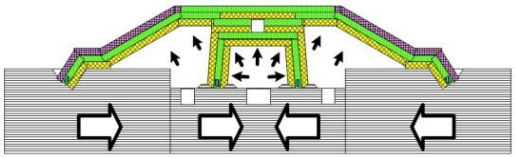
A Layers "4" to "7" are wrapped around drum respectively to build-up Zone (1) chamber.



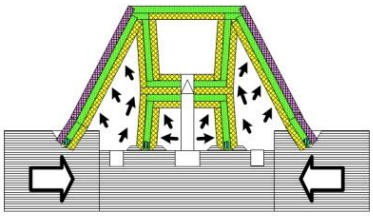
B Zone (2) chamber is built-up independently from layers "9" to "11" then folded into thin flat layer.



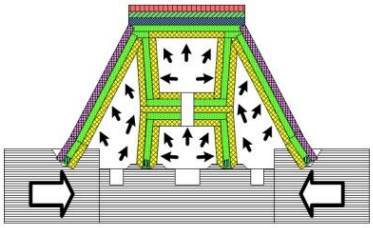
C Layers "8", followed by zone (2) chamber & then layers "12" to "14" are wrapped around drum respectively.



D Zone (1) chamber is inflated, drums move inward & side zones are inflated partially.



E Side zones are fully inflated and a puncture is made in zone (1) for inflation to pop-up zone (2).



F Zone (2) is fully inflated and layers "15", "16" & "17" are wrapped around drum respectively.

Figure 8.1 Proposed On-Drum Building Approach of II-1-1B-20 Design [292]

After the on-drum building phase, the tyre is cured to fuse the different tyre layers into one solid structure and give the tyre its physical profile and properties as seen in Figure 8.2. Besides the conventional curing mould housing, an internal mould is suggested to be assembled inside the tyre to surround and hold the structure of the inner chambers during the curing process in order to help give the inner chambers their final physical shape and properties as indicated in Figure 8.2.

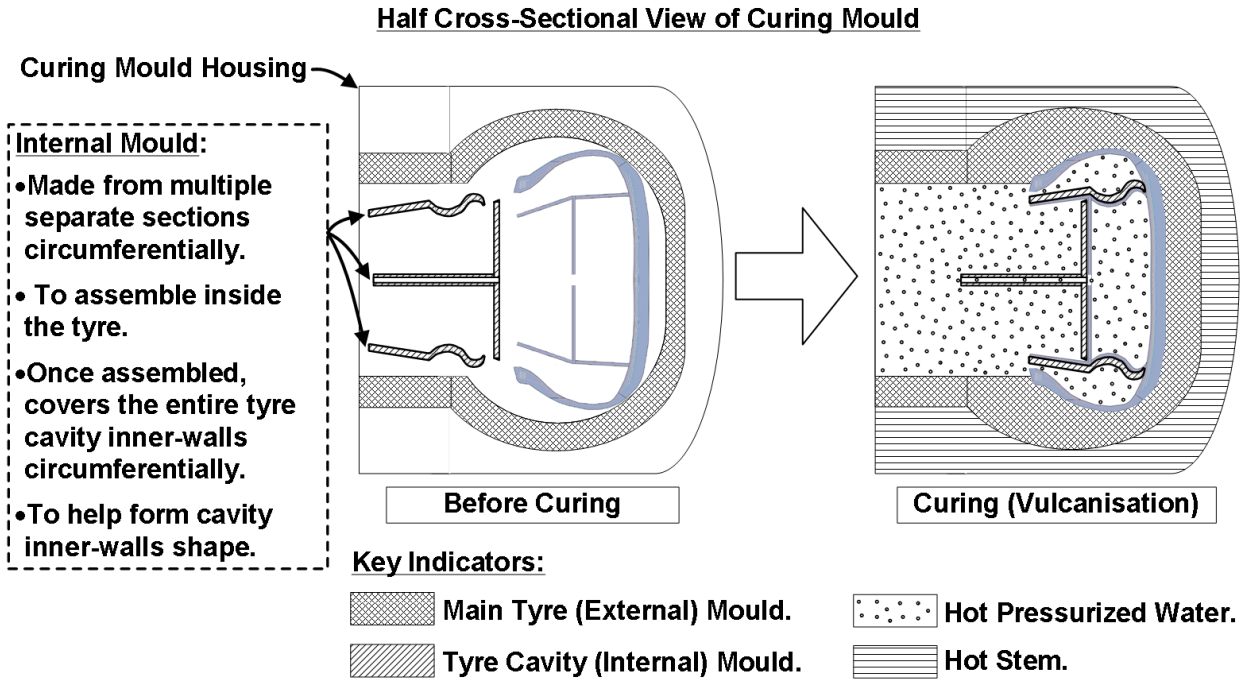


Figure 8.2 Suggested Curing Method of II-1-1B-20 Design [292]

In addition to the proposed manufacturing method, a further aspect of the II-1-1B-20 design that needs to be considered and developed to ensure the design feasibility is the inflation mechanism of the inner chambers. A net of flexible air channels is suggested to be developed to link each zone chamber with the closest valve stem on the wheel in

which those channels are used to inflate the chambers without being bent or getting damaged easily during normal tyre operation. The II-1-1B-20 design can be inflated manually at a single mode of inflation only for all time operation and this mode is the normal inflation mode. Another option is to have two interchangeable modes of inflation of the II-1-1B-20 design based on the driving/road conditions at hand and those modes are the normal and economy modes as indicated previously in this research. Those two modes can be inflated and controlled by an automatic inflation mechanism such as or similar to that of Goodyear AMT and Aperia's Halo in which zone 2 inflation will be the only inflation to change between those two modes.

APPENDICES

APPENDIX (A): BASIC BACKGROUND ABOUT PNEUMATIC TYRES

A.1 Main Function(s)

As the only link between the vehicle and the road, normally, the pneumatic tyre has multiple crucial functions to carry-out to deliver the mechanical drive (i.e. vertical, longitudinal and lateral forces) between the vehicle and the road surface in the safest, most efficient and effective manner possible under various driving conditions. As an example, such functions are as follows [28, 152, 296]:

a) To offer a proper mechanical grip between the vehicle and the road for traction, cornering, braking and parking under various road conditions such as coarse, fine, flat, steep, dry and wet surfaces.
b) To provide the vehicle with the optimum control and handling performance during interaction with road surface by transmitting and generating the required longitudinal and lateral forces for proper acceleration, braking and cornering conditions.
c) To support and withstand the vehicle's weight under all realistic loading and driving conditions.
d) To act as a cushion to absorb or reduce the impact of road surface irregularities on vehicle chassis for a more comfortable and stable ride.

A.2 General Construction

In general, the vehicle's tyres are very complex and anisotropic [25, 297]. Although, this makes them being able to perform the various challenging functions indicated earlier; at the same time, this makes them not something simple and easy to analyse, predict and describe [5, 152, 297].

A.2.1 Outer Geometrical Profile

Commonly, vehicle's tyres come as a circular tubular casing in shape with distinguishable key features and they are the "tread", the "sidewalls" and the "beads" as seen in Figure A.0.1:

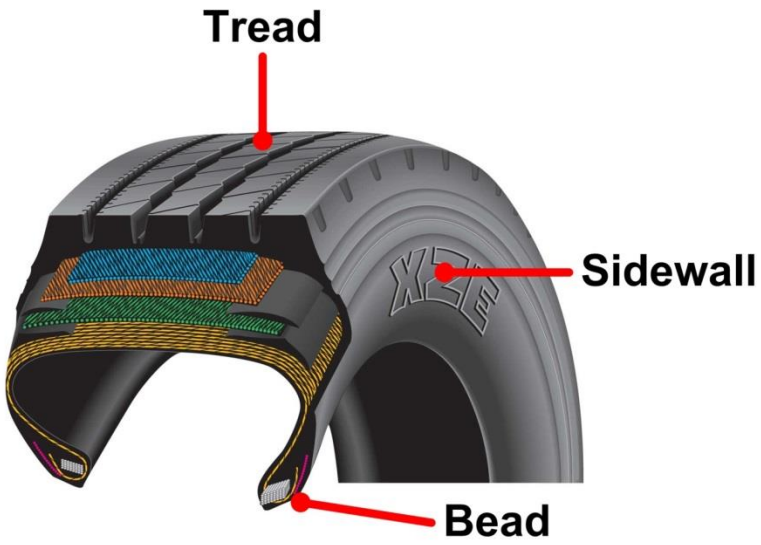


Figure A.0.1 Outer Layout of Today's Vehicle Tyre and its Key Features **[298]**

In Figure A.0.1, the "tread" is the outer interface surface of the tyre (i.e. circumferential crown part) in contact with the road surface. It is made from rubber that is compounded

with other chemicals and reinforcement plies for hardness, strength and durability [152, 299-301]. The surface of the tyre's tread comes with different zigzag-like patterns to provide sufficient road grip for traction, braking and cornering along with expelling water from under the tyre in case of wet road surface [152, 300]. Also, the tyre's tread is expected to offer the minimum rolling-resistance and the optimum handling performance possible for the vehicle [152].

For the "sidewalls", it is the outside lateral walls of the tyre carcass that fall between the tread and the bead as indicated in Figure A.0.1. It is made of rubber compounds and reinforcing fabric plies [152, 299]. Sidewalls are used to support the tread, strengthen the tyre's capacity for carrying loads and guard the tyre's carcass against external damages [152, 301, 302]. This is besides maintaining the shape of the tyre and its air volume when inflated, loaded/unloaded, and subject to road irregularities while being very flexible to cushion the tyre [152, 300, 301].

The "beads" are the tyre's edges that are in contact with the wheel-rim and they come as rubber covered cords of steel wires in the shape of hoops surrounding the rim [300, 301]. This is to fasten and hold the tyre to the rim firmly, seal the air inside the tyre, and support the normal loads on the tyre [152, 299, 301].

Besides the common key features of the tyres' shape, there are common geometrical dimensions for vehicles' tyres. From the most basic and commonly used tyre's dimensions that help in determining the tyre's geometrical specifications and hence

tyre's suitability to a wheel-rim and a vehicle as well, the following basic tyre dimensions that are shown in Figure A.0.2 below [300, 301]:

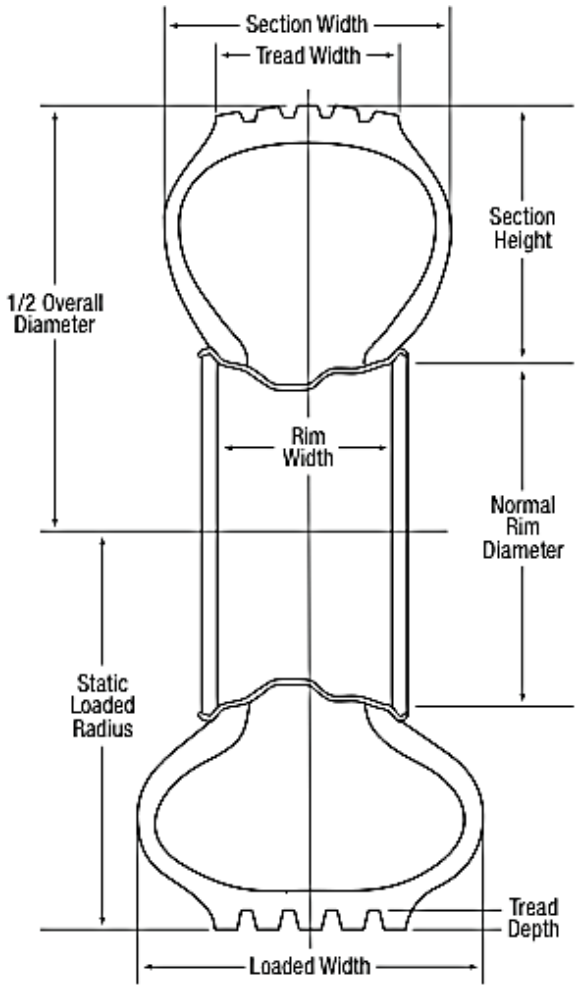


Figure A.0.2 Basic Geometrical Dimensions of Common Vehicle's Tyre [303]

A.2.2 Body Structure

Since the "tubeless radial tyres" are the most common and dominant type to use in the automotive sector around the globe, particularly for passenger vehicles, the detailed construction of the "tubeless radial tyre" will be explored here. In the tubeless radial tyre,

the traditional tyre's tube is compensated by an innermost thin and air-sealed rubber layer called the "inner liner", as indicated in Figure A.0.3 below:

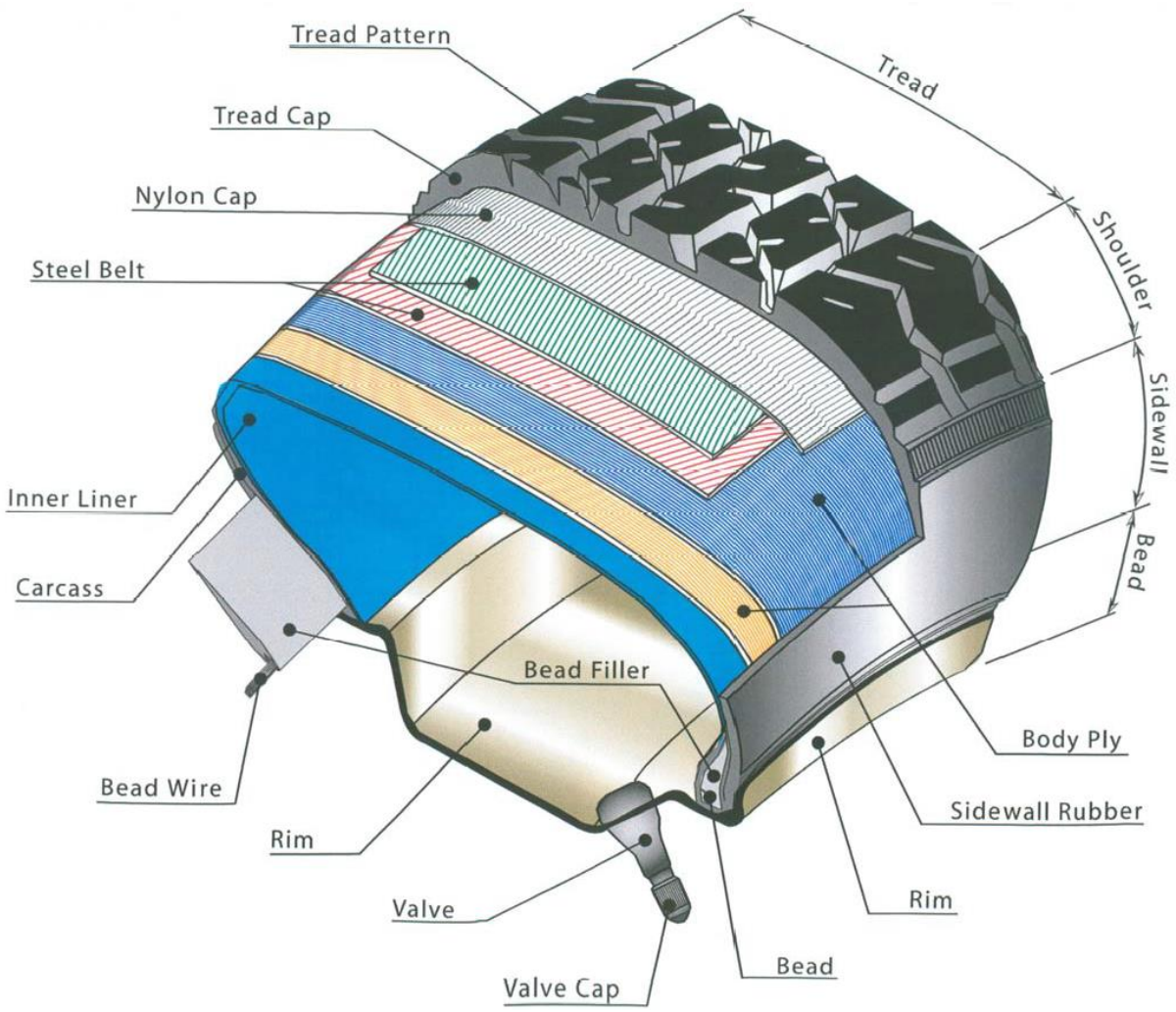


Figure A.0.3 Detailed Radial Tyre Construction [304]

Each of the tread and the sidewall has its own different constructional plies in order to enhance their performance characteristics and enable them to do their functions more efficiently (i.e. More strength and stability to tread and more flexibility to sidewalls). The

body plies are placed radially from one bead to the next on the other side of the tyre at 90 degrees to the tread's centre-line. This is to give the tyre its outline and loading/strength characteristics [152, 299]. From such plies, the body plies for sidewalls are formed.

In the tread section, a number of steel-belt plies are placed diagonally to the tread's centre-line over the radial body plies to strengthen the tread to resist punctures and maintain its flatness for a better road contact. Over the steel-belt layers and under the tread, a layer of fabric cap ply is added circumferentially to stabilise the crown region against the centrifugal forces during high-speed rolling.

A.2.3 Material(s)

The pneumatic tyre has visco-elastic material properties that provide it with resilience, strength, durability, heat/cold resistance, high coefficient of friction, air-seal casing and many other features to handle and withstand normal and extreme driving conditions and still keep its vital properties [269, 304, 305]. Such capabilities are gained by the tyre through the many various ingredients that enter into manufacturing the final tyre material as indicated in Figure A.0.4 below [304]:

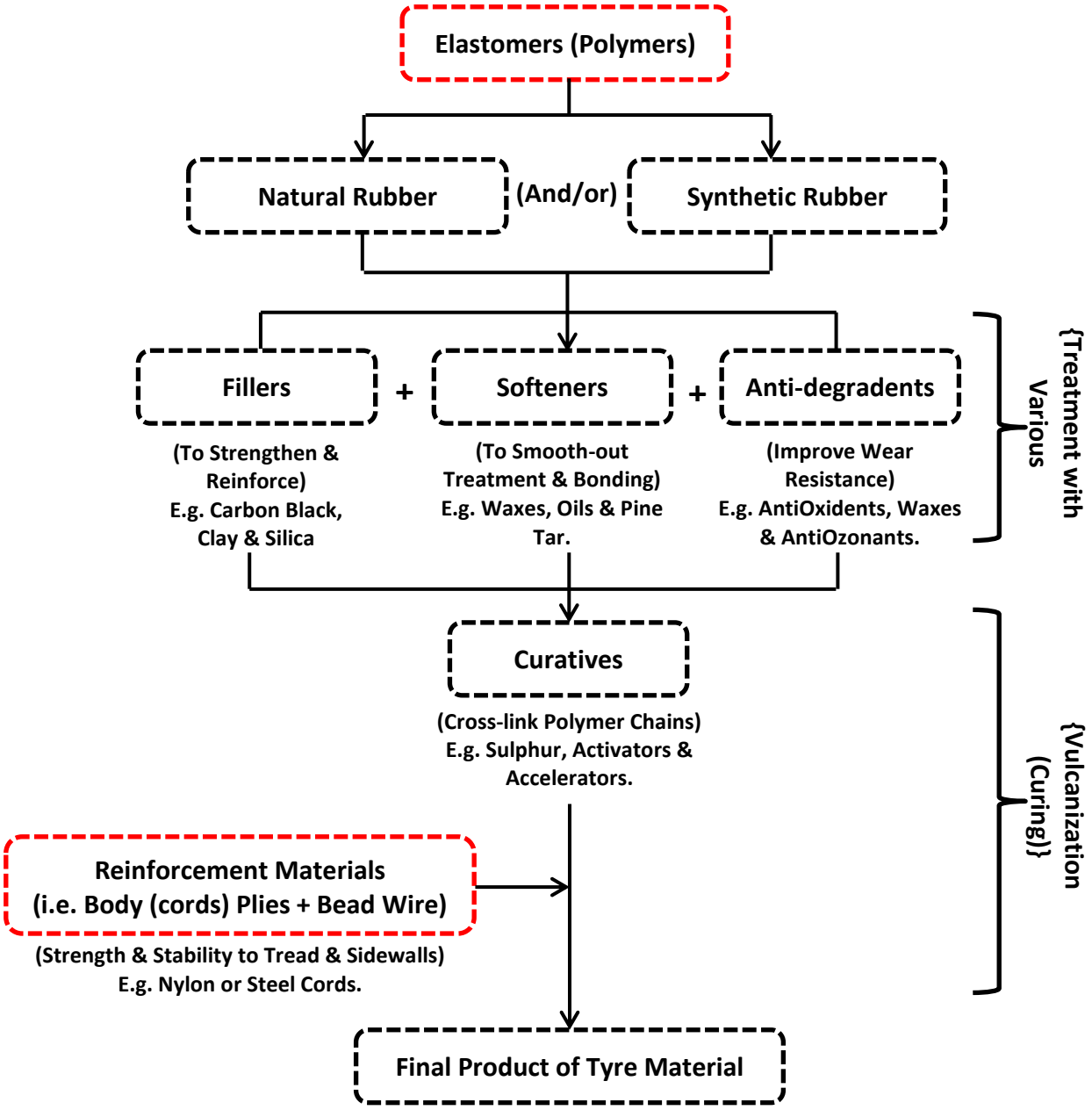


Figure A.0.4 General Ingredients of Final Tyre's Material(s)

As indicated previously, the modern pneumatic tyre has a complex blend of numerous ingredients which according to Lindemuth [28], Gent [305], Smith [25], Miller [302] and Anne and Evans [304] can be classified to the following categories in general:

First of all, the core ingredient that is the basis of the tyre's material is "Polymers". Basically, polymers represent the rubber composites of the tyre, which come either as natural and/or synthetic rubber, that are soft and elastic with good contact-surface grip in nature. However, rubber alone will not be sufficient to handle and withstand the multiple functions required from the tyre in a vehicle. That is why the rubber is to be treated with various chemicals (i.e. "Fillers", "Softeners" and "Anti-degradents") and then heated under a process called "vulcanising or curing" with the aid of "Curatives" to gain the targeted properties/capabilities such as strength and resilience.

Besides the rubber treatment chemicals, there are the "Reinforcement materials" to the tyre structure that are used for strengthening the loading, constancy and sealing properties. Mainly, those reinforcement materials are used in the tyre in the form of "cap ply", "belts", "body plies" and "bead wires". Both cap and body plies can be made from nylon, polyester, rayon, or aramid. The "belts" can be manufactured from steel, aramid or polyester. For the bead wire, it is generally made from carbon steel and coated with bronze.

APPENDIX (B): FE VALIDATION FOR PROTOTYPE 0.5 TYRE

B.1 Prototype 0.5 Tyre (Experimental Prototype)

As further validation of the author's FE modelling approach of multi-chamber tyre solution in comparison to practice, a more complex experimental prototype of the multi-chamber solution was used. This experimental prototype has five inner chambers inside a 205/50 ZR15 tyre as shown in Figure A.0.5. A look inside this experimental prototype was not possible since it is a prototype that belongs to Fusion Innovation and has commercial confidentiality especially to the way to how it is manufactured [186].

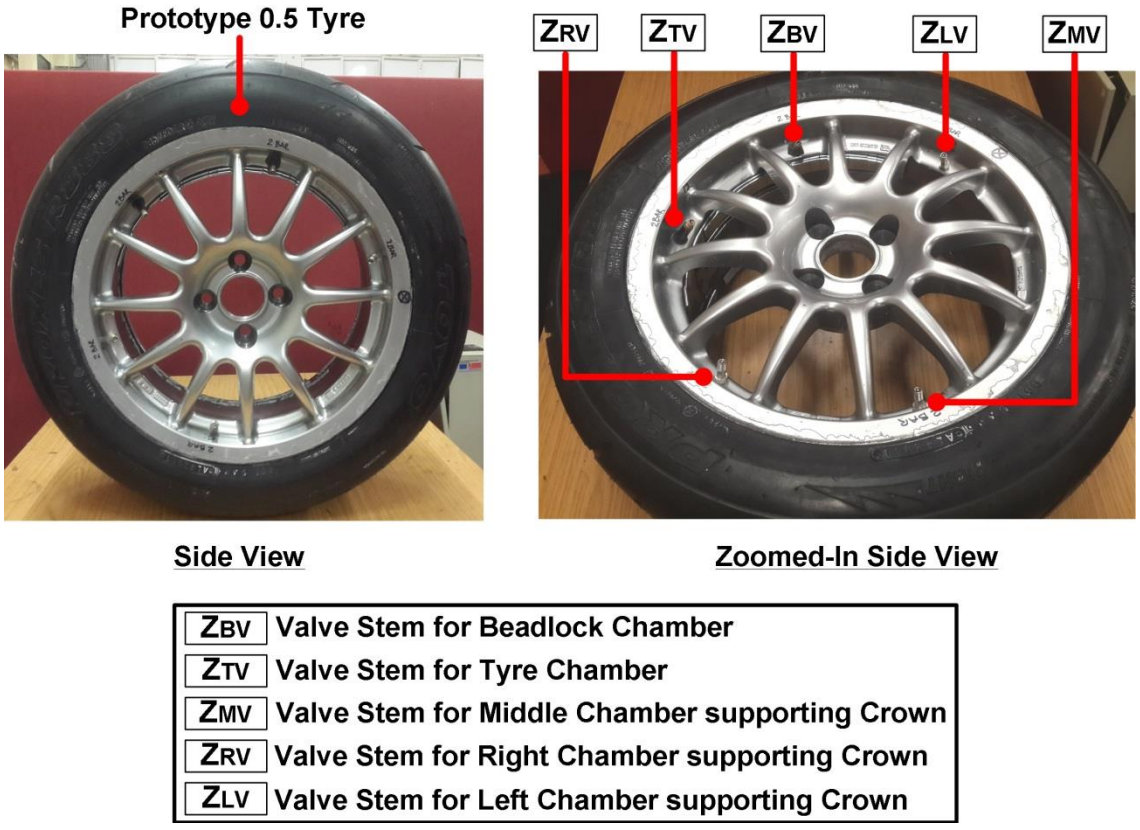


Figure A.0.5 Experimental Prototype 0.5 Tyre

B.2 Material Properties

As an essential part of FE modelling inputs, the relevant material properties were captured for both the rubber and reinforcement components of prototype 0.5 tyre using the same methodology and equipment as in chapter (3). An example of the material testing done is the uniaxial tensile testing for rubber hyperelasticity and viscoelasticity shown in Figure A.0.6. These captured material properties are listed in Table A.0.1, Table A.0.2, Table A.0.3 and Table A.0.4 below.

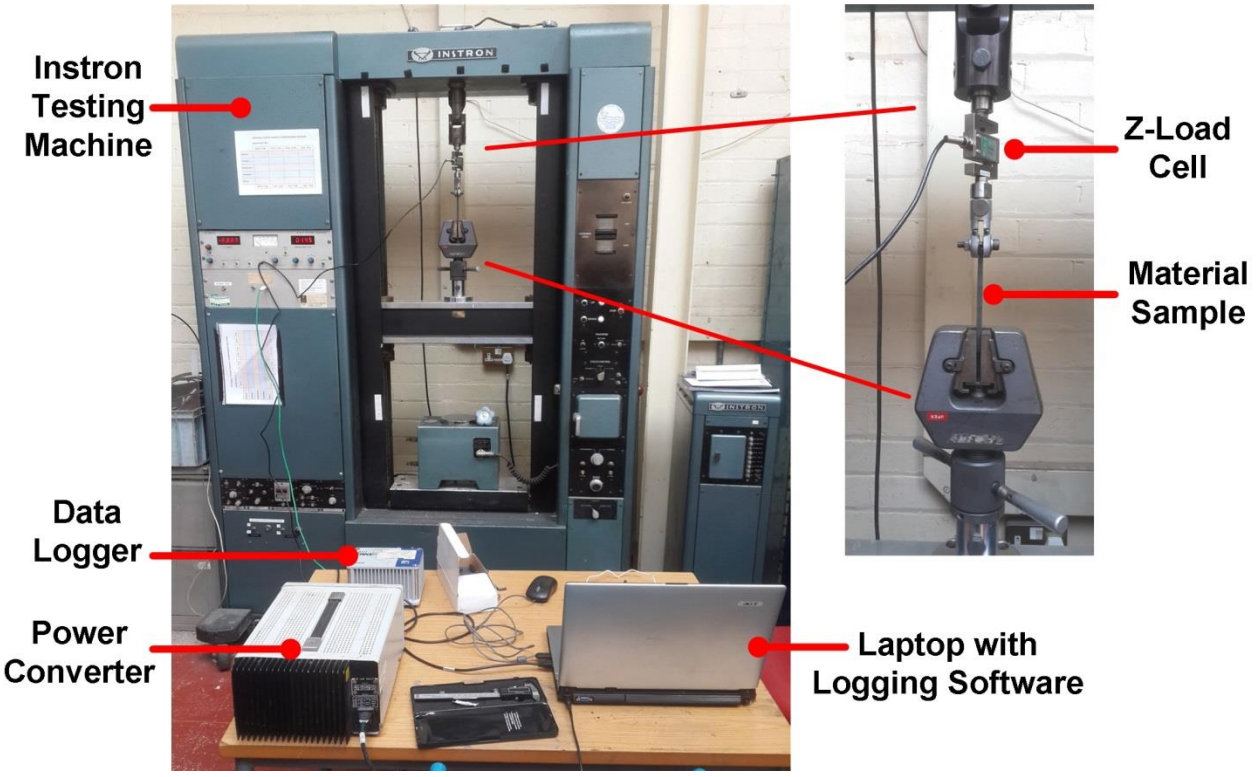


Figure A.0.6 Uniaxial Tensile Test using Instron Machine

Table A.0.1 Material Model Coefficients for Hyperelasticity and Viscoelasticity of Rubber Components

Material Model Parameters		Tyre Rubber Component(s)				
		Tread	**Sidewall**	**Apex**	**Inner Walls**	**Inner Tubes**
Yeoh	**C10**	0.332	0.390	2.281	0.356	0.236
	C20	-0.070	-0.024	-3.763	-0.343	-0.043
	C30	0.0173	0.003	8.353	0.369	0.013
PRF (Power-Law Strain Hardening)	**SR1**	0.150	0.696	0.073	0.070	0.040
	SR2	0.101	0.037	0.072	0	0.088
	SR3	0.040	0.006	0.063	0.246	0.134
	SR4				0.140	0.039
	A1	0.932	0.165	0.638	0.046	26.059
	n1	1.0	2.129	1.287	1	1
	m1	-0.479	-0.889	0.0	-0.087	-0.028
	A2	0.127	0.091	0.050	0.091	0.818
	n2	1.0	1.0	1.001	1.422	1
	m2	-0.325	-0.273	-0.287	-0.396	-0.007
	A3	0.010	0.006	0.005	0.092	0.098
	n3	1.0	1.011	1.111	1.068	1.039
	m3	-0.0315	-0.008	-0.209	-0.095	-0.285
	A4				0.007	0.028
	n4				1	1.039
	m4				-0.151	-0.042

Table A.0.2 Density for Rubber Components

Rubber Parts	**Density (Kg/m^3)**
Tread	1200
Sidewall	
Apex	
Inner Walls	
Inner Tubes	

Table A.0.3 Elastic Properties for Reinforcement Components

Reinforcements	Young's Modulus (MPa)	Poisson's Ratio	Density ($\mathbf{Kg/m^3}$)
Cap Ply	4000	0.3	1300
CarCass	4600	0.3	1500
Steel Belts	200000	0.3	7800
Beads	200000	0.3	7800
Beadlock Chamber Housing	154000	0.35	1470

Table A.0.4 Lay-Up of Reinforcement Components in Tyre Structure

Reinforcements	Area-per-Bar ($\mathbf{mm^2}$)	Spacing ($\mathbf{mm}$)	Orientation Angle (Degree)
Cap Ply	0.1	0.7	90
CarCass	0.1	0.8	0
Steel Belt 1	0.104	0.6	65
Steel Belt 2	0.104	0.6	115
Steel Belt 3	0.104	0.6	115
Beads	0.885	0.05	90

B.3 FE Model

With the material properties obtained in section A.2 incorporated into prototype 0.5 FE model, another essential input to the FE model is the tyre geometry which was acquired applying the image capturing and processing approach in chapter (4) in addition to the relevant information provided by Teqniqa Systems Ltd about the prototype's chamber construction [186]. Based on the captured profile, as in chapter (4), a 2D axisymmetric model was created in Abaqus 6.13-1 from which then a full 3D model of prototype 0.5 tyre with road drum was developed as seen in Figure A.0.7 and Figure A.0.8 below.

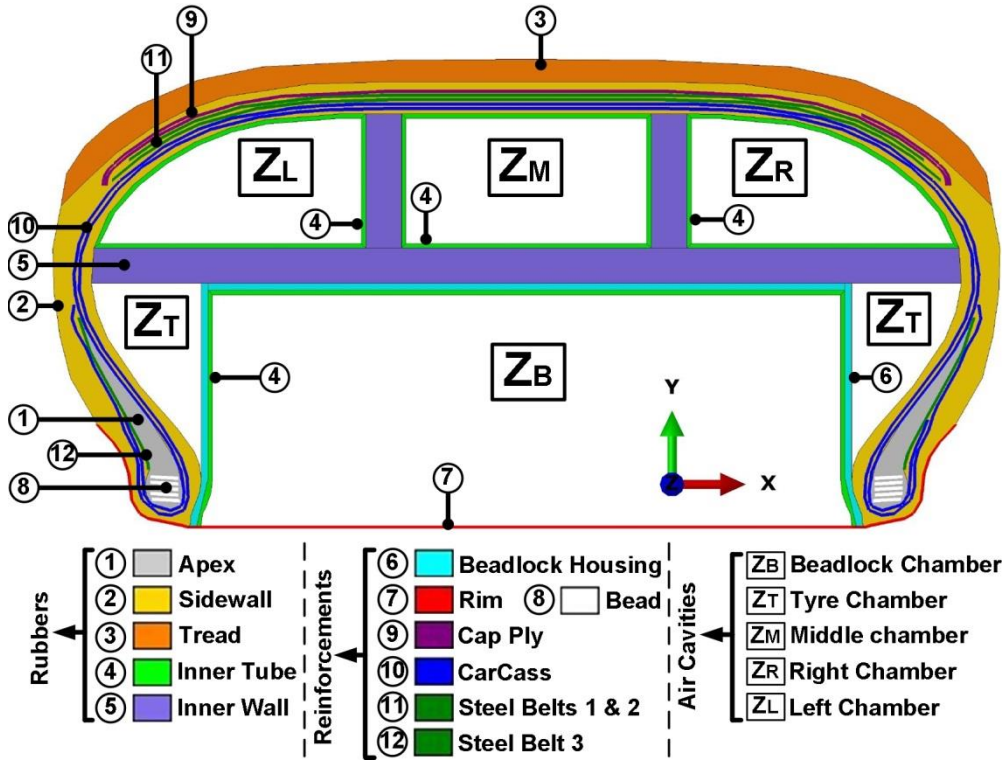


Figure A.0.7 2D Axisymmetric Model of Prototype 0.5

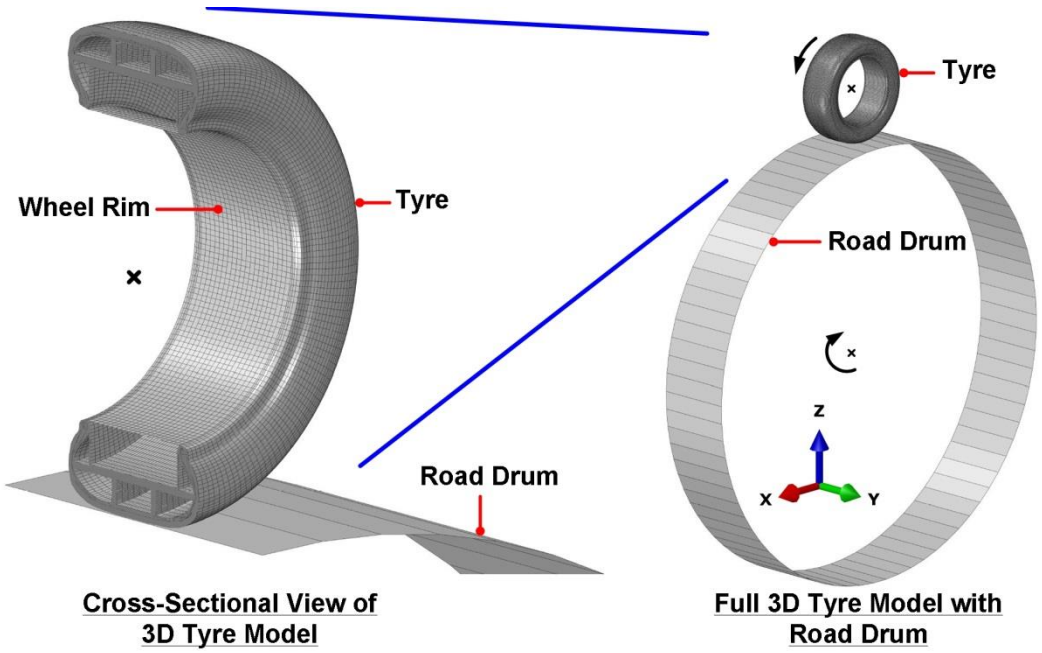


Figure A.0.8 3D Model of Prototype 0.5

B.4 FE Validation

Using the same simulation (analysis) steps in chapter (4), the full 3D model developed in section A.3 was subjected to mesh refinement and energy output validity in which a mesh density of 180 sectors circumferentially was found to yield accurate, consistent and valid solution numerically. To validate the credibility of the FE model to simulate tyre behaviour as that of practice, the same methodology and equipment used in chapter (4) were applied to run both FE model and its experimental counterpart to measure a variety of static and dynamic tyre properties (i.e. geometrical inflation, vertical stiffness, footprint, rolling-resistance, and cornering) respectively. The corresponding experiments were done using the Faro scanner for the inflation validation and the tri-axial elector-hydraulic tyre/drum rig for the static and dynamic contact validations as shown in Figure A.0.9 and Figure A.0.10 respectively.

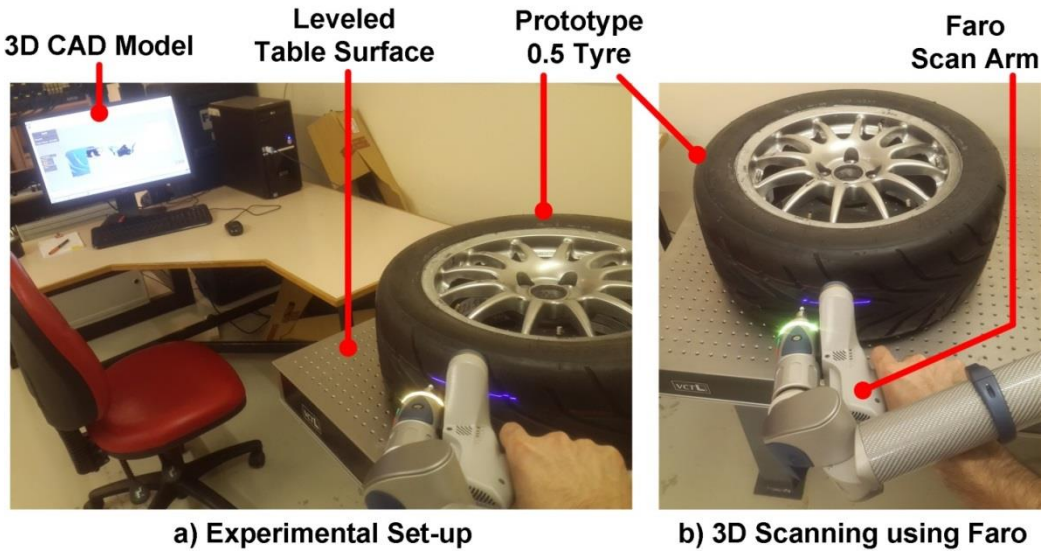


Figure A.0.9 Experimental Set-Up for Inflation Validation of Prototype 0.5

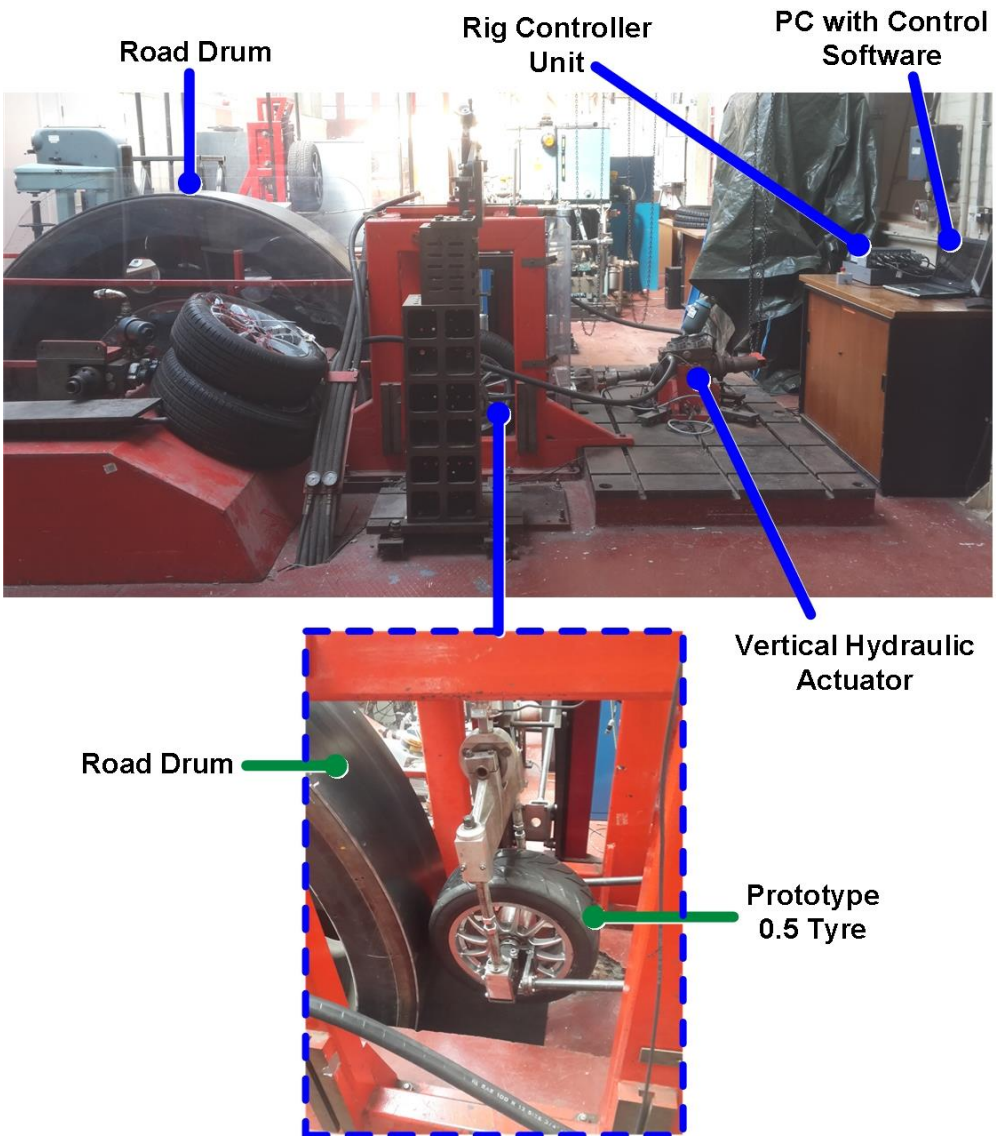


Figure A.0.10 Experimental Set-Up for Static and Dynamic Contact Validation of Prototype 0.5

All the validation tests were conducted at the economy inflation mode of prototype 0.5 tyre shown in Table A.0.5 except for the inflation validation. A good agreement is found between the FE model and its corresponding experiment for different tyre properties as

shown in Figure A.0.11, Figure A.0.12, Figure A.0.13, Figure A.0.14 and Figure A.0.15 respectively indicating the validity and suitability of the FE modelling to predict the multi-chamber tyre solution as in practice.

Table A.0.5 Economy Inflation Mode of Prototype 0.5

Chamber Name	Inflation Pressure (KPa)
Beadlock (ZB)	340
Tyre (ZT)	220
Middle (ZM)	290
Right (ZR)	220
Left (ZL)	220

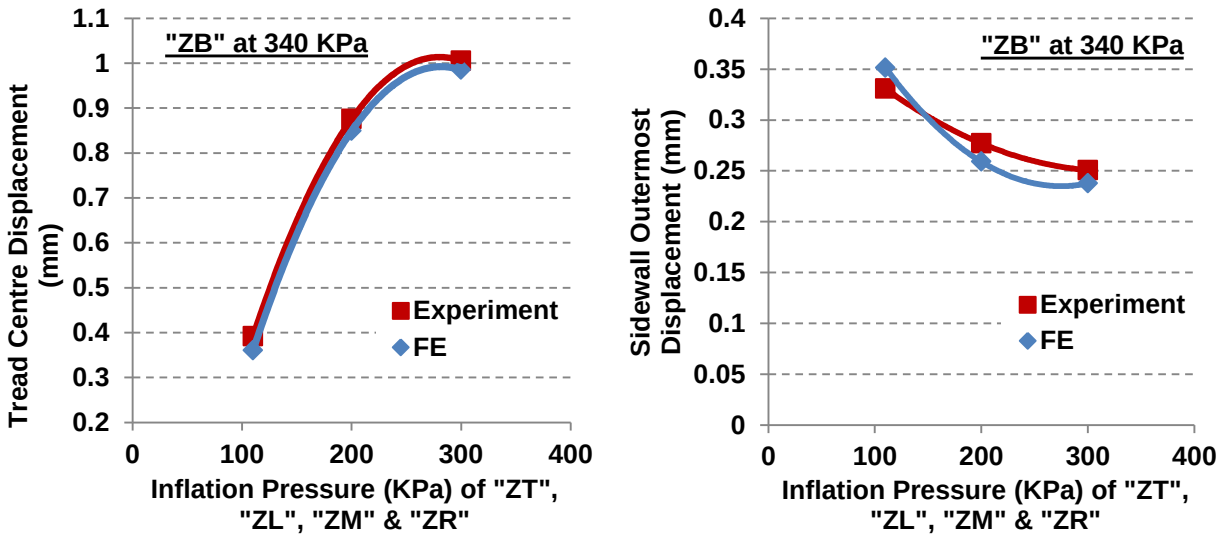


Figure A.0.11 Inflation Validation of Prototype 0.5 at (a) Tread Centre and (b) Sidewall Outermost Point

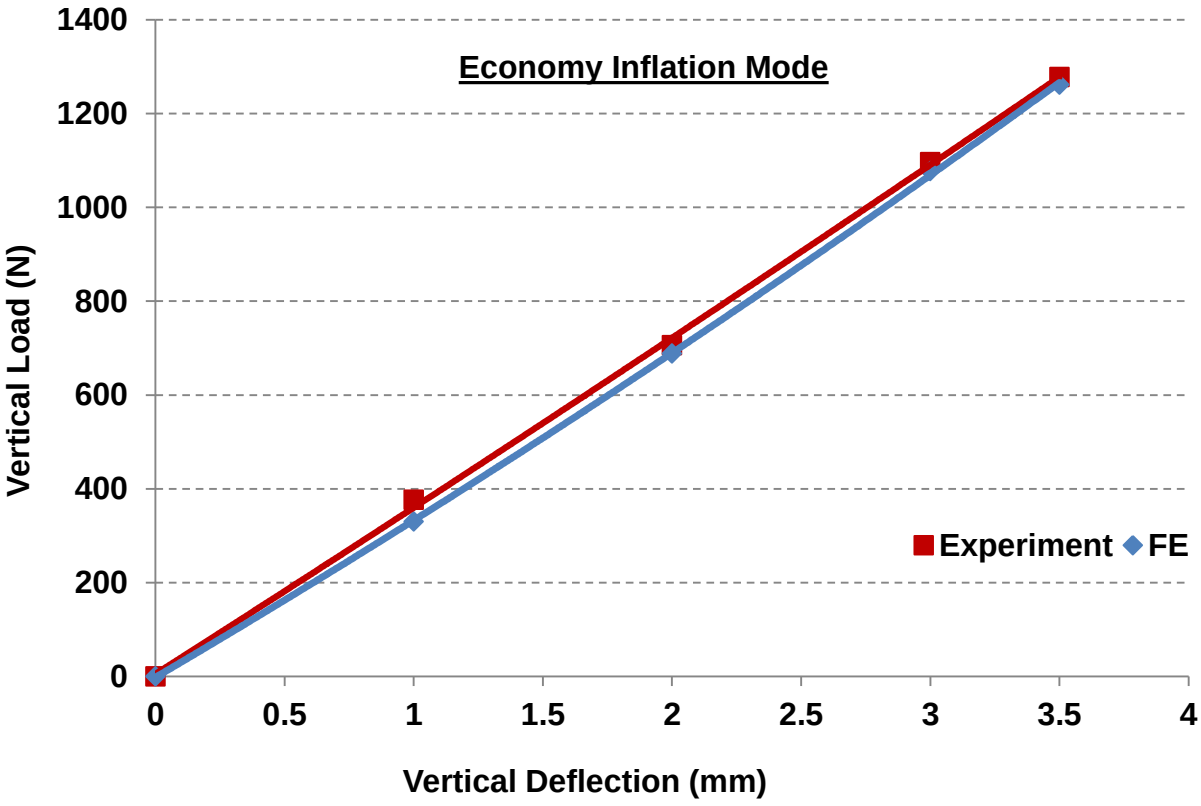


Figure A.0.12 Vertical Stiffness Validation of Prototype 0.5

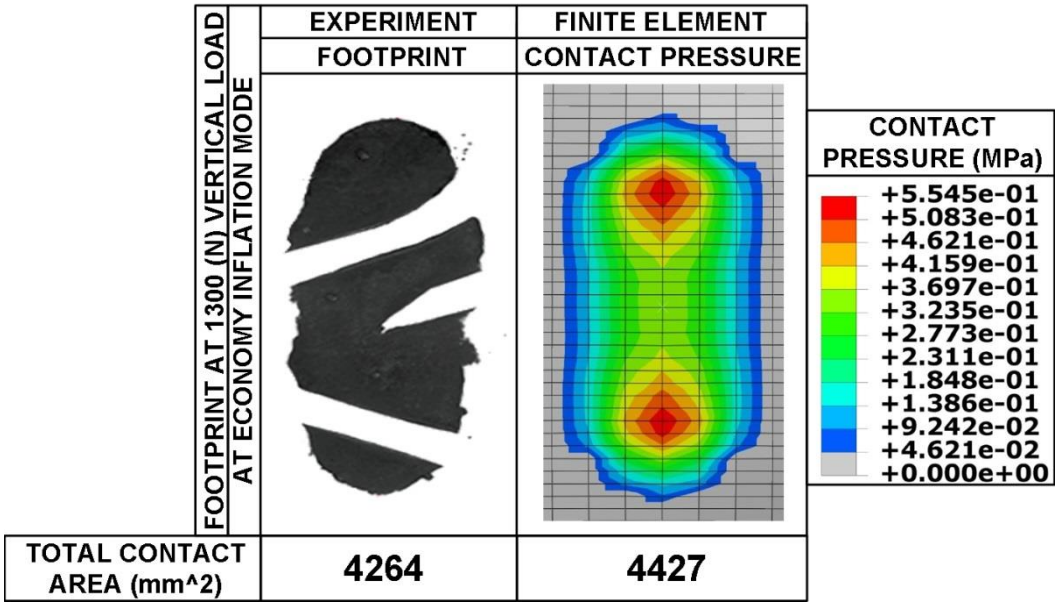


Figure A.0.13 Footprint Validation of Prototype 0.5

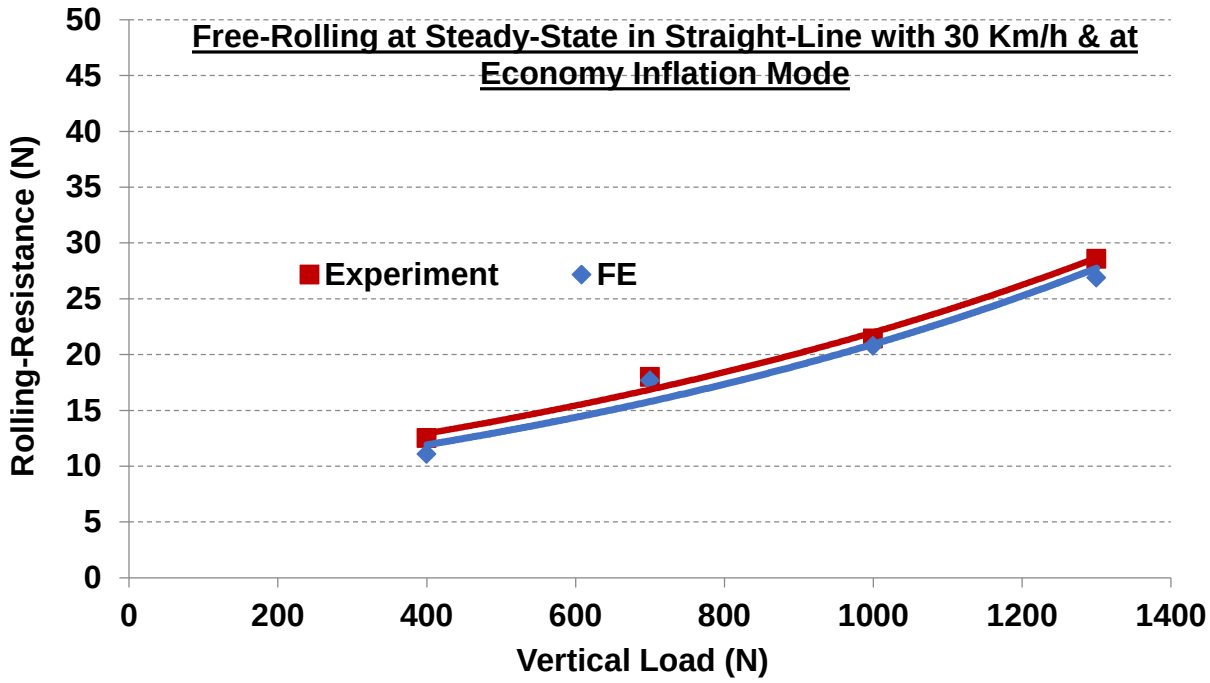


Figure A.0.14 Rolling-Resistance Validation of Prototype 0.5

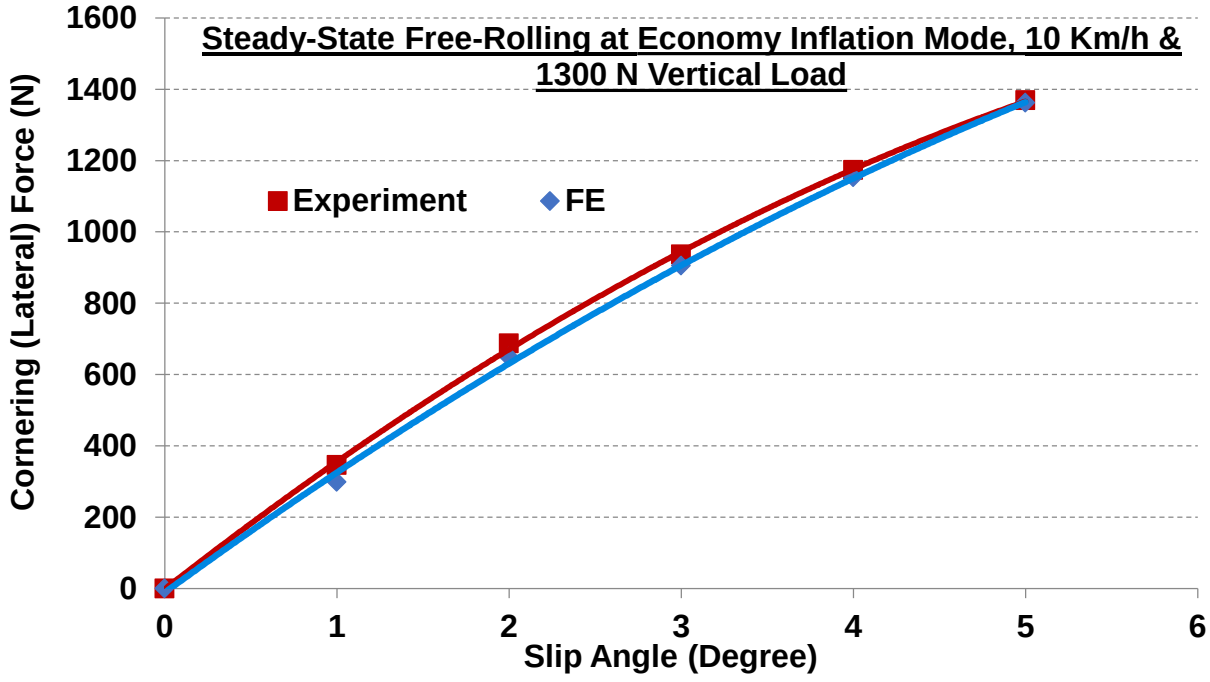


Figure A.0.15 Cornering Validation of Prototype 0.5

APPENDIX (C): WRITTEN PERMISSION FOR PROTOTYPE 0.5 TYRE

FW: FW: Need Written Permission

Oluremi Olatunbosun (Department of Mechanical Engineering)
Sent:16 November 2018 12:20
To: Hamad Aldhufairi (PhD Mechanical Engineering FT)

Dear Hamad,

Please see the email trail below. Greg Hall, the MD of Fusion Innovations Ltd has given permission to use the test data from the ECORR yre prototype 0.5 for validation your tyre models.

Kind regards,
Remi

From: ghall@fusion-innovations.com <ghall@fusion-innovations.com>
Sent: 16 November 2018 09:24
To: Oluremi Olatunbosun (Department of Mechanical Engineering) <O.A.OLATUNBOSUN@bham.ac.uk>
Subject: Re: FW: Need Written Permission

Hi Remi

Sorry for not getting back to you. This is all patented other than my new method using Shape memory polymers so is fine to go ahead and also publish. I hope you are coping okay, as before thoughts are with you.

Kind regards

Greg

Gregory Hall

Managing Director

Fusion Innovations Ltd

Tel 07788 562605
www.fusion-innovations.com

On Thu, 15 Nov 2018 at 22:59, Oluremi Olatunbosun <O.A.OLATUNBOSUN@bham.ac.uk> wrote:

> Hi Greg,
>
> I sent you the Abstract of Hamad's thesis several weeks ago as discussed (see attached). All he needs from you is an email or letter from you giving him permission to use the results of the tests we carried out on the ECORR prototype 0.5 to validate his simulation results. We can place an embargo on public access to the thesis for 3 years if you wish.
>
> It is obviously of great importance that he is able to validate him FE models so this would be of great help to him.
>
> I would appreciate a response from you one way or the other at your earliest convenience.
>
> Kind regards,
> Remi

APPENDIX (D): FULL-FACTORIAL DoE RUNS FOR DIFFERENT VOLUME SETTINGS OF II-1-1B DESIGN

Table A.0.6 Evaluation Results of 25 Different Volume Versions of II-1-1B Design

				Straight Free-Rolling at Normal Inflation Mode		
Run No	Design Version	LW's Height (mm)	LW's Width (mm)	Rolling-Resistance (N) (Energy Lost per Unit Distance)	Contact-Area (mm^2)	Vertical Stiffness (N/mm)
1	II-1-1B-1	245.896	110.000	29.105	15895.551	211.092
2	II-1-1B-2	245.896	120.962	34.585	16122.290	189.220
3	II-1-1B-3	245.896	131.923	32.611	15691.076	200.704
4	II-1-1B-4	245.896	142.885	34.200	15953.663	196.820
5	II-1-1B-5	245.896	153.846	30.972	15761.403	210.761
6	II-1-1B-6	253.521	110.000	31.970	15320.599	196.973
7	II-1-1B-7	253.521	120.962	31.516	16083.130	201.971
8	II-1-1B-8	253.521	131.923	33.106	15867.009	200.648
9	II-1-1B-9	253.521	142.885	33.761	16118.180	197.484
10	II-1-1B-10	253.521	153.846	38.257	15907.767	190.090
11	II-1-1B-11	261.146	110.000	29.258	15775.674	209.586
12	II-1-1B-12	261.146	120.962	30.263	15619.492	218.712
13	II-1-1B-13	261.146	131.923	30.753	15763.458	217.978
14	II-1-1B-14	261.146	142.885	31.373	15952.179	218.902
15	II-1-1B-15	261.146	153.846	32.710	16205.062	213.883
16	II-1-1B-16	269.396	110.000	30.013	15458.286	213.893
17	II-1-1B-17	269.396	120.962	30.772	15935.396	218.548
18	II-1-1B-18	269.396	131.923	31.111	14353.479	218.192
19	II-1-1B-19	269.396	142.885	32.043	16069.886	217.178
20	II-1-1B-20	269.396	153.846	32.376	16324.025	218.483
21	II-1-1B-21	276.396	110.000	30.740	14560.580	215.922
22	II-1-1B-22	276.396	120.962	35.385	14901.145	222.284
23	II-1-1B-23	276.396	131.923	31.432	15160.763	217.531
24	II-1-1B-24	276.396	142.885	33.913	14471.301	219.728
25	II-1-1B-25	276.396	153.846	36.992	16251.072	213.831

APPENDIX (E): FULL-FACTORIAL DoE RUNS FOR DIFFERENT INFLATION SETTINGS OF II-1-1B-20 DESIGN

Table A.0.7 Evaluation Results of Nine Different Inflation Versions of II-1-1B-20 Design

		Inflation (KPa)			Straight Free-Rolling			Cornering	
Run No	II-1-1B-20 Designs	Zone (1)	Zone (2)	Side Zones (R & L)	Rolling-Resistance (N) (Energy Lost per Unit Distance)	Vertical Stiffness (N/mm)	Straight Footprint Area (mm^2)	Cornering Footprint Area (mm^2) at 3° Slip	Cornering Stiffness (N/deg)
1	II-1-1B-20-1	320	200	200	42.987	182.745	16937.795	17944.2	977.028
2	II-1-1B-20-2	320	200	220	38.491	199.087	16749.873	17863.1	967.532
3	II-1-1B-20-3	320	200	240	40.074	214.393	17180.288	17616.8	1059.084
4	II-1-1B-20-4	320	220	200	41.579	219.425	16560.240	17618.5	995.232
5	II-1-1B-20-5	320	220	220	32.376	218.483	16324.025	17619.2	1009.278
6	II-1-1B-20-6	320	220	240	36.263	205.665	15904.342	17402.6	907.724
7	II-1-1B-20-7	320	240	200	35.744	222.100	13774.531	16944.9	903.114
8	II-1-1B-20-8	320	240	220	31.657	222.029	14632.963	17516.9	959.649
9	II-1-1B-20-9	320	240	240	29.542	225.620	14403.599	17527.3	966.906

LIST OF REFERENCES

1. Andrzejewski R, Awrejcewicz J. Nonlinear dynamics of a wheeled vehicle: Springer Science & Business Media; 2006.

2. IMARC. Tire Market: Global Industry Trends, Share, Size, Growth, Opportunity and Forecast 2018-2023. USA.2018.

3. Staff TB. Global tire demand to rise 4% annually — Freedonia [Internet]. 2015 [cited 2015 23 December]. Available from: https://www.tirebusiness.com/article/20151223/NEWS/151229969/global-tire-demand-to-rise-4-annually-freedonia.

4. Świeczko-Żurek B, Ejsmont J, Ronowski G. Reduction of Tire Rolling Resistance by Optimization of Road Surfaces and Tires. Troisième Congrès Tunisien de Mécanique. 2014.

5. Yang X. Finite element analysis and experimental investigation of tyre characteristics for developing strain-based intelligent tyre system [PhD Thesis]. Birmingham, UK: University of Birmingham; 2011.

6. Beken S. From an ancient Mayan ball game to rocket fuel: the limitless application of rubber [Internet]. 2016 [cited 2016 08 November]. Available from: https://ktn-uk.co.uk/perspectives/the-limitless-application-of-rubber.

7. Wei C. A finite element based approach to characterising flexible ring tire (FTire) model for extended range of operating conditions [PhD Thesis]. Birmingham, UK: University of Birmingham; 2015.

8. Aldhufairi HS, Olatunbosun OA. Developments in tyre design for lower rolling resistance: a state of the art review. Proceedings of the Institution of Mechanical Engineers, Part D: Journal of Automobile Engineering. 2018;232(14):1865–82. doi: https://doi.org/10.1177/0954407017727195

9. Pillai PS. Effect of tyre overload and inflation pressure on rolling loss (resistance) and fuel consumption of automobile and truck/bus tyres. Indian Journal of Engineering & Materials Sciences. 2004;11:406-12.

10. LaClair T. The pneumatic tire: Rolling resistance. NHTSA Report. Washington DC: US department of Transportation: National Highway Traffic Safety Administration.2006.

11. Mavros G. Tyre models for vehicle handling analysis under steady-state and transient manoeuvres [PhD Thesis]. UK: Loughborough University; 2005.

12. Hall DE, Moreland JC. Fundamentals of Rolling Resistance. Rubber Chemistry and Technology. 2001;74(3):525-39. doi: 10.5254/1.3547650

13. Khanger R, Bardhan A. Challenges in developing low rolling resistance tyre. SAE Technical Paper.2015. Report No.: 0148-7191.

14. Stein D, Bernard J, Eagleburger J. Tires and passenger vehicle fuel economy: informing consumers, improving performance. Washington, DC.2006. Report No.: 286-78.

15. Juhala M. 14 - Improving vehicle rolling resistance and aerodynamics A2 - Folkson, Richard. Alternative Fuels and Advanced Vehicle Technologies for Improved Environmental Performance: Woodhead Publishing; 2014. p. 462-75.

16. Agency IE. IEA Work for the G8: 2008 Messages. Hokkaido, Japan.2008.

17. Jae E. Data directory: future market insights on specialty silicas. Tire Technology International. 2015;11:70-1.

18. Shaw D. Interview: New force rising: Hee-Jong Lee, Nexen: The tech center chief on Nexen's European expansion. Tire Technology International 2015;11:30-4.

19. Heeps G. Expo interview: Dufournier: A new tire labeling and R&D test facility. Tire Technology International. 2015;11:36-8.

20. Michelin. The Tyre: Rolling Resistance and Fuel Savings. Clermont–Ferrand, France: Société de Technologie; 2003.

21. Katz J. Automotive aerodynamics. Wast Sussex, United Kingdom: John Wiley & Sons; 2016.

22. Andersen LG, Larsen JK, Fraser ES, Schmidt B, Dyre JC. Rolling resistance measurement and model development. Journal of Transportation Engineering. 2014;141(2):04014075.

23. Bosch R. Automotive Handbook. 4 ed. Stuttgart, Germany: Bentley Publishers; 1996.

24. Walter J. Fuel economy and effective mass: The tire's place in fuel economy. Tire Technology International. 2016;3:16.

25. Smith ND. Understanding parameters influencing tire modeling. Department of Mechanical Engineering, Colorado State University. 2004.

26. Savage AJ, inventor; Savage Tire Company, assignee. Vehicle-tire. Washington, DC patent 1203910. 1916.

27. Mullineux N. Light vehicle tyres. Shrewsbury, UK: iSmithers Rapra Publishing; 2004.

28. Lindemuth B. Chapter 1: An overview of tire technology. The pneumatic tire. Washington DC: National Highway Traffic Safety Administration, US department of Transportation; 2006. p. 1-27.

29. Aldhufairi HS, Essa K. Tire Rolling-Resistance Computation based on Material Viscoelasticity Representation. Advances in Automotive Engineering. 2019;1(2):167-83. doi: https://doi.org/10.12989/aae.2019.1.2.167

30. Aldhufairi HS, Essa K, Olatunbosun OA. Multi-chamber Tire Concept for Low Rolling-Resistance. SAE International Journal of Passenger Cars - Mechanical Systems. 2019;12(2):111-26. doi: https://doi.org/10.4271/06-12-02-0009

31. ISO. ISO 4223-1:2017. Definitions of some terms used in the tyre industry — Part 1: Pneumatic tyres. Switzerland: International Organization for Standardization; 2017.

32. Wong JY. Theory of ground vehicles. Canada: John Wiley & Sons; 2008.

33. Blundell M, Harty D. Multibody systems approach to vehicle dynamics. Oxford: Elsevier; 2004.

34. Jazar RN. Chapter 2 Vibration Dynamics. Advanced Vibrations: A Modern Approach. UK: Springer; 2013.

35. Erdogan G. Tire Modeling: Lateral and longitudinal tire forces. Tire Modeling lecture. Minnesota, US: University of Minnesota - Department of Mechanical Engineering; 2009.

36. Gillespie TD. Fundamentals of vehicle dynamics. US: SAE International; 1992.

37. Pacejka Hans B. Tire and vehicle dynamics. Warrendale: SAE. 2006.

38. Guiggiani M. Chapter 2: Mechanics of the Wheel with Tire. The Science of Vehicle Dynamics: Handling, Braking, and Ride of Road and Race Cars. 1 ed. Netherlands: Springer 2014.

39. Pottinger MG. Chapter 8: Forces and Moments. The pneumatic tire. Washington DC: National Highway Traffic Safety Administration, US department of Transportation; 2006. p. 286-363.

40. Nandi B, Dalrymple T, Yao J, Lapczyk I, editors. Importance of capturing non-linear viscoelastic material behavior in tire rolling simulations. Presented at the Meeting of the Tire Society; 2014 8-10 September 2014; USA.

41. Jana KK, Patel M, Rana D, Maiti P. Nonlinear viscoelasticity of one dimensional filler reinforced elastomer composites. Non-Linear Viscoelasticity of Rubber Composites and Nanocomposites. Switzerland: Springer; 2014. p. 15-41.

42. Marković G, Marinović-Cincović M, Jovanović V, Samaržija-Jovanović S, Budinski-Simendić J. Modeling of Non-Linear Viscoelastic Behavior of Filled Rubbers. Non-Linear Viscoelasticity of Rubber Composites and Nanocomposites. Switzerland: Springer; 2014. p. 193-271.

43. Hodge KF. Field and experimental constraints on the deformation and breakup of injected magma [PhD Thesis]. Canada: University of British Columbia; 2012.

44. Moore DF. The Friction of Pneumatic Tyres. Amsterdam: Elsevier Scientific Publishing Company; 1975.

45. Council NR. Assessment of fuel economy technologies for light-duty vehicles. Washington, DC: National Academies Press; 2011.

46. Gough V. Tyre-to-ground contact stresses. Wear. 1958;2(2):107-26.

47. Crum W. Road and dynamometer tire power dissipation. SAE Technical Paper.1975. Report No.: 0148-7191.

48. Schuring D, editor A new look at the definition of tire rolling loss. Tire Rolling Losses and Fuel Economy—An R&D Planning Workshop; 1977; Warrendale, Pennsylvania1977.

49. Segel L, Lu X. Vehicular resistance to motion as influenced by road roughness and highway alignment. Australian Road Research. 1982;12(4):211-22.

50. Sandberg U. Rolling resistance–basic information and state-of-the-art on measurement methods. Linköping, Sweden: Swedish National Road and Transport Research Institute.2011.

51. Clark SK, Dodge RN. A handbook for the rolling resistance of pneumatic tires. Michigan: Industrial Development Division: Institute of Science and Technology, The University of Michigan; 1979.

52. Clark S, editor A Brief-History of Tire Rolling Resistance. Rubber Chemistry And Technology; 1983: AMER Chemical Soc Inc Rubber Div Univ Akron PO BOX 499, Akron, OH 44309-0499.

53. Vorachek J, Dill R, Montag R, editors. Effect of passenger tire reinforcing materials on rolling resistance. Society of Automotive Engineers Conference Proceedings, Tire rolling losses and fuel economy, P-74; 1977; Cambridge, MA: Michigan: Society of Automotive Engineers.

54. Hoever C. The simulation of car and truck tyre vibrations, rolling resistance and rolling noise [PhD Thesis]. Göteborg, Sweden: Chalmers University of Technology; 2014.

55. Ridha R, Clark S. Tire stress and deformation. Mechanics of Pneumatic Tires. Washington, DC: US Goverment Printing Office; 1981. p. 475-540.

56. Li Z, Li ZR, Xia YM. An implicit to explicit FEA solving of tire F&M with detailed tread blocks. Tire Science and Technology. 2012;40(2):83-107.

57. Stutts D, Soedel W. A simplified dynamic model of the effect of internal damping on the rolling resistance in pneumatic tires. Journal of Sound and Vibration. 1992;155(1):153-64.

58. Kim S-J, Savkoor AR. The contact problem of in-plane rolling of tires on a flat road. Vehicle System Dynamics. 1997;27(S1):189-206.

59. Miège A, Popov A. Truck tyre modelling for rolling resistance calculations under a dynamic vertical load. Proceedings of the Institution of Mechanical Engineers, Part D: Journal of Automobile Engineering. 2005;219(4):441-56.

60. Li B, Zhao Y, Zang L, Wang J, Zhang M. Analytical model of tire rolling resistance based on elastic hysteresis theory. Transactions of the Chinese Society of Agricultural Engineering. 2014;30(17):56-62.

61. Smith G. Better rolling resistance measurement. Tire Technology International. 2015;11:120.

62. Singh D, Hu C, Valentin J, Liu ZL, editors. Geo-China 2016: Innovative and Sustainable Solutions in Asphalt Pavements. The Fourth Geo-China International Conference; 2016; Shandong, China: ASCE.

63. Ejsmont J, Taryma S, Ronowski G, Swieczko-Zurek B. Influence of load and inflation pressure on the tyre rolling resistance. International journal of automotive technology. 2016;17(2):237-44.

64. Hernandez JA, Al-Qadi IL, Ozer H. Baseline rolling resistance for tires' on-road fuel efficiency using finite element modeling. International Journal of Pavement Engineering. 2017;18(5):424-32.

65. Ghosh S. Investigation on role of fillers on viscoelastic properties of tire tread compounds [PhD Thesis]. India: Maharaja Sayajirao University of Baroda; 2011.

66. Ghoreishy MHR. A state of the art review of the finite element modelling of rolling tyres. Iranian Polymer Journal. 2008;17(8):571-97.

67. Wei C, Olatunbosun OA, Behroozi M. Simulation of tyre rolling resistance generated on uneven road. International journal of vehicle design. 2016;70(2):113-36.

68. Wei Y-T, Tian Z-H, Du X. A finite element model for the rolling loss prediction and fracture analysis of radial tires. Tire science and technology. 1999;27(4):250-76.

69. Luchini J, Peters J, Arthur R. Tire rolling loss computation with the finite element method. Tire Science and Technology. 1994;22(4):206-22.

70. Ebbott T, Hohman R, Jeusette J-P, Kerchman V. Tire temperature and rolling resistance prediction with finite element analysis. Tire Science and Technology. 1999;27(1):2-21.

71. Cho J, Lee H, Jeong W, Jeong K, Kim K. Numerical estimation of rolling resistance and temperature distribution of 3-D periodic patterned tire. International Journal of Solids and Structures. 2013;50(1):86-96.

72. Shida Z, Koishi M, Kogure T, Kabe K. A rolling resistance simulation of tires using static finite element analysis. Tire science and technology. 1999;27(2):84-105.

73. Ma G-l, Xu H, Cui W-y. Computation of rolling resistance caused by rubber hysteresis of truck radial tire. Journal of Zhejiang University-SCIENCE A. 2007;8(5):778-85.

74. Golbakhshi H, Namjoo M. An Efficient Numerical Scheme for Evaluating the Rolling Resistance of a Pneumatic Tire. International Journal of Automotive Engineering. 2015;5(2).

75. Ghosh P, Saha A, Mukhopadhyay R, editors. Prediction of tyre rolling resistance using FEA. Proceedings of the Third European conference on Constitutive Models for Rubber; 2003 Sep 15-17; London, UK. Netherlands: A.A. Balkema Publishers.

76. Pillai P, Fielding-Russell G. Tire rolling resistance from whole-tire hysteresis ratio. Rubber chemistry and technology. 1992;65(2):444-52.

77. Kim T-W, Kim H-H, Jeong H-Y, Park H-C, Kim Y-H, Choe J-H. Determination of Prony Series Parameters and Rolling Resistance Simulation of a Tire. In: Yao Z, Yuan M, Zhong W, editors. Sixth World Congress on Computational Mechanics in conjunction with the Second Asian-Pacific Congress on Computational Mechanics; Beijing, China. Beijing: Tsinghua University Press & Springer; 2004.

78. Schuring D. The rolling loss of pneumatic tires. Rubber Chemistry and Technology. 1980;53(3):600-727.

79. Rafei M, Ghoreishy MHR, Naderi G. Computer simulation of tire rolling resistance using finite element method: Effect of linear and nonlinear viscoelastic models. Proceedings of the Institution of Mechanical Engineers, Part D: Journal of Automobile Engineering. 2018. doi: https://doi.org/10.1177/0954407018804117

80. Nyaaba W, Frimpong S, Somua-Gyimah G, Galecki G. FEA Prediction of Off-Road Tire Temperature Distribution. Science in the Age of Experience; Boston, MA: Dassault Systèmes 2016.

81. Schuring D, Futamura S. Rolling loss of pneumatic highway tires in the eighties. Rubber Chemistry and Technology. 1990;63(3):315-67. doi: http://dx.doi.org/10.5254/1.3538261

82. Hunt J, Walter J, Hall G, editors. The effect of tread polymer variations on radial tire rolling resistance. Tire Rolling Losses and Fuel Economy—An R&D Planning Workshop; 1977 18-20 October; Cambridge (MA): Society of Automotive Engineers.

83. Clark J, Schuring D. Load, speed and inflation pressure effects on rolling loss distribution in automobile tires. Tire Science and Technology. 1988;16(2):78-95.

84. Srirangam SK, Anupam K, Kasbergen C, Scarpas A, Cerezo V. Study of influence of operating parameters on braking friction and rolling resistance. Transportation Research Record: Journal of the Transportation Research Board. 2015(2525):79-90. doi: 10.3141/2525-09

85. Thieme HvE, Dijks A, Bobo S. Measurement of tire properties. In: SK C, editor. Mechanics of Pneumatic Tires. 8. Washington D.C.: Department of Transportation; 1981. p. 541-720.

86. Potter T. Dynamics and stability of rolling viscoelastic tires [PhD Thesis]. Berkeley: University of California 2013.

87. Norbye JP, Dunne J, Oertle VL. Tires for Your Car. Popular Science. 1968:134-48.

88. Prevorsek D, Beringer C, Kwon Y. Design of Tire Cords-Optimization of Viscoelastic Properties. Polymers for Fibers and Elastomers. 24. Washington, DC: American Chemical Society; 1984. p. 371-95.

89. Kwon Y, Prevorsek D. Formation of standing waves in radial tires. Tire Science and Technology. 1984;12(1):44-63. doi: https://doi.org/10.2346/1.2150982

90. Taborek JJ. Mechanics of Vehicles. Cleveland (Ohio): Penton Publishing Co; 1957.

91. Jonsson P. Effect of tire pressure on fuel consumption-methodology and results. VTI Rapport. 2007(564).

92. Obringer LA. How Self-inflating Tires Work [Internet]. 2004 [cited 2017 23 March]. Available from: http://auto.howstuffworks.com/self-inflating-tire.htm.

93. Ajas M, Aiswarya T, Adersh V. Tire pressure monitoring and automatic air filling system. IJREAT: International Journal of Research in Engineering & Advanced Technology. 2014;2(02):1-6.

94. Klingemann. Self-Inflating Tires…Soon To Be A Reality? [Internet]. 2016 [cited 2017 23 March]. Available from: http://klingemanncarcare.com/blog/view/self-inflating-tires-soon-to-be-a-reality.

95. Vishnuram K, Dinesh R, Krishna N. Self inflating tyres. International Journal on Applications in Mechanical and Production Engineering. 2015;1(5):5-6.

96. Harley M. Self-inflating tire technology captures innovation award [Internet]. 2009 [cited 2017 23 March]. Available from: http://www.autoblog.com/2009/02/23/self-inflating-tire-technology-captures-innovation-award/.

97. Skydel S. Tire Pressure monitoring & automatic inflation systems. Fleet Equipment. 2011;37:32-6.

98. Quick D. Goodyear's self-inflating tire tech for commercial vehicles leaves the lab [Internet]. 2012 [cited 2017 23 March]. Available from: http://newatlas.com/goodyear-air-maintenance-technology-tires/24229/.

99. Peckham M. Self-Inflating Tires Have Been Around for Awhile [Internet]. 2014 [cited 2017 22 March]. Available from: http://time.com/13022/self-inflating-tires-have-been-around-for-awhile/.

100. GoodYear. Debut of Goodyear Self-Inflating Technology for Commercial Tires at the Internationale Automobil-Ausstellung (IAA) Commercial Vehicle Show [Internet]. 2012 [cited 2017 22 March]. Available from: https://corporate.goodyear.com/en-US/media/news/Debut-of-Goodyear-Self-Inflating-Technology-for-Commercial-Tires-at-the-International-Automobil-Ausstellung--IAA--Commercial-Vehicle-Show-1426100350223.html.

101. Ashley S. Rolling tires power self-inflation pumps. SAE International. 2012.

102. Woollaston V. End of the flat tire? Goodyear develops self-inflating wheels that constantly maintain the perfect air pressure [Internet]. 2014 [cited 2017 22 March]. Available from: http://www.dailymail.co.uk/sciencetech/article-2860406/End-flat-tyre-

Goodyear-develops-self-inflating-wheels-constantly-maintain-perfect-air-pressure.html#ixzz4cxK5sX4D.

103. Bureau PN. Self Inflating Tyres. Polymers & Tyre Asia. 2012:64-5.

104. Klamp W, editor Power consumption of tires related to how they are used. "Conference Proceedings of Tire Rolling Losses and Fuel Economy-An R & D Planning Workshop" 1977 18-20 October Cambridge (MA): Society of Automotive Engineers.

105. Campbell K, editor A Comparison of Radial And Non-Radial Tire Construc-tion With Respect to Rolling Resistance And Vehicle Fuel Economy. Tire Rolling Losses and Fuel Economy – An R&D Workshop; 1977 18-20 October; Cambridge (MA): Society of Automotive Engineers.

106. Pauwelussen JP. Essentials of Vehicle Dynamics: Elsevier Ltd.; 2015.

107. Thompson G, Myriam T, editors. Variations in Tire Rolling Resistance Tire Rolling Losses and Fuel Economy – An R&D Workshop; 1977 18-20 October; Cambridge (MA): Society of Automotive Engineers.

108. Yurjevich MA. The effect of stabilizer ply geometry on rolling resistance and cornering force properties. SAE Transactions. 1981:236-50. doi: 10.4271/810065

109. Walter SL. The effects of five basic design and construction parameters on radial tire rolling resistance and cornering force. SAE Transactions. 1983:579-91. doi: 10.4271/830160

110. Keefe R, Koralek A, editors. Precision measurement of tire rolling resistance. Rubber division symposia; 1983; Akron: American Chemical Society, Rubber Div. Akron, OH.

111. Williams AR, editor The influence of tyre and road surface design on tyre rolling resistance. Technical papers 1981 Proceedings of IP/DGMK Joint Meeting; 1981 27-29 May; London: Institute of Petroleum.

112. Gerresheim M, editor Dependence of Vehicle Fuel Consumption on the Tyre-Wheel Assembly. Proceedings of the Conference Automobile Wheels and Tyres; 1983 18-19 October; Penns Hall Hotel, Sutton Coldfield, England: Mechanical Engineering Publications Limited.

113. Knight R. Correlation of truck tire rolling resistance as derived from fuel economy and laboratory tests. USA: Society of Automotive Engineers.1982. Report No.: 0148-7191.

114. Sandstrom PH, Goldstein AA, Darab JM, Oblizajek KL, Rodgers WR, Ryba JL, et al., inventors; Goodyear Tire and Rubber Co GM Global Technology Operations LLC, assignee. Stiffness enhanced tread patent US20160001605A1. 2016.

115. Rhyne TB, Cron SM. Development of a non-pneumatic wheel. Tire Science and Technology. 2006;34(3):150-69.

116. Aboul-Yazid A, Emam M, Shaaban S, El-Nashar M. Effect of Spokes Structures on Characteristics Performance of Non-Pneumatic Tires. International Journal of Automotive & Mechanical Engineering. 2015;11:2212-23. doi: http://dx.doi.org/10.15282/ijame.11.2015.4.0185

117. Kubba AIS. Intelligent tyre technologies [PhD Thesis]. Birmingham, UK: University of Birmingham; 2018.

118. Veeramurthy M, Ju J, Thompson LL, Summers JD. Optimisation of geometry and material properties of a non-pneumatic tyre for reducing rolling resistance. International Journal of Vehicle Design. 2014;66(2):193-216.

119. Bridgestone. Bridgestone Corporation Reveals Second Generation "Air Free Concept (Non-Pneumatic) Tire": Targeting Future Practical Viability by Bolstering Functionality [Internet]. 2013 [cited 2016 04 March]. Available from: https://www.bridgestone.com/corporate/news/2013112101.html.

120. Umesh G, SN AK. Design and analysis of non-pneumatic tyre (NPT) with honeycomb spokes structure. International Journal of Engineering Science and Computing. 2016;6(9):2136-40.

121. Sassi S, Ebrahemi M, Al-Mozien M. New design of flat-proof non-pneumatic tire. International Journal of Mechanical Systems Engineering. 2016;2(114). doi: http://dx.doi.org/10.15344/2455-7412/2016/114

122. Kaufman G, Triana D, Blouin V, Cole C, Joseph P, Summers J, editors. Wear resistance of lunar wheel treads made of polymeric non-woven fabrics. SAE World Congress and Exhibition: Tire and Wheel Technology; 2009 20-23 April Cobo Center, USA: SAE.

123. Ju J, Ananthasayanam B, Summers JD, Joseph P. Design of cellular shear bands of a non-pneumatic tire-investigation of contact pressure. SAE International Journal of Passenger Cars-Mechanical Systems. 2010;3(1):598-606.

124. Ma J, Ju J, Summers JD, Joseph P, Ananthasayanam B, editors. Effects of cellular shear bands on interaction between a non-pneumatic tire and sand. SAE World Congress and Exhibition: Tire and Wheel Technology; 2010 13-15 April Cobo Center, USA: SAE Technical Paper.

125. Rutherford W, Bezgam S, Proddaturi A, Thompson L, Ziegert JC, Rhyne TB, et al. Use of orthogonal arrays for efficient evaluation of geometric designs for reducing vibration of a non-pneumatic wheel during high-speed rolling. Tire Science and Technology. 2010;38(4):246-75.

126. Narasimhan A, Ziegert J, Thompson L. Effects of material properties on static load-deflection and vibration of a non-pneumatic tire during high-speed rolling. SAE International Journal of Passenger Cars-Mechanical Systems. 2011;4(**1**):59-72.

127. Howard FA, inventor; Frank A Howard assignee. Safety pneumatic tire patent US2969824A. 1961.

128. Kenneth K, Brook O, inventors; Eng K. Kenneth assignee. Multi-chamber safety tire patent US20030131918A1. 2003.

129. Mazhar MS, inventor; US Secretary of Army, assignee. Multi-chamber pressurizable tube for a tire patent US6076580A. 2000.

130. Seyed K, inventor; Khalil Seyed assignee. Tire patent US2525752A. 1950.

131. Huber VR, inventor; Uniroyal Goodrich Tire Co, assignee. Tire patent US3487870A. 1970.

132. Cupp HN, inventor; Harry N Cupp, assignee. Automobile tire patent US1989402A. 1935.

133. Mclean WD, inventor; Willard D. McLean, assignee. Supplemental Shoe for Automobile Tires patent US2735471A. 1956.

134. Mcleod NW, inventor; Norman W Mcleod assignee. Multi-chambered vehicle tire patent US2780266A. 1957.

135. Lambe DM, inventor; Lambe Donald M assignee. Dual-chamber pneumatic tire patent US4293017A. 1981.

136. Francesco M, Maria M, Marina M, inventors; Curtiss-Wright Corp, assignee. Tire for vehicles, composed of two concentric annular chambers patent US2925845A. 1960.

137. Coyote. Coyote Boltless Beadlock System [Internet]. 2014 [cited 2017 19 September]. Available from: https://www.coyoteents.com/beadlocks/.

138. Bridgestone. Multi-chamber tyre extends thinking on stability. European Automotive Design. 2006;10(5):12.

139. Evans R. Concept Tires: Future Proofs. Tire Technology International. 2015;3.

140. Hall G, inventor; Fusion Innovations Ltd assignee. Pneumatic Tyre with Multiple Chambers patent WO2014057282A1. 2014.

141. Pillai P, Fielding-Russell G. Effect of aspect ratio on tire rolling resistance. Rubber chemistry and technology. 1991;64(4):641-7. doi: http://dx.doi.org/10.5254/1.3538579

142. Treichel D, editor Possibilities of reducing the rolling resistance of commercial vehicle tyres and effects on fuel consumption. Proceedings of the 19th International Fisita Congress; 1982 8-12 November Melbourne: Society of Automotive Engineers.

143. Yoshimura N, Yamagishi K, Togashi M. The present status of research on rolling resistance in Japan. Rubber Chemistry and Technology. 1983;56(2):497-8.

144. Klingbeil W, editor The effect of aspect ratio on rolling loss of radial passenger car tires. ASTM F-9 Committee on Tires; 1989 November; Richfield, Ohio.

145. Balbis M, editor Effect of aspect ratio on tyre rolling loss. Proceedings of the Conference Automobile Wheels and Tyres; 1983 18-19 October; Penns Hall Hotel, Sutton Coldfield, England: Mechanical Engineering Publications Limited.

146. Mathevet A, editor Selecting a tyre for reduced rolling resistance, aerodynamic drag, fuel consumption and weight. Proceedings of the Conference Automobile Wheels

and Tyres; 1983 18-19 October; Penns Hall Hotel, Sutton Coldfield, England: Mechanical Engineering Publications Limited.

147. Clark S, editor Geometric effects on the rolling resistance of pneumatic tires. Tire Rolling Losses and Fuel Economy – An R&D Workshop; 1977 18-20 October; Cambridge (MA): Society of Automotive Engineers.

148. Curtiss W. Low power loss tires. SAE Technical Paper. 1969. doi: 10.4271/690108, 1969

149. Dijks A. Rolling Resistance Measurements with a Piezo-EIectric Measuring System. Netherlands: Delft University of Technology – Vehicle Research Laboratory.1981. Report No.: 0148-7191.

150. Rhode D, editor Investigation into the influence parameters on rolling resistance and the development of an energy optimized tire. 6th Annual Meeting of Tire Society; 1987 24-25 March Akron University: Tire Society.

151. Bosik A, Dunn T, Critch C. Comparison of laboratory and on-long road truck tire rolling resistance for various tire tread depths. SAE Technical Paper. 1988. doi: 10.4271/880584

152. Redrouthu BM, Das S. Tyre modelling for rolling resistance [Master Thesis]. Göteborg, Sweden: Chalmers University of Technology; 2014.

153. Evans I. The rolling resistance of a wheel with a solid rubber tyre. British Journal of Applied Physics. 1954;5(5):187.

154. Bennetts A. Bay Systems: Thermal measurement. Tire Technology International. 2015;11:111.

155. Martino M. Speaker Spotlight: Fiat Chrysler Automobiles. Tire Technology International. 2015;11:102.

156. Lawson T. Low profile tyres: how low can you go? [Internet]. 2014 [cited 2016 20 February]. Available from: https://www.caradvice.com.au/291176/low-profile-tyres-how-low-can-you-go/.

157. Michelin. An unknow object: the tire materials [Internet]. 2019 [cited 2019 09 April]. Available from: https://thetiredigest.michelin.com/an-unknown-object-the-tire-materials.

158. Rodgers B, Waddell W. Tire engineering. In: Eirich FR, editor. Science and Technology of Rubber. Third ed. USA: Elsevier: Academic Press; 2005. p. 653-94.

159. Trinko MJ. Chapter 6: Tire Stress Analysis. The pneumatic tire. Washington DC: US department of Transportation: National Highway Traffic Safety Administration; 2006. p. 206-30.

160. Volk H, Struebel C, Mueller N, inventors; Continental Reifen Deutschland GmbH, assignee. Pneumatic vehicle tire patent US20160016435A1. 2016.

161. Martini M. Passenger Tire Rolling Loss: A Tread Compounding Approach and Its Tradeoffs. Rubber Chemistry and Technology. 1983;56(2):507-8.

162. Bond R, Morton G, Krol L. A tailor-made polymer for tyre applications. Polymer. 1984;25(1):132-40. doi: 10.1016/0032-3861(84)90278-7

163. Funt J, editor Dynamic properties and compound performance. Rubber Chemistry and Technology; 1986: American Chemical Society.

164. Yoshioka A, Komuro K, Ueda A, Watanabe H, Akita S, Masuda T, et al. Structure and physical properties of high-vinyl polybutadiene rubbers and their blends. Pure and Applied Chemistry. 1986;58(12):1697-706.

165. Takao H, Imai A, editors. Polymer design for lower rolling resistance rubbers. International Rubber Conference Proceedings: IRC ’85; 1985 15-18 October; Kyoto: Japan Society of Rubber Industry.

166. Kern W, Futamura S. Effect of tread polymer structure on tyre performance. Polymer. 1988;29(10):1801-6. doi: 10.1016/0032-3861(88)90394-1

167. Fujimaki T, Ogawa M, Yamaguchi S, Tomita S, Okuyama M, editors. Solution polymerised SBR terminated with tin-compound. II. tyre application. International Rubber Conference Proceedings: IRC'85; 1985 15-18 October Kyoto: Japan Society of Rubber Industry.

168. Oshima N, Tsutsumi T, Sakakibara M, editors. Newly developed solution SBRs for low rolling resistance tires. International Rubber Conference Proceedings: IRC'85; 1985 15-18 October Kyoto: Japan Society of Rubber Industry.

169. Felix DG, SivaKumar G. Nano particles in automobile tires. IOSR Journal of Mechanical and Civil Engineering. 2014;11(4):07-11.

170. Kopcha J. Still a segmented market: UHP tires: every driver seems to want more than performance. Modern Tire Dealer–The Industry's Leading Publication. 2015;96(2):18-24.

171. Chen S. A preliminary discourse on tunable rolling resistance of electrorheological fluid containing polymer composites [PhD Thesis]. Akron: University of Akron; 2015.

172. Nair S, Chandra A, Mohamed P. Reducing rolling resistance with improved tread design and new materials. Tire Technology International. 2008.

173. Nordsiek K. The "integral rubber" concept—an approach to an ideal tire tread rubber. Kautschuk und Gummi, Kunststoffe. 1985;38(3):178-85.

174. Aggarwal S, Hargis I, Livigni R, Fabris H, Marker L. Structure and properties of tire rubbers prepared by anionic polymerization. Advances in elastomers and rubber elasticity: Springer; 1986. p. 17-36.

175. Baker C, Gelling I, Newell R. Epoxidized natural rubber. Rubber chemistry and Technology. 1985;58(1):67-85. doi: http://dx.doi.org/10.5254/1.3536059

176. Aher S, Desarda A, Shelke J, Chaudhari M. A review on smart materials: future potentials in engineering. Intertional Journal of Science Technology and Management. 2015;4(10):7-16.

177. Kaushal A, Vardhan A, Rawat R. Intelligent material for modern age: a review. IOSR Journal of Mechanical and Civil Engineering. 2016;13(3):10-5.

178. Forsell U. The market is changing and it is now about offering the best ESC, the best TPMS, all at the right price. Tire Technology International. 2009;7:26.

179. Matsuzaki R, Todoroki A. Wireless monitoring of automobile tires for intelligent tires. Sensors. 2008;8(12):8123-38. doi: 10.3390/s8128123

180. Mueller M. Interview: Ulrich Giese, DIK: A focus on future materials and natural rubber's potential. Tire Technology International 2015;11:20-4.

181. ASTM. D412 − 15a. Standard Test Methods for Vulcanized Rubber and Thermoplastic Elastomers—Tension. West Conshohocken, PA: ASTM International; 2016.

182. ISO. ISO 4664-1. Rubber, vulcanized or thermoplastic — Determination of dynamic properties — Part 1: General guidance. Switzerland: International Organization for Standardization; 2005.

183. ASTM. D885/D885M − 10a (2014)E1. Standard Test Methods for Tire Cords, Tire Cord Fabrics, and Industrial Filament Yarns Made from Manufactured Organic-Base Fibers. West Conshohocken, PA: ASTM International; 2014.

184. Ponnamma D, Thomas S. Non-Linear Viscoelasticity of Rubber Composites and Nanocomposites: Influence of Filler Geometry and Size in
Different Length Scales. Switzerland: Springer; 2014.

185. Behroozi MH. Finite element analysis of aircraft tyres [PhD Thesis]. Birmingham: University of Birmingham; 2014.

186. Mahmoodi N. InterjetRR IDP12: Q6 Review UK innovate, fusion innovation. University of Birmingham 2018.[20 April 2018]. Report No.: 65187-464180.

187. Aldhufairi HS, Olatunbosun OA, Essa K. Determination of a Tyre's Rolling Resistance using Parallel Rheological Framework. SAE Technical Paper. 2019. doi: https://doi.org/10.4271/2019-01-5069

188. Hogan R. 6 Influences on Uncertainty in Measurement Results [Internet]. 2013 [cited 2018 24 November]. Available from: https://www.isobudgets.com/6-influences-on-uncertainty-in-measurement-results/.

189. ASTM. E4-16. Standard Practices for Force Verification of Testing Machines. West Conshohocken, PA: ASTM International; 2016.

190. ISO. ISO 5893:2002. Rubber and plastics test equipment - Tensile, flexural and compression types (constant rate of traverse) - Specification. Switzerland: International Organization for Standardization; 2002.

191. ISO. ISO 37:2005. Rubber, vulcanized or thermoplastic - Determination of tensile stress-strain properties. Switzerland: International Organization for Standardization; 2005.

192. UNC. Measurements and Error Analysis. 2011. In: College Physics Labs Mechanics [Internet]. Chapel Hill: Advanced Instructional Systems, Inc. and the Universtiy of North Carolina, [cited 16 April 2016]. Available from: https://www.webassign.net/question_assets/unccolphysmechl1/measurements/manual.html.

193. ISO. ISO 7500-1. Metallic materials - Verification of static uniaxial testing machines - Part 1: Tension/compression testing machines - Verification and calibration of the force-measuring system. Switzerland: International Organization for Standardization; 2004.

194. Systèmes D. Abaqus Analysis User's Guide. 2251 Hyperelastic behavior of rubberlike materials. RI, USA: Dassault Systèmes Simulia Corp.; 2013.

195. Ghosh P, Saha A, Bohara P, Mukhopadhyay R. Material property characterization for finite element analysis of tires. Rubber world. 2006;233(4).

196. Fung Y-c. Biomechanics: motion, flow, stress, and growth. New York: Springer Science & Business Media; 2013.

197. ISO. ISO 23529. Rubber — General procedures for preparing and conditioning test pieces for physical test methods. Switzerland: International Organization for Standardization; 2010.

198. Martin JW, Ryntz RA, Chin J, Dickie R. Service life prediction of polymeric materials: global perspectives. New York: Springer Science & Business Media; 2008.

199. Clark SK. Mechanics of pneumatic tires. Washington, D. C.: U.S. Department of Transportation; 1981.

200. Fleming RA, Livingston DI. Tire Reinforcement and Tire Performance. Philadelphia: ASTM International; 1979.

201. Smith EH. Mechanical engineer's reference book. 12th ed. Oxford, UK: Butterworth-Heinemann; 2013.

202. ASTM. E328 − 13 Standard Test Methods for Stress Relaxation for Materials and Structures. West Conshohocken, PA: ASTM International; 2014.

203. ISO. ISO 6914:2008. Rubber, vulcanized or thermoplastic - Determination of ageing characteristics by measurement of stress relaxation in tension. Switzerland: International Organization for Standardization; 2008.

204. Systèmes D. Abaqus Analysis User's Guide. 2271 Time domain viscoelasticity. RI, USA: Dassault Systèmes Simulia Corp.; 2013.

205. García-Barruetabeña J, Cortés F, Abete JM, Fernández P, Lamela MJ, Fernández-Canteli A. Experimental characterization and modelization of the relaxation and complex moduli of a flexible adhesive. Materials & Design. 2011;32(5):2783-96.

206. Systèmes D. Abaqus Analysis User's Guide. 2282 Parallel rheological framework. RI, USA: Dassault Systèmes Simulia Corp.; 2013.

207. Obbink-Huizer C. Simuleon FEA Blog Material calibration using Abaqus (and Isight) [Internet]. 2016 [cited 2018 07 March]. Available from: https://info.simuleon.com/blog/material-calibration-using-abaqus-and-isight.

208. Barrett PR. Debugging Complex Finite Element Analysis Using a Single Element Model [Internet]. 2014 [cited 2017 27 September]. Available from: https://www.engineering.com/DesignSoftware/DesignSoftwareArticles/ArticleID/8705/Debugging-Complex-Finite-Element-Analysis-Using-a-Single-Element-Model.aspx.

209. Osborne M. Single-element characterization of the LS-DYNA MAT54 material model [Master Thesis]. Washington, USA: University of Washington; 2013.

210. Dalrymple T. Calibration of Polypropylene, Washington Penn grade PPC3TF2-Black. Ann Arbor, Michigan: axel physical testing services.2014.

211. Wood LA, Bekkedahl N, Roth FL. Measurement of Densities of Synthetic Rubbers. Journal of Research of the National Bureau of Standards. 1942;29(1939):391-6.

212. Engineering-Department. Materials Data Book. Cambridge, UK: Cambridge University; 2003. Available from: http://www-mdp.eng.cam.ac.uk/web/library/enginfo/cueddatabooks/materials.pdf.

213. ASTM. D1776/D1776M − 16. Standard Practice for Conditioning and Testing Textiles. West Conshohocken, PA: ASTM International; 2016.

214. ASTM. D2969-04. Standard Test Methods for Steel Tire Cords. West Conshohocken, PA: ASTM International; 2014.

215. Baranowski P, Malachowski J, Janiszewski J, Wekezer J. Detailed tyre FE modelling with multistage validation for dynamic analysis. Materials & Design. 2016;96:68-79.

216. Chandra S. Challenges in the Finite Element Analysis of Tire Design using ABAQUS. American Engineering Group. 2000.

217. Heeps G. Another fine mesh. Tire Technology International. 2015;11:50-6.

218. Bekakos C-A, Papazafeiropoulos G, O'Boy D, Prins J, editors. Pneumatic tyres interacting with deformable terrains. Journal of Physics: Conference Series; 2016: IOP Publishing.

219. Systèmes D. Abaqus Analysis User's Guide. 2811 Solid (continuum) elements. RI, USA: Dassault Systèmes Simulia Corp.; 2013.

220. Hale S. Engineering Advantage: Why worry about hourglassing in explicit dynamics part I [Internet]. 2015 [cited 2018 04 January]. Available from: https://caeai.com/blog/why-worry-about-hourglassing-explicit-dynamics-part-i.

221. Hale S. Engineering Advantage: Why Worry About Hourglassing in Explicit Dynamics? Part II [Internet]. 2015 [cited 2018 04 January]. Available from: https://caeai.com/blog/why-worry-about-hourglassing-explicit-dynamics-part-ii.

222. Yang X, Behroozi M, Olatunbosun OA. A neural network approach to predicting car tyre micro-scale and macro-scale behaviour. Journal of Intelligent Learning Systems and Applications. 2014;6(01):11.

223. Wei C, Olatunbosun OA, Yang X. A finite-element-based approach to characterising FTire model for extended range of operation conditions. Vehicle System Dynamics. 2017;55(3):295-312. doi: https://doi.org/10.1080/00423114.2016.1264613

224. Steen vdR. Enhanced friction modeling for steady-state rolling tires [PhD Thesis]. Netherlands: Technische Universiteit Eindhoven; 2010.

225. Moisescu R, FRĂŢILĂ G. Finite element model of radial truck tyre for analysis of tyre-road contact stress. UPB Sci Bull. 2011;73(3).

226. Wang H, Al-Qadi IL, Stanciulescu I. Simulation of tyre–pavement interaction for predicting contact stresses at static and various rolling conditions. International Journal of Pavement Engineering. 2012;13(4):310-21. doi: https://doi.org/10.1080/10298436.2011.565767

227. Yang X, Olatunbosun O, Bolarinwa E. Materials testing for finite element tire model. SAE International Journal of Materials and Manufacturing. 2010;3(2010-01-0418):211-20.

228. Systèmes D. Abaqus Analysis User's Guide. 1151 Surface-based fluid cavities: overview. RI, USA: Dassault Systèmes Simulia Corp.; 2013.

229. Ask T. Engineering for Industrial Designers and Inventors: Fundamentals for Designers of Wonderful Things: O'Reilly Media, Inc.; 2016.

230. Myers R. The basics of chemistry. London, UK: Greenwood Publishing Group; 2003.

231. Zheng R, Li M, Wu B. Autoregressive Model for Automobile Tire Pressure and Temperature Based on MATLAB. In: Jin D, Lin S, editors. Advances in Computer Science and Information Engineering; Verlaf Berlin Heidelberg: Springer; 2012. p. 513-20.

232. Zenner H. Intelligence Call It Smarts: Update Yourself-Step by Step: Xlibris Corporation; 2012.

233. LS-DYNA. What are the differences between implicit and explicit? [Internet]. 2018 [cited 2018 252 September]. Available from: https://www.dynasupport.com/faq/general/what-are-the-differences-between-implicit-and-explicit.

234. Abaqus. Lecture 1: Overview of Abaqus/Explicit. USA: Abaqus, Inc; 2005.

235. Systèmes D. Abaqus Analysis User's Guide. 633 Explicit dynamic analysis. RI, USA: Dassault Systèmes Simulia Corp.; 2013.

236. Abaqus. Lecture 5: Quasi-Static Analyses. USA: Abaqus, Inc; 2005.

237. Nikola J, Karl-Fredrik N. Numerical Simulation of the One Meter Drop Test on a Bar for the Castor Cask-Preliminary Analysis. Luxembourg: Institute for Energy JRC) D-GJRCD.2007. Report No.: EUR 22470 EN.

238. Systèmes D. Getting Started with Abaqus: Interactive Edition. 241 Choosing between implicit and explicit analysis. RI, USA: Dassault Systèmes Simulia Corp.; 2013.

239. Hirt T. Implicit vs. Explicit Numerical Methods [Internet]. 2018 [cited 2018 25 September]. Available from: https://www.flow3d.com/resources/cfd-101/numerical-issues/implicit-versus-explicit-numerical-methods/.

240. Ogmaia D, Tasel SET. Simulation of vehicle crash into bridge parapet using Abaqus/Explicit [Master Thesis]. Stockholm, Sweden: KTH Royal Institute of Technology; 2015.

241. Bekakos C-A, Papazafeiropoulos G, O'Boy DJ, Prins J. Finite element modelling of a pneumatic tyre interacting with rigid road and deformable terrain. International Journal of Vehicle Performance. 2017;3(2). doi: 10.1504/IJVP.2017.083359

242. Yazdandoost F, Taheri S. Finite element tyre model for antilock braking system study. International Journal of Vehicle Design. 2016;72(3):248-61.

243. Simulia. An Integrated Approach for Transient Rolling of Tires. RI, USA: ABAQUS, Inc.2011. Report No.: TB-03-TRT-1.

244. Zuo S, Ni T, Wu X, Wu K, Yang X. Prediction procedure for wear distribution of transient rolling tire. International Journal of Automotive Technology. 2014;15(3):505-15. doi: 10.1007/s12239−014−0053−3

245. Henry JJ. Evaluation of pavement friction characteristics. Washington, D.C.: Transportation Research Board; 2000.

246. Wang H, Al-Qadi IL, Stanciulescu I. Effect of surface friction on tire–pavement contact stresses during vehicle maneuvering. Journal of Engineering Mechanics. 2014;140(4):04014001. doi: 10.1061/(ASCE)EM.1943-7889.0000691

247. ADAMS M. Material Contact Properties Table. 2005. In: MSC ADAMS Help Manual [Internet]. California: MSC Software Corporation.

248. Tomita H. Friction coefficients between tires and pavements surfaces. Port Hueneme, California: U. S. Naval Civil Engineering Lab.1964. Report No.: R303.

249. Systèmes D. Abaqus Analysis User's Guide. 3713 Contact damping. RI, USA: Dassault Systèmes Simulia Corp.; 2013.

250. Systèmes D. Abaqus Analysis User's Guide. 612 Defining an Analysis: Precision Level of the Abaqus/Explicit Executable. RI, USA: Dassault Systèmes Simulia Corp.; 2013.

251. Systèmes D. Abaqus Analysis User's Guide. 911 Restarting an Analysis: Controlling the precision of output to the Abaqus/Explicit state file. RI, USA: Dassault Systèmes Simulia Corp.; 2013.

252. Narasimha Rao K, Kumar RK. Simulation of tire dynamic behavior using various finite element techniques. International Journal for Computational Methods in Engineering Science and Mechanics. 2007;8(5):363-72. doi: 10.1080/15502280701471566

253. Systèmes D. Abaqus/CAE User's Guide. 1761 Verifying your Mesh RI, USA: Dassault Systèmes Simulia Corp.; 2013.

254. Systèmes D. Getting Started with Abaqus: Interactive Edition. 44 Mesh Convergence RI, USA: Dassault Systèmes Simulia Corp.; 2013.

255. Systèmes D. Abaqus Analysis User's Guide. 422 Abaqus/Explicit output variable identifiers. RI, USA: Dassault Systèmes Simulia Corp.; 2013.

256. Optimec. Significance of Energies in FE Simulation – Part-1 [Internet]. 2018 [cited 2018 02 April]. Available from: http://optimec.ca/news/significance-of-energies-in-fe-simulation-part-1/.

257. Clarhed D. Stress Analysis of PTFE Sleeves in Industrial Valves [Master Thesis]. Lund, Sweden: Lund University; 2008.

258. Shahabi B. A structural investigation to develop guidelines for the finite element analysis of the Mini-Baja vehicle [Master Thesis]. Ontario, Canada: University of Windsor; 2012.

259. Systèmes D. Getting Started with ABAQUS/Explicit: Keywords Version. 43 Example: hourglassing in a rubber block. RI, USA: Dassault Systèmes Simulia Corp.; 2009.

260. Tanlak N, Sonmez F, Talay E. Detailed and simplified models of bolted joints under impact loading. The Journal of Strain Analysis for Engineering Design. 2011;46(3):213-25.

261. ISO. ISO 18164:2005. Passenger car, truck, bus and motorcycle tyres - Methods of measuring rolling resistance. Switzerland: International Organization for Standardization; 2005.

262. ISO. ISO 28580:2009. Passenger Car, Truck and Bus Tyres—Methods of Measuring Rolling Resistance—Single Point Test and Correlation of Measurement Results. Switzerland: International Organization for Standardization; 2009.

263. Vayalat TM. Tire Contact Patch Characterization through Finite Element Modeling and Experimental Testing [Master Thesis]. Blacksburg, VA: Virginia Polytechnic Institute and State University; 2016.

264. Kumar U, Goyal S, Unnikrishnan G, Thomas TK. Application Of Improved Simulation Approach For Tire Foot Print Contact Pressure Estimation. International Journal of Mechanical And Production Engineering. 2015;3(5):97-9.

265. Michelin. The Tyre: Mechanical and Acoustic Comfort: Société de technologie Michelin; 2002.

266. Mawby WD, Sauls J, inventors; Michelin Recherche Et Technique, S.A.Societe De Technologie Michelin assignee. Improvement of tire uniformity through identification of process effects using singlet tire regression analysis patent WO2012002949A1. 2012.

267. Hall J, Smith KL, Titus-Glover L, Wambold JC, Yager TJ, Rado Z. Guide for pavement friction. USA: Transportation Research board of the National Academies.2009. Contract No.: 108.

268. Steyn WJv, Ilse M. Evaluation of tire/surfacing/base contact stresses and texture depth. International Journal of Transportation Science and Technology. 2015;4(1):107-18.

269. Michelin. The tyre grip. Clermont–Ferrand, France: Société de Technologie Michelin 2001.

270. Khameneifar F, Arzanpour S, editors. Energy harvesting from pneumatic tires using piezoelectric transducers. ASME Conference Proceedings of Smart Materials, Adaptive Structures and Intelligent Systems; 2008 October 28–30; Ellicott City, Maryland, USA: Aerospace Division.

271. Pottinger MG, Marshall KD, Arnold GA. Effects of test speed and surface curvature on cornering properties of tires. SAE Transactions. 1976:95-104.

272. Nordeen DL, Cortese AD. Force and moment characteristics of rolling tires. SAE Transactions. 1964:325-47.

273. Lee C-R, Kim J-W, Hallquist JO, Zhang Y, Farahani AD. Validation of a FEA tire model for vehicle dynamic analysis and full vehicle real time proving ground simulations. SAE Technical Paper.1997. Report No.: 0148-7191.

274. Stallmann MJ, Els PS. Parameterization and modelling of large off-road tyres for ride analyses: Part 2–Parameterization and validation of tyre models. Journal of Terramechanics. 2014;55:85-94.

275. Hernandez JA, Gamez A, Shakiba M, Al-Qadi IL. Numerical prediction of three-dimensional tire-pavement contact stresses. Urbana-Champaign: University of Illinois.2017. Report No.: 0197-9191 Contract No.: ICT-17-004.

276. Narasimha Rao K, Kumar RK, Bohara P. A sensitivity analysis of design attributes and operating conditions on tyre operating temperatures and rolling resistance using finite element analysis. Proceedings of the Institution of Mechanical Engineers, Part D: Journal of Automobile Engineering. 2006;220(5):501-17.

277. Akutagawa K. Technology for reducing tire rolling resistance. Tribology Online. 2017;12(3):99-102.

278. Vorotović GS, Rakicević BB, Mitić SR, Stamenković DD. Determination of cornering stiffness through integration of a mathematical model and real vehicle exploitation parameters. FME Transactions. 2013;41(1):66-71.

279. Hac A, Simpson MD. Estimation of vehicle side slip angle and yaw rate. SAE 2000 World Congress; March 6-9; Detroit, Michigan. USA: Society of Automotive Engineers, Inc; 2000.

280. Katz J. Aerodynamics of race cars. Annual Review of Fluid Mechanics. 2006;38:27-63. doi: 10.1146/annurev.fluid.38.050304.092016

281. Parisouz S. Experimental rubber friction modelling and its applications in tyre finite element analysis [PhD Thesis]. Birmingham, UK: University of Birmingham; 2018.

282. Pugh S. Total design: integrated methods for successful product engineering. Michigan: Addison-Wesley; 1991.

283. Kennedy R, editor Performance Assessment from the Tire's Point of View. Road Profile Users Group Conference; 2016 November 1-4; San Diego, California: The Transtec Group.

284. Goodyear. Tire Performance Criteria [Internet]. 2016 [cited 2018 11th March]. Available from: https://www.goodyear.com.ph/learn/tire-performance-criteria.

285. Petersen G. How to Choose the Right Car Tires [Internet]. 2016 [cited 2018 11th March]. Available from: https://www.consumerreports.org/tires/how-to-choose-the-right-car-tires/.

286. Allen J. Jeep 4x4 Performance Handbook: MotorBooks International; 1998.

287. Schuring D, Skinner G, Rae W. Contained Air Flow in a Radial Tire. SAE Transactions. 1981:705-12.

288. Rae WJ, Skinner GT. Measurements of Air Flow Velocity Distributions Inside a Rolling Pneumatic Tire. SAE Technical Paper.1984. Report No.: 0148-7191.

289. KuliKowsKi K, Szpica D. Determination of directional stiffnesses of vehicles' tires under a static load operation. Eksploatacja i Niezawodność. 2014;16(1):66-72.

290. Soltani A, Goodarzi A, Shojaeefard MH, Saeedi K. Optimizing tire vertical stiffness based on ride, handling, performance, and fuel consumption criteria. Journal of Dynamic Systems, Measurement, and Control. 2015;137(12):121004.

291. Mhaske N, Narwade P, Nagarkar M. Stiffness Analysis of Passenger Car Tire Using Nitrogen. International Journal of Scientific and Research Publications. 2016;6(1):140-8.

292. Aldhufairi HS, Olatunbosun OA, Essa K. Multi-Chamber Tyre Designing for Fuel Economy. Proceedings of the Institution of Mechanical Engineers, Part D: Journal of Automobile Engineering. 2019. doi: https://doi.org/10.1177/0954407019857026

293. Ji T. Concepts for designing stiffer structures. The Structural Engineer. 2003;81(21):36-42.

294. Wei Y, Oertel C, Shen X. Tyre rolling kinematics and prediction of tyre forces and moments: part II–simulation and experiment. Vehicle system dynamics. 2012;50(11):1689-706. doi: https://doi.org/10.1080/00423114.2012.694453

295. Haney P. The racing & high-performance tire: using the tires to tune for grip and balance. USA: McFarland; 2003.

296. Ridha R, Theves M. Advances in tyre mechanics: iSmithers Rapra Publishing; 1994.

297. Schmid M. Tire Modeling for Multibody Dynamics Applications [PhD Thesis]. Madison: University of Wisconsin; 2011.

298. careocar.com. tire-section. India: Indtree Software Pvt. Ltd.; 2017.

299. Denton T. Automobile mechanical and electrical systems. Oxford, UK: Butterworth-Heinemann: Elsevier; 2011.

300. Hillier VAW, Coombes P. Fundamentals of motor vehicle technology: Nelson Thornes; 2004.

301. Heisler H. Advanced vehicle technology: Elsevier; 2002.

302. Miller RC. Tire [Internet]. 2007 [cited 2016 23 September]; 1. Available from: http://www.madehow.com/Volume-1/Tire.html.

303. bridgestonetyres.com. Truck_define. Australia: Bridgestone; 2016.

304. Anne, Evans R. The Composition of a Tyre: Typical Components. Oxon: The Old Academy.2006. Report No.: TYR0009-02.

305. Gent AN. Chapter 2: Mechanical Properties of Rubber. The pneumatic tire. Washington DC: National Highway Traffic Safety Administration, US department of Transportation; 2006. p. 28-79.